Peroxidase Catalyzed Degradation of Partially Hydrolyzed Polyacrylamide

By

William Joe Rivie Gilbert

B.Sc. Environmental Science, Haskell Indian Nations University, Lawrence, Kansas, 2008

Submitted to the graduate degree program in the Department of Chemical and Petroleum Engineering and the Graduate Faculty of the University of Kansas in partial fulfillment of the requirements for the degree of Doctor of Philosophy.

Committee members:

_____

Aaron Scurto

(Chairperson)

_____

Reza Barati

(Co-chairperson)

_____

Kevin Leonard

_____

Belinda Sturm

_____

Jyun-Syung Tsau

_____

Stephen J. Johnson

Date defended: August 23, 2016

The Dissertation Committee for William Joe Rivie Gilbert certifies that this is the approved version of the following dissertation:

Peroxidase Catalyzed Degradation of Partially Hydrolyzed Polyacrylamide

_____

Aaron Scurto

(Chairperson)

_____

Reza Barati

(Co-chairperson)

_____

Kevin Leonard

_____

Belinda Sturm

_____

Jyun-Syung Tsau

_____

Stephen J. Johnson

Abstract

Recently developed technologies such as directional drilling, multi-stage fracturing, and friction reducing fracturing fluids, have allowed access to previously unattainable resources. These technologies were adapted to deal with the extremely low rock permeability where conventional fracturing practices were unsuccessful. Although there are many similarities in the fracturing ideologies between conventional and unconventional fracturing processes, one main component that differs greatly is the fracture fluid makeup, composition, and quantity. In most conventional fracturing practices, high viscosity cross-linked cellulosic polymers are used in order to transport and suspend proppant in the fracture. On the other hand, high molecular weight partially hydrolyzed polyacrylamide (HPAM) is used as a friction reducer in unconventional "slickwater" fracturing. In both cases, these polymer additives have been shown to decrease the productivity of the well by damaging the fracture conductivity and fracture face permeability. Moreover, water usage and disposal has created social and political pressures for recycling or cleaning reproduced fracture fluids. Major advances have been made to recover damage created in conventional fracturing fluids enzymatically as opposed to chemically. A few studies have investigated the oxidative chemical breakdown of HPAM but no known enzymatic processes have shown to directly degrade the polymer. The purpose of this study was to develop an enzymatic method for degrading HPAM polymer.

For this study the oxidative enzyme Horseradish Peroxidase (HRP) Type II was used in conjunction with hydrogen peroxide, and β-nicotinamide adenine dinucleotide (NADH). This system was chosen for its ability to form hydroxyl free radicals though the breakdown of hydrogen peroxide. NADH was added to act as stable electron carrier during free radical formation. In addition, pilot studies, observing HPAM viscosity reduction, using soybean peroxidase was

investigated as an economical alternative to HRP. Partially hydrolyzed polyacrylamide (HPAM; MW = 6,000 kDa) Alcoflood 935 was used as a commercially available polymer.

Initially, studies investigated the reduction of HPAM viscosity after exposure to the HRP/NADH system using low, moderate and high peroxide concentrations in aqueous solution. Results of this study show that there was a significant reduction in viscosity 17.6 % ± 5.16, 37.7% ± 6.1, and 63.4% ± 3.9 respectively when reaction were conducted at 37°C for 24 hours. In addition, studies were conducted to observe viscosity reduction in the absence of NADH and with varying HRP concentrations. Periodic sampling over a 24-hour period showed that most viscosity reduction takes place within the first 4-5 hours for all peroxide concentrations.

Size exclusion chromatography was used to confirm that the reduction in viscosity was directly related to reduction in molar mass. It was determined that the weight average molecular weight of Alcoflood 935 is $6.14 \pm 0.66 \times 10^6$ Da. Reductions of 15.0 ± 3.0%, 40.2 ± 2.7%, and 66.8 ± 11.0% were observed for low, medium, and high peroxide concentrations respectively. In anticipation of core flooding studies, molecular weight reductions were also measured in 2% potassium chloride (KCl) brine. There was no significant difference in molecular weight reduction in brine when compared to studies conducted in water. Periodic sampling of molecular weight revealed that there are two kinetically distinct regions. Further studies investigated the kinetics of the reaction using different polymer concentrations.

Filter cake studies were performed using 0.1-micron nylon filter. In this study filter cake was formed using polymer and/or polymer plus different components of the enzyme system to determine the most effective treatment. The resulting damage to flow from filter cake formation was greater than 99%. The best recovery (14.0 % ± 7.4) in flowrate was observed when the filter cake was formed using HPAM and HRP followed by NADH and peroxide treatment.

Core flooding studies, using low permeability (1-4 md) Indiana Limestone, investigated the enzyme's ability to recover HPAM damage to porous media. Permeability to 2% KCl was measured for the undamaged, damaged, and treated cores to determine flow damage and recovery. Recoveries were measured by rigorously flowing all components through the core. This study resulted in an average recovery of 9.7 ± 3.3% using free HRP in solution. Further investigation revealed additional damage (28.0% ± 0.7%) to permeability caused by flowing HRP treatment through the core. For this reason, HRP was covalently immobilized on Ottawa fracturing sand as a means of enzyme application.

Enzyme immobilization was achieved by covalently binding HRP to Ottawa sand using (3-aminopropyl)triethoxysilane (APTES) and glutaraldehyde. This technique resulted in an immobilized concentration of 1.03 mg HRP/g sand and a specific activity of 1.1 ± 0.6 U/g sand. Using HPAM solutions, immobilized HRP resulted in a viscosity reduction of by about 65% but to a lesser degree than free enzyme in the presence of sand. Application of this system during core flooding resulted in a mean recovered permeability of 28.0 ± 0.4 percent, which is a considerable improvement, compared to free enzyme treatment (9.7 ± 3.3%).

In summary, a novel approach for degrading partially hydrolyzed polyacrylamide was investigated using hydrogen peroxide and horseradish peroxidase. This sustainable HRP/H_2O_2 system degraded the polymer in solution, reducing its viscosity and molecular weight. Molecular weight measurements confirmed that the viscosity reduction was due to a significant degradation of the polymer backbone and not primarily by amide hydrolysis or rearrangement, etc. Furthermore, the un-optimized treatment method was able to increase the permeability in HPAM damaged cores. Indiana limestone core samples with low permeability (< 4 md) were damaged and then the HRP/H_2O_2 treatment was used to improve the flow. It was noticed that the

enzyme treatment method actually both increases and decreases the damage in unidirectional flow system; which would not occur in an actual field treatment. However, immobilizing the enzyme on sand alleviated any further damage due to the enzyme plugging pores and increased the recovery of the damaged cores. This immobilized system may be a useful platform for remediation of polymer damage in hydraulic fracturing operations.

Acknowledgement

I would like to express my deep gratitude to all of my committee members for their guidance and support. I would especially like to thank my committee chair, Prof. Aaron Scurto, for his patience, extensive knowledge, and insight during the duration of this study. In addition, I would like to thank Dr. Stephen Johnson and Dr. Jyun-Syung Tsau for their support and advice in the laboratory. I would also like to thank Prof. Reza Barati for his support and knowledge dealing with unconventional reservoirs and enzyme systems. I would also like to acknowledge Prof. Jenn-Tai Liang (Texas A&M) for acting as my committee chair for the first half of my graduate studies.

This research would not have been possible without the assistance and support of Dr. Karen Peltier and Mr. Scott Ramskill. I greatly appreciate Dr. Peltier's assistance with laboratory equipment and procedures and Mr. Ramskill's ingenuity and technical assistance.

I would also like to acknowledge Madison and Lila Self for their generous contributions to The University of Kansas and the School of Engineering. The Madison and Lila Self Graduate Fellowship provided me with invaluable opportunities and experiences. Furthermore, I would like to thank Cathy D. Dwigans, Sharon Graham, Patty Dannenberg, and Howard Mossberg for making all of the fellowship events possible.

I would like to thank Prof. James Orr for his Baccalaureate and Post-Baccalaureate mentorship and support. Without Prof. Orr's guidance and mentorship, graduate school would not have been in my future. In addition, I would like to thank Prof. Orr and Dr. Marigold Linton for all of their hard work in supporting programs such as the Post-Baccalaureate Research Education Program (PREP) and Bridge Program. These programs were essential in preparing me for graduate school and providing valuable research experiences.

This is dedicated to my parents Tom and Nancy, whose unwavering love and support made everything possible.

Table of Contents

List of Figures

List of Tables

1 Introduction

The introductory chapter presents background information regarding hydraulic fracturing technology, application, and issues. It focuses on the use of polyacrylamide in water based fracturing fluids. Section 1.1 gives a brief introduction into the evolution of fracturing which has led to the water based technology used today. Section 1.2 outlines the differences between conventional and unconventional reservoirs, production from these reservoirs, and reservoir characterization. Section 1.3 describes the complexity of fractures created in shale reservoirs and gives a general description of fracturing fluid quantity, composition, and procedure. Section 1.4 gives a detailed description of fracture fluid components and challenges associated with the use of the additives. Section 1.5 describes the damage created in porous media, degradation mechanism, past chemical and biological degradation research, and governing kinetic equations related to random scission. Section 1.6 gives a detailed description of horseradish peroxidase structure, classification, reaction mechanism/activity, and applications. This section describes bioremediation studies and the use of free and immobilized enzyme, the substrates used, immobilized enzyme stability, and emphasizes on enzyme immobilization using silica and natural substrates. Section 1.7 outlines the research objective and gives a brief description on how those objectives were achieved.

1.1 A Brief History on Hydraulic Fracturing

The purpose of fracturing is to initiate and propagate fractures in the production zone to increase the rock matrix permeability and productivity. A Civil War veteran named Edward A.L. Roberts developed the first documented fracturing technique in 1865. His invention, called the Torpedo, consisted of 15-20 pounds of explosive powder that was lowered into the well and detonated.[1]

Later developments in the technology lead to the use of nitroglycerin but the use of this explosive was dangerous and unpredictable. The first fracturing innovation to follow the Torpedo was acid fracturing. In the 1930's it was discovered that corrosive liquids could be used to open channels in the rock and was a desirable alternative to using volatile nitroglycerine.[2]

The birth of modern day hydraulic fracturing took place in 1947 at the Hugoton gas field located in southwestern Kansas.[3] This experimental well was treated with 1000 US gallons of gelled gasoline, similar to napalm, and the technology was later commercialized in 1949.[2] The first year of commercialization, hydraulic fracturing proved to be a big advancement leading to an average production increase of 75% in 332 wells.[2] Since the commercialization of hydraulic fracturing by Halliburton in 1949, many advancements have been made but the main practice and concepts have stayed the same. In 1952, advancements allowed for multi-stage fracturing in vertical wells and became common practice throughout the industry.[4] Advancements in polymer technology has allowed the industry to move toward safer alternatives to gelled gasoline.

Horizontal wells were first used in around the early 1930's but were rarely used until the 1970's at which time, horizontal wells were mainly used as a tool for gas coning control.[5] Multistage fracturing in horizontal wells was first studied the late 1980's[6] and later became common practice. As conventional high permeability oil was depleted, the need for production in low permeability, unconventional zones became apparent. In the 1980's, George P. Mitchell discovered natural fractures in shale and in the early 1990's and further developed the use of horizontal drilling, including the use of water based "slickwater" fracturing fluid, for shale gas production.[7] Today, horizontal, multistage fractured wells have allowed gas and oil producers to gain access to previously inaccessible, unconventional resources such as shale. The development of horizontal extensions allowed production of oil and gas beneath developed locations, such as the Dallas-Fort

Worth airport, and allowed for greater contact with the production zone. The use of friction reducing fracture fluids, in conjunction with horizontal drilling, created the opportunity to produce oil and gas from previously inaccessible, low permeability rock.

The ability to produce from unconventional resources has catapulted the United States from one of the world's greatest energy importers to one of the greatest energy producers. The onset of technical advances has opened up 24.4 trillion cubic meters (tcm) of technologically recoverable shale gas, which more than triple the 7.7 proven gas reserves.[8] According to the United States Energy Information Administration (EIA), unconventional gas resources from tight gas, coal bed methane, and shale have increased 40%, 138%, and 900% respectively from 1995 to 2010 and is only projected to increase.[9]

1.2 Differences between Conventional and Unconventional Reservoirs

The purpose of this section is to identify the differences between conventional and unconventional reservoirs and practices. In general, the same concepts apply for both but there are key differences in rock properties that dictate drilling and completion procedures. Figure 1.1 illustrates the differences in vertical and horizontal well orientation and shows examples of conventional and unconventional oil and gas resources. In this figure, conventional oil and gas sources are shown to accumulate due to entrapment from impermeable rock (cap rock) where the trapped hydrocarbon originates in the shale source rock and undergoes migration over time. In addition, conventional reservoirs are usually considered as needing little stimulation for fluid flow due to the higher rock matrix permeability. These reservoirs can be categorized as having permeability in the millidarcy to darcy range and are cheaper to produce, require less technology, but contain less gas than unconventional sources.[10] Well completion in conventional reservoirs is

relatively straightforward because the well is drilled, perforated, stimulated (if needed), then produced. Often, as shown in Figure 1.1, vertical well orientation is used but this is not always the case. Unconventional reservoirs are low permeability (micro to nanodarcy range) and require increased investment to produce with the three most common reservoir type consisting of shale, tight gas, and coal bed methane.[11] These reservoirs require extensive stimulation, through the use of horizontal drilling and multistage fracturing, in order to produce an economically feasible quantity.

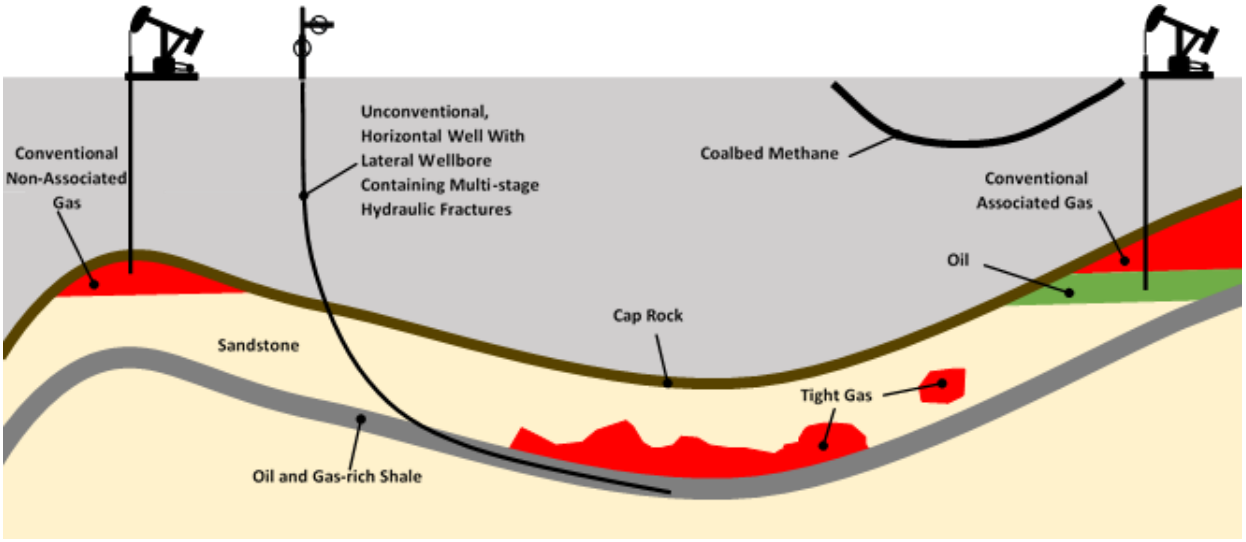

Figure 1.1 Illustration showing the type of oil and gas sources and difference between vertical and horizontal wells (Photo derived from EIA).

1.2.1 Reservoir Characterization

The reservoir conditions (i.e. temperature and pressure) and hydrocarbon composition dictate the type of reservoir. Examples of typical reservoir types are oil or gas cap reservoirs, dry gas, wet gas, and condensate. Figure 1.2 depicts a generic liquid-vapor, two-phase envelope for a hydrocarbon system.[12] These phase diagrams vary considerably depending on the hydrocarbon composition with gas reservoirs being comprised of mostly light hydrocarbon components. For the single phase gas reservoir, if the temperature remains constant then no fluid will exist. This

can be seen from the pressure reduction path (A_1) and is representative of reservoir conditions. Single-phase reservoirs are considered dry gas if production conditions do not cross the two-phase envelope. If the dew point is reached, condensate is formed (as shown by path A_2) and in this case, a wet gas exists. Dew point or gas condensate reservoirs initially contain gas but are unique in the fact that reservoir pressure reduction will first cause condensation (B_1 to B_2) then vaporization (B_2 to B_3). These reservoirs can cause near wellbore fluid blockage that can decrease the well productivity.[13] Production of this type of reservoir will be evident by increasing gas-oil ratio (GOR) during the condensation phase and decreasing GOR during vaporization. Bubble point reservoirs contain single-phase liquid state above the bubble point pressure (C). Above bubble point, the producing GOR is equivalent to the dissolved GOR and the oil is considered under saturated because the oil phase could dissolve more gas if it were present. At the bubble point, (C_1) light components in the oil phase are extracted and gas begins to form. As the reservoir pressure continues to drop, free gas is formed creating a solution-gas drive and gas cap (C_2). Initially, free gas saturation is small and immobile and the producing GOR is slightly reduced. As the pressure continues to fall the free gas become mobile and the producing GOR increases with time. Point (D) in the phase diagram represents a reservoir that initially contains two phases (oil and gas). This type of reservoir would contain a saturated oil that releases additional gas as pressure decreases and would contain both volumetric gas drive (as seen with single phase and condensate reservoirs) as well as solution-gas drive.

Conventional reservoirs can be any of the previously explained types but unconventional sources are typically more specific. For example, coal bed methane is considered a single-phase gas reservoir and can contain wet and dry gas composition.[14] Tight gas formations produce mainly dry gas[10] but some have shown to be retrograde gas-condensate reservoirs.[15] On the other

hand, shale reservoirs contain source organics, such as kerogen, that have gas generation potential through primary and secondary cracking.[16] Shale reservoirs can be categorized as being biogenic or thermogenic[17] but can also contain a mixture of the two. Biogenic shales, such as the Antrim shale, contain dry gas that is adsorbed to the organic matter.[18] Thermogenic shales are classified as having high or low thermal maturity. Examples of low thermal maturity shales are found in New Albany shale and Illinois basin and high thermal maturity basins are the Barnett and Fort Worth formations. A study conducted on the Barnett shale showed a linear correlation between the thermal maturity, initial GOR, and the type of produced hydrocarbon.[19] This correlation showed that the lower thermal maturity produced oil and wet gas- condensate, where higher maturity resulted in dry gas.

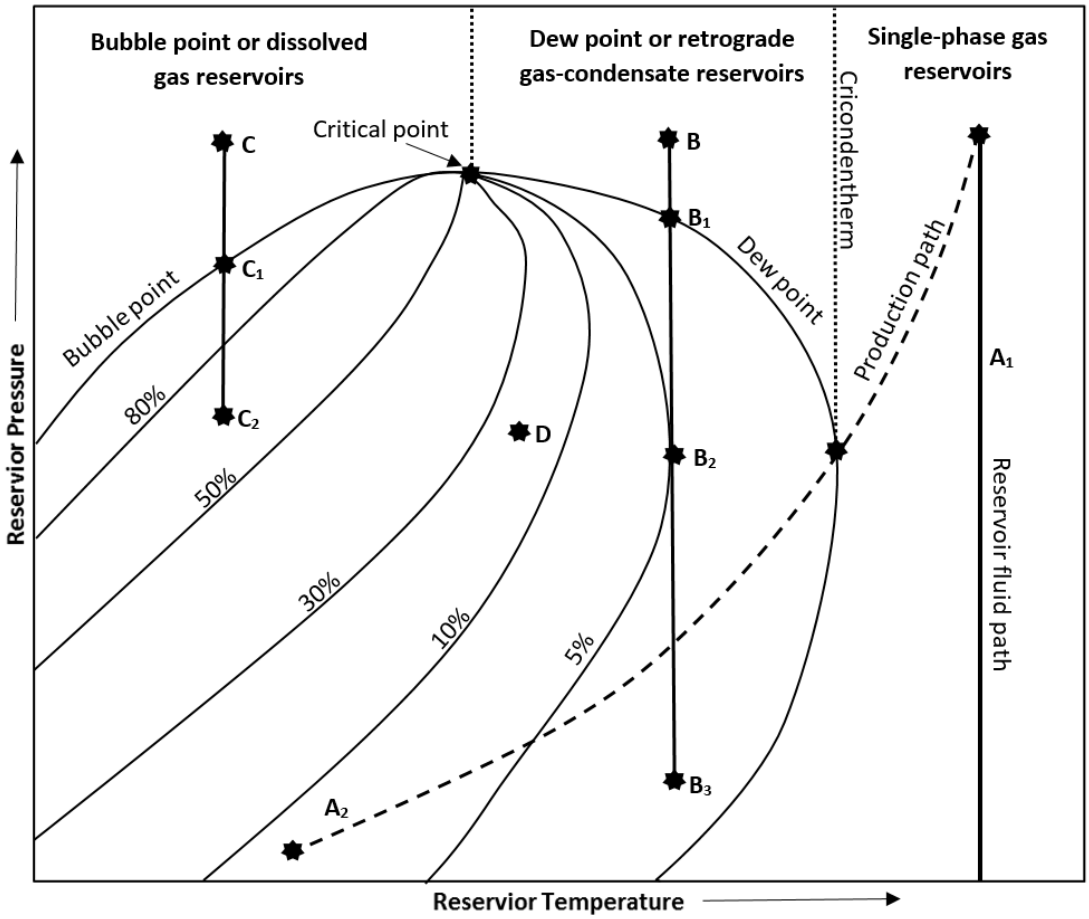

Figure 1.2: Phase diagram depicting a generic hydrocarbon liquid-vapor oil and gas system (Image derived from Terry and Rogers[12])

1.3 Fracturing in Unconventional Reservoirs

Fracturing has been the mainstream technology used to increase productivity in wells since its development in the 1940's. Up until recent years, wells were usually vertically oriented and shown to be successful in formations with a matrix permeability that allows fluid drainage from a large radial extent. The intent of fracturing conventional reservoirs is to reverse damage created from drilling (or skin factor) and stimulate the near wellbore region. On the other hand, the goal of fracturing in unconventional reservoirs is to create fractures throughout the entire reservoir. While there are some differences between fracturing conventional and unconventional reservoirs the overall goal still applies. In both cases, a polymer solution is injected under high pressure creating

highly conductive fluid flow pathways. In both cases proppant is added to the fracturing fluid, usually consisting of sand or ceramic beads, to "prop" open the newly created fractures after the pumping pressure is released. Furthermore, additives such as biocides, clay stabilizers, and scale inhibitors are added for flow assurance. The decision to apply one fracturing technique over the other is dictated by the rock properties in the target zone and therefore well type (i.e. vertical or horizontal).

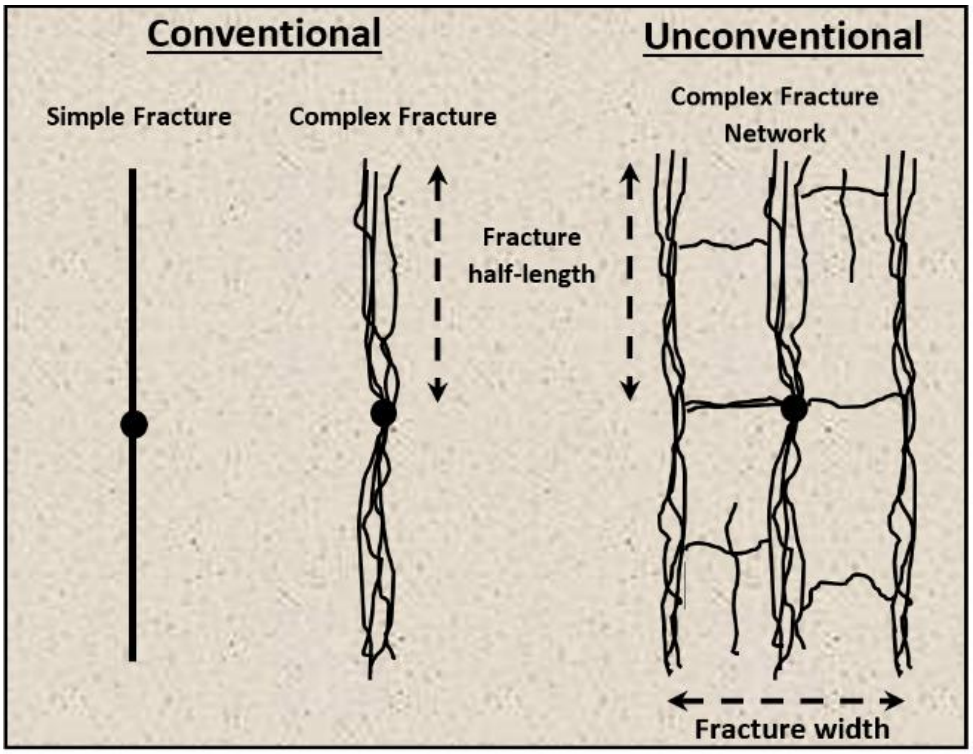

Figure 1.3: Fracture complexity in unconventional fracturing (Image derived from Fisher *et al.*[20]).

Unconventional fracturing is applied in very low permeability formations, such as tight gas and shale reservoirs, where conventional fracturing techniques are unsuccessful. The goal of this fracturing technique is to create fractures throughout the entire target zone. Furthermore, the fractures created are not simple, as seen in conventional formations, but consist of a complex network of fractures as visualized by microseismic techniques.[20,21] Figure 1.3 illustrates the

difference in fracture complexity observed in conventional and unconventional fracturing processes as described by Fisher *et al.*[20] The complexity created by hydraulically fractured shale is due to the presence of natural fractures, well orientation to the natural (preexisting) fractures, and interfacial friction.[22,23] Characterization of these fractures is conducted using complex models in conjunction with microseismic observation.

Fracturing in shale formations is conducted through multiple horizontally drilled wells that are often placed on multi-well pads. Wells are drilled through the target formation with the optimal distance between laterals being dictated by the effective fracture half-length. Next, multistage perforation and fracturing is conducted incrementally along the horizontal extension with recommended spacing of 400-600ft.[24] Fracturing fluid is injected into the well at high rates and volumes. After fractures are created, the well is produced to rid the well of fracture fluid.

Frictional losses become a significant factor when fracturing long horizontal wells. To reduce the friction loss, a new fracture fluid formulation was developed that contains uncrosslinked, high molecular weight polymer. The high molecular weight polymer, such as partially hydrolyzed polyacrylamide (HPAM), is shear thinning and acts as a friction reducer when injecting the fluid. The shear thinning characteristics of the fluid reduces the overall pump power need to fracture these wells. Furthermore, the volume of fluid injected can range from 5.0×10^5 to 1.5×10^6 gallons in the Barnett shale[20] but can reach volumes as high as 4 million gallons in the Marcellus Shale.[25] Fracture fluids are injected at significantly higher rates in unconventional processes (greater than 100 barrel/min) when compared to 20 barrel/min used in conventional fracturing.[2] The high pump rate not only facilitates the propagation of the fracture but is also used to transport proppant. The fracture fluid is mainly (>95%) composed of water but does contains additives such as friction reducer, proppant, biocide, scale inhibitors, among others.[26]

1.4 Water-based (Slickwater) Fracture Fluid Components

As stated above, unconventional fracturing processes use a fluid composition that differs from conventional practices. In both cases, the fracturing fluid makeup is specifically tailored to the each unique fracturing situation but the general composition of each technique stays the same. One of the greatest differences for slickwater applications is the low concentration of additives per volume of water. In most cases, the composition of the fluid is no greater than 5% chemical additives (as shown in Table 1.1).[27] In addition to the list presented, chemical breakers have been studied to degrade HPAM polymers injected. These breakers are covered in detail in Section 1.5. The purpose of this section is to outline the different fluid additives, issues associated with them, and to explain the reason behind their use.

Table 1.1 Common list of additives, the percent composition, and purpose as presented by Gregory *et al*.[27] from data collected by the Environmental Protection Agency (2004) and the American Petroleum Institute (2009).

Additive	Composition (% vol)	Example	Additive purpose
Water and Proppant	99.5	Fresh with addition of sand, resin coated sand, or ceramic beads as proppant	Hold fracture open
Friction reducer	0.088	Polyacrylamide or mineral oil	Minimize friction loss during pumping operations
Surfactant	0.085	Isopropanol	Increases viscosity
Salt	0.06	Potassium chloride (KCl)	Prevents clay swelling
Scale inhibitor	0.043	Phosphoric acid salt	Prevent salts from forming precipitants
pH-adjusting agent	0.011	Sodium or potassium carbonate	Maintains effectiveness of other additives
Acid	0.0123	Hydrochloric or muriatic acids	Dissolves minerals and initiates fractures
Iron control	0.004	Citric acid	Prevent precipitation of metal oxides
Corrosion inhibitor	0.002	n,n-dimethyl formamide	Prevents pipe corrosion
Biocide	0.001	Glutaraldehyde	Prevents bacterial growth

1.4.1 Friction Reducer

In horizontal wells, lateral extensions can reach thousands of feet. For example, a paper published on horizontal wells drilled in the United States reported laterals as long as 9000 ft. as early as 2004.[28] Due to the length of the lateral, a significant amount of pump energy is lost especially while trying to transport a viscous fluid. To alleviate some of this friction loss a high molecular weight, vinyl polymer such as polyacrylamide is added in low concentration as a friction reducer in place of conventional crosslinked polymer. The high molecular weight of the polymer creates the shear thinning effect through polymer-polymer interaction. The two main interactions are hydrogen bonding and polymer entanglement. At low shear rates the polymer interaction

creates a viscous fluid, but when shear is applied hydrogen bonds are broken and polymer molecules align creating a thinning effect. This shear thinning effect reduces the overall pump power needed for fluid transport.

High molecular weight polyacrylamide is the most common polymer used in slickwater applications. Due to the high molecular weight, low concentrations of this polymer can significantly increase the viscosity. Polyacrylamide (PAM) is co-polymerized with various monomers to create nonionic, anionic, and cationic forms. Figure 1.4 shows examples of polyacrylamide in the three forms were anionic acrylic acid or cationic monomers such as 3-(methacrylamidopropyl)trimethylammonium chloride (MAP-TAC)[29] is copolymerized with acrylamide monomer. For most applications, the optimum charge density is around 30%.[30]

A case study in the Marcellus shale stated that typical amounts of PAM used was 5 pounds dry polyacrylamide per thousand gallons and is equivalent to about 0.6 g/L.[31] An undesired consequence of using a friction reducer is residual fracture damage.[32] The use of PAM and HPAM for proppant transport and friction reduction can create formation and fracture damage.[33,34] Because of damage created, the polymer must be degraded using breakers to take advantage of the increased surface area provided by the fractures. PAM and HPAM polymers contain C-C backbones and are stable at temperatures as high as 200°C[35] making degradation especially difficult even when exposed to oxidizing breakers. [36,37] A majority of prior research has focused on degradation using harsh oxidative, chemical breakers with little focus on more sustainable and environmentally conscious alternatives. The degradation of polyacrylamide is covered in detail in Section 1.5.

Non-Ionic polyacrylamide from acrylamide monomer

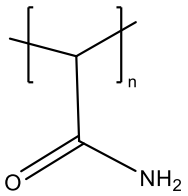

Anioinic polyacrylamide from acrylamide and acetic acid copolymerization. (HPAM)

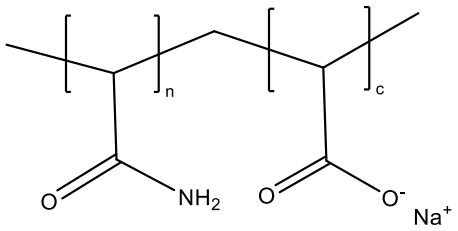

Cationic polyacrylamide from acrylamide and 3- (methacry1amido)propyl)trimethylammonium chloride

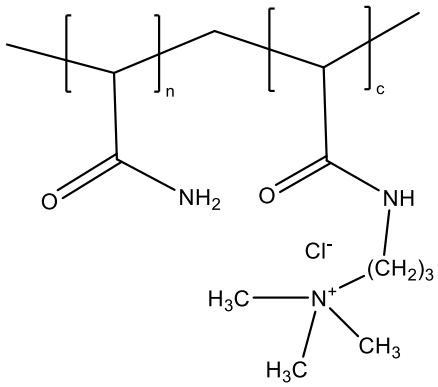

Figure 1.4 Structures of nonionic, anionic, and cationic polyacrylamide. The anionic form is representative of partially hydrolyzed polyacrylamide (HPAM).

1.4.2 Proppants

Proppants are used to "prop" or hold the fracture open after the pumping pressure is released. A majority of proppants consist of silica sand, resin coated sand, and ceramic or a combination of the three.[38] Proppant size and type are selected for the ability to maintain a highly conductive, productive channel for oil and gas production under the specific well conditions and pressure. Table 1.2 lists the sieve size and corresponding grain size distribution for fracturing fluid proppants.[39] In general, the fracture conductivity is determined by the proppant strength and

uniformity with the strongest, most uniform proppant resulting in the highest production yields.[40] The more uniform, crush resistant, and spherical the proppant the better the fracture conductivity but also higher the price (Figure 1.5). On the other hand, sand is the primary proppant used in the United States and accounts for around 90% of wells with total proppant consumption of 4.3 million pounds per well in 2013.[41] The use of sand is driven by the price of proppant due to the large amounts used. Average price per pound of ceramic proppant is \$0.40-\$0.50 and average price of sand is \$0.08-\$0.10.[42] In general the main assumption is that the price difference between silica sand and ceramic proppant is \$0.50 per pound and the difference between resin coated sand and silica sand is \$0.10 per pound higher.[43] Amounts of proppant used can reach 1.0×10^6 pounds per well in the Horn river basin[44] and can vary from 8.0×10^4-1.8×10^5 pounds per stage in the Lower Wolfcamp Shale (west Texas).[45] In the Bakken shale, as many as 48 fracturing stages per well can be found resulting in 7 million pounds of proppant.[43]

One of the cheapest and most commonly used proppants is silica sand. These sands are generally categorized into monocrystalline and multicrystalline sands. White sands such as Ottawa and Jordan sands are stronger because they are made up of single crystal structure.[46] Multicrystalline sands, such as Brandy sand, are composed of multiple crystals and are therefore weaker in nature.[46] The strength of these sands is important because crushing under pressure causes the release of fine particles that ultimately reduce the fracture conductivity and cause the well to "sand off". Ottawa fracturing sand properties were used as a model for creating sand standards by the International Organization for Standards (ISO) and the American Petroleum Institute (API).[47] Ottawa sand contains high silica content (>99%), is monocrystalline, and is highly crush resistant. For these reasons, Ottawa fracturing proppant was used in the immobilization experiments in the current study (explained in the Materials and Methods section).

Table 1.2 Proppant sieve sizes and equivalent grain diameters.[39]

Proppant Size	Grain Diameter (inches)
50/70	0.008-0.012
40/60	0.01-0.017
30/50	0.011-0.023
20/40	0.017-0.033
16/30	0.023-0.047
12/20	0.033-0.066

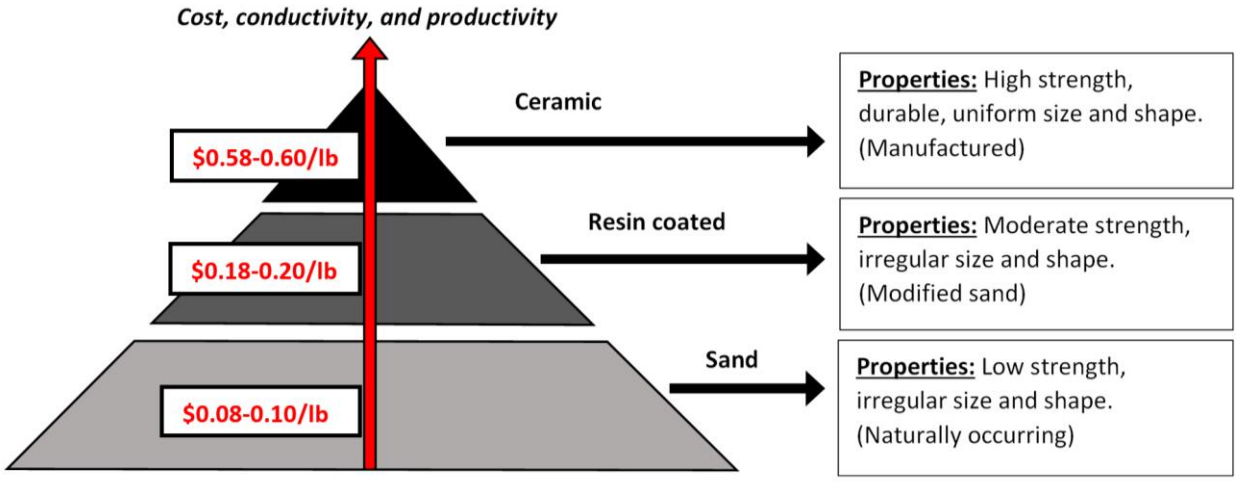

Figure 1.5: Proppant type, property, and trends (Image derived from Gallagher [48]).

One method for increasing the strength and reducing the release of fine particles is to resin coat the sand. The coating can be made from a variety of materials, depending on the requirements, but generally there are two types of resin-coated sand: pre-cured and partially cured or curable

resins.[49,50] Pre-cured resin coating is used to increase strength and durability of the proppant before injection. Partially cured and curable resin coatings have a couple of additional benefits when compared to pretreated proppant. First, these resins have the ability to bond to other sand grains in the fracture, which in turn reduces the overall stress applied to the individual sand grains. This decreases the chances for crushing and the release of fines. Secondly, the bonds created between sand grains reduce the chance for proppant embedment into the fracture face over time.[51] This is extremely important in narrow fractures, such as those seen in unconventional formations, because embedment will reduce fracture width and overall productivity.

Ceramic proppant is made from sintered bauxite, kaolin, or a mixture of both along with additional additives to achieve chemical and physical proppant requirements.[52] Additional benefits to strength and durability of ceramic proppants are the ability to create specialized, low-density proppants.[53] The advantage of low-density ceramic proppants is reduction of proppant settling, sedimentation, and increase saltation to achieve better transport and distribution.[54]

1.4.3 Scale Inhibitors

Scale inhibitors are chemicals added to the fracture fluid to prevent precipitation of solids due to changes in temperature and pressure. During the fracturing process, the injected water can dissolve scale minerals and deposits can form during flow back. The amount of scale that will precipitate is dependent on the water incompatibility, mineral content, pressure, and temperature. These deposits can form in and around the wellbore, coating the casing, valves, clogging perforations, and downhole equipment resulting in equipment failure and decreased production.[55] Some of the most common oilfield scales are calcium carbonate ($CaCO_3$) and sulfate in the form

of gypsum ($CaSO_4$-$2H_2O$), hemihydrate ($CaSO_4$-$1/2H_2O$), anhydrite ($CaSO_4$), barium sulfate ($BaSO_4$), and strontium sulfate ($SrSO_4$) among others.[56]

Removal of scale can be conducted using hydrochloric acid (for carbonate material) or chelating agents (for sulfate based scale).[57] For processes other than hydraulic fracturing, the scale inhibitor is injected in the formation by a process called squeeze treatment where the formation is treated after fracturing.[58] For scale inhibition, as used in hydraulic fracturing, a number of phosphate based molecules and polymers can be used to disrupt crystal growth rates.[57] During fracturing, the scale inhibitor is added to the fracturing fluid to prevent the buildup of scale during the different pressurization and depressurization stages. In both processes, the amount of inhibitor that is retained in the formation is dependent on the formation composition. Some common inhibitors added to fracturing fluids are carboxylic acids, sodium acrylate, sodium polycarbonate, and phosphoric acid salts.[59,60]

1.4.4 Biocides

Biocides are widely used for sterilization, disinfection, and preservation. These chemicals are used in healthcare, food preservation, water treatment, and among many other industries such as oil and gas. Biocides are added to the fracturing fluid to prevent the growth of bacteria in the well, which can cause plugging and ultimately reduce the permeability and productivity. Some notable biocides found in the literature are glutaraldehyde (glut), tetra-kis-hydroxylmethylphosphonium sulfate, dimethyl benzyl ammonium chloride, and dibromonitrilopropionamide.[61] One of the main concerns with biocide use is incompatibility with the friction reducer. A recent study shows that 3,5-dimethyl-1,3,5,-thiadiazinane-2-thione (Thione) does not interfere with friction reducing polymers.[26]

1.4.5 Salts for Clay Control

Shale reservoirs can contain clay material, such as illite, kaolinite, chlorite, and smectite, that are prone to swelling.[30,62] Clay swelling is caused by formation hydration due to ionic interactions and water/brine incompatibility can drastically reduce the productivity of the well.[63] Furthermore, clay incompatibility can cause sediment migration.[64] For these reasons simple salts, such as calcium chloride (NaCl) and potassium chloride (KCl) can be added as a temporary means of reducing the effects of clay swelling. A common brine used in fracturing fluids is 2% KCl because it is less expensive than NaCl and has better temperature stability.[65,66] Economically 2-4% KCl is commonly preferred although but in some shales higher salt concentration has shown to be slightly more effective.[67] Today, the use of produced brine can reduce the cost of adding KCl or other synthetic stabilizers. Some examples of synthetic shale stabilizers include monocationic, oligocationic, and polycationic tertiary amines.[68]

1.4.6 Other Additives

Some other fracturing fluid components are surfactants, corrosion inhibitors, iron control agents (citric acid), pH- adjusting agent (hydrogen chloride). Surfactants are added to increase the viscosity of fracturing fluids and aid in proppant transport through the formation micelles or lamellar structures or vesicles. Some categories of surfactants are viscoelastic surfactant fluids (VES) and foams that form micelles and lamellar or vesicles, alcohol and CO_2 based fluids, liquid CO_2 fluids and foams, and liquefied petroleum gas (LPG).[69] Corrosion inhibitors are used to prevent pipe corrosion when using acids. Some commonly used corrosion inhibitors are n,n-dimethyl formamide, gelatin, and methanol.[70] Additionally, citric acid can be added to the fracturing fluid to control the precipitation of metal oxides. Breakers, such as potassium persulfate,

can be added to oxidize the carbon backbone of the friction-reducing polymer PAM. The degradation of PAM is covered in detail in Section 1.5.

1.4.7 Challenges Associated with Unconventional Fracturing

In addition to the formation damage and chemical component or formation incompatibility issues, the overall volume of water used is means for concern. Because of the volume of fresh water used (>1.0×10^6 gallons), concerns over methods of disposal, cleaning, and reuse arise. Furthermore, many studies have cited that some chemical components used in fracturing fluids are toxic and can be environmentally detrimental as covered in the following discussion.

Due to large volumes of fresh water consumed, fracture fluid flow back cleaning and reuse has become a concern. Currently flow back fluids are disposed of by reinjecting for disposal, reverse osmosis, thermal distillation and crystallization, reuse for fracturing, or discharged into public water treatment facilities.[27] Reinjecting for disposal has its own challenges due to the limited number of disposal wells and formation uptake[71] and resulting seismic activity.[72] Filtering the flow back water using reverse osmosis or thermal distillation and crystallization can be energy intensive and maybe economically unfeasible for fluids containing large total dissolved solids (TDS, > 4.0×10^4 mg/L and 3.0×10^5 mg/L respectively).[27] Some examples of water cleaning can be found in the literature and use a variety of the mentioned methods in addition to biological processes for removal of dissolved organic matter.[73] Disposal into treatment facilities is not a sustainable option due to regulatory restrictions on received and expelled TDS.[74]

Overall, the toxicity of fracturing fluid components are of concern due to environmental and health implications. Biocides used in fracturing fluids are of main concern with many causing toxicity in lab animals, or are known carcinogens, with the exception of glutaraldehyde N-bromo,

and peracetic acid.[61] A study conducted by Stringfellow *et al.*[75] outlined the environmental and health implications of many fracturing fluid components. In this study, it was found that corrosion inhibitors are both toxic and carcinogenic. Inorganic oxidants used for breakers are considered to have low environmental impact but do carry considerable risk during transportation and industrial use and some are listed as level 4 toxins under the Globally Harmonized System (GHS). Overall 81 fracturing fluid chemicals were examined with some being GHS level 1 and 2 inhalation toxins, three level 2 oral toxins, and at least 5 confirmed of suspected carcinogens.

1.5 Degradation of Polyacrylamide

Polyacrylamide (PAM) can be a dry powder, suspended in solution, or gelled (crosslinked) and can undergo degradation under a variety of conditions and states. In aqueous solutions PAM can undergo degradation via mechanical (shear),[76] thermal,[77] chemical, biological, photocatalytic,[78] and radiative (sonication)[79] means. As previously stated, high molecular weight polyacrylamide is used as a friction reducer in unconventional, water-based fracturing fluid. Although a low concentration of PAM is used the large volume of fluid can cause significant formation damage. Due to the damage created, free radical induced degradation of PAM is conducted using chemical breakers. For the purpose of this section, uncrosslinked, aqueous polyacrylamide is discussed and the degradation mechanisms are restricted to biological and free radical degradation by chemically catalyzed means. The following section outlines the damage created in porous media, degradation mechanism, past chemical and biological degradation research, and governing kinetic equations.

1.5.1 Polyacrylamide Damage in Porous Media

A majority of literature showing damage in consolidated core samples is conducted for drilling, polymer, and chemical flooding purposes. Although these reservoirs are higher permeability (k,

millidarcy (md) to Darcy), damage is still created in the form of adsorption. In polymer flooding, polyacrylamide is utilized as a water thickener that reduces the mobility ratio and enhances overall sweep efficiency in the reservoir. Increased sweep efficiency takes place by polymer adsorption, which reduces the flow through highly swept areas and diverts the flow to poorly swept areas. In these studies, the reduction in permeability is often expressed as the residual resistance factor (RRF) and describes the reduction in pressure after polymer flood over the pressure before the polymer flood at a constant flowrate (Equation 1).[80] In hydraulic fracturing of low permeability unconventional reservoirs, adsorption still plays a significant role but additional damage is created on the fracture face though fluid loss.[34] The mechanism of fluid leak off, or fluid loss, creates an increased concentration of polymer on the fracture face by filtering the fluid as it moves into the rock matrix. The literature below outlines examples of both mechanisms but restricts the discussion to uncrosslinked PAM and HPAM polymer.

Formation damage using polyacrylamides was noted as early as 1977 in acid fracturing applications.[81] This study showed nonionic and anionic PAM displayed poor stability, undergoing hydrolysis in the presence of hydrochloric acid and well simulated temperatures. On the other hand, cationic forms showed a greater resistance to hydrochloric acid. A study conducted using Botucatu sandstone, brine permeability (K_w=60.5-140.4 md), flooded the core with 6 pore volumes 2000 parts per million (ppm) non-hydrolyzed, polyacrylamide (molecular weight=$7.6x10^6$ Da). The RRF, described by Equation 1, was 5 and the adsorbed layer thickness was 0.84μm. PAM friction reducer has been shown to cause considerable damage in Bossier Shale when 5-8 pore volumes (1 part per thousand gallons, pptg) of friction reducer was injected and allowed to set for 2 hours.[32] In this study ammonium persulfate breaker (1 pptg) breaker showed 56% permeability recovery at a temperature of 150°F.[32] Cationic, nonionic, and anionic PAM (15-20 million

molecular weight) was studied for the adsorption at the pore level.[82] The authors concluded that greater polymer volumes injected created thicker polymer layers. Furthermore, thicker polymer layers resulted in reduced hydraulic conductivity. The use of PAM and HPAM for proppant transport and friction reduction can create formation and fracture damage.[33,34] Fracture conductivity tests have shown that polyacrylamide does reduce fracture conductivity at higher fracture stress (5000 psi) using sand proppant and residual damage remained after treatment with a commercial oxidizing breaker at 200°F for 24 hours.[34]

$$RRF = \frac{\Delta P_{w\,(after\ polymer)}}{\Delta P_{w\,(before\ polymer)}} \qquad 1$$

1.5.2 Mechanism of Polyacrylamide Free Radical Degradation

These mechanisms are all oxidative processes that create free radicals and degrade the polymer. As previously mentioned, PAM is considered extremely stable compared to other polymers but it has been shown to degrade with time.[83] Much of the degradation due to aging can be attributed to photo degradation but this process can take a very long time under normal conditions. Degradation mechanisms that are more thoroughly studied include mechanical, thermal, and chemical degradation. These are important degradation mechanisms because they catalyze the breakdown of PAM and can create favorable or unfavorable conditions depending on the application. Furthermore, biological degradation has shown to be an important mechanism for the catalyzed breakdown of PAM and is extremely important in environmental applications. Free radicals can degrade the polymer chain at the points illustrated in Figure 1.6.[84,85] Assuming simultaneous

radical generation of low molecular weight compounds, reactivity ratios of the three sites have been shown: (1):(2):(3)=1:2:8.[84]

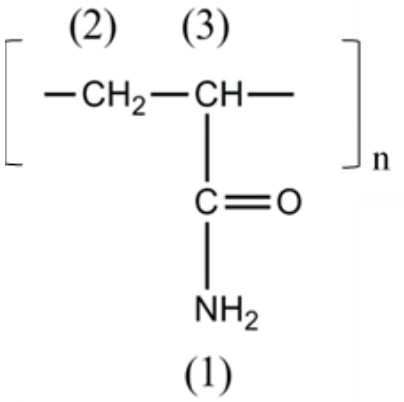

Figure 1.6 PAM repeating unit and the sites vulnerable to free radical attack.

After free radicals are introduced, PAM can undergo a variety of mechanisms. Figure 1.7 depicts the theoretical mechanism responsible for C-C backbone cleavage.[86] In this mechanism it is assumed that the radical initiates the reaction by attacking site 3 (Figure 1.6) where the R groups on the PAM chain can represent partially hydrolyzed polyacrylamide (HPAM) as well as the unhydrolyzed side groups (Figure 1.7A). Furthermore, the radical may undergo chain transfer and chain propagation in addition to the termination mechanisms shown. Chain transfer would not result in chain propagation or degradation but would simply act as a conduit for radical movement. Termination can take place via two scenarios. The first consists of two radical containing chains coming together to quench the reaction (Figure 1.7B). When two radical containing chains come together, either recombination or disproportionation can occur. The preferred termination mechanism is disproportionation and guarantees molecular weight reduction. The second involves the addition of the oxidized polymer chain and the radical carrier (Figure 1.7c). The steps, and kinetics, of radical transfer are covered in detail in Section 1.5.5.

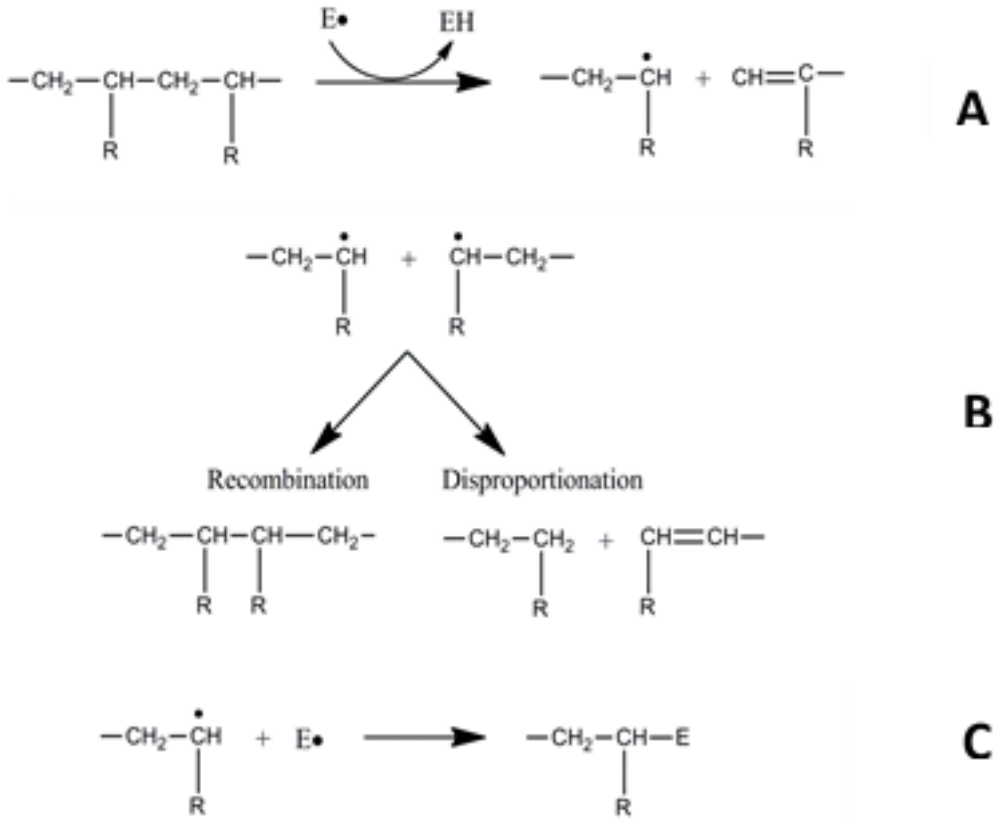

Figure 1.7 Depicts mechanisms during free radical attack. **A**: PAM backbone cleavage by free radical attack. **B**: Termination mechanism through radical containing polymer-polymer interaction. **C**: Termination mechanism by polymer-radical carrier.

1.5.3 Chemically Induced Degradation of Polyacrylamide

Degradation of PAM can take place via changes in the polymer side chain (hydrolysis) or by backbone cleavage with the latter being more difficult. Hofmann degradation can be performed on PAM side chains using a slight excess of hydrochloric acid.[87] The hydrolysis of PAM can be conducted under elevated temperature and alkaline conditions using a variety of additives.[88-91] Hydrolysis of PAM under alkaline conditions is very slow resulting in 60-70% hydrolysis in 30 days at 35°C in the presence of 1% sodium carbonate.[88] In addition, the same study showed both PAM and HPAM undergo hydrolysis with a very fast initial stage followed by a slower later stage.

The degree of hydrolysis was shown to be a function of pH and temperature with the less hydrolysis observed at lower pH and temperatures. The hydrolysis of PAM resulted in a viscosity increase of about 40 centipoise. Furthermore, hydrolysis has shown to increase intrinsic viscosity and would create the opposite effect needed to recover fracture conductivity and rock matrix permeability.[92] In order to significantly reduce the viscosity and molecular weight, carbon backbone cleavage must occur which can be achieved through the production of free radicals.

Chemical oxidizers, such as Fenton reagents and persulfates can cleave the C-C backbone of PAM by free radical attack. Ramsden *et al.*[93,94] conducted two studies showing carbon backbone cleavage of PAM in the presence of Fenton reagent and Fe^{2+}. This study showed reduced molecular weight of 5% wt. PAM (5.2×10^6 molecular weight, hydrolysis < 3%) to 2.4×10^6, 0.97×10^6, 0.56×10^6, 0.22×10^6 in the presence of 1, 10, 20, and 50 ppm Fenton reagent at 20°C.[94] In an additional study, 1% PAM was degraded at 20°C in the presence of unchelated and chelated Fe^{2+} using a variety of chelating agents.[93] The results showed that unchelated Fe^{2+} produced the greatest reduction in viscosity at pH= 6 with little to no reduction observed from pH=1 to pH=3 and at pH= 8. Furthermore, viscosities were tested over a 6 day period with the greatest reductions of buffered (about 53%) and unbuffered (about 35%) observed on the sixth day. In addition to Fe^{2+} PAM was degraded in the presence of Fe(III) catalyst in aqueous solution.[95] Results showed that $Fe(NO_3)_3$ was a better catalyst than $FeSO_4$. Overall Fe_2O_3/Al_2O_3 catalysts that contained trace amounts of Cu resulted in the highest catalytic activity (about 94% molecular weight reduction in 90 minutes) when the reaction was run at 60°C. In a more general study, degradation of six cationic and anionic PAMs were tested under a variety of oxidation processes.[96] Results revealed that cationic samples were less susceptible to photochemical oxidation when compared to anionic samples. Fenton agent showed slow and ineffective oxidation of most samples when the reaction was conducted at 25°C.

On the other hand, photochemical processes showed very effective oxidation of both anionic and cationic PAMs. Furthermore, PAM exposure to potassium ferrate (VI) showed similar results as Fenton reagent. A hybrid photo-Fenton experiment showed efficient removal of PAM (5 x10^6 M_w, 30% hydrolysis).[97] Fe(III)-SiO_2 catalyst was created using $Fe(NO_3)_3$ and $FeSO_4$ precursor. The study concluded that the catalyst derived from the $FeSO_4$ precursor was more effective resulting in 94% degradation of PAM in 90 minutes and 70% total organic carbon (TOC) removal in 180 minutes. This was done with an initial pH of 6.8 and 100 mg/L PAM concentration.

Potassium persulfate is the most widely used oxidizing breakers in oilfield fracturing applications.[98] Persulfate oxidizers are highly temperature and concentration dependent. Gao. *et al.*[99,100] showed the viscosity and molecular weight reduction of PAM (initial molecular weights 12.0×10^6 and 15.0×10^6 Da) in the presence of persulfates with potassium persulfate being most effective and no change in the presence of hydrogen peroxide alone. Furthermore, these studies showed a greater degree of degradation with increasing molecular weight, persulfate concentration, and temperature. More specifically, the reduction in apparent viscosity of HPAM friction reducer was demonstrated using persulfate oxidizers in both fresh water and brine based solutions above 100°C.[101] In this study, HPAM was degraded using persulfates, organic peroxides, inorganic peroxides, and other oxidizers at elevated temperatures (100-180°F). Results showed that all breaker groups reduced the viscosity of HPAM at 180°F. Persulfates were shown to be very effective at this temperature even at low concentrations. Furthermore, persulfate oxidizers performed better than the organic and inorganic peroxides. Increase in breaker concentration reduced the time of viscosity reduction. Only one persulfate (called A1) was an effective breaker at 120°F and low concentration but was also effective at 100°F and higher concentrations of 5 and 10 ppt. The degree of degradation has been shown dependent upon oxygen concentration with no

degradation in the absence of oxygen.[102] Potassium persulfate has also been shown to recover permeability loss from PAM in Ohio sandstone at 150°F.[103]

A very thorough study conducted by Yang and Treiber [102] tested the degradation of PAM under different reservoir conditions and over many days (5-500 days). The study concluded that oxidative degradation of PAM stops when oxygen is completely consumed in the presence of limited oxygen. The rate and degree of viscosity loss is initially attributed to the amount of oxygen in solution and then the reservoir temperature. Furthermore, the rate and degree of degradation is increased in the presence of metal ions, hydrogen sulfide, among other redox reactions. Metal ions do not reduce the viscosity of solutions in the absence of oxygen. For pH>7 little viscosity loss is seen with limited oxygen at temperatures below 100°F. At temperatures greater than 140°F, degradation is prevalent in the presence of oxygen (in brine) but can be limited with addition of oxygen scavengers. Under acidic conditions, metal ions accelerate oxidative degradation. Methanol and thiourea act as effective antioxidants for long-term solution exposure to oxygen. At elevated temperatures, an increase in rate and magnitude of viscosity was observed due to polymer hydrolysis. The rate of viscosity increase was greater in brine solutions of higher ionic strength but resulted in lesser magnitude of viscosity increase. In an oxygen-free environment, the increase in viscosity of polymer solutions was 2-3 time higher in freshly prepared brines and elevated temperatures. The viscosity of the solution was not affected by the presence of glutaraldehyde, ethoxylated sulfated alcohol, or ferrous sulfide in the absence of oxygen.

1.5.4 Biological Degradation of Polyacrylamide

Biologically, PAM and HPAM has also been shown to be susceptible to microbial degradation by several bacterial strains but with very low efficiency. Seven PAM degrading oil field bacteria

were isolated from wastewater with four of the bacteria associated with Actinobacteria, two with Alphaproteobacteria, and one with Bacillus.[104] Wen *et al.*[105] reported two bacteria, identified as *Bacillus cereus* and *Bacillus flexu*, which can slowly utilize PAM as the sole carbon source. These bacteria were isolated from oilfield wastewater and could utilize PAM as the sole carbon source. *Bacillus cereus* and *Bacillus flexu* utilized PAM at different rates but were shown to consume 70% of PAM within about 70-90 hours. In a similar study, *Bacillus cereus* was used to remove PAM in a contact oxidation reactor (COR) and a sequencing batch reactor (SBR).[106] Results of the COR study showed 70% removal of PAM after 7 days and remained the same after 45 days after a single inoculation. Also, SBR showed 70% removal after the first operation cycle and remained relatively the same following 8 cycles after a single inoculation.

Bacteria isolated from oilfield polymer flooding showed the ability to utilize HPAM as both nitrogen and carbon source.[107] In addition, the amide group on the side chain of HPAM could serve as a nitrogen source and that the carbon backbone was partially utilized as a carbon source. HPAM removal efficiency was relatively low with the highest (about 37%) observed for experiments where HPAM was used as the sole carbon and nitrogen source. *Enterobacter agglomerans* and *Azomonas macrocytogenes* were isolated from soil samples located at Hokkaido University.[108] Both strains were shown to utilize PAM as sole carbon and nitrogen source. Over 27 hours cultivation, the molecular weight of PAM was reduced from 2.0×10^6 to 0.5×10^6 Da with consumption of about 20% total organic carbon (TOC). Although these bacteria have the potential for bioremediation of PAM and HPAM in aerobic (surface) conditions, the same would not be true in an anaerobic reservoir.

Enzymatically, only a few studies exist for the degradation of PAM. Asparaginase enzyme has been patented as a means of hydrolyzing PAM but there is no evidence that it can create carbon

backbone cleavage.[109] One study showed that degradation of PAM could be catalyzed by superoxide radical formation through reduction of dissolved oxygen (Harder-Weiss reaction) during the xanthine oxidase catalyzed oxidation of xanthine.[110] A microbial study conducted by Nakamiya *et al.*[111] led to the isolation of a hydroquinone peroxidase enzyme, from *Azobacter beijerinckii*, that was shown to facilitate the degradation of PAM, poly(acrylic acid) (PAA), polyethylene glycol (PEG), and polyvinyl acetate (PVA). Degradation of 1g/L, 2.0×10^6 molecular weight PAM was achieved at 30°C using hydroquinone peroxidase in the presence of peroxide and tetramethylhydroquinone and peroxide. These peroxidase enzymes require cofactors for polymer degradation, thus three reagents in all: enzyme, H_2O_2, and cofactor. Although few enzymes have been shown to degrade PAM, all are more exotic than horseradish and soybean peroxidases and therefore may be more expensive to produce for industrial applications.

1.5.5 Degradation and Kinetics for Random Chain Scission

The rate of degradation induced by free radicals is a function of a variety of radical transfer events and experimental conditions. The rate of the radical mechanisms dictate the overall rate of polymer degradation. The random degradation kinetics of long chain polymer molecules was first studied in the early 1930's and 1940's.[112-114] The random backbone cleavage of polymers can be achieved using a variety of catalysts (such as radical generation and acid hydrolysis) but is dependent upon the backbone chemical makeup. For example, as previously mentioned vinyl polymers are relatively stable and backbone cleavage can only be achieved with exposure to free radicals. In addition, carbohydrate polymers such as Guar are susceptible to degradation via the glycosidic bonds using acid hydrolysis and direct enzymatic cleavage. The following section

describes the kinetic relationships for the random chain scission of high molecular weight polymers.

One of the earliest and most widely used kinetic equations is shown in Equation 2 and describes the first order, continuous kinetics of random cleavage.[115] In this equation, the inverse difference in the initial molecular weight (M_0) and molecular weight at any time (M_t) can be plotted versus time (t) and the linear slope is a function of the first order rate constant (k, s^{-1}) divided by the monomer molecular weight (m). Although the equation is a good general description of simple random polymer cleavage, many variations of the expression have been developed to fit specific studies.

$$\frac{1}{M_t} - \frac{1}{M_o} = \left(\frac{k}{m}\right) t \qquad 2$$

A study conducted on the acid hydrolysis of dextran by Basedow *et al.*[116] scaled the general kinetic equation (Equation 2) to fit the produced data. Equation 3 shows the differential equation used where (a) is the scaling constant and *(m)* is the monomer molecular weight. This relationship was derived by setting the rate proportional to the number of polymer bonds. Equation 4 is the integrated version where an a =2/3. The linearized data and the derived correlation was used to find the initial molecular weight (M_{no}, intercept) and rate constant (k) from the slope. As an example, the data from the study is plotted in Figure 1.8 and depicts the molecular weight relationships before scaling (according to Equation 2) and after scaling.

$$\left(-\frac{1}{M_n}\right)\left(\frac{dM_n}{dt}\right) = k\left(\frac{M_n}{m}\right)^a \quad (3)$$

$$\frac{1}{{M_{nt}}^{2/3}} = \frac{1}{{M_{no}}^{2/3}} + \frac{2}{3}\left(\frac{k}{m^{\frac{2}{3}}}\right)t \quad (4)$$

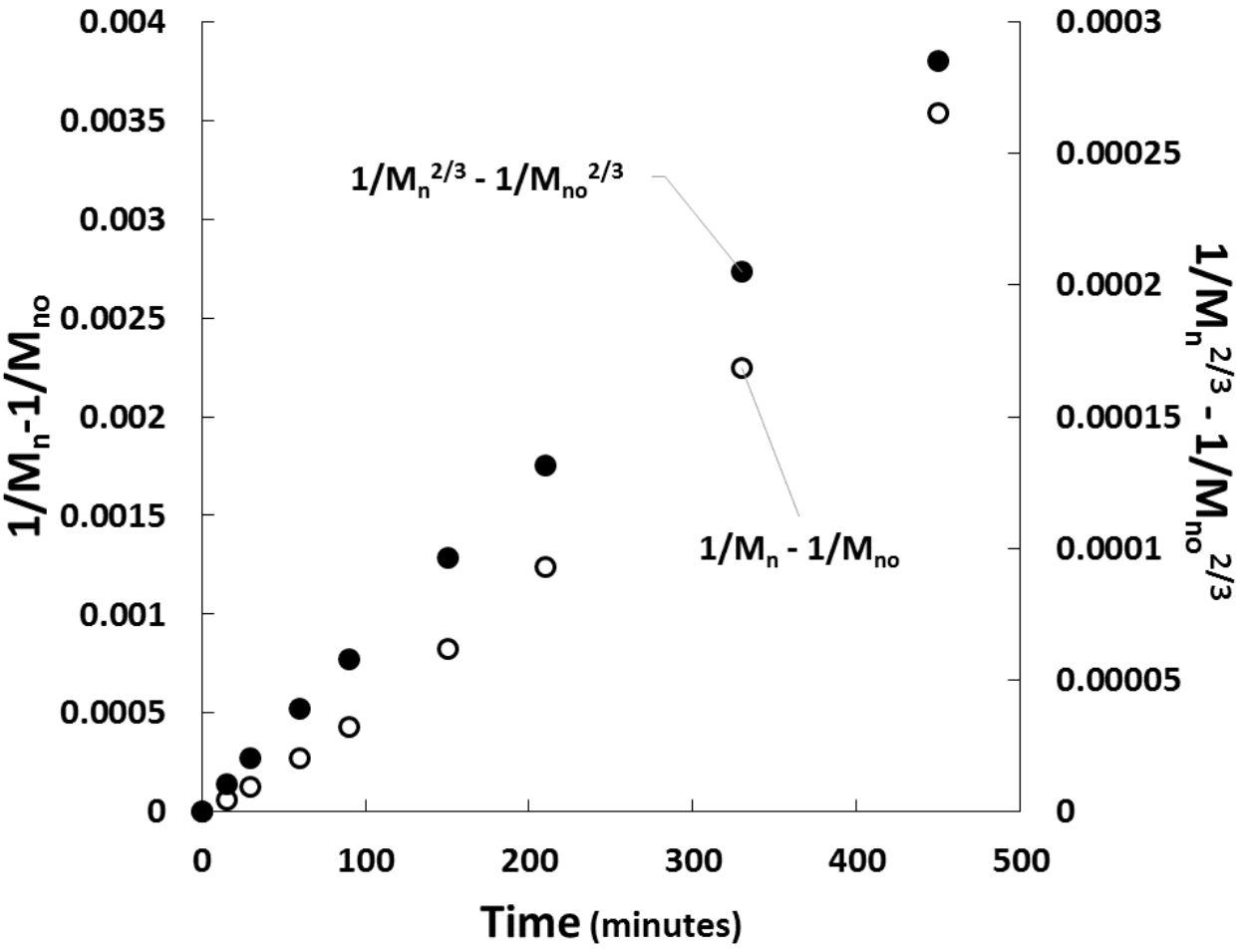

Figure 1.8 Figure showing the linearization of data presented by Basedow *et al.*[116] when applying Equation 4. Data linearized when a=2/3.

In addition to slightly curved data, some polymer degradation studies can exhibit two kinetically distinct regions. As previously stated, the general conception is that random polymer

backbone cleavage is representative of first order kinetics. By assuming a random molecular weight distribution and that the molecular weight of the polymer is much greater than the monomer, the kinetics can be expressed by Equation 5 for any order (n).[117-119] Using this expression, m is the monomer molecular weight and N_0 is the total number of molecules. This study demonstrated that previously reported data from literature displayed initial zero order kinetics to time *t'* followed by first order kinetics up to time *t*. An example of the simplified zeroth and first order expressions are shown in Equations 6 and 7 and data fitting the expressions would fit the general trend depicted in Figure 1.9. Similar qualitative results have been reported in a large number of polymer degradation studies for random chain hydrolysis of polymers using chemical and enzymatic reagents and catalysts. For example, the hydrolysis of alginate,[120] cellulose linters,[121] carrageenan,[115] and glucomannan[118] with chemical reagents or enzymes results in two distinct kinetic regions.

$$\left[\left(1-\frac{m}{M_{nt}}\right)^{1-n}-\left(1-\frac{m}{M_{n'}}\right)^{1-n}\right]=\left(\frac{k(n-1)}{{N_0}^{1-n}}\right)(t) \qquad 5$$

$$\frac{1}{M_{n'}}-\frac{1}{M_{no}}=\left(\frac{k}{mN_0}\right)t' \qquad 6$$

$$\frac{1}{M_{nt}}-\frac{1}{M_{n'}}=\left(\frac{k_1}{m}\right)(t-t') \qquad 7$$

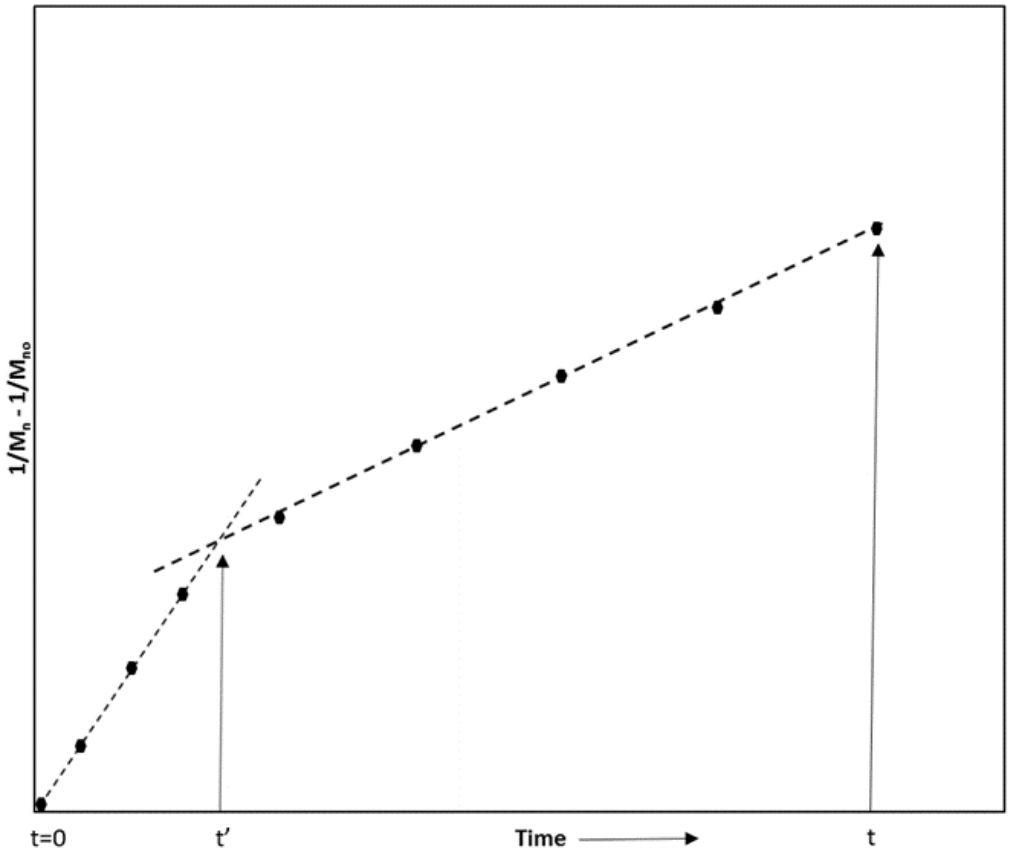

Figure 1.9 Generic example of two kinetically distinct regions observed from plotting $1/M-1/M_o$ versus time. Bottom (x-axis) shows representative times for application of Equations 6 and 7.

Data is presented in Section 3.4 describing the degradation of HPAM using radicals generated from the decomposition of hydrogen peroxide. In this process, the breakdown of peroxide creates two free radicals that are able to attack the carbon backbone of HPAM. Although peroxides and persulfates should exhibit similar chemistries, it is later shown that this kinetic relationship differs in the presence of peroxidase enzyme. Although this is the case, the following study is mentioned as reference. Shukla *et al.*,[122] derived the kinetic relationship for the oxidative (radical) degradation of poly (acrylic acid) using potassium persulfate. In the derivation, represented by Equation 8, it was assumed that the initiator (potassium persulfate) created two radical species that can degrade

the vinyl polymer. Therefore, the degree of degradation is a function of the initial persulfate concentration (C_{2i}) and time squared (t^2).

$$\frac{1}{M_n} - \frac{1}{M_{no}} = C_{2i} k t^2 \qquad 8$$

In addition to the continuous kinetics mentioned above, expressions using the final molecular weight have been established. Madras and Chattopadhyay[123] studied the degradation of polyvinyl acetate in the presence of benzyl peroxide. In this expression, the initial peroxide concentration (C_{po}) is plotted versus $1/M_n$ -$1/M_{no}$ as seen in Equation 9. In this study, the initial drop in molecular weight was fast and after a period showed little change with time. This relationship uses the "endpoint" molecular weight to determine the kinetics after the reaction was completed.

$$\frac{1}{M_{nf}} - \frac{1}{M_{no}} = k C_{po} \qquad 9$$

1.6 Horseradish Peroxidase

Peroxidase enzymes can be found in many plant, animal, and microorganism tissues and are present to catalyze the general reaction shown in Reaction 10. In the reaction, peroxidase enzyme is responsible for catalyzing the oxidation of hydrogen peroxide in the presence of a reductant. The enzymatic cycle, mechanism, and kinetics are described later in Section 1.6.3. The oxidation reaction, shown below, was first observed in the early 1800's but the peroxidase enzyme was not specifically named until nearly a century later. We now know that a variety of peroxidase enzymes exist that can be separated in superfamilies, families, and classes that contain numerous sequences

and isoenzymes. These isoenzymes have similar structure and function but vary in molecular weights, activities, and isoelectric points.

$$H_2O_2 + 2AH_2 \rightarrow 2H_2O + 2AH\bullet \qquad 10$$

Horseradish peroxidase (HRP) is one of the most studied plant peroxidases and has been used as a model peroxidase for research, industrial, biomedical, and bioremediation applications. In nature, this catalyst is responsible for a variety of roles such as crosslinking of cell wall polymers,[124] lignification,[125] indole-3-acetic acid metabolism,[126] and a defense mechanism for infections.[127] The purpose of this section is to describe the background knowledge pertaining to peroxidase, and more specially horseradish peroxidase enzymes with emphasis on remediation processes.

1.6.1 Peroxidase Discovery

Peroxidase enzymes are found in a variety of sources including some animal tissues and most plant cells. The evolution of peroxidase discovery started in the early 1800's by investigation the enzymatic oxidation of guatiac tincture. A dissertation written by Ernest Clark in 1910 outlines the studies of plant oxidase and more specifically the existence of peroxidase enzymes.[128] At this time, it was stated that peroxidase and oxidase enzymes could not be separately distinguished by distribution and properties, therefore were considered together. The first to find peroxidase was Schönbein, but no significance was recognized because guaiac tincture could not be oxidized in the absence of peroxide. During Schönbein's studies, it was thought that all enzymes had the ability to catalyze the decomposition of hydrogen peroxide, and therefore it was not unusual for enzymes

not to display activity until peroxide addition.[129] A study conducted by Jacobson in 1892, showed that heating diastase (to 60°C) did affect the ability to breakdown hydrogen peroxide but did not affect the enzymes diastatic ability.[130] This finding prompted a study conducted by Loew, which concluded the decomposition of hydrogen peroxide and the direct oxidation of substances (such as guaiac tincture) were catalyzed by different enzymes.[131] A study conducted by Bourquelot showed that the enzymes responsible for indirect oxidation (requiring peroxide) of guaiacum were more resistant to heat than direct oxidizing enzymes.[132] In 1898, Linossier showed that hydrogen peroxide was required for in leukocyte oxidation reactions and was the first to suggest the name "peroxidase".[133] Pure, crystalline peroxidase was first obtained from horseradish and milk (lactoperoxidase) in 1943 by Nobel Prize winner Hugo Theorell.[134] Since HRP isolation, studies regarding the enzyme started to escalate in the mid 1960's, peaked in 1985 with around 1000 publications for the year, and remains around 400 publications per year today.[135] Furthermore, horseradish peroxidase (HRP) remains a model for most studies allowing for a more complete understanding of the enzyme structures and reaction mechanism.

1.6.2 Peroxidase Structure and Classifications

Peroxidase enzymes were once separated into three superfamilies and were classified by evolutionary origin and similarities in structure. These superfamilies consisted of prokaryotic (Class I), fungal (Class II), and classical sensory plant peroxidases (Class III).[136] Today, peroxidase enzymes are more easily separated into superfamilies consisting of heme-containing and non-heme peroxidases. Under this classification, peroxidase enzymes have 5 non-heme and 6 heme-containing superfamilies.[137] As seen in Table 1.3 the heme containing and non-heme containing peroxidase superfamilies are shown and separated into families, classes, and subclasses. Table 1.3 also shows groups of peroxidase enzymes, the number of sequences within the group, and the

distribution within the major kingdoms.[138] For each of these groups, specific sources, and/or sequences can be identified. Peroxidase enzymes isolated from plants, such as horseradish and soybean, are classified as Class III heme-containing peroxidase and make up a majority of this superfamiliy.

For each source, such as horseradish, numerous isoenzymes can be identified. Isoenzymes are very similar in structure and function but can vary in molecular weight, isoelectric point (pI), and enzymatic activity. Table 1.4 lists the 19 known isoenzymes isolated from HRP. Furthermore, the table lists the differences in molecular weight, isoelectric point, and corresponding GenBank reference number.[139] The isoenzymes show isoelectric points ranging from 4.84 to 9.30, molecular weighs that range from 31.3 to 35.9 kDa, and 2-9 N-glycosylation sites. HRP extraction from horseradish roots have shown to contain varying amounts of these isoenzymes with the specific content being influenced by environmental factors.[140]

The enzyme structure and amino acid sequence of plant peroxidase isoenzymes C1A and cytochrome c peroxidase was first characterized in the late 1970's.[141-143] The characterization of HRP isoenzyme C1A showed that it was composed of 308 amino acid residues with an average molecular weight of 40,000 Da. HRP also contains four disulfide bridges, one buried salt bridge, and two buried calcium-binding sites which are all characteristic of heme-containing peroxidases and essential for the structure and function of the enzyme. The full enzyme structure is illustrated in Figure 1.10 and a detailed illustration of the heme group (active site) is shown in Figure 1.11. In Figure 1.10, the active site is colored by molecule type and calcium bridges are represented with black dots.[144] Furthermore, HRP C1A contains nine potential N-glycosylation sites that have been defined by N-X-S/T motif where X is any amino acid (except proline). Of the nine N-glycosylation sites, eight are shown to contain neutral carbohydrate side chains and the ninth Asn316 site is

unoccupied. The heme-containing active site is ferriprotoporphyrin IX prosthetic and is shown in Figure 1.11. At the active site, the His170 forms a bond to the iron (Fe) atom and acts as the primary bond between the heme group and enzyme. The two calcium atoms located within HRP have been shown to contribute to the overall activity.

Table 1.3 Superfamilies, families, and groups of peroxidase enzymes as sorted by PeroxiBase with respect to distribution within the major kingdoms.[145] *** Shows horizontal gene transfer resulting in marginal sequence detection.[138]

	Prokaryotes	Plants	Fungi	Animals	Other eukaryotes	Total Sequences
Heme Peroxidase						
Catalase (Kat)	X	X	X	X	X	22
Dyp-type peroxidase	X					6
Di-Heme cytochrome c peroxidase (DiHCcP)	X					5
Haloperoxidase (HalPrx)			X		X	49
Non-animal peroxidase						
Class I peroxidase						
- Ascorbate peroxidase (APx)		X		***		352
- Catalase peroxidase (CP)	X	***	***		***	299
- Cytochrome c peroxidase (CcP)			X		X	94
- Hybrid ascorbate cytochrome c perox (APx-CcP)					X	4
Class II peroxidase						
- Lignin peroxidase (LiP)			X			26
- Manganese peroxidase (MnP)			X			69
- Versatile peroxidase (VP)			X			14
- Other Class II peroxidase (CII)			X			10
Class III peroxidase		X				2625
Other non animal peroxidase (NAnPrx)		X		X		5
Animal perox/perox-cycloxygenase superfamily						
Prostaglandin H synthase/cyclooxygenase (PGHS)	X		X	X		59
Linoleate diol synthase, PGHS-like (LDS)			X			2
Alpha dioxygenase (aDox)		X				7
Dual oxidase (DuOx)				X		15
Peroxidasins (Pxd)				X		29
Peroxinectins (Pxt)	X			X	X	61
Non-mammalian vertebrate peroxidase (AnPOX)				X		2
Thyroid peroxidase (TPO)				X		9
Myelo-peroxidase (MPO)				X		12
Lacto-peroxidase (LPO)				X		10
Eosinophil peroxidase (EPO)				X		6
Non-heme Peroxidase						
Manganese catalase (MnCat)	X					5
NADH peroxidase (NadPrx)	X					2
Thiol peroxidase						
Glutathione peroxidase (GPx)	X	X	X	X	X	196
Peroxiredoxin						
- 1-Cysteine peroxiredoxin (1CysPrx)	X	X	X	X	X	95
- Typical 2-cysteine peroxiredoxin (2CysPrx/AhpC)	X	X	X	X	X	191
- Atypical 2-cysteine peroxiredoxin (Prx II,Prx X,PrxGrx)	X	X	X	X	X	105
- Atypical 2-cysteine peroxiredoxin (PrxQ,BCP)	X	X	X		X	95
Haloperoxidases						
No heme, no metal haloperoxidase (HalNPrx)	X					6
No heme, Vanadium haloperoxidase (HalVPrx)	X				X	5
Alkylhydroperoxidase D-like superfamily						
Alkylhydroperoxidase D (AhpD)	X					68
Carboxymuconolactone decarboxylase, perox activity (CMD)	X					42
Carboxymuconolactone decarboxylase, no perox activity (CMDn)	X		X			23
Hydrolase-CMD fusion, peroxidase activity (HCMD)						0
Hydrolase-CMD fusion, no peroxidase activity (HCMDn)	X		X			22
Double CMD, peroxidase activity (DCMD)	X					3
Double CMD, no peroxidase activity (DCMDn)	X					21
Other Alkylhydroperoxidase, peroxidase activity (AlkyPrx)	X					0
Other Alkylhydroperoxidase, no peroxidase activity (AlkyPrxn)	X					10

Table 1.4 List of HRP isoenzymes with the corresponding isoelectric points (pI), molecular weight (MW), potential N-glycosylation sites, and GenBank reference number.[139]

Isoenzymes	pl	MW (kDa)	N-X-S/T	GeneBank
C1A	5.41	35.82	9	HE963800.1
25148.1 (C1C)	6.13	35.86	7	HE963802.1
25148.2 (C1D)	6.50	35.89	7	HE963803.1
04627 (C2)	8.38	35.67	4	HE963804.1
C3	7.05	35.48	3	HE963805.1
A2A	4.84	32.09	9	HE963806.1
A2B	4.84	32.12	9	HE963807.1
E5	8.99	33.92	3	HE963808.1
1805	5.75	35.96	5	HE963809.1
22684.1	6.39	35.06	4	HE963810.1
22684.2	6.00	35.15	4	HE963811.1
1350	8.47	31.42	3	HE963812.1
5508	8.22	31.35	3	HE963815.1
6351	5.99	32.89	2	HE963816.1
22489.1	8.24	31.37	2	HE963818.1
22489.2	8.24	31.39	2	HE963819.1
17517.2	9.30	32.69	4	HE963823.1
08562.4	8.91	33.26	3	HE963825.1
08562.1	8.89	33.81	3	HE963824.1

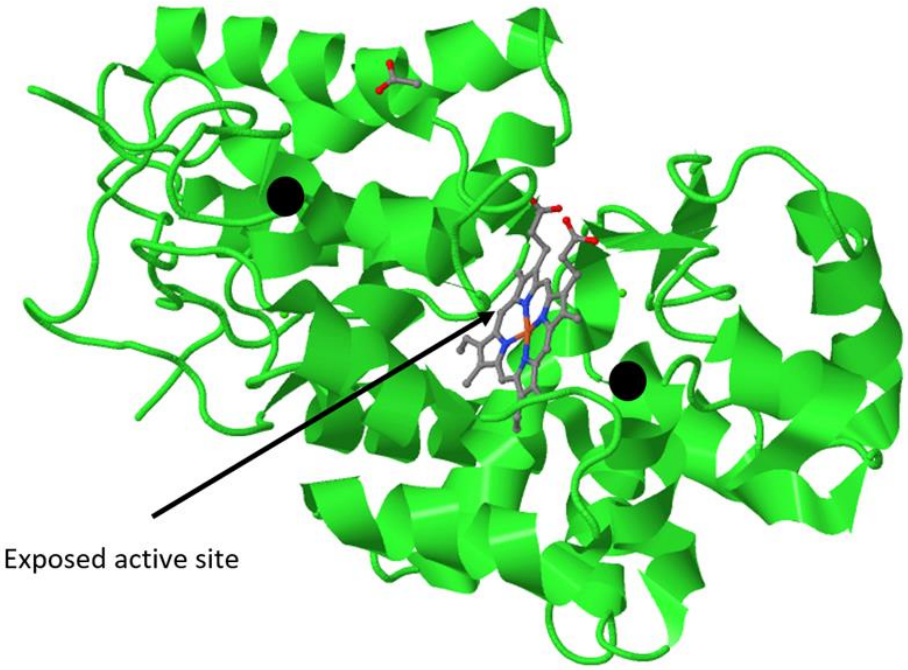

Figure 1.10 Protein structure of ferrous horseradish peroxidase C1A. Image created using 3D visualization from Protein Data Bank in Europe from data published by Berglund.[144] Green compounds are amino acid sequences, black dots are calcium bridges.

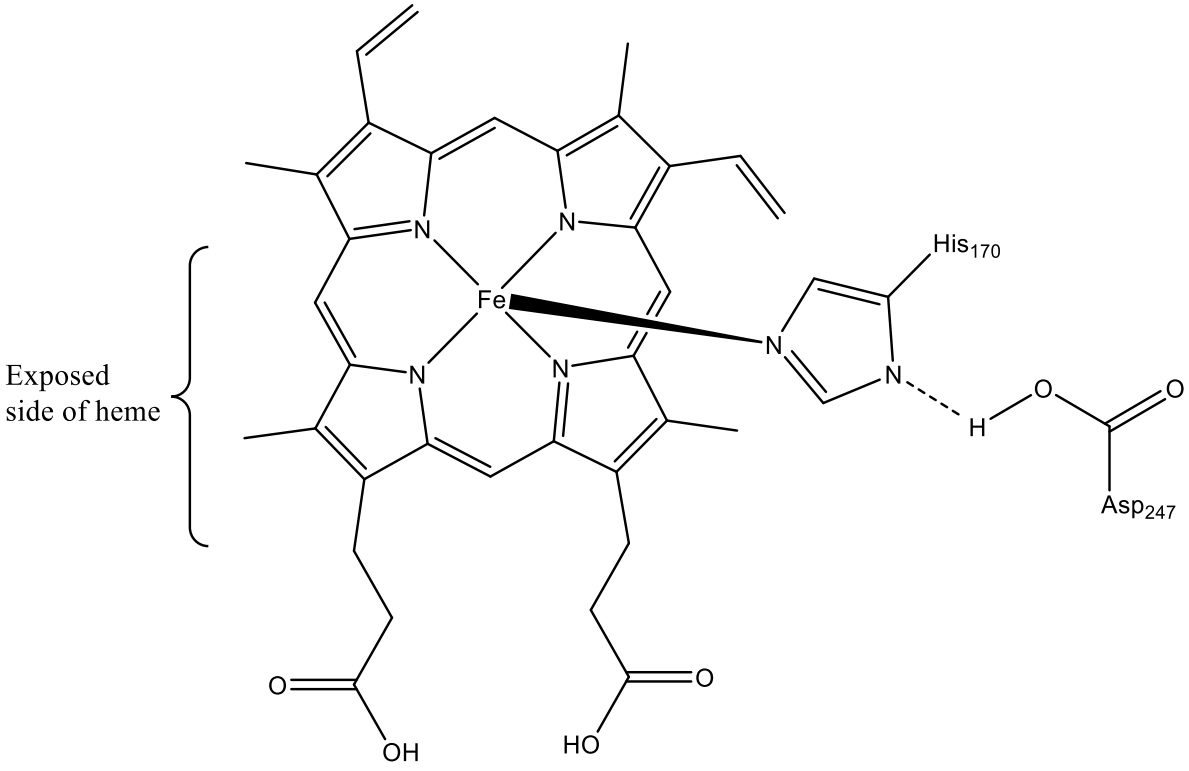

Figure 1.11 Structure of horseradish peroxidase isoenzyme C1A active site.

1.6.3 Horseradish Peroxidase Mechanism and Activity

Horseradish peroxidase is well known for the ability to create hydroxyl radicals in the presence of hydrogen peroxide and a reductant. The general reaction scheme is shown in Equations 11-13 where Equation 14 is the overall material balance and Compounds I and II are the oxidized forms of HRP.[146,147] The first step in this reaction shows that HRP, in the presence of hydrogen peroxide, is converted to an intermediate called Compound I. Then, Compound 1 is converted to another intermediate called Compound II in the presence of the reductant (AH_2). Finally, the Compound II intermediate is converted back to native HRP in the presence of an additional reductant molecule. In the overall material balance, HRP catalyzes the breakdown of hydrogen peroxide in the presence of a reductant. Furthermore, two reductants are required to every peroxide molecule and the products are two water molecules and two radicalized reductant molecules. Due to the production of radicals, HRP has been shown to be an effective tool in degradation processes as outlined in Section 1.6.5.

$$HRP + H_2O_2 \rightarrow Compound\ I + H_2O \quad (11)$$

$$Compound\ I + AH_2 \rightarrow Compound\ II + AH\bullet \quad (12)$$

$$Compound\ II + AH_2 \rightarrow HRP + AH\bullet + H_2O \quad (13)$$

$$H_2O_2 + 2AH_2 \rightarrow 2AH\bullet + 2H_2O \quad (14)$$

In the absence of a reductant, hydrogen peroxide can act as both the oxidant and reducing substrate.[148-150] The simplified reaction mechanism is shown in Reactions 15-17 where Reaction 18 is the overall balance. In the more complex reaction scheme, Compound II can undergo further oxidation to produce Compound III resulting in enzyme deactivation. In addition, hydroxyl and superoxide radicals created as from peroxide decomposition can degrade the polymer but can also

cause enzyme deactivation. The deactivation of proteins takes place through oxidation of amino acids and amino acid residues.[151]

$$HRP + H_2O_2 \rightarrow Compound\ I + H_2O \quad (15)$$

$$Compound\ I + H_2O_2 \rightarrow Compound\ II + HO_2\bullet \quad (16)$$

$$Compound\ II + H_2O_2 \rightarrow HRP + HO_2\bullet + H_2O \quad (17)$$

$$3H_2O_2 \rightarrow 2HO_2\bullet + 2H_2O \quad (18)$$

To improve the efficiency of these reactions, naturally occurring and synthetic electron carriers can be added to the reaction and act as a reductant (AH_2).[152,153] The electron carrier nicotinamide adenine dinucleotide (NADH) is a naturally occurring electron transfer agent that is used in cellular metabolism and is considered a model compound. The addition of NADH has been shown to create the oxidized form of NADH (NAD•) in the cycle. The neutral, oxidized and radical forms of NADH are shown in Figure 1.12. The radical form of NAD• can react with O_2 to create a superoxide radical in an additional oxidative cycle. Figure 1.13 illustrates the reaction cycle in the presence of NADH or a reductant (AH_2) and shows the additional oxidative cycle produced through the addition of NADH. Furthermore, the addition of a reductant has been shown to protect against peroxide inactivation.[154,155] Kinetically, the catalytic cycle has been characterized using computer simulation of 11 elementary reactions and 9 rate equations.[156]

In order to quantify peroxidase activity, Bach first outlined a method by indirectly measuring the conversion of pyrogallol to purpurogallin.[157] Today, similar spectrophotometric methods are used in order to quantify the breakdown of peroxide to reductant radical carriers. By observing the

continuous spectrophotometric absorbance of the oxidized reductant, explained in later in Section 2.6.2, the maximum velocity of conversion (V_{max}) can be established. In order to define unit activity a standard mass of reductant conversion with time, temperature, and pH must be established. Two common reductants used for activity assays are pyrogallol and guaiacol but many other reductants exist.[158-160]

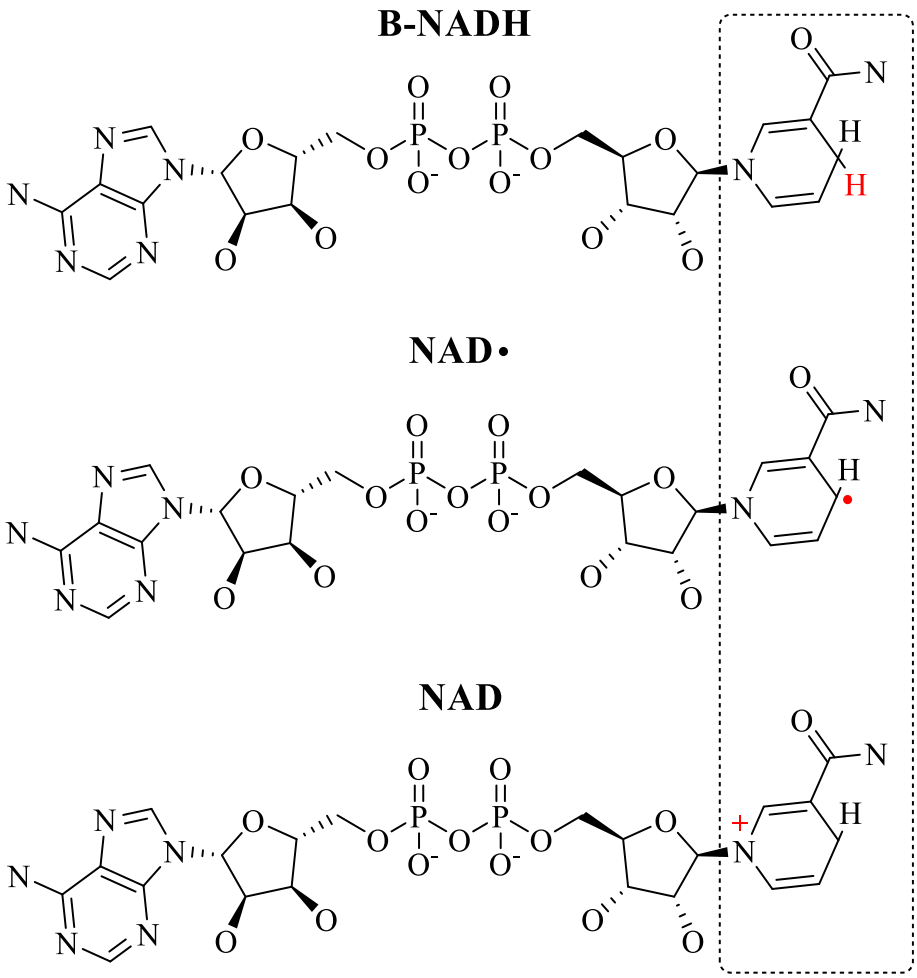

Figure 1.12 Oxidized, radical, and reduced forms of nicotinamide adenine dinucleotide (NADH).[161]

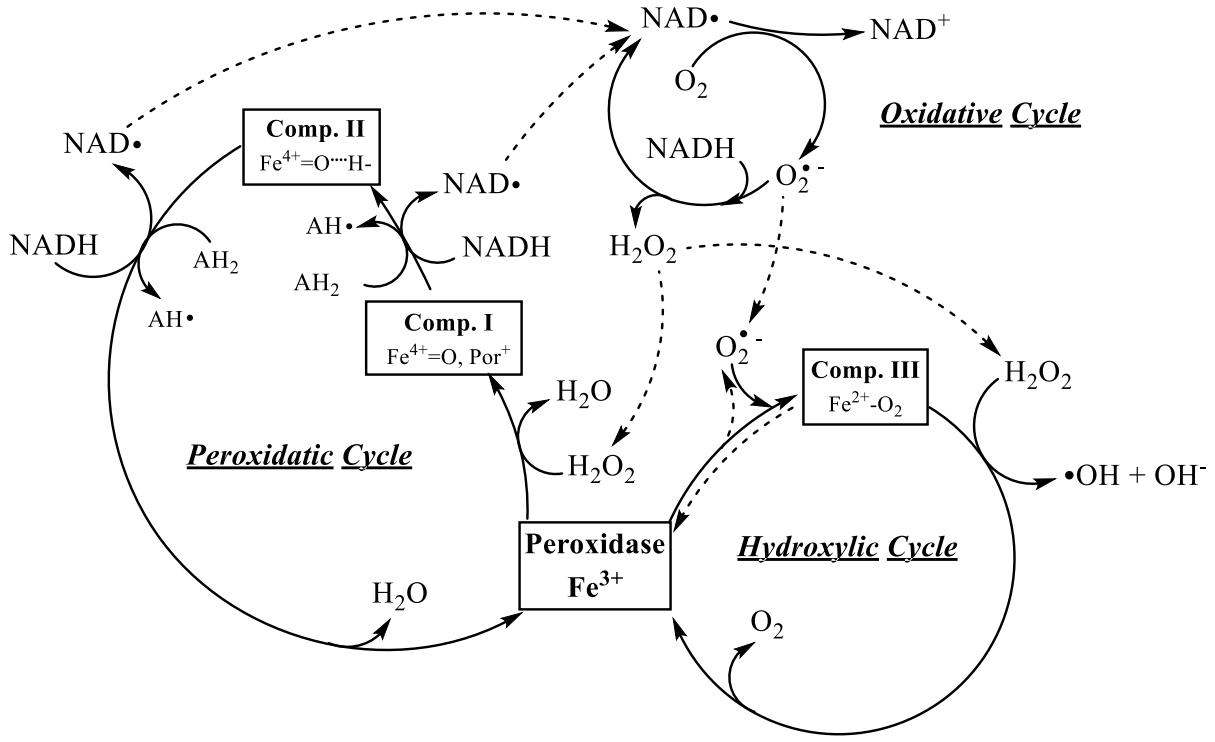

Figure 1.13: Peroxidase cyclic reaction scheme for catalyzed degradation of PAM/HPAM in the presence of NADH after Chen and Schopfer.[162]

In addition to the colorimetric assays, chemiluminescent (CL) and enhanced chemiluminescent (ECL) methods can be used to demine the activity of peroxidase enzymes. This method oxidizes cyclic diacylhydrazides that create the emission of light.[163] One common CL method measures light emission created by the oxidation of luminal under alkane conditions but many other molecules exist.[164] The ECL methods are better than traditional CL methods due to the greater light emission. This method utilizes luminal in the presence of enhancing molecules such as sodium hydroxide, some phenols, naphthols, ect.[165]

1.6.4 Horseradish Peroxidase Applications

Horseradish peroxidase is a versatile enzyme with a number of uses. One of the traditional uses is as a reporter enzyme. HRP has been used in Enzyme-linked immunosorbent assay (ELISA) to

improve the sensitivity.[166] It can be used to detect products such as the mycotoxin, ochratoxin,[167] and tyramine[168] in screen-printed biosensors. HRP can be used in conjunction with graphene oxide in chemiluminescent biosensors to detect DNA.[169] Amperometric sensors were developed using HRP for hydrogen peroxide, choline, and acetylcholine.[170] The detectors immobilized HRP and a redox polymer to measure the electron transfer between the two. HRP was used to develop a highly sensitive hydrogen peroxide biosensor.[171] In addition, HRP biosensors have been developed to detect glucose, ethanol, RNA, L-phenylalanine, citrinin, pyrogallol, hydroquinone, phenols, β-lactoglobulin, rotavirus titers, and tumor markers.[172]

HRP can be used as a biocatalyst in polymer polymerizations. The enzyme has been used to polymerize phenol copolymer,[173] para-functionalized phenol derivatives,[174] various wastewater compounds,[175] and many other phenol monomers in polymerization reactions via enzyme coupling, enzyme hydroxylation, and enzyme nitration and sulfoxidation.[176] HRP has been shown to facilitate the formation of hydrogels *in-situ* for implantable biomaterials and biomedical applications.[177] Recent advancements in cancer research have shown that HRP, in conjunction with the plant hormone indole-3-acetic acid, can cause cytotoxicity and apoptosis in cancer cells.[172] In addition to biosensor, biocatalyst, and medicinal uses HRP has been thoroughly studied in the bioremediation of many phenol and phenol-like compounds.

1.6.5 Horseradish Peroxidase for Pollutant Remediation

The literature describes a number of compounds that can be degraded using HRP both in solution and immobilized on a substrate. Most of the compounds can be categorized as phenols or phenol-like but degradation of more exotic compounds (such as carbon nanotubes) can be found.[178] A major category of bioremediation using HRP is degradation of synthetic dyes. These studies

have shown varying efficiency in removal depending on dye chemistry. For example, Bhunia *et al.*[179] studied the removal of industrial dyes (three Remazol and three Cibacron dyes). In this study, HRP (0.1-1 units/ml, pH=6) was reacted with .0002M/L peroxide for degradation of 15-1000 mg/ml dye at 25°C. It was found that degradation of Ramacol blue was inhibited above pH=6. The greatest percent dye removal was observed with multiple peroxide and HRP additions. About 40% Remazol blue and 50% Crystal violet was removed after 9 hours when 1.2 μM peroxide and 3.4 units of HRP was added after 3 and 6 hours. Kinetics, by linear regression, gave k_m and V_{max} values of 0.044 (mmol/L) and 0.015 (mmol/L-min) for Remazol blue and 0.021 (mmol/L) and 0.0028 (mmol/L-min) for Crystal violet respectively. Ulson de Souza *et al.*[180] conducted a similar study on the removal of Remazol Turquoise Blue G 133% and Lanaset Blue 2R textile dyes and further evaluated the reduction in toxicity. Dye removal was tested using variations in pH (range evaluated= 2.0-9.0), dye concentrations (10-100 mg/L), enzyme concentration (2.985-29.85 U/ml), and peroxide concentration (0.001-0.02 mM/L). Optimum conditions were found to be pH=4-5, 100 mg/L, 29.85 U/ml, and 0.002 mM/L respectively. A discoloration efficiency of about 60% was achieved for Remazol Turquoise blue G 133% after 45 mins whereas, 90% was observed for Lanaset Blue 2R after 10 hours. The toxicity of treated solutions showed a decrease mortality toward two bacteria species. Another study conducted by Onder *et al.*[181] decolored the industrial azo dye naphthol blue black. Activity of free enzyme was 1781 U/mg and a concentration of 5.88 U/ml was used in conjunction with 10μl, 3% peroxide. The optimized pH for degradation was 4-5 and 80-90% discoloration was observed within 5 minutes at temperatures ranging from 25-70°C. After 60 minutes of treatment the discoloration was not affected by temperature change at pH= 4-6 but showed a decline in discoloration with increased temperature at pH=7-8. In addition to the

dyes mentioned above, HRP has shown the ability to remove acid black 10BX, direct yellow 11, direct yellow 12, orange II, bromophenol blue, and methyl orange with varying efficiency.[182]

In addition to dye removal, HRP has been shown to remove many phenol waste compounds. For example, Sakuyama *et al.*[183] studied the removal of bisphenols (2,2-bis(4-bydroxypbenyl)propane; BPA), p-nonylpbenol (p-NP), and p-octylpbenol (p-OP) using HRP at room temperature. Using 66.7 U/ml HRP and 200mM peroxide, the results revealed that the optimum pH was 8, 7, and 5 for BPA, p-NP, and p-OP respectively with the highest oxidation activity for BPA. Optimum temperature for BPA degradation was found to be 20°C. Degradation of BPA was shown to be concentration dependent with the highest concentration (66.7 U/ml) resulting in greater than 99% removal. BPA product produced after degradation was determined to be 4-isopropylphenol. Additional peroxide added to the reaction did not show additional degradation indicating HRP inactivation. Another study conducted by Wagner and Nicell[184] used HRP to degrade phenols in the foul condensate from Kraft pulping. HRP and peroxide concentrations were varied consisting of 0.01-3.0 U/ml and 0-0.9 mM respectively. The results show the greatest degradation of phenols when peroxide concentration is greater than 0.46 mM and 0.76 mM depending on wastewater sample. Furthermore, the reduction in phenol content was linear with peroxide and HRP concentration. The greatest reduction in phenol content was observed with the highest HRP concentration (3.0 U/ml) and pH= 6-9. HRP has also been shown to effectively remove steroid estrogens from waste water,[185] 2,4,6-trinitrotoluene (TNT),[186] and many other compounds with multiple reviews published.[187-189]

One major trend in the remediation of dyes and phenol compounds is HRP removal efficiency being dependent on enzyme mobility (free in solution or immobilized on a surface). Table 1.5 lists examples, from various sources, of removal efficiencies for various phenol compounds using free

and immobilized enzyme.[189,190] Although phenol removal in these systems is conducted under different conditions, a similar trend of higher removal efficiency can be found throughout the literature. The increase in removal efficiency, for immobilized samples, can be attributed to the enzyme stability.

Table 1.5 Comparison of free and immobilized HRP removal efficiency for various phenol compounds.

Compound	% Removal (Free Enzyme)	% Removal (Immobilized Enzyme)
p-Chlorophenol	58	100
2,4-Dichlorophenol	82	100
2,4,5-Trichlorophenol	36	99
2,4,6-Trichlorophenol	97	98
2,3,4,6-Trichlorophenol	81	99
Petrachlorophenol	55	97
Phenol	57.1	64
4-Methoxyphenol	69.5	69.0
2-Methoxyphenol	66	68
3-Aminophenol	67.4	72.7
Catechol	83.4	87.6
2-Cholorophenol	16.1	20.4
2,4-Dimethyloxyphenol	17.6	34.4

1.6.6 Horseradish Peroxidase Immobilization: Substrates and Stability

The immobilization of HRP, for remediation processes, produces higher removal yields, increased enzyme stability and reusability. Covalently binding the enzyme to a solid substrate can help stabilize the enzyme, retaining the activity of the enzyme, for months at a time in aqueous environments.[191] Immobilizing HRP has been of particular interest for bioremediation and biosensor applications.[192,193] Furthermore, immobilization for remediation processes have utilized

a variety of substrates. Some of the most popular immobilization substrates are mesoporous silica or controlled pore glass because of the high surface area. HRP has shown greater remediation of acid azo dye (Acid Black 10 BX) when immobilized with acrylamide gel beads (80%) when compared to alginate beads (55%) after 45 minutes of exposure. [194] In this same study, immobilization in an acrylamide matrix showed better remediation than free enzyme while immobilization in alginate was inferior. Immobilization on Celite R-646 porous beads removed 90% azo dye orange II after 36 hours of reactor operation and immobilized enzyme showed much better storage stability.[195] In this study, free enzyme showed complete loss of activity after 50 days and immobilized enzyme retained about 90% relative activity. HRP immobilization on graphene oxide (GO) retained higher activity at pH=10 (36%), temperature stability (measured between 40-60°C), much higher storage stability, and removal of 2-cholorophenol and 2,4-dimetheoxyphenol compared to free enzyme.[196] HRP immobilized on magnetic poly(glycidylmethacrylate-co-methylmethacrylate) (poly(GMA-MMA)) beads showed higher temperature tolerance, storage and operational stability, and higher phenol conversion compared to free enzyme.[197] Immobilization in electro spun fibrous membranes (EFM) showed 60% relative activity remaining after eight repeated runs and degradation was increased using immobilized enzyme with removal percentages of 47% for free enzyme and 83% for immobilized enzyme.[198] In addition to these substrates, HRP has been successfully immobilized using a reverse micelle system,[190] polypropylene hollow fiber membranes (HF),[199] on graphene oxide,[200] carbon nanotubes,[201] gold surfaces,[202] indium tin oxide,[203] magnetic beads,[204] chitosan,[205] Amberlite IRA-400 ion exchange paper,[206] and can be entrapped in a variety a matrices.[207]

1.6.7 Peroxidase Immobilization on Silica and Natural Substrates

For covalent immobilization of the enzyme to a glass or silica, the surface is modified using bifunctional silane molecule followed by covalent binding, or crosslinking, of the protein. In some cases, an acid or base pretreatment is needed before silaneization to clean the surface of the solid substrate. Some examples of silane molecules used in surface modification are (3-glycidyloxypropyl)trimethoxysilane (3-GPS), (3-aminopropyl)triethoxysilane (APTES), aminophenyltrimethoxysilane , (3-mercaptopropyl)trimethoxysilane (3-MPTS), and haloacetamidosilanes.[208] After surface modification, a hetero or homo bifunctional cross linker is applied to covalently attach the protein to the surface activated substrate. In many immobilization studies, a decrease in activity is observed in immobilized samples and can be attributed to active site hindrance or protein unfolding and conformational changes the degree dependent upon functional group.[209,210] Glutaraldehyde cross linker is reactive toward amine groups found in APTES and lysine residues. Native HRP contains six lysine groups available for binding[211] and studies using APTES-glutaraldehyde binding technique retains much of the original activity for remediation processes.

Table 1.6 lists some studies that immobilized HRP using glutaraldehyde cross linker. In this table, activity is either reported as percent retained activity or specific activity depending on reported values. A study conducted by Gomez *et al*.[212] compared phenol removal for free and immobilized HRP and soybean peroxidase (SBP). This study concluded that immobilized enzyme, using glutaraldehyde, showed good activity (resulting in removal as high as 95%), increased storage capability, and created a protective effect against protein inactivation by peroxide. Bodalo *et al.*[213] confirmed the protective effects for immobilized SBP and HRP for the removal of 4-chlorophenol but achieved lower retained HRP activity due to higher enzyme loading.[213] One

particular study conducted by Lai *et al.*[214] showed that immobilized HRP retained a higher activity at increased pH (8-9.5) and temperature (about 65-80°C). This study also found that higher enzyme loading (from 5.63 -9.6 mg HRP/g support) produced a 30% lower specific activity and was thought to be due to steric hindrance and mass transfer limitations.

Table 1.6 List of some HRP immobilizations on glass beads using glutaraldehyde crosslinking. * designates immobilization conducted in reactor, ** designates concentrations determined by absorbance at 403 nm.

Substrate	Substrate cleaning	Activation	Crosslinking	Immobilization	Concentration	Activity	Author
200-400 mesh, controlled pore glass beads (PG-75-400, Sigma)	5% HNO_3 at 80°C for 1 hour.	10% APTES in water adjusted to pH 3-4 at 75°C for 2 hours.	Glutaraldehyde (2.5% v/v) in 50 mM PBS (pH=7) for 1 hour.	2 mg/ml HRP or SBP at 4°C overnight*	SBP=35 mg/g dry support (45.2%) HRP= 18 mg/g dry support (40.6%)	SBP=74% HRP=78%	Gomez *et al.*[212]
200-400 mesh, controlled pore glass beads (PG-75-400, Sigma)	5% HNO_3 at 80°C for 1 hour.	10% APTES in water adjusted to pH 3-4 at 75°C for 2 hours.	Glutaraldehyde (2.5% v/v) in 50 mM PBS (pH=7) for 1 hour.	2 mg/ml HRP or SBP at 4°C overnight*	SBP=42.3 mg/g dry support (45.2%) HRP= 23.1 mg/g dry support (40.6%) **	SBP=82.4% HRP=52.5%	Bodalo *et al.*[213]
200-400 mesh porous aminopropyl glass beads (pore diameter = 170 nm)	NONE	NONE	Glutaraldehyde (2.5% v/v) in 50 mM PBS (pH=7) for 8 hours.	2.5 mg/ml HRP in 50 mM PBS (pH=7) at 4°C for various times	9.6 mg HRP/g support**	5.3 U/g substrate	Yi-Chen and Sung-Chyr[214]
Zirconia coated arylamine and alkylamine glass beads (55nm pore diameter)	2ml, 2N HCl in ice bath with addition of 50 mg NaNO3 for 30 minutes	Pre activated with arylamine and alkylamine	Glutaraldehyde (2.5% v/v) in 50 mM PBS (pH=7) for 2 hours.	2.8 U/ml HRP in 0.1M PBS (pH=7) at 4°C for 48 hours	arylamine = 28 mg HRP/g alkylamine= 16 mg HRP/g	arylamine = 77% alkylamine= 39%	Pundir *et al.* [215]
Alkylamine controlled pore glass (80–120 mesh, 700Å pore size)	NONE	NONE	Glutaraldehyde (5% v/v) in 0.1 M PBS (pH=7) for 2 hours.	20 mg/ml HRP in 0.1 M PBS (pH=7) at 4°C for 18 hours*	21 mg HRP/g support	17.4 U/cm3	Azevedo *et al.*[216]

Very little research has been done on enzyme immobilization using sand. The literature has shown that ligand concentrations for controlled pore glass (CPG) vary depending on the type but two publications reported values of 33.8 and 47.6 μmol/g for CPG-2000 and CPG 500

respectively.[217,218] Silanization of Celite, a naturally occurring siliceous sedimentary rock, resulted in slightly lower values of ligand concentration (20.1 μmol/g).[219] A study conducted by Brotherton *et.al* [220] showed that sand contained the lowest ligand concentration resulting in 3.0 μmol/g. The lower concentration of available binding sites on sand will result in lower immobilized enzyme concentrations when compared to glass and other substrates. In addition to Celite and sand, enzyme immobilization has been studied using other naturally occurring substances such as vermiculite,[221] kaolinite, hornblende, biotite, muscovite, and feldspar.[222] Johnson and Thornton[222] compared immobilization of lactoperoxidase on porous glass, hornblende, biotite, muscovite, feldspar, and sand using APTES and glutaraldehyde binding method in addition to a metal linking method. The results of this study showed that APTES-glutaraldehyde method resulted in no detectable activity for sand. Using a metal linking method, the highest specific activity was observed for hornblende (5.74 U/g) with the lowest activity of 0.23 U/mg observed for sand. On the other hand, studies have shown that trypsin can be covalently bound to sand. One study using APTES and glutaraldehyde cross linker showed that the amount of trypsin binding achieved from iron and non-iron containing sand.[223] The results showed that between 1.88 and 2.31 mg/g bound protein was achieved regardless of iron content. In addition, the study showed that protein binding is covalent and more prevalent with quartz sand. The immobilization of enzyme catalysts to proppant (or quartz sand) would create a means of breaker transport and would act as reaction bed for removal of fracturing polymers.

1.7 Research Objectives

With the growing use of slickwater fracturing applications, and use of polyacrylamide, new and environmentally friendly applications for fracture cleanup are necessary. Currently, no enzymes are used in the degradation of PAM/HPAM in oilfield applications but the use of

enzymes has been well established for conventional fracturing fluids that utilize crosslinked guar polymer. The objective of this research is to evaluate the ability of peroxidase, specifically horseradish peroxidase (HRP) and soybean peroxidase (SBP), to degrade high molecular weight HPAM in the presence and absence of the intermediate reductant NADH. HRP is used in this study because it is considered a model plant peroxidase but the use of SBP would be more economically feasible for industrial upscaling. First, viscosity measurements were conducted to quickly determine degradation of HPAM in the presence of HRP and peroxide. Viscosity experiments were conducted in the presence and absence of NADH. These results were compared to the reduction in viscosity achieved using SBP in the presence of NADH and peroxide. Furthermore, viscosity and molecular weight reduction was observed with respect to time using HRP. Reduction in HPAM molecular weight was observed for solutions containing varying peroxide concentrations in both aqueous and brine solutions. As a prelude to core flooding, filtration tests were conducted to measure flowrate recovery by HRP after HPAM filter cake was formed. Finally, core flooding tests measured permeability recovery in HPAM damaged limestone using both free and immobilized HRP. A novel approach was tested by immobilizing HRP on Ottawa fracturing sand and core flooding results were compared to those achieved using free enzyme. After HRP immobilization was achieved the bound concentration and activity was quantified using spectrophotometric analysis and further testing was conducted to observe viscosity reduction of NADH solution.

1.8 References

1. Eobeets, E. A., Improvement in method of increasing capacity of oil-wells. US59936 A, 1866
2. Montgomery, C. T.; Smith, M. B., J. Petrol. Techn. 62, 26 2010.
3. Medvedev, A. V.; Kraemer, C. C.; Pena, A. A.; Panga, M. K. R. SPE Hydraulic Fracturing Technology Conference, 2013. Document ID: SPE-163836-MS
4. King, G. E. SPE Annual Technical Conference and Exhibition, 2014. Document ID: SPE-170952-MS

5. Joshi, S. D., Horizontal well technology; PennWell Books, 1991.
6. Overbey, W.; Yost, A.; Wilkins, D. SPE Annual Technical Conference and Exhibition, 1988. Document ID: SPE-18249-MS
7. Heinberg, R., Snake oil: How fracking's false promise of plenty imperils our future; Clairview Books, 2014.
8. Howarth, R. W.; Ingraffea, A.; Engelder, T., Nature 477, 271 2011.
9. McGlade, C.; Speirs, J.; Sorrell, S., Energy 55, 571 2013.
10. Holditch, S. A., J. Petrol. Techn. 58, 86 2006.
11. Holditch, S. A.; Madani, H., J. Petrol. Techn. 62, 42 2010.
12. Terry, R. E.; Rogers, J. B., Applied petroleum reservoir engineering; Pearson Education, 2013.
13. Ahmed, T.; Evans, J.; Kwan, R.; Vivian, T. SPE Eastern Regional Meeting, 1998. Document ID: SPE-51050-MS
14. Arri, L.; Yee, D.; Morgan, W.; Jeansonne, M. SPE Rocky Mountain Regional Meeting, 1992. Document ID: SPE-24363-MS
15. Engineer, R. SPE California Regional Meeting, 1985. Document ID: SPE-13650-MS
16. Jarvie, D. M.; Hill, R. J.; Ruble, T. E.; Pollastro, R. M., AAPG Bull. 91, 475 2007.
17. Claypool, G., AAPG Bull. 82, 5 1998.
18. Martini, A. M.; Walter, L. M.; Ku, T. C.; Budai, J. M.; McIntosh, J. C.; Schoell, M., AAPG Bull. 87, 1355 2003.
19. Zhao, H.; Givens, N. B.; Curtis, B., AAPG Bull. 91, 535 2007.
20. Fisher, M.; Heinze, J.; Harris, C.; Davidson, B.; Wright, C.; Dunn, K. SPE Annual Technical Conference and Exhibition, 2004. Document ID: SPE-90051-MS
21. Cipolla, C. L.; Fitzpatrick, T.; Williams, M. J.; Ganguly, U. K. SPE Reservoir Characterisation and Simulation Conference and Exhibition, 2011. Document ID: SPE-146876-MS
22. Olson, J. E.; Taleghani, A. D. SPE Hydraulic Fracturing Technology Conference, 2009. Document ID: SPE-119739-MS
23. Weng, X.; Kresse, O.; Cohen, C.-E.; Wu, R.; Gu, H., SPE Prod. Oper. 26, 368 2011.
24. Roussel, N. P.; Sharma, M. M., SPE Prod. Oper. 26, 173 2011.
25. Lee, D. S.; Herman, J. D.; Elsworth, D.; Kim, H. T.; Lee, H. S., KSCE J. Civ. Eng. 15, 679 2011.
26. Kaufman, P. B.; Penny, G. S.; Paktinat, J. SPE Shale Gas Production Conference, 2008. Document ID: SPE-119900-MS
27. Gregory, K. B.; Vidic, R. D.; Dzombak, D. A., Elements 7, 181 2011.
28. Wiley, C.; Barree, B.; Eberhard, M.; Lantz, T. SPE Annual Technical Conference and Exhibition, 2004. Document ID: SPE-90697-MS
29. Shubin, V.; Linse, P., J. Phys. Chem. 99, 1285 1995.
30. Paktinat, J.; O'Neil, B. J.; Aften, C. W.; Hurd, M. D. SPE Production and Operations Symposium, 2011. Document ID: SPE-141356-MS
31. Fontaine, J. S.; Johnson, N. J.; Schoen, D. SPE Eastern Regional/AAPG Eastern Section Joint Meeting, 2008. Document ID: SPE-117772-MS
32. Sun, H.; Stevens, R. F.; Cutler, J. L.; Wood, B.; Wheeler, R. S.; Qu, Q. SPE Tight Gas Completions Conference, 2010. Document ID: SPE-136807-MS
33. Barati, R.; Johnson, S. J.; McCool, S.; Green, D. W.; Willhite, G. P.; Liang, J.-T., J. Appl. Polym. Sci. 126, 587 2012.
34. Cooke Jr, C., J. Petrol. Techn. 27, 1 1975.
35. Caulfield, M. J.; Hao, X.; Qiao, G. G.; Solomon, D. H., Polymer 44, 1331 2003.
36. Wang, X.; Sun, H.; Zhou, J.; Guerin, M.; Li, L. SPE European Formation Damage Conference and Exhibition, 2015. Document ID: SPE-174280-MS

37. Guerin, M.; Sun, H.; Cutler, J.; Zhou, J.; Wang, X. SPE Production and Operations Symposium, 2015. Document ID: SPE-173608-MS
38. Rightmire, C. M.; Leshchyshyn, T. T.; Vincent, M. C. SPE Annual Technical Conference and Exhibition, 2005. Document ID: SPE-96962-MS
39. Grieser, B.; Hobbs, J.; Hunter, J.; Ables, J. SPE Production and Operations Symposium, 2003. Document ID: SPE-80933-MS
40. Palisch, T.; Duenckel, R.; Wilson, B., SPE Prod. Oper. 30, 76 2015.
41. Patel, P.; Robart, C.; Ruegamer, M.; Yang, A. SPE Hydraulic Fracturing Technology Conference, 2014. Document ID: SPE-168645-MS
42. Kurz, B.; Schmidt, D.; Beddoe, S. S. C.; Lindeman, C.; Mibeck, B.; University Of North Dakota: 2012, p Medium: ED.
43. Hu, K.; Sun, J.; Wong, J.; Hall, B. E. SPE Western North American and Rocky Mountain Joint Meeting, 2014. Document ID: SPE-169566-MS
44. Demong, K. L.; Boulton, K. A.; Elgar, T.; Longmuir, K. C.; Affleck, B. SPE Eastern Regional Meeting, 2013. Document ID: SPE-165673-MS
45. Yang, M.; Economides, M. J.; Wei, C.; Gao, C. SPE Annual Technical Conference and Exhibition, 2013. Document ID: SPE-166299-MS
46. Zwolle, S.; Davies, D. R., J. Petrol. Techn. 35, 1 1983.
47. Benson, M. E.; Wilson, A. B. Frac Sand Sources in the United States, 2015. Website: http://www.rockproducts.com/frac-sand/14379-frac-sand-sources-in-the-united-states.html#.V5aOTs6cGAg
48. Gallagher, D. G., J. Petrol. Techn. 63, 18 2011.
49. Zahid, S.; Bhatti, A. A.; Ahmad Khan, H.; Ahmad, T. Production and Operations Symposium, 2007. Document ID: SPE-107053-MS
50. Palisch, T. T.; Duenckel, R. J.; Chapman, M. A.; Woolfolk, S.; Vincent, M. C. SPE Hydraulic Fracturing Technology Conference, 2009. Document ID: SPE-119242-MS
51. Penny, G. SPE Annual Technical Conference and Exhibition, 1987. Document ID: SPE-16900-MS
52. McDaniel, G. A.; Abbott, J.; Mueller, F. A.; Anwar, A. M.; Pavlova, S.; Nevvonen, O.; Parias, T.; Alary, J. SPE Annual Technical Conference and Exhibition, 2010. Document ID: SPE-135360-MS
53. Wood, W. D.; Brannon, H. D.; Rickards, A. R.; Stephenson, C. SPE Annual Technical Conference and Exhibition, 2003. Document ID: SPE-84309-MS
54. Rickards, A. R.; Brannon, H. D.; Wood, W. D., SPE Prod. Oper. 21, 212 2006.
55. Paul, J.; Fieler, E. SPE Annual Technical Conference and Exhibition, 1992. Document ID: SPE-24847-MS
56. Yeboah, Y.; Somuah, S.; Saeed, M. SPE International Symposium on Oilfield Chemistry, 1993. Document ID: SPE-25166-MS
57. Crabtree, M.; Eslinger, D.; Fletcher, P.; Miller, M.; Johnson, A.; King, G., Oilfield Rev. 11, 30 1999.
58. Powell, R.; Gdanski, R.; McCabe, M.; Buster, D. SPE International Symposium on Oilfield Chemistry, 1995. Document ID: SPE-28999-MS
59. Montgomery, C. ISRM International Conference for Effective and Sustainable Hydraulic Fracturing, 2013. Document ID: ISRM-ICHF-2013-035
60. Ferrer, I.; Thurman, E. M., Trends Environ. Anal. Chem 5, 18 2015.
61. Kahrilas, G. A.; Blotevogel, J.; Stewart, P. S.; Borch, T., Environ. Sci. Tech. 49, 16 2014.
62. Boek, E.; Coveney, P.; Skipper, N., J. Am. Chem. Soc. 117, 12608 1995.
63. Steiger, R. P., J. Petrol. Techn. 34, 1 1982.
64. Paktinat, J.; Pinkhouse, J. A.; Little, J. B.; Lash, G. G.; Penny, G. S. SPE Eastern Regional Meeting, 2007. Document ID: SPE-111063-MS

65. Shuler, P. J.; Tang, H.; Lu, Z.; Tang, Y. SPE Canadian Unconventional Resources Conference, 2011. Document ID: SPE-147531-MS
66. O'Brien, D. E.; Chenevert, M. E., J. Petrol. Techn. 25, 1 1973.
67. Carman, P. S.; Lant, K. S. SPE Eastern Regional Meeting, 2010. Document ID: SPE-139030-MS
68. Patel, A. D. SPE International Symposium on Oilfield Chemistry, 2009. Document ID: SPE-121737-MS
69. Samuel, M.; Polson, D.; Graham, D.; Kordziel, W.; Waite, T.; Waters, G.; Vinod, P.; Fu, D.; Downey, R. SPE Rocky Mountain Regional/Low-Permeability Reservoirs Symposium and Exhibition, 2000. Document ID: SPE-60322-MS
70. Batley, G. E.; Kookana, R. S., Envir. Chem. 9, 425 2012.
71. McCurdy, R. USEPA Technical Workshops for the Hydraulic Fracturing Study: Water Resources Management, Arlington, VA, May; United States Environmental Protection Agency, Office of Research and Development, 2011. Document ID: NA
72. Ellsworth, W. L., Science 341, 1225942 2013.
73. Lester, Y.; Ferrer, I.; Thurman, E. M.; Sitterley, K. A.; Korak, J. A.; Aiken, G.; Linden, K. G., Sci. Total Environ. 512, 637 2015.
74. Vidic, R. D.; Brantley, S. L.; Vandenbossche, J. M.; Yoxtheimer, D.; Abad, J. D., Science 340, 1235009 2013.
75. Stringfellow, W. T.; Domen, J. K.; Camarillo, M. K.; Sandelin, W. L.; Borglin, S., J. Hazard. Mat. 275, 37 2014.
76. Abdel-Alim, A.; Hamielec, A., J. Appl. Polym. Sci. 17, 3769 1973.
77. Yang, M.-H., Polym. Test. 17, 191 1998.
78. Vijayalakshmi, S.; Madras, G., J. Appl. Polym. Sci. 100, 3997 2006.
79. Yen, H.-Y.; Yang, M.-H., Polym. Test. 22, 129 2003.
80. Maia, A. M.; Borsali, R.; Balaban, R. C., Mater. Sci. Eng. C 29, 505 2009.
81. Woodroof Jr, R. A.; Anderson, R. W. SPE Annual Fall Technical Conference and Exhibition, 1977. Document ID: SPE-6812-MS
82. Grattoni, C.; Luckham, P.; Jing, X.; Norman, L.; Zimmerman, R. W., J. Pet. Sci. Eng. 45, 233 2004.
83. Lam, C.; Jefferis, S. A., Proc. Inst. Civ. Eng. Constr. Mater. 0, 1 2015.
84. Gröllmann, U.; Schnabel, W., Polym. Degrad. Stabil. 4, 203 1982.
85. Laurenti, E.; Ghibaudi, E.; Ardissone, S.; Ferrari, R. P., J. Inorg. Biochem. 95, 171 2003.
86. Kurenkov, V. F.; Hartan, H. G.; Lobanov, F. I., Russ. J. Appl. Chem. 75, 1039 2002.
87. Tanaka, H.; Senju, R., Bull. Chem. Soc. Jpn. 49, 2821 1976.
88. Levitt, D. B.; Pope, G. A.; Jouenne, S., SPE Reservoir Eval. Eng. 14, 281 2011.
89. Muller, G., Polym. Bull 5, 39 1981.
90. Muller, G.; Fenyo, J.; Selegny, E., J. Appl. Polym. Sci. 25, 627 1980.
91. Muller, G., Polym. Bull 5, 31 1981.
92. Zeynali, M. E.; Rabbii, A., Iran. Polym. J. 11, 269 2002.
93. Ramsden, D. K.; McKay, K., Polym. Degrad. Stabil. 15, 15 1986.
94. Ramsden, D.; McKay, K., Polym. Degrad. Stabil. 14, 217 1986.
95. Hu, Y.; Lu, S., Int. J. Eng. Sci. Technol. 2, 110 2010.
96. De Sena, R. F.; Moreira, R. d. F.; José, H. J., Chem. Eng. Comm. 200, 235 2013.
97. Liu, T.; You, H.; Chen, Q., J. Hazard. Mat. 162, 860 2009.
98. Albonico, P.; Cobianco, S.; Bianchi, D.; D'Aloisio, R. European Formation Damage Conference, 2007. Document ID: SPE-107757-MS
99. Gao, J.; Lin, T.; Wang, W.; Yu, J.; Yuan, S.; Wang, S., Macro. Symp. 144, 179 1999.
100. Gao, J., J. Appl. Polym. Sci. 69, 791 1998.

101. Carman, P. S.; Cawiezel, K. SPE Hydraulic Fracturing Technology Conference, 2007. Document ID: SPE-106162-MS
102. Yang, S.; Treiber, L. SPE Annual Technical Conference and Exhibition, 1985. Document ID: SPE-14232-MS
103. Goldstein, B.; Josyula, K.; VanZeeland, A.; Aboushabana, M.; Tran, T.; O'Connell, L.; Conway, M. SPE Unconventional Resources Technology Conference (URTEC), 2015. Document ID: SPE-178518-MS
104. She, Y.; Zhang, F.; Wang, Z.; Zhao, L.; Yu, L. 2009 3rd International Conference on Bioinformatics and Biomedical Engineering, 2009, pp 1. Document ID: 2151-7614
105. Wen, Q.; Chen, Z.; Zhao, Y.; Zhang, H.; Feng, Y., J. Hazard. Mat. 175, 955 2010.
106. Wen, Q. X.; Zhang, H. C.; Chen, Z. Q.; Zhao, Y.; Feng, Y. J., J. Environ. Sci. Health A 47, 358 2012.
107. Bao, M.; Chen, Q.; Li, Y.; Jiang, G., J. Hazard. Mat. 184, 105 2010.
108. Nakamiya, K.; Kinoshita, S., J. Ferment. Bioeng. 80, 418 1995.
109. Gupta, D. S., Method of using asparaginase as a polyacrylamide enzyme breaker. US9090815 B2, 2015
110. Ramsden, D. K.; Fielding, S.; Atkinson, N.; Boota, M., Polym. Degrad. Stabil. 17, 49 1987.
111. Nakamiya, K.; Ooi, T.; Kinoshita, S., J. Ferment. Bioeng. 84, 213 1997.
112. Montroll, E. W.; Simha, R., J. Chem. Phys. 8, 721 1940.
113. Mark, H.; Simha, R., Trans. Faraday Soc. 35, 611 1940.
114. Simha, R., J. Appl. Phys 12, 569 1941.
115. Masson, C., Can. J. Chem. 33, 597 1955.
116. Basedow, A. M.; Ebert, K. H.; Ederer, H. J., Macromol. 11, 774 1978.
117. Davis, A.; Golden, J. H., Makromol. Chem. 78, 16 1964.
118. Li, G.; Qi, L.; Li, A.; Ding, R.; Zong, M. in Macro. Symp.; Wiley Online Library: 2004, p 165.
119. Tayal, A.; Kelly, R. M.; Khan, S. A., Macromol. 32, 294 1999.
120. Bouhadir, K. H.; Lee, K. Y.; Alsberg, E.; Damm, K. L.; Anderson, K. W.; Mooney, D. J., Biotech. Prog. 17, 945 2001.
121. Marx-Figini, M., J. Appl. Polym. Sci. 33, 2097 1987.
122. Shukla, N. B.; Daraboina, N.; Madras, G., Polym. Degrad. Stabil. 94, 1238 2009.
123. Madras, G.; Chattopadhyay, S., Chem. Eng. Sci. 56, 5085 2001.
124. Francoz, E.; Ranocha, P.; Nguyen-Kim, H.; Jamet, E.; Burlat, V.; Dunand, C., Phytochemistry 112, 15 2015.
125. Marjamaa, K.; Kukkola, E. M.; Fagerstedt, K. V., J. Exp. Bot. 60, 367 2009.
126. Kim, D.-S.; Jeon, S.-E.; Park, K.-C., Cell. Signal. 16, 81 2004.
127. Mlíčková, K.; Luhová, L.; Lebeda, A.; Mieslerová, B.; Peč, P., Plant Physiol. Biochem. 42, 753 2004.
128. Clark, E. D., The plant oxidases; Eschenbach printing Company, 1910.
129. Schoenbien, C., Journa. f. prakt. Chemie 89, 323 1863.
130. Jacobson, J., Zts. Physiol Chem. 16, 340 1892.
131. Loew, O., US Department of Agriculture Report number 681901.
132. Bourquelot, E., Compt. Rend. Soc. Biol. 50, 381 1898.
133. Linossier, G., Semaine Medicale, 141 1898.
134. Theorell, H., Enzymologia 10, 250 1942.
135. Krainer, F. W.; Glieder, A., Appl. Microb. Biotech. 99, 1611 2015.
136. Welinder, K. G., Curr. Opin. Struct. Biol. 2, 388 1992.
137. Koua, D.; Cerutti, L.; Falquet, L.; Sigrist, C. J. A.; Theiler, G.; Hulo, N.; Dunand, C., Nuc. Acids Res. 37, D261 2009.
138. Passardi, F.; Zamocky, M.; Favet, J.; Jakopitsch, C.; Penel, C.; Obinger, C.; Dunand, C., Gene 397, 101 2007.

139. Krainer, F. W.; Pletzenauer, R.; Rossetti, L.; Herwig, C.; Glieder, A.; Spadiut, O., Protein Express. Purif. 95, 104 2014.
140. Passardi, F.; Cosio, C.; Penel, C.; Dunand, C., Plant Cell Rep. 24, 255 2005.
141. Welinder, K. G., FEBS Letters 72, 19 1976.
142. Takio, K.; Titani, K.; Ericsson, L. H.; Yonetani, T., Arch. Biochem. Biophys. 203, 615 1980.
143. Poulos, T. L.; Freer, S. T.; Alden, R. A.; Edwards, S. L.; Skogland, U.; Takio, K.; Eriksson, B.; Xuong, N.; Yonetani, T.; Kraut, J., J. Biol. Chem. 255, 575 1980.
144. Berglund, G. I.; Carlsson, G. H.; Smith, A. T.; Szoke, H.; Henriksen, A.; Hajdu, J., Nature 417, 463 2002.
145. Passardi, F.; Theiler, G.; Zamocky, M.; Cosio, C.; Rouhier, N.; Teixera, F.; Margis-Pinheiro, M.; Ioannidis, V.; Penel, C.; Falquet, L.; Dunand, C., Phytochemistry 68, 1605 2007.
146. Dunford, H., Peroxidases in Chemistry and Biology 2, 1 1991.
147. Poulos, T. L.; Fenna, R. E., Met. Ions Biol. Syst. 30, 25 1994.
148. Hiner, A. N.; Ruiz, J. H.; López, J. N. R. g.; Cánovas, F. G. a.; Brisset, N. C.; Smith, A. T.; Arnao, M. B.; Acosta, M., J. Biol. Chem. 277, 26879 2002.
149. Hernandez-Ruiz, J.; Arnao, M. B.; Hiner, A. N.; Garcia-Canovas, F.; Acosta, M., Biochem. J 354, 107 2001.
150. Valderrama, B.; Ayala, M.; Vazquez-Duhalt, R., Chem. Biol. 9, 555 2002.
151. Stadtman, E., Annu. Rev. Biochem. 62, 797 1993.
152. Anne, A.; Hapiot, P.; Moiroux, J.; Neta, P.; Saveant, J. M., J. Phys. Chem. 95, 2370 1991.
153. Halliwell, B.; Rycker, J. d., Photochem. Photobiol. 28, 757 1978.
154. Arnao, M.; Acosta, M.; Del Rio, J.; Garcia-Canovas, F., Biochim. Biophys. Acta 1038, 85 1990.
155. Acosta, M.; Arnao, M.; Del Rio, J.; Garcia-Canovas, F., Biochim. Biophys. Acta 996, 7 1989.
156. Yokota, K.; Yamazaki, I., Biochem. 16, 1913 1977.
157. Bach, A., Ber. Chem. Gesell 37, 3750 1904.
158. Nicell, J. A.; Wright, H., Enzyme Microb. Technol. 21, 302 1997.
159. Chance, B.; Maehly, A. C. In Methods in Enzymology; Academic Press, 1955.
160. Conyers, S. M.; Kidwell, D. A., Anal. Biochem. 192, 207 1991.
161. Kirkor, E. S.; Scheeline, A., Eur. J. Biochem. 267, 5014 2000.
162. Chen, S. x.; Schopfer, P., Eur. J. Biochem. 260, 726 1999.
163. Arakawa, H.; Maeda, M.; Tsuji, A., Anal. Biochem. 97, 248 1979.
164. Kricka, L. J., Clin. Chem. 37, 1472 1991.
165. Thorpe, G. H. G.; Kricka, L. J. In Methods in Enzymology; Academic Press, 1986.
166. Acharya, A. P., J. Polym. Sci., Part A: Polym. Chem. 53, 206 2015.
167. Alonso-Lomillo, M. A.; Domínguez-Renedo, O.; Román, L. d. T.-d.; Arcos-Martínez, M. J., Anal. Chim. Acta 688, 49 2011.
168. Calvo-pérez, A.; Domínguez-renedo, O.; Alonso-lomillo, M. A.; Arcos-martínez, M. J., Electroanal. 25, 1316 2013.
169. Luo, M., Chem. Comm. 48, 1126 2012.
170. Garguilo, M. G.; Nhan, H.; Proctor, A.; Michael, A. C., Anal. Chem. 65, 523 1993.
171. Tangkuaram, T.; Ponchio, C.; Kangkasomboon, T.; Katikawong, P.; Veerasai, W., Biosens. Bioelectron. 22, 2071 2007.
172. Krainer, F. W., Appl. Microb. Biotech. 99, 1611 2015.
173. Lv, S.; Li, D.; Ju, H.; Ma, Y.; Qiu, C.; Zhang, G., J. Appl. Polym. Sci. 128, 523 2013.
174. Pang, Y.; Ritter, H.; Tabatabai, M., Macromol. 36, 7090 2003.
175. Nicell, J. A.; Saadi, K. W.; Buchanan, I. D., Bioresour. Technol. 54, 5 1995.
176. Lopes, G. R., RSC Advances 4, 37244 2014.
177. Bae, J. W.; Choi, J. H.; Lee, Y.; Park, K. D., J. Tissue. Eng. Regen. Med. 9, 1225 2015.

178. Allen, B. L.; Kotchey, G. P.; Chen, Y.; Yanamala, N. V. K.; Klein-Seetharaman, J.; Kagan, V. E.; Star, A., J. Am. Chem. Soc. 131, 17194 2009.
179. Bhunia, A.; Durani, S.; Wangikar, P. P., Biotech. Bioeng. 72, 562 2001.
180. Ulson de Souza, S. M. A. G.; Forgiarini, E.; Ulson de Souza, A. A., J. Hazard. Mat. 147, 1073 2007.
181. Onder, S.; Celebi, M.; Altikatoglu, M.; Hatipoglu, A.; Kuzu, H., Appl. Biochem. Biotechnol. 163, 433 2010.
182. Husain, Q., Rev. Environ. Sci. Biotechnol. 9, 117 2010.
183. Sakuyama, H.; Endo, Y.; Fujimoto, K.; Hatana, Y., J. Biosci. Bioeng. 96, 227 2003.
184. Wagner, M.; Nicell, J. A., Water Res. 35, 485 2001.
185. Auriol, M.; Filali-Meknassi, Y.; Adams, C. D.; Tyagi, R. D.; Noguerol, T.-N.; Piña, B., Chemosphere 70, 445 2008.
186. Beom Lee, K.; Bock Gu, M.; Moon, S.-H., Water Res. 37, 983 2003.
187. Kalsoom, U., Appl. Biochem. Biotechnol. 176, 1529 2015.
188. Eibes, G.; Arca-Ramos, A.; Feijoo, G.; Lema, J.; Moreira, M., Appl. Microb. Biotech. 99, 8815 2015.
189. Kolhe, P., Annu. Res. Rev. Biol. 8, 1 2015.
190. Hong-Mei, L.; Nicell, J. A., Bioresour. Technol. 99, 4428 2008.
191. Sheldon, R. A., Adv. Synth. Catal. 349, 1289 2007.
192. Rad, A. S.; Mirabi, A.; Binaian, E.; Tayebi, H., Int J Electrochem Sci 6, 3671 2011.
193. Durán, N.; Esposito, E., Appl. Catal., B 28, 83 2000.
194. Mohan, S. V.; Prasad, K. K.; Rao, N. C.; Sarma, P. N., Chemosphere 58, 1097 2005.
195. Shim, J.; Kim, G.-Y.; Yeon, K.-H.; Cho, S.-H.; Woo, J.-J.; Moon, S.-H., Kor. J. Chem. Eng. 24, 72 2007.
196. Zhang, F.; Zheng, B.; Zhang, J.; Huang, X.; Liu, H.; Guo, S.; Zhang, J., J. Phys. Chem. C 114, 8469 2010.
197. Bayramoğlu, G.; Arıca, M. Y., J. Hazard. Mat. 156, 148 2008.
198. Niu, J.; Xu, J.; Dai, Y.; Xu, J.; Guo, H.; Sun, K.; Liu, R., J. Hazard. Mat. 246, 119 2013.
199. Moeder, M.; Martin, C.; Koeller, G., J. Memb. Sci. 245, 183 2004.
200. Zhang, J.; Zhang, F.; Yang, H.; Huang, X.; Liu, H.; Zhang, J.; Guo, S., Langmuir 26, 6083 2010.
201. Lee, Y.-M.; Kwon, O.-Y.; Yoon, Y.-J.; Ryu, K., Biotech. Lett. 28, 39 2006.
202. Xiao, Y.; Ju, H.-X.; Chen, H.-Y., Anal. Chim. Acta 391, 73 1999.
203. Lin, J.; Qu, W.; Zhang, S., Anal. Biochem. 360, 288 2007.
204. Bayramoğlu, G.; Arıca, M. Y., J. Hazard. Mat. 156, 148 2008.
205. Bindhu, L.; Abraham, E. T., J. Appl. Polym. Sci. 88, 1456 2003.
206. Peralta-Zamora, P.; Esposito, E.; Pelegrini, R.; Groto, R.; Reyes, J.; Durán, N., Environ. Technol. 19, 55 1998.
207. Zhao, Z.; Lei, W.; Zhang, X.; Wang, B.; Jiang, H., Sensors 10, 1216 2010.
208. Halliwell, C. M.; Cass, A. E., Anal. Chem. 73, 2476 2001.
209. Wilchek, M.; Miron, T., J. Biochem. Bioph. Methods 55, 67 2003.
210. Turková, J., J. Chromatogr. B 722, 11 1999.
211. Mogharrab, N.; Ghourchian, H.; Amininasab, M., Biophys. J. 92, 1192 2007.
212. Gomez, J.; Bodalo, A.; Gomez, E.; Bastida, J.; Hidalgo, A.; Gómez, M., Enzyme Microb. Technol. 39, 1016 2006.
213. Bódalo, A.; Bastida, J.; Máximo, M. F.; Montiel, M. C.; Gómez, M.; Murcia, M. D., Bioprocess Biosyst. Eng. 31, 587 2008.
214. Lai, Y.-C.; Lin, S.-C., Process Biochem. 40, 1167 2005.
215. Pundir, C.; Malik, V.; Bhargava, A.; Thakur, M.; Kalia, V.; Singh, S.; Kuchhal, N., J Plant Biochem Biotechnol. 8, 123 1999.

216. Azevedo, A.; Vojinović, V.; Cabral, J.; Gibson, T.; Fonseca, L., J. Molec. Cat. B 28, 121 2004.
217. Janolino, V. G.; Swaisgood, H. E., Biotech. Bioeng. 24, 1069 1982.
218. Swaisgood, H., Food Enzymology 2, 309 1991.
219. Huang, X. L.; Catignani, G. L.; Swaisgood, H. E., J. Biotech. 53, 21 1997.
220. Brotherton, J. E.; Emery, A.; Rodwell, V. W., Biotech. Bioeng. 18, 527 1976.
221. Chellapandian, M., Process Biochem. 33, 169 1998.
222. Johnson, D. B.; Thornton, D.; Ryan, P. D., Biochem. Soc. Trans. 2, 494 1974.
223. Puvanakrishnan, R.; Bose, S.; Reddi, B., J. Biosci 4, 51 1982.

2 Experimental Materials and Methods

The intent of this study is to evaluate the degradation of partially hydrolyzed polyacrylamide (HPAM) friction reducer using horseradish peroxidase (HRP) enzyme. This chapter outlines the methods and materials utilized for quantifying the degradation of HPAM. Section 2.1 gives a general description of viscosity and non-Newtonian fluids. In addition, this section describes the solutions used for viscosity measurements and methods used to evaluate the HPAM degradation for endpoint (24 hour) and periodic sampling measurements. Section 2.2 explains size exclusion chromatography (SEC) and the methods used in evaluating the molecular weight of degraded HPAM samples. This section also give a description of solutions and methods used for evaluating endpoint (24-hour) molecular weights, in brine and fresh water, and periodic sampling. Section 2.2.2 explains the methods and materials used in the polymer filtration tests. These tests evaluated the HRP system ability to recover flowrate in HPAM damaged filter paper before conducting core flooding. Section 2.4 outlines the methods used to evaluate the amount of oxygen generated by the breakdown of hydrogen peroxide. These experiments were conducted to evaluate the pressure needed to retain the oxygen in solution during preliminary core flooding experiments. Section 2.5 outlines the methods and materials used to conduct core flooding studies. In addition to the final results, preliminary experimental protocol and equipment is included to help explain the reasoning behind the final core flooding setup. Section 2.6 outlines the methods used to evaluate immobilized HRP. This encompasses the methods used for immobilization and evaluating immobilized HRP activity and concentration. Furthermore, methods are included for determining viscosity reduction of HPAM solutions and permeability recovery in core flooding applications.

2.1 Viscosity Reduction of Polyacrylamide Solutions

Solution viscosity can be described as the fluid's resistance to flow. With this in mind, higher viscosity fluids will have a higher resistance to flow than low viscosity fluids. Unit and dimensional analysis of viscosity is described in Equation 19, where (*F*) is a tangential force, (*r*) is the distance between layers, (*A*) is the area, and (*v*) is velocity. This results in the SI units of Pascal (N/m^2)-second or Poise that can be converted to any number of viscosity units such as centipoise (cp) which is widely used in the oil industry.

$$\eta = \frac{Fr}{Av} = \frac{(N * m)}{m^2 * (m/s)} = \frac{N - s}{m^2} = \frac{\mathrm{M}}{\mathrm{LT}} \qquad 19$$

$$\tau_{yx} = -\eta \frac{dV_x}{dy} = \eta\sigma \qquad 20$$

In order to define viscosity in Cartesian coordinates, Figure 2.1 depicts the flow of a fluid between two plates. In this figure, a constant tangential force is applied at the y = 0 plane (in the positive x direction) and the flow of fluid is fully developed, laminar flow. By rearranging Equation 19 we can describe the system in the figure as Equation 20 where (*F/A*) is called shear stress (σ), (τ_{yx}) is the momentum flux, and the differential change in velocity with respect to distance (*dV/dy*) is called shear rate (γ). Equation 20 is also known as Newton's law of viscosity and fluids described by this equation are known as Newtonian fluids. For Newtonian fluids, the viscosity is constant regardless of the shear rate and the relationship between shear rate and shear stress is linear (Figure 2.2). Some examples of Newtonian fluids include water and organic solvents.

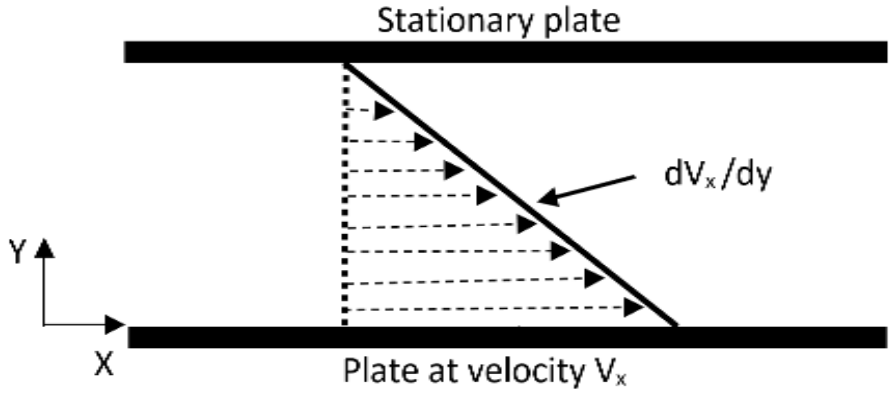

Figure 2.1 Laminar viscosity profile for flow between two plates.

Non-Newtonian fluids include polymeric solutions, slurries, foams, and many others. Some examples of shear rate vs. shear stress and viscosity relationships are shown in Figure 2.2. The most closely related to Newtonian fluid is the ideal Bingham plastic. Bingham solutions act like a solid until the initial shear stress, or yield stress, is overcome. After the yield stress is exceeded the fluid acts Newtonian, or pseudo plastic in nature. Some common examples of Bingham plastics are toothpaste and mayonnaise.

Shear thickening, or dilatant, solutions show increasing viscosity with respect to shear rate. Some of the most common examples of these solutions are cornstarch and water mixtures and water saturated sand. Shear thinning, or pseudo plastic, solutions have decreasing viscosity with respect to shear rate. There are many examples of shear thinning solution but some of the most common are blood, paint, ketchup, and many polymer solutions or mixtures.

In general shear thinning solutions have three characteristic regions to the viscosity profile (Figure 2.3). Located at very low and very high shear rates are the upper (η_i) and lower (η_∞) Newtonian regions. In the middle of the two Newtonian regions is a shear thinning region where a linear correlation occurs when plotting the viscosity vs shear rate on log-log scale. The shear

thinning fluid viscosity profile can be fitted using a number of correlations that are applicable to all or part of the total trend. The Cross and Carreau models are able to fit the entire range of data. Equations 21 and 22 are the Cross[224] and Carreau[225] models respectively. These models calculate the apparent viscosity (η_a) where (α_c) and (λ_c) are related to the polymer relaxation time, or structural breakdown, of the polymer in solution.

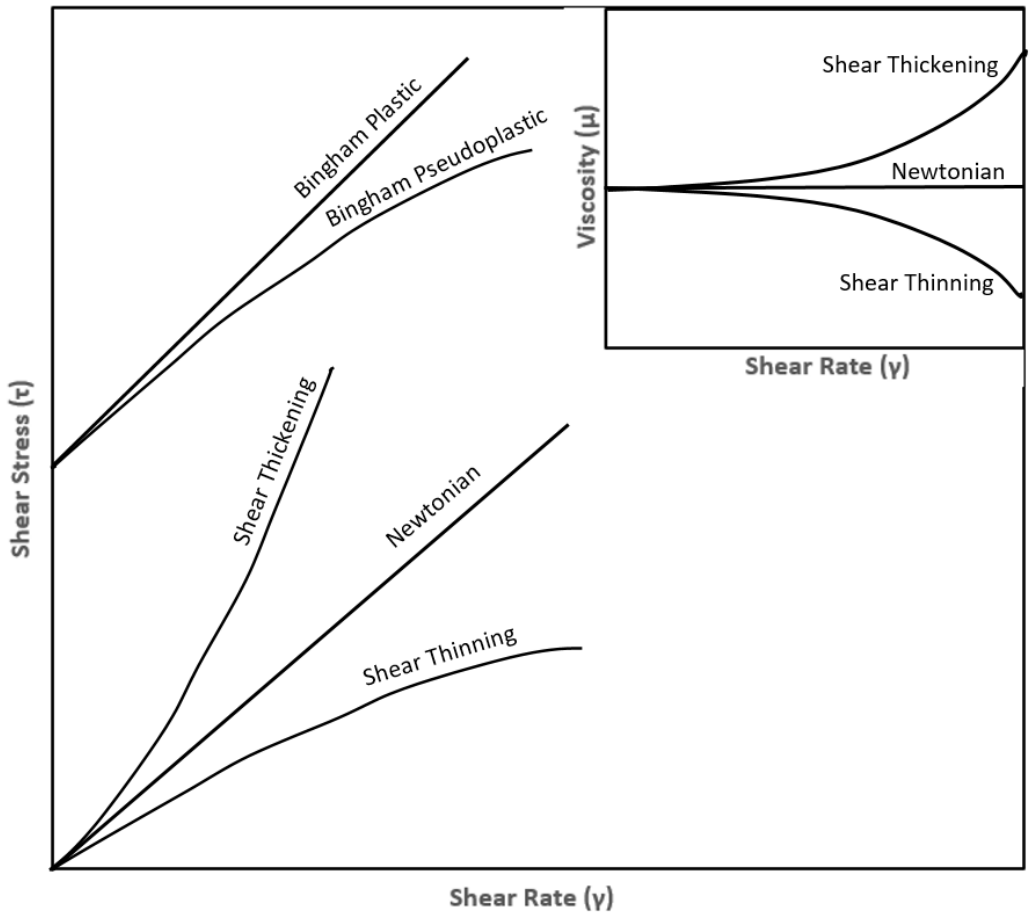

Figure 2.2 Shear rate vs shear stress and viscosity relationships for various types of fluids.

For example, higher values of these constants result in relaxations at lower shear values. Changes in (α_c) and (λ_c) result in curve shift along the x-axis without change in shear thinning

slope or magnitude of upper lower Newtonian regions. The exponents (z) and (N) are dimensionless constants that are determined graphically.

$$\eta_a = \eta_\infty + \frac{\eta_i - \eta_\infty}{1 + (\alpha_c \gamma)^z} \quad 21$$

$$\eta_a = \eta_\infty + \frac{\eta_i - \eta_\infty}{(1 + (\lambda_c \gamma)^2)^N} \quad 22$$

The Sisko Model[226] is shown in Equation 23 and fits data that includes the shear thinning and lower Newtonian regions (η_∞).

$$\sigma = \eta_\infty \gamma + K_s \gamma^{n_s} \quad 23$$

The shear-thinning region is fit with a power law equation, or Ostwald de Waele Model [227] (Equation 24). For the power law model, viscosity is a product of the flow consistency index (K), the shear rate, and the power law index (n) where $n = 1$ is a Newtonian fluid, $n > 1$ is a shear thickening fluid, and $n < 1$ is a shear thinning fluid. Under the condition n=1 the flow consistency index is equal to the viscosity. As shown in Figure 2.3, and from Equation 24, plotting viscosity or shear stress versus shear stress on log-log scale results in a straight line with intercept (K) and slope (n). The power law region is easy to measure using most rheological equipment and is often used to describe trends in shear thinning and thickening fluids. This region was used in the current study to describe rheological behavior of initial and degraded solutions.

$$\eta = K\gamma^{n-1} \ or \ \sigma = K\gamma^n \quad 24$$

In all studies, viscosity was measured using the cone and plate configuration but different rheometers and viscometers were used. The cone/plate geometry, as shown in Figure 2.4, measures the viscosity of a solution by measuring the force necessary to shear a fluid given cone geometry and rotational speed. More specifically, the viscosity of the fluid (η) will determine the torque (τ) necessary to maintain the revolutions per minute (RPM) or angular frequency (Ω). The angle of the cone (θ) ensures that the shear rate applied to the fluid is constant at all locations under the cone.

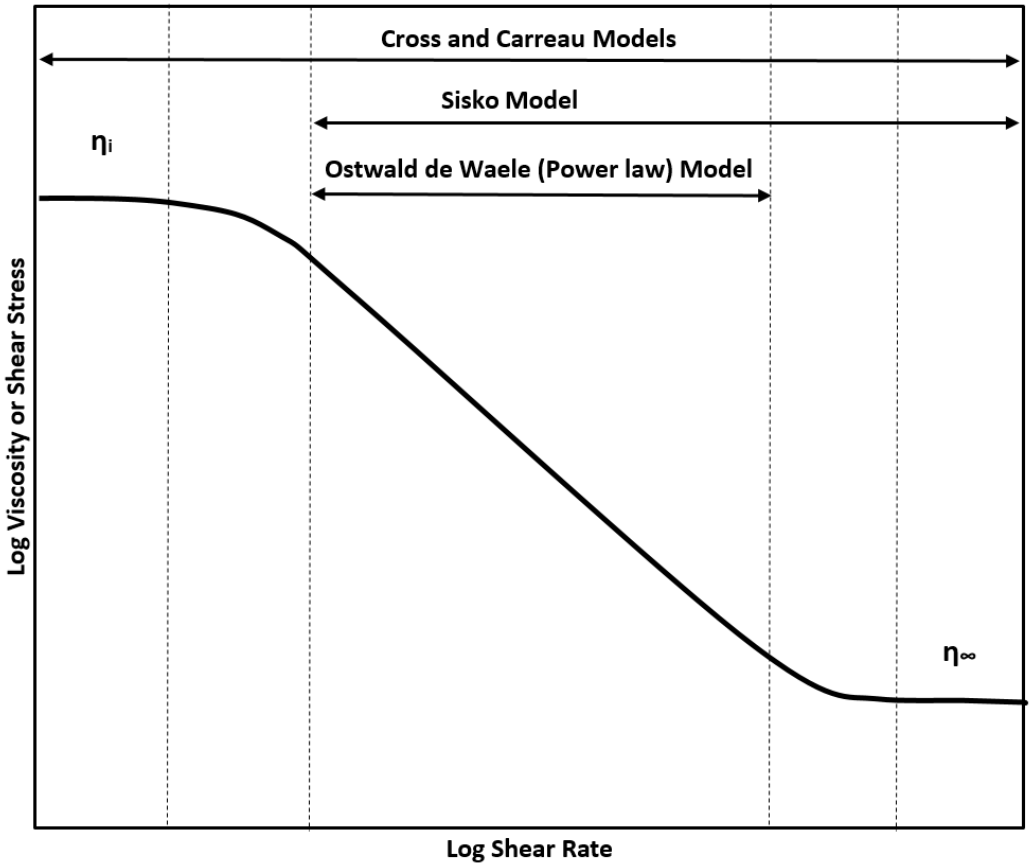

Figure 2.3 Example of full shear thinning viscosity profile plotted on log-log scale. Profile shows upper Newtonian (η_o) and lower Newtonian (η_∞) in conjunction with applicable models for fitting the profile.

The derivation of governing equations are straightforward. First, the fluid contact area (A) on the surface of the cone at any radius (R) is shown in Equation 25. As the derived area spins, the

shear rate (γ) relationship is determined by dividing the linear speed by the area under the cone (Equation 26). The force balance can be developed by multiplying Equation 25 and Equation 26 by the viscosity of the fluid and the resulting equation is given in Equation 27. By integrating Equation 27 over the radial distance of R=0 and R=r the equation for torque can be obtained (Equation 28). From this derived relationship, the viscosity of the solution be can be directly determined. The shear stress (σ) associated with this system is shown in Equation 29 where we can assume that tan (θ) ≈ sin (θ) at the low cone angles. The cone angles used for this study was instrument specific but was < 1° in all cases. The specific equations related to the Brookfield DV-II+ viscometer are provided in the next section.

$$A = \frac{2\pi R dR}{\cos\theta} \tag{25}$$

$$\gamma = \frac{R\Omega}{\mathrm{R}\tan\theta} = \frac{\Omega}{\tan\theta} \tag{26}$$

$$F = A\gamma\eta = \left(\frac{2\pi R dR}{\cos\theta}\right)\left(\frac{\Omega}{\tan\theta}\right)\eta = \frac{2\pi R dR\eta\Omega}{\sin\theta} \tag{27}$$

$$\tau = \frac{2\pi R dR\eta\Omega}{\sin\theta}\int_0^r R^2 dR = \frac{2\pi\eta\Omega r^2}{3\sin\theta} \tag{28}$$

$$\sigma = \eta\gamma = \frac{\mu\Omega}{\tan\theta} = 3\tau/2\pi r^3 \tag{29}$$

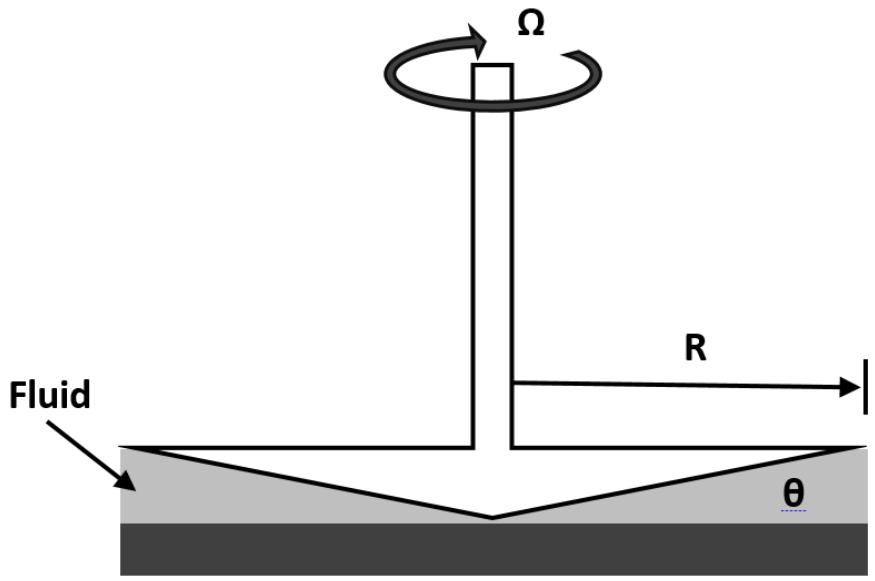

Figure 2.4 Cone and plate configuration used in viscosity measurements.

2.1.1 Preliminary Studies

Preliminary tests were conducted on the Brookfield DV-II+ viscometer. The equations describing the Brookfield viscometer outputs are given in Equations 30-33. The accuracy and repeatability the viscosity measurement using the Brookfield DV-II+ Viscometer are ± 1% and ± 2% of the full-scale viscosity range respectively. The measurement range of the Brookfield viscometer is determined by the rotational speed of the spindle, the size and shape of the spindle, and the full-scale torque of the calibrated spring. Normal operating range for the viscometer is between 10 and 100 torque percent. The constants used for viscosity calculations are given in Table 2.1 and correspond to the CP-40 cone and plate configuration used in experiments. Samples were tested by placing 0.6 ml solution into the cup then the cup was secured and the gap was set according to specifications.

$$\eta(cp) = \frac{100}{RPM} * TK * SMC * Torque \quad (30)$$

$$Shear\ rate\ \left(\frac{1}{s}\right) = RPM * SRC \quad (31)$$

$$Shear\ Stress\ \left(\frac{dynes}{cm^2}\right) = TK * SMC * Torque \quad (32)$$

$$Full\ Scale\ Viscosity\ Range\ (cp) = TK * SMC * 10000/RPM \quad (33)$$

Table 2.1 Constants used in Equations 43-46 for Brookfield DVII+ viscometer.

TK=	Torque constant	= 0.09373
SMC=	Spindle multiplier constant	= 0.327 for CP-40
SRC=	Spindle shear rate constant	= 7.5 for CP-40

The purpose of these studies was to establish working solutions and to test theory. These experiments used were first conducted using 50 % polyacrylamide (PAM, M_w=10000 Da) obtained from Sigma. Horseradish peroxidase Type II (HRP, *Mw*=44000 Da), essentially salt free, lyophilized powder, 150-250 units/mg solid (using pyrogallol) (Sigma) was used in conjunction with β-nicotinamide adenine dinucleotide (NADH, M_w= 709 Da) (Sigma-Aldrich) and 30% hydrogen peroxide (Fisher Scientific) to test degradation. Viscosity of solutions were tested using the Brookfield DVII+ Pro instrument equipped with an SP-40 0.8°/40 mm cone and plate (Brookfield Engineering, Middleboro, MA). Initial 10000 Mw PAM concentration was

determined by tested the viscosity of 50% PAM solutions diluted with 18MΩ reverse-osmosis water (LabconcoWaterPro RO/PS system). These tests determined that 18% PAM solutions were at an acceptable viscosity range for testing on the Brookfield viscometer. Initial component concentrations were determined by fixing the HRP concentration added to the polymer solution and varying the addition of NADH and hydrogen peroxide. HRP concentration was fixed at 45.3 μM (2 mg HRP/ml PAM) then NADH and 30% peroxide were added at 1:2 molar ratio. Most of the initial testing took place using 2-13 mg/ml (2.82-18.3 mM) additions of NADH. Varying amounts of 30% hydrogen peroxide were used to initiate the reaction. These solutions were tested periodically for up to 2 hours at 25°C and elevated temperatures of 35°C. Later tests incubated samples at 35° C for 24 hours before testing the change in viscosity. The solution pH was also adjusted to observed effects on viscosity over a 2-hour period.

Because 10000 M_w PAM is not analogous to the fracture additive, the partially hydrolyzed polyacrylamide (HPAM; M_w = 6,000 kDa) AlcoFlood 935, Lot A2247BOV was obtained from Ciba Specialty Chemicals for further testing. Solutions were made as described in the next section but NADH concentration was adjusted. Initial NADH concentrations of 18.3 mM were adjusted to 1.4 mM because tests showed that HPAM solution viscosity is highly dependent on NADH concentration. A higher initial viscosity was needed to quantify differences between degraded and initial HPAM samples.

2.1.2 Final Solution Components and Concentrations

For the final set of experiments, a higher molecular weight PAM polymer was selected for all subsequent testing. Partially hydrolyzed polyacrylamide (HPAM; Mw = 6,000 kDa) AlcoFlood 935, Lot A2247BOV was obtained from Ciba Specialty Chemicals and is analogous to the polymer used in fracturing applications. Polymer solutions were made by addition of Alcoflood 935 to room

temperature 18MΩ reverse-osmosis water (LabconcoWaterPro RO/PS system) or 2% (w/vol) potassium chloride (Fisher Scientific) solution to form a 2 mg/ml polymer stock solution (2000 ppm). The solution was stirred slowly for approximately 12 hours to ensure complete dissolution of the polymer. A slow stir rate was chosen to ensure that shear degradation of the polymer was avoided. The polymer solution was vacuum filtered through an 8μm filter paper (Micron Separations Inc.) to remove any undissolved polymer aggregates. After filtration, HPAM solutions were refrigerated until needed. Again, Horseradish peroxidase Type II (HRP; Mw = 44,000), essentially salt-free, lyophilized powder, 150-250 units/mg solid (using pyrogallol) (Sigma) and β-nicotinamide adenine dinucleotide (NADH) (Sigma-Aldrich) were added to the Alcoflood 935 stock solution immediately before each experiment. In addition to HRP, soybean peroxidase (SBP, Mw = 41000, Bio Research Products Inc.) was tested using equivalent concentrations.

Test solutions were made by adding components to the Alcoflood 935 stock solution at varying concentrations. Tests were conducted on solutions containing varying HRP and peroxide concentration in the absence and presence of NADH. In all samples containing NADH, a concentration of 1.41 mM (1 mg/ml) was used. Solutions containing varying HRP concentrations were made by the addition of 2, 1, and 0.25 mg HRP/ml HPAM stock solution resulting in concentrations of 45.3, 22.7, and 5.6 μM HRP respectively. Reactions were initiated by addition of 10 μL/ml (peroxide solution/polymer solution) at concentrations of 9.77, 4.89, and 0.977 M. The resulting diluted peroxide concentrations after addition were 9.69, 48.4, and 96.9 mM. For samples not containing peroxide, water was added to maintain a constant dilution of other components. After peroxide/water dilution, the final concentrations of HPAM, HRP, and NADH were 1980 ppm, 45.0 μM, and 1.40 mM respectively. Final solution concentrations are used to designate specific concentrations throughout the results. The pH of 1980 ppm Alcoflood solution

without the addition of the reagents 7.6 ± 0.01. However, with reagents, the pH was between 6.5 and 7.4 with maximum deviation of ± 0.05.

2.1.3 Viscosity after 24-hour Incubation

Viscosities were measured using two digital cone-and-plate viscometers at 25°C (± 0.1°C). Data collected after initial experiments were measured using a Bohlin CS10 Rheometer (Malvern Instruments Ltd, Worcestershire, UK) with a 4°/40 mm cone and plate geometry or an Anton Paar MCR 302 model rheometer (Anton Paar, Graz, Austria) equipped with a CP-50, 1°/50 mm attachment. With the Bohlin CS10 Rheometer, the temperature bath was set to 25°C at least 15 minutes before measurements were taken. The gap was set to the distance 1mm using the provided gap tool. The tool was placed between the cone and plate, the cone was lowered, then the knob at the top of the rheometer was adjusted until the tool made little to no contact with the cone. Initial endpoint measurements, after 24-hour incubation, were tested using the Bohlin CS10 Rheometer at 75 s^{-1} and 25°C (± 0.1°C). A 1.5ml aliquot was used for testing and viscosity was determined immediately after incubation. Viscosity was measured at a shear rate of 75 s^{-1} with a 30-seceond integration time. Measurements with the Bohlin CS10 Rheometer showed deviations of 1.0-0.1% depending on shear rate and viscosity. Reported results are the mean from a minimum of three separate runs/measurements. Reported error is the standard deviation from the mean.

After the method was completely developed, the Anton Paar MCR 302 model rheometer was used for testing. Procedures using this instrument are simplified because the instrument is automated. The temperature is controlled internally by a Peltier temperature control system. The gap is automatically adjusted before viscosity measurement by measurement of the normal force when the cone meets the plate. Testing is conducted by pipetting 0.5 ml of sample onto the plate

and initiating the computer program. The cone automatically lowered via a slide rail and the sample was trimmed. The program allowed 15 viscosity measurements to be recorded for shear rates ranging from 0.1 to 500 s^{-1}. Viscosity was tested before and after incubation at a variety of shear rates.

All samples were prepared in triplicate and incubated at 37˚C. Initial viscosities (η_o) were obtained by measuring samples diluted with water in place of peroxide. The viscosity results were fit with the Ostwald de Waele Model (Equation 24) where the flow consistency index (K) and the power law index (n) are reported in the graphical legends. The power law index can indicate solution trend changes where n = 1 is a Newtonian fluid, n > 1 is a shear thickening fluid, and n < 1 is a shear thinning fluid.

2.1.4 Continuous and Periodic Sampling

Continuous sampling was attempted for reaction solutions using the Brookfield viscometer. In these experiments, solutions containing HPAM, NADH, and HRP were made as previously mentioned with a final peroxide concentration of 96.9 mM. After peroxide addition, 0.6 ml reaction solution was placed in the cup and tested continuously for 15 hours at 35°C. Sample evaporation was prevented by placing electricians tape around the cup to seal junction between cup and instrument. For some samples, the RPM was adjusted from $75s^{-1}$ to $150s^{-1}$ after 4.5 hours of testing to ensure that the viscometer was running within acceptable torque range. Results showed unfavorable outcomes due to instrument limitations so identical experiments were attempted using the Bohlin CS10 Rheometer.

The Bohlin CS10 Rheometer (Malvern Instruments Ltd, Worcestershire, UK) with a 4°/40 mm cone and plate geometry was also used for continuous sampling. Before experiments, the gap and temperature was set as previously mentioned. Concentrations of HPAM, NADH, and HRP were

made a previously stated. After peroxide activation, a 1.5 ml aliquot reaction solution was pipetted onto the plate and the cone was lowered onto the sample. To prevent evaporation, Cannon viscosity standard (28.89 cP at 25°C, Cannon Instrument Company, Cannon Falls, MN) was placed around the sample. The reacting sample viscosity was measured at 35°C for 15 hours at a shear rate of 75 s^{-1}. Again, results revealed definite trends but also showed erroneous results due to oxygen production. Because of the oxygen production, periodic sampling was conducted to capture the reduction in viscosity with time. In order to conduct periodic sampling, 14ml solutions were made and incubated at 37˚C. These solutions were sampled periodically over a 24 hour period by removing a 1.5ml aliquot and immediately determining the viscosity using the Bohlin CS10 Rheometer at 75 s^{-1} and 25˚C (± 0.1°C). Samples were tested at times of 0, 1, 2, 3, 5, 7, 9, 14.5, and 24 hours.

2.2 Size Exclusion Chromatography and Molar Mass Reduction

Size exclusion chromatography (SEC) is a liquid chromatographic technique that separates molecules by size. This technique uses a column containing dual porous material that creates a more torturous flow path for smaller molecules. Figure 2.5 shows an example of column packing and particle flow path. In this illustration, larger molecules cannot fit into the smaller pores creating a more direct flow path and therefore earlier elution times. On the other hand, small molecules can fit into the smaller pores creating a more torturous flow path. Because of flow path, larger molecules elute at earlier times as shown in the Figure 2.5. The resulting peaks from separated partials called chromatograms. The column packing and length, particle molecular weight, pump flow rate, mobile phase composition, and temperature all influence molecule elution times. In order to find the molecular weight of unknown samples, known molecular weight standards are used to create a calibration curve under the same sampling conditions as

unknown samples. Chromatograms created using standards are analyzed for elution time plotted using a semi-log plot of molecular weight versus elution time. This plot will result in a linear correlation that is used to determine the molecular weight of unknown samples.

The number average (M_n) and weight average (M_w) molecular weight of unknown samples are determined using Equations 34 - 36.[228] In order to determine the molecular weight directly from the chromatograms, the representative curves can be broken into arbitrary time or volume (ΔV) increments. Equation 34 is the number of moles polymer (n_i) in a volume increment. The number of moles is a function of incremental concentration (c_i) and molecular weight (M_i). In terms of detector readout (Q_o), the number of moles can be expressed as a function of a proportionality constant (k_p) because $c_i = Q_o/k_p$. Assuming a constant volume increment, and that (M_i) is the same for small incremental volumes, Equations 35 and 36 can be used to determine the average molecular weights directly from the detector output. Polydispersity Index (*PDI*) describes the magnitude of molecular weight distribution and is given in Equation 37. For example, monodisperse samples have a *PDI* of 1.0 with most carefully synthesized polymers exhibiting values close to one and while some very disperse polymers can exhibit values greater than 7.[229]

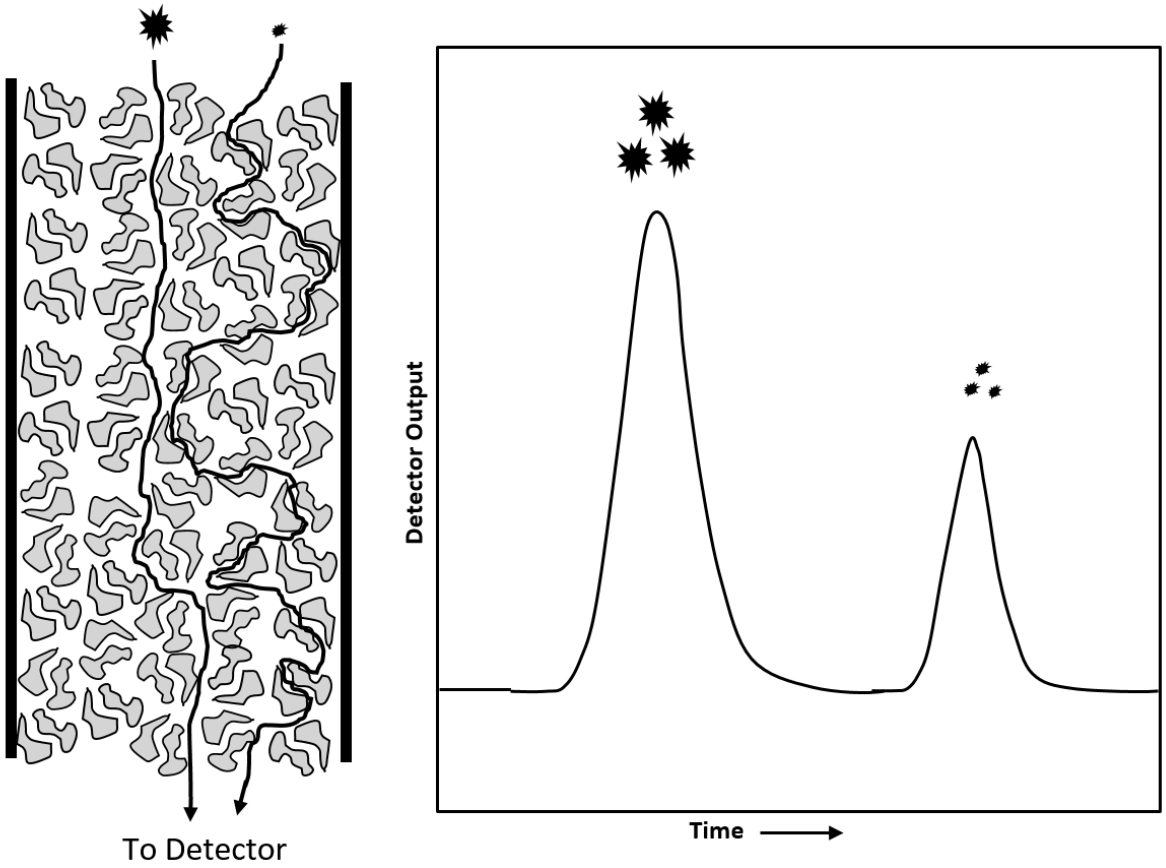

Figure 2.5 Example of particle separation using size exclusion chromatography. Picture left shows particle movement through column. Picture right shows an example of peak elusion with respect to size and time.

$$n_i = \frac{c_i \Delta V}{M_i} = \frac{Q_o \Delta V}{k_p M_i} \tag{34}$$

$$\overline{Mn} = \frac{\sum_i n_i \, M_i}{\sum_i n_i} = \frac{\sum_i Q_o}{\sum_i (Q_o / M_i)} \tag{35}$$

$$\overline{Mw} = \frac{\sum_i n_i M_i^2}{\sum_i n_i M_i} = \frac{\sum_i (Q_o / M_i)}{\sum_i Q_o} \tag{36}$$

$$PDI = \frac{\overline{Mw}}{\overline{Mn}} \tag{37}$$

2.2.1 24-hour Incubation and Periodic Sampling

Molecular weight of the polymer was obtained using two ViscoGEL 08025 GMPWXL columns (Viscotek, Houston, TX) connected in series to a PL-2100 ELSD evaporative light scattering detector (Polymer Laboratories Ltd., Amherst, MA). The detector has a sensitivity range of 1-50 ng on the column. Samples were injected using a Varian Prostar model 410 auto sampler (relative standard deviation < 0.5% using partial loop) and the mobile phase was delivered using dual model 210 Varian Prostar solvent delivery modules (Varian, Palo Alto, CA) with flowrate accuracy of ±1.0% and reproducibility of ± 0.1%. The mobile phase was 20% acetonitrile (Fisher Scientific, Pittsburg, PA) and 80% 0.1M ammonium acetate (Fisher Scientific Pittsburg, PA). Samples were tested at room temperature with a mobile phase flow rate of 1 mL/min and a sample injection volume of 45.0 µL. Molecular weight standards of 27.5, 53.2, 99.0, 201, 1100 (American Polymer Standards, Mentor, OH) and 5000 KDa (Polysciences Inc, Warrington, PA) were used for calibration. The number average (M_n) and weight average (M_w) molecular weights were determined from the chromatograms using Equations 35 and 36. Reported results are the mean from at least three separate runs and error reported is standard deviations from the mean.

For endpoint measurements, samples were incubated at 37°C for 24 hours. To test samples, at least 1 ml of reacted sample was transferred from 15 ml, Nunc centrifuge tubes (Thermo Scientific) into a 2 ml glass sampling vial for use in the auto sampler. For periodic sampling, the reaction took place in the glass-sampling vial for direct transfer to and from the incubator and auto sampler.

2.2.2 Molecular Weight Calibration and Adjustments

Before each set of experiments, the PAM molecular weight standards were tested using the same mobile phase as tested Alcoflood samples. Figure 2.6 depicts the chromatograms obtained

from injecting PAM standards at 1 ml/min. This example is the calibration used for calculating molecular weights for 1980 ppm periodic sampling data depicted in Chapter 3, Figure 3.16. As seen from the calibration standards, size exclusion chromatography results in higher molecular weight components eluting at earlier times. Chromatograms are used to construct a calibration curve by plotting Log_{10} of the known molecular weight versus the elution time (Figure 2.7). Using this correlation, the molecular weights eluted at any time for unknown samples are calculated as previously described.

During the attempt to quantify the kinetics, different concentrations of HPAM were used to find the kinetic order of the reaction. While running the 990 ppm Alcoflood samples and standards there were some observed increases in column pressure for high molecular weight polymer standards and un-degraded HPAM samples. In addition to increased pressure, later elution time was observed. The shift in time was only observed for the initial, un-degraded HPAM sample and 4900 kDa standard resulting in a lower molecular weight values inconsistent with previous data. In order to test for discrepancies, an internal, low molecular weight control was used to ensure peak alignment. The internal control was a small, unidentified peak, found upon HRP addition. Figure 2.8 shows an example of a typical chromatogram collected at time zero and after 24 hours for degradation studies using 990 ppm Alcoflood 935. At first glance, HPAM peaks seem to be consistent, but all other peaks show inconsistency with shift to longer time seen for initial measurement. Peaks obtained for HRP and NADH could be used as an internal standard but were not because peak maximums were not visible due to detector limits. The NADH and HRP peaks only exceeded the detector limits for the 990 ppm HPAM experiments because a larger injected volume was required in order to have a HPAM peak with acceptable noise/peak height ratio.

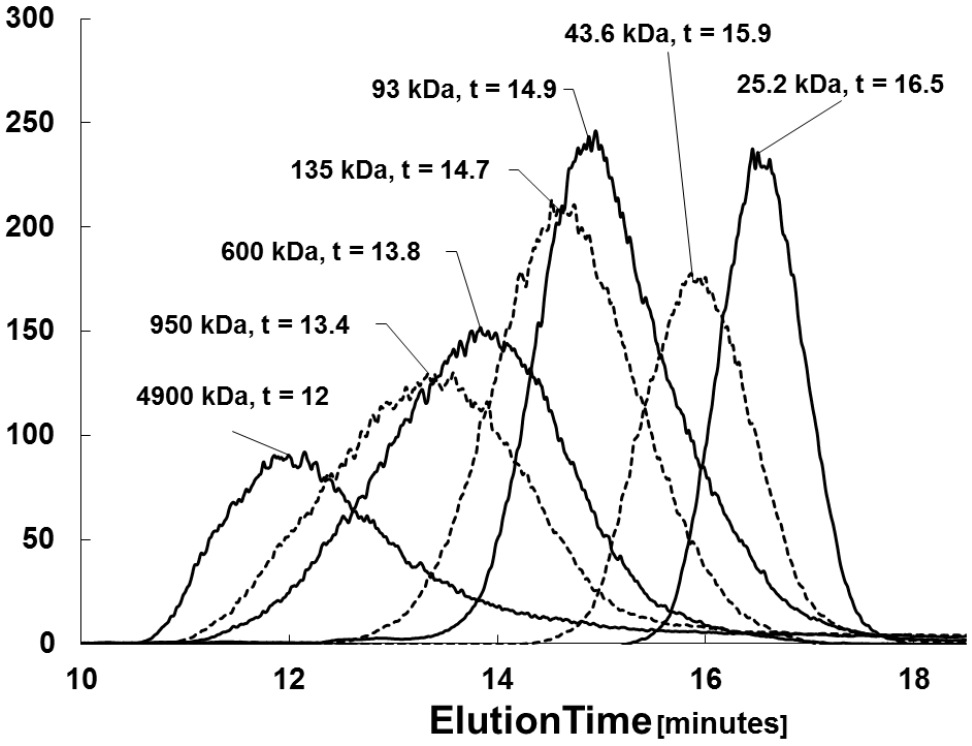

Figure 2.6 Chromatograms showing molecular weight and elution time of PAM standards.

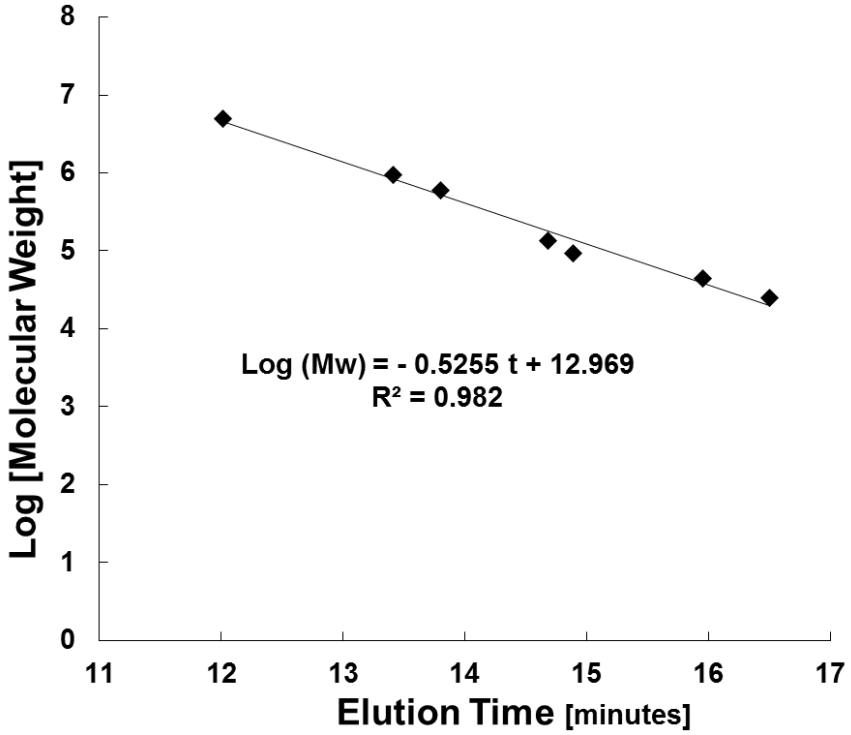

Figure 2.7 Calibration curve constructed using known molecular weight standards from chromatograms shown in Figure 2.6.

To evaluate if the small peak was acceptable as an internal standard, a set of control experiments was conducted to test the consistency of the peak in the absence of HPAM. First, solutions consisting of HRP, NADH and peroxide were tested over a 24-hour period while incubated at 37°C (Figure 2.9). The results from this experimental set show that there is no change in the internal standard elution time (22.35 minutes) with respect to time or peroxide addition when subjected to the same conditions as test samples. Furthermore, the test suggests that the later observed elution time is due to column plugging by the un-degraded, high molecular weight HPAM. In addition, the elution time of the internal standard peak from this study correlates well with the same peak from Figure 2.8 at 24-hours (22.4 minutes). This suggests that the lower molecular weight, degraded HPAM does not cause a shift in the chromatograms. Observations from these tests resulted in mean time shifts of 0.29, 0.39, 0.49 minutes for the three experimental sets. The shift in elution time showed greater differences with the number of sample sets tested which is a result of further plugging. The kinetic order of the reaction was not determined because column plugging ultimately became an issue. Chromatograms in Figure 2.8 are not indicative of HRP and NADH concentrations and show detector overload as indicated by flat plateaus. The high concentration of smaller components does not affect the polymer molecular weight measurement.

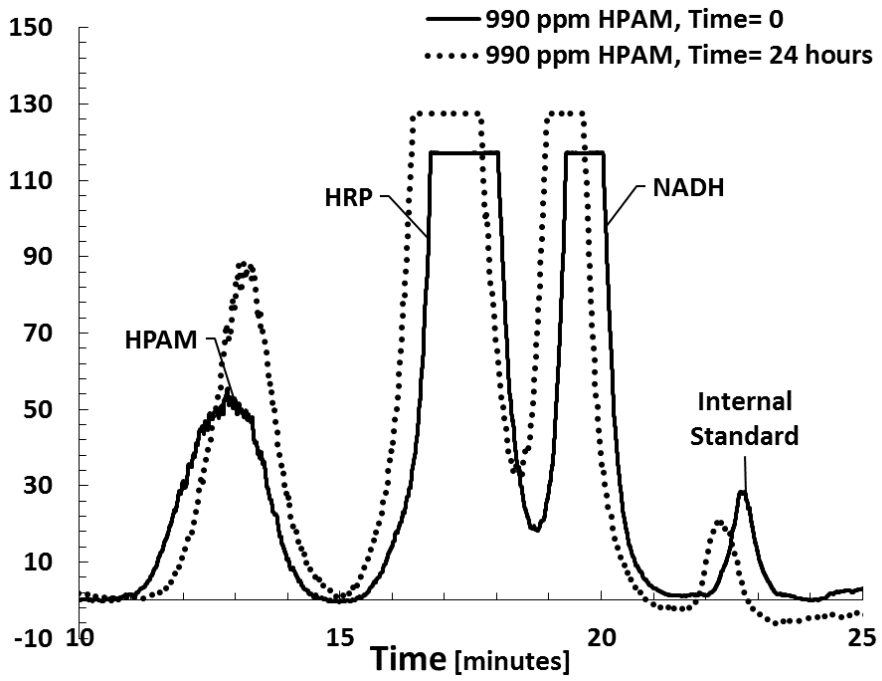

Figure 2.8 Chromatograms showing HPAM, HRP, NADH, and internal standard peaks for 990 ppm HPAM at time zero and 24 hours.

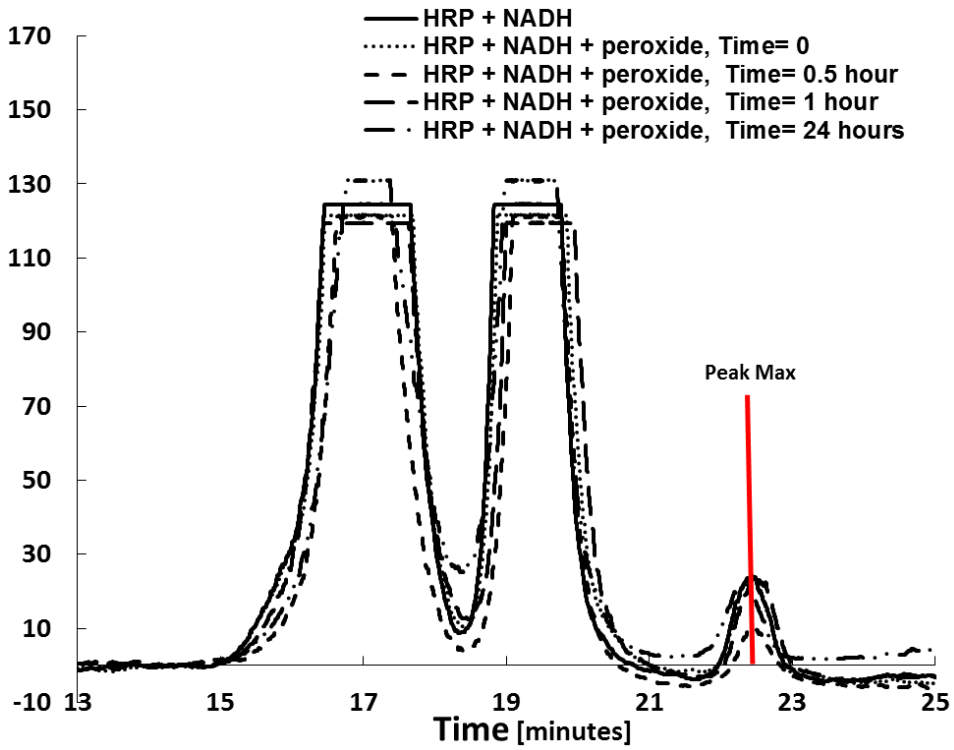

Figure 2.9 Chromatograms depicting no shift in internal standard observed for samples containing HRP, NADH, and peroxide without HPAM.

2.3 Polymer Filtration to Determine Flow Rate Recovery

Filtration experiments tested the HRP/peroxide system effectiveness to degrade filter cake. In addition, these tests were conducted to find the correct concentrations and order of component addition to achieve the best flowrate recovery. The filtration apparatus allowed constant pressure application so that the effluent mass could be measured and the change in flowrate quantified. Tests were conducted using the apparatus shown and described in Table 2.2. All PVC tubing and fittings were purchased from McMaster Carr (Elmhurst, IL). The apparatus used a variety of components to convert from PVC to 0.125 inch tubing. Swagelok (Solon, OH) was utilized to convert from National Pipe Taper Thread (NPT) to 1/8 inch tubing. An Advantec 47mm polypropylene filter holder (Advantec MFS Inc, Dublin, CA) was used in conjunction with 0.1 μm Magna filters (47mm, nylon, Fisher). The PVC valve located under the filter holder is used for fluid shutoff and effluent mass was measured using A&D HF-2000G scale (San Jose, CA).

For all stages of filtration, a constant pressure of 20 psi was applied to the system. Different combinations of system components were used to create the filter cake and the treatment solutions were varied (Table 2.3). Solution concentrations were the same as those used in previous viscosity and molecular weight experiments and were comprised of 2000 ppm Alcoflood 935, 45.0 μM HRP, 1.4 mM NADH, and 96.9 mM hydrogen peroxide in water. Data was recorded using LabVIEW software (National Instruments, Austin, TX)). All flow rate measurements were conducted with water and no air was allowed into the system after initial filter saturation.

Table 2.2 Filtration apparatus numbered by component with corresponding description.

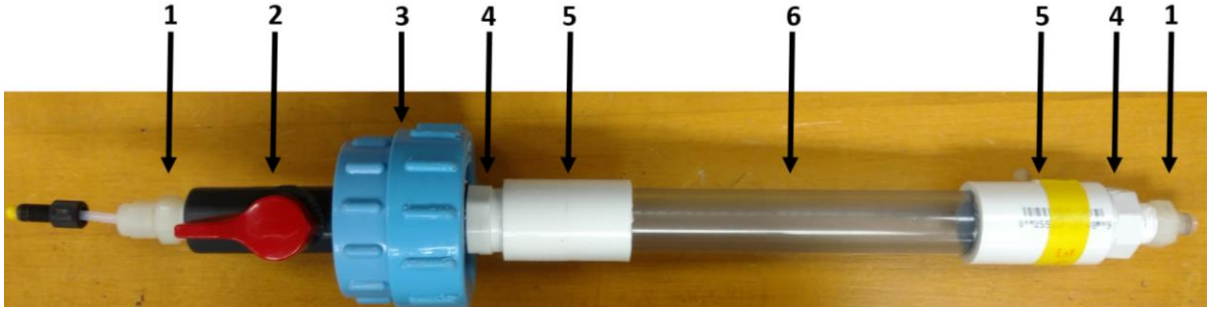

Component #	Component Description
1	0.25 NPT to 0.125 inch male Swagelok connector
2	0.25 inch NPT, PVC ball valve
3	Advantec 47mm polypropylene filter holder
4	0.5 to 0.25 inch NPT reducers
5	0.5 inch PVC coupler
6	0.5 inch outer diameter (OD) Excelon clear PCV/VI, nylon-R-4000

Table 2.3 Description of components used to create filter cake for applied treatment.

Expt #	Filter cake formation	24 hour treatment
1	HPAM	Peroxide
2	HPAM	Peroxide + HRP
3	HPAM	HRP + NADH + Peroxide
4	HPAM+HRP	Peroxide
5	HPAM+HRP	NADH + Peroxide
6	HPAM+HRP+NADH	Peroxide

Procedurally, filter paper was placed in the downstream section of the disassembled filter holder. Then, the filter was saturated with RO water to ensure that no air was present under the filter. The filter holder was assembled and the fluid reservoir was half filled with water. A 25 ml syringe was used to flush residual air out of the system. With the effluent valve shut, the fluid

reservoir was completely filled with water and the air supply was connected. Data acquisition was started, a pressure of 20-psi supplied, and the effluent valve was opened. The mass of effluent water was measured with respect to time. The effluent valve was shut before air reached the filter holder and data acquisition was stopped. From data collected, the initial flowrate (Q_i) through the filter was calculated. Next, the excess water was carefully vacuum suctioned off and 10 ml of 2000 ppm HPAM was placed into the reservoir. Pressure to the system was applied and the polymer solution was filtered. Again, the flowrate to water was obtained to quantify damaged flowrate (Q_d). Then, 10 ml treatment solution was applied to the reservoir. To ensure treatment contact with polymer cake, 2 ml of treatment solution was flushed through the filter holder at 20 psi. The treatment was applied for 24 hours at room temperature, then the excess treatment solution was carefully vacuum suctioned off. The flowrate to water was again obtained for the treated filter cake and the recovered flowrate (Q_r) was calculated. Percent damage and recoveries were calculated using Equations 38-39. A minimum of three samples were collected for each data set and error is reported as standard deviation from the mean.

To observe the effects of cake dissolution, enzyme reaction, and chemical exposures during filtration tests, additional control experiments were conducted. Dissolution of the filter cake (during 24 hour treatment) was measured by creating a cake with 10 ml polymer solution. Procedures for applying treatment mimicked those used in previous experiments but 10 ml water is used in place of treatment solution. The cake set for 24 hours then the excess water was vacuum suctioned off. The flowrate to water was measured and compared to the initial flowrate using Equation 39. The second control experiment observed the effect of peroxide on the filter and filtration system. First, initial flow rate was measured with water, and then 10 ml of 96.9 mM peroxide was added. Again, 2 ml of solution was flushed through the filter and the treatment was

allowed to sit for 24 hours. After 24 hours, the flowrate to water was obtained and compared to the initial flowrate. The final control experiment observed the effect of the total enzyme reaction on the filter. Again, after obtaining the initial flowrate, the treatment solution was added and 2 ml was flushed through filter. The treatment solution sat for 24 hours and then was vacuum suctioned off. The recovered flowrate to water was measured and difference in flowrates were compared as previously described. The equation for calculating percent change was modified for control experiments testing peroxide and enzyme reaction. Since there was no initial damage, the percent change between initial and recovered flowrates were compared.

$$\%\, Damage = (Qi - Qd)/Qi * 100 \quad (38)$$

$$\%\, Recovery = (Qr - Qd)/Qi * 100 \quad (39)$$

2.4 Peroxide Consumption/O_2 Generation and Pressure Effects

For all experiments, oxygen generation by the enzyme reaction created an additional challenges for measuring fluid properties and performance. The following studies were performed to determine the pressure required to keep molecular oxygen in solution. This is particularly important for two reasons. First, if reaction solution is in a core sample, the generated oxygen can change the brine saturation and therefore the permeability. This can cause recovered values to misrepresent the true recovery. Secondly, the increased pressure is indicative of real world application and could affect the degradation of the polymer since oxygen content has shown to directly affect degradation of polymers in the presence of hydroxyl radicals. The first method

observed the consumption of hydrogen peroxide spectrophotometrically. The second directly measured the pressure required to retain oxygen in solution.

2.4.1 Spectrophotometric Monitoring of H_2O_2 Consumption

The spectrophotometric experiment observed the change in peroxide concentration over time. Using a Cary 60 UV-Vis Spectrophotometer (Agilent Technologies, Santa Clara, CA), and 3 ml quartz cuvette, baseline scans of peroxide, water, HRP, and NADH where conducted to obtain peak absorbance values (Table 2.4). A 2 ml reaction mixture of 45.3 µM HRP and 1.41 mM NADH was used to zero the baseline at 240 nm before addition of peroxide. After the baseline was established, addition of 20 µL of 30% peroxide initiated the reaction. Final HRP, NADH, and peroxide concentrations were equivalent to previously used values (45.0 µM, 1.4 mM, and 96.9 mM respectively). The absorbance was monitored for two hours and the consumed peroxide concentration (C) was calculated using Beers law (Equation 40) with extinction coefficient (εl) of 43.6 $(m\text{-}cm)^{-1}$ for hydrogen peroxide.

$$Abs = C\varepsilon l \qquad 40$$

Table 2.4 Absorbance values for components in reaction mixture.

Horseradish peroxidase (HRP)	450 nm
β-nicotinamide adenine dinucleotide (NADH)	340 nm
Hydrogen peroxide	240 nm

2.4.2 View Cell

The view cell experiment directly tested the amount of oxygen produced from the reaction and data was compared to values measured spectrophotometrically. This experiment observed oxygen

solubility in a high-pressure view cell (volume≈ 5ml) as shown in Figure 2.10. An Isco 260D syringe pump (Teledyne Isco, Lincoln NE) and Eldex pump (Eldex Laboratories, Inc, Napa, CA, max 5 ml/min) were used in parallel to deliver enzyme and peroxide solutions. The Isco pump was loaded with a solution consisting of HRP and NADH at concentrations of 90.6 μM and 2.8 mM respectively. A peroxide solution made in 2% KCl at a concentration of 193.8 mM, by addition of 20 μL 30% peroxide per ml water, was delivered using the Eldex pump. These solution concentrations were diluted two fold by pumping each solution into the view cell at equal pump rates. This method ensured that the reaction did not start before the solution reached the view cell. Solutions were pumped into the view cell at a combined rate of 10 ml/min using a backpressure of 2000 psi. After thoroughly flushing the cell with mixed solution, the cell was incubated at 30°C for 24 hours with the pressure maintained at 2000 psi. While internally stirred the pressure was incrementally released until, oxygen visibly appeared in solution. This pressure was use as a minimum pressure in preliminary core flooding studies (using Hassler-type core holder) and results were compared to the spectrophotometric study.

Figure 2.10 High-pressure view cell with backpressure regulator.

2.5 Core Flooding to Determine Recovery in HPAM Damaged Cores

Core flooding studies were conducted to quantify the permeability recovered from HPAM damaged rock using the HRP enzyme treatment. Permeability is an important rock property that is directly related to the rate of oil and gas production. Before placing the core in the core flooding apparatus, important properties were measured for all cores. First, the core dimensions were measured using digital Vernier calipers (Fowler, Newton, MA) with accuracy of 0.001 inch or 0.02 mm. After the dimensions were obtained, the dry mass of the core was determined. The core was the placed into a vacuum desiccator and the air was evacuated at 28 in-Hg in 2% KCl using a Precision model DD 20 vacuum pump (Precision Plus, Sanborn, NY). Core saturation took place for a minimum of 3 hours, or until bubbles no longer formed on the outside of the core. The core was removed from the desiccator and excess brine was removed from the outside

of the core using a brine saturated Kimwipe (Kimtech Science). After measuring the saturated mass, the porosity was calculated using Equation 41.

$$Porosity\ (\phi) = \frac{\frac{saturated\ weight - dry\ weight}{brine\ density}}{bulk\ volume} = \frac{pore\ volume}{bulk\ volume} \quad 41$$

In these studies, brine permeability was quantified for the undamaged, damaged, and treated rock. The permeability (K_b) is often expressed in units of Darcy (D) and is a measurement of a porous material's ability to allow fluid to pass through it. In linear flow, permeability is calculated using Equation 42 and is function of flowrate (Q), cross sectional area (A), pressure drop (ΔP), fluid viscosity (η), and core length (L). Figure 2.11 illustrates the relationship for variables in Darcy equation (Equation 42). In order to ensure that permeability reading is within acceptable error, initial permeability to brine was calculated using a range of flowrates and corresponding pressures. Plotting a variety of flowrates and corresponding pressures should produce a straight line with slope (m_b) and intercept of zero. Equation 43 describes the line generated from plotting flowrate versus pressure drop.

$$Q = \frac{K_b A \Delta P}{\eta L} \quad 42$$

$$K_b = \frac{Q\mu L}{\Delta P A} = \frac{m_b \eta L}{A} \quad 43$$

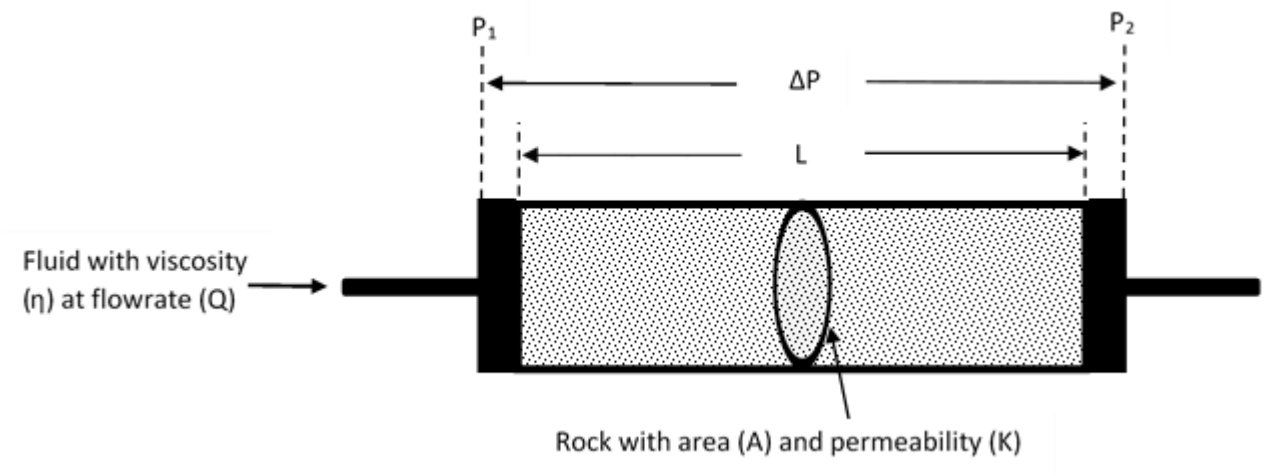

Figure 2.11 Description of variables used in Darcy's equation.

2.5.1 Initial Core Flooding Studies

Initially, permeability was tested for a variety of rock types to determine which rock would be acceptable to use. After base permeability measurements, 1 mL slugs of 2000 ppm Alcoflood was pumped into the core followed by brine flush in between slugs. Pressure was monitored over time to observe changes that would be indicative of polymer damage. From these studies it was determined that Indiana limestone (K_b=1-5 md) showed measurable damage after 1-2 ml polymer injection.

Preliminary experiments consisted of a variety of failed methods due to equipment limitations. These methods are included here to show the reasoning behind the final experimental setup. Some of the earliest work was conducted on a static fluid loss system that was donated by Schlumberger. Figure 2.12 depicts the fluid loss cell disassembled into three sections. On the right is the core holder, in the center is the fluid cell, and on the left is the inlet nitrogen port. Using this apparatus,

the fluid is added to the top of the core and the inlet nitrogen cap is placed on the fluid cell. The assembled cell is situated into a heater vertically and flow is initiated by applying positive nitrogen pressure to the top of the fluid. The mass of the effluent is measured with time and can be used to compare flow properties before and after filter cake formation and recovery. One experiment was conducted using this technique but permeability calculations showed little accuracy. Accurate flowrate and pressure measurements are needed due to the large variation in values that can be created when using low permeability Indian Limestone rock.

Figure 2.12 Fluid loss cell with inlet nitrogen port (left), cylindrical fluid cell (center), and core holder (right).

A Hassler-type core holder was used for all other preliminary core flooding experiments. Modifications were made as experiments progressed and are explained later. A Hassler-type core holder (1-inch inner diameter, made in house) was used to test permeability recovery (Figure 2.13). The middle of the Hassler core holder consists of a 1-inch Viton rubber sleeve where the core is placed. A void space between the rubber sleeve and the outer metal shell creates an annulus filled with oil. When the holder is fully assembled (as shown), the port in the side can be used to apply an overburden pressure to the sleeve that prevents fluid from bypassing the core. Overburden pressure was applied using an Enerpac P392 hand pump (Milwaukee, WI). The gauge on the side of the core holder indicates applied overburden pressure. This core holder allowed fluid to be

pumped though the core at accurate flowrates and the pressure drop could be determined directly using pressure transducers. Two Validyne pressure sensors (Validyne Engineering, Northridge, CA) were used with maximum pressures of 50 and 500 psi for accurate reading over low and high ranges. Pressure data was recorded using LabVIEW software (National Instruments, Austin, TX) and pressure data collected was within 0.1% of maximum pressure for each sensor. An Isco 260D-syringe pump (Teledyne Isco, Lincoln NE) and Eldex pump (Eldex Laboratories, Inc, Napa, CA, max 5 ml/min) were used in parallel to deliver enzyme and peroxide solutions. The Isco pump was used to deliver brine for permeability measurements and enzyme/NADH solution for damage treatment. During treatment stage, the Isco pump was loaded with a solution consisting of HRP and NADH at concentrations of 90.6 μM and 2.8 mM respectively. The peroxide solution was made in 2% KCl brine at a concentration of 193.8 mM, by addition of 20 μL 30% peroxide per ml brine, was delivered using the Eldex pump. As described in the view cell experiments, these solution concentrations were diluted in half by pumping each solution into the core at equal pump rates.

Figure 2.13 Hassler core holder for flooding one-inch diameter cores.

In all experiments, 2% KCl brine was used to make polymer solutions, treatment solutions, and perform permeability measurements. Furthermore, all experiments measured the initial (undamaged) permeability, damaged core with 2000 ppm Alcoflood, measured damaged permeability, applied treatment, and measured recovered permeability. Initial brine permeability is calculated using the linear correlation between pressure and flowrate (Equation 43). All subsequent fluid flows were conducted at 0.2 ml/min. Damage was created using the Eldex pump to deliver various HPAM polymer volumes. After polymer injection, damaged permeability to brine was calculated using Darcy's law when flow pressure was stable (Equation 42). Treatments were applied using varying volumes injected and allowed to sit for 24 hours at 30°C. The recovered permeability to brine was measured to brine after 15 hours flow time. The first few experiments only utilized the dual pumps, Hassler core holder, and pressure transducers. The following experiments led to the evolution of experimental apparatus and procedure resulting in the final experimental setup illustrated in Figure 2.14. The following describes the reasons for using additional equipment:

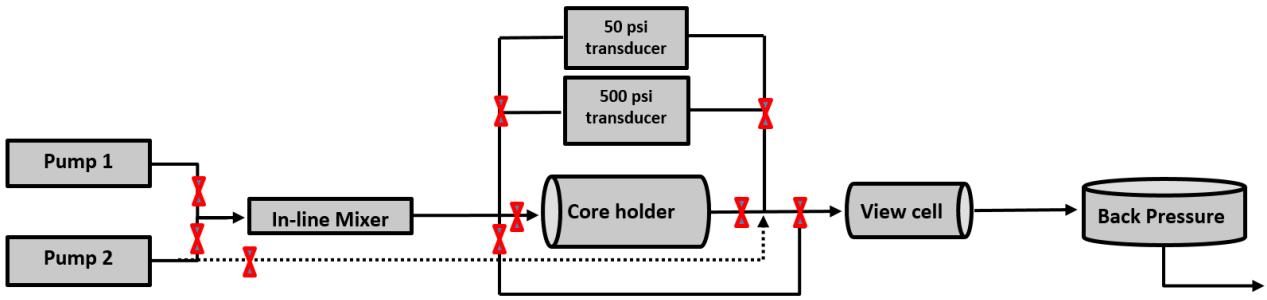

Figure 2.14 Final core flooding setup using the Hassler core holder.

1. The first experiment applied 10 ml Alcoflood 935, and then applied 16 ml HRP treatment. This experiment used no backpressure and oxygen generation by reaction proved to be a problem. A backpressure regulator and high-pressure view cell was incorporated and

system pressure was maintained at minimum of 600 psi for subsequent experiments. The view cell was used to observe if any visible oxygen was in the core effluent after enzyme reaction occurred.

2. In the next experiment, damage was created using 15 ml polymer solution and recovery was tested using 17 ml HRP treatment. Backpressure was 1000 psi and large enzyme aggregates were visible after treatment. Further damage was thought to be a result of enzyme aggregation at high pressure. Treatment volume was lowered to 2 ml and backpressure was reduced to 600 psi for subsequent experiments.
3. Further damage and aggregation was observed for lower backpressure and lower treatment volume. A flow loop around core holder was incorporated so flow could be reversed when measuring permeability. Reversed flow also prevented enzyme solution from being flushed through the core.
4. Additional damage was still observed and a significant amount of HPAM damage was recovered by reverse flow. Observations revealed ridges in the Viton rubber sleeve used in core holder. In addition, black residue was observed on inlet side of core thought to be causing permeability damage. Further investigation showed that rubber sleeve was not resistant to free radicals. Due to rubber incompatabiltiy, thin wall fluorinated ethylene propylene (FEP) heat shrink (McMaster Carr) was placed around core to prevent contact with a new rubber sleeve (Figure 2.15). Core and inlet lines were saturated with brine before heat was applied to prevent loss of core saturation.

Figure 2.15 Core and spacers held together using heat shrink.

5. Further damage was observed regardless of flow direction. An inline mixer was incorporated, before the core holder, to ensure peroxide and HRP mixing during treatment application. Treatment volume was reduced to 0.5 ml. The inline mixer was 3/16 inch outer diameter, 24 element (Cole-Parmer Instrument Co, Vernon Hills, IL) placed tightly in steel tubing and connected inline using Swagelok fittings (Figure 2.16).

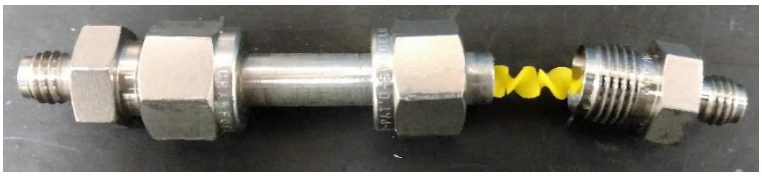

Figure 2.16 Inline mixer incorporated before core holder to ensure HRP/peroxide mixing.

Unfavorable results in all experiments, regardless of modification, showed the need for a new approach. The new approach needed to be free radical resistant, accurately measure permeability, and treat the surface of the core without reaction solution entering the core. At this stage surface treatment is particularly important due to additional damage by the enzyme, generation of oxygen by the reaction, and because it simulates treatment conditions in the reservoir.

2.5.2 Final Core Flooding Experiments using Resin Encapsulated Cores

In order to solve issues mentioned using the Hassler core holder, cores were encapsulated in clear PVC. Cores were cut to 1 inch diameter, 0.7 inch length and encapsulated in 1 inch length,

schedule 80 clear PVC (1.5 inch outer diameter, McMaster Carr). Encapsulation was conducted in a plastic mold (made in house) with Play-Doh molding compound (Hasbro, Pawtucket, RI) as shown in Figure 2.17. In the center of the plastic mold, a 0.125-inch cutout provided a place to put the molding compound. As seen in the figure, the molding compound fills the cutout but is level with the next layer in the mold. Before encapsulating, the outside of the cores were coated with a thin coat of epoxy using a Easypoxy K-2 repair kit (Cytec Solvay Group, Woodland Park, NJ) and allowed to cure for 24 hours. Pre-coating the cores with a thick epoxy prevented the thinner resin, used for filling, from entering the pore space in the core. The resin-coated core was gently pushed into the molding compound and the excess compound was removed. The PVC is centered on the core and space between the core and PVC was filled with Armstrong C-4 resin and D activator (Easton, MA) at a ratio of 4:1. The resin was allowed to cure in the mold for 24 hours. After being removed from the mold, the side contacting the molding compound was sanded flush using Norton P120 grit and Gator grit 320-B sand papers (McMaster Carr)

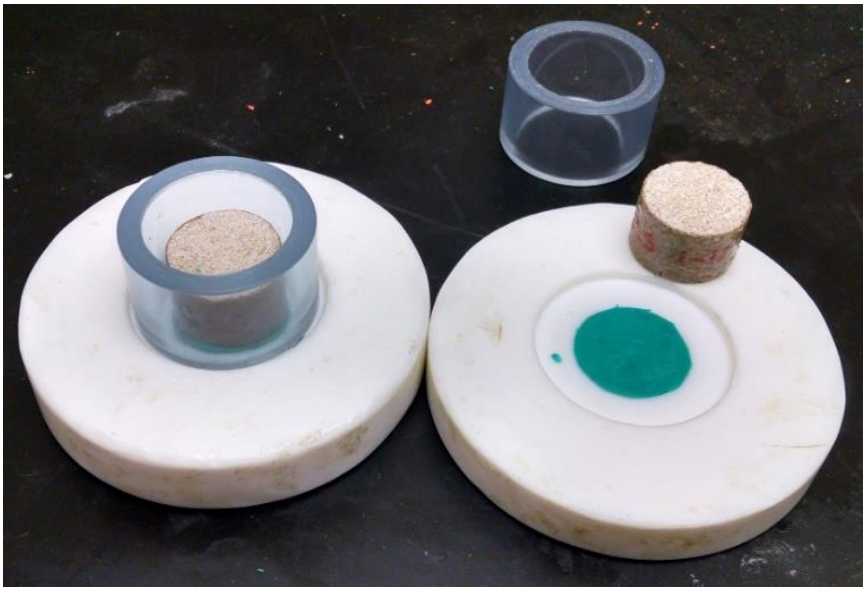

Figure 2.17 Core encapsulation using plastic mold, molding compound and PVC.

The experimental setup in Figure 2.18 was used to accommodate the new holder. An Isco 260D-syringe pump (Teledyne Isco, Lincoln NE) and Eldex pump (Eldex Laboratories, Inc, Napa, CA, max 5 ml/min) were used in parallel to deliver enzyme and peroxide solutions separately. The Isco pump was used to measure brine permeability and deliver enzyme/NADH solutions for damage treatment. During the treatment stage, the Isco pump was loaded with a solution consisting of 12 ml HRP and NADH at concentrations of 90.6 μM and 2.8 mM in 2% KCl brine respectively. A peroxide solution made in 2% KCl brine at a concentration of 193.8 mM by addition of 20 μL, 30% peroxide per ml brine was delivered using the Eldex pump. The inline mixer shown in Figure 2.16 was used to ensure treatment mixing. Two Validyne pressure sensors (Validyne Engineering, Northridge, CA) were used with max pressures of 50 and 500 psi for accurate reading over low and high ranges. Experiments were conducted at atmospheric pressure and treatment was applied for 24 hours at 30°C.

The core holder was made in house and could be used with aluminum-encapsulated or PVC-encapsulated cores. Figure 2.18 shows the disassembled core holder (bottom left), the final PVC encapsulated core (bottom center), and the assembled core holder with enzyme solution (bottom right). The free space above the core was about 10 ml. The top of the core holder contained two ports positioned across from one another. One port was used to create brine cross flow for air evacuation and the port opposite was used for venting and effluent waste. The orientation of the core holder allowed fluid to enter the top and fill the void space. This apparatus acts similar to the traditional fluid loss cell but can measure the permeability accurately. In addition, treatment can be applied to the core surface without disturbing the filter cake. The core encapsulation method alleviates the chance of rubber degradation by free radical generation as seen with traditional, Hassler core flooding setups. The following steps were taken for core preparation and testing:

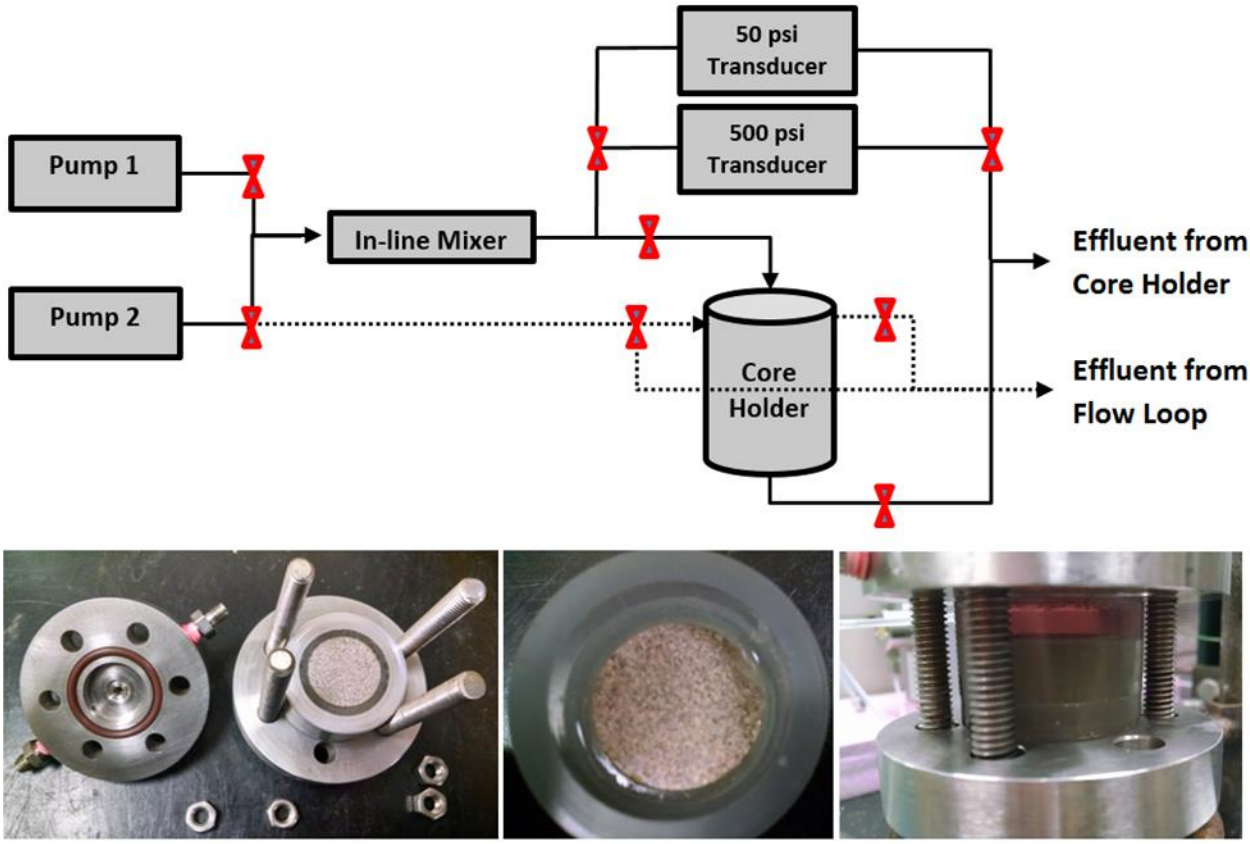

Figure 2.18: Top: Schematic of the entire core flooding apparatus. Bottom left: Picture of core holder with aluminum/epoxy encapsulated core. Bottom middle: Picture of the PVC and epoxy encapsulated core. Bottom right: Encapsulated core in core holder. Picture also depicts application of enzyme treatment.

1. Core dimensions and porosity was obtained using procedure described in Section 2.5 and Equation 41.
2. The core was placed into the flooding apparatus and air in the void space was displaced with 2% KCl brine. The pressure drop versus flowrate relationship was created (Figure 2.19). The permeability of the core to brine was determined using Darcy's Equation relationship (Equation 43) where (m_b) is the slope of the line.
3. A 1 ml slug of 2000 ppm Alcoflood 935 was then injected at a flowrate of 0.2 ml/min followed by brine injected at the same flowrate until the pressure stabilized (Figure 2.20).

The pressure stabilized between 1-2 hours after initial brine injection. The pressure and flowrate, after pressure had stabilized, was used to determine the damaged permeability using Equation 42.

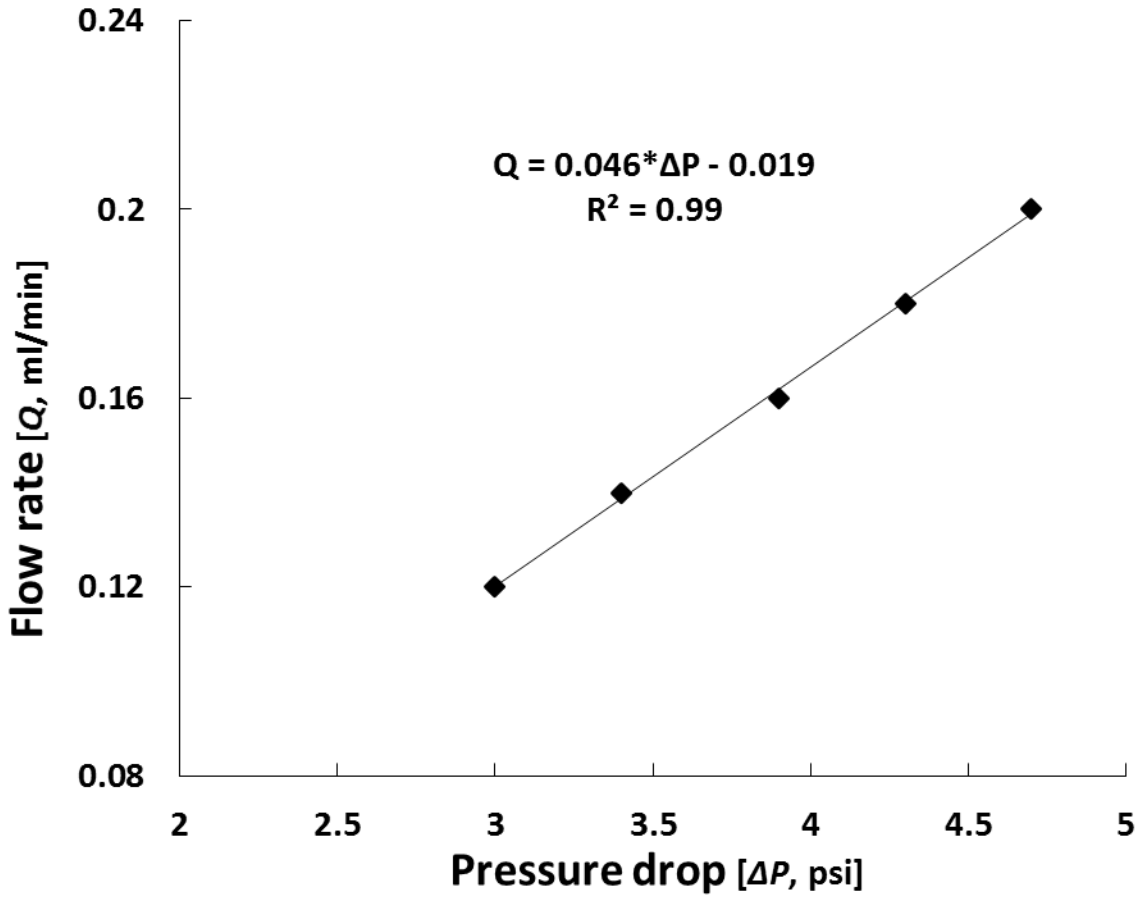

Figure 2.19 Pressure vs flowrate correlation for core ILS 1-3. Data was used to calculate undamaged permeability.

4. A void space was made above the core using air pressure to push brine through the core. Air pressure was applied using the Isco syringe pump at the same pressure as the final value observed during permeability measurement of damaged core. Careful observation was used to ensure that no air was injected into the core. After the void space was created, the valve

on the effluent (downstream side of core) side was shut and the top of the core was vented to atmospheric pressure.

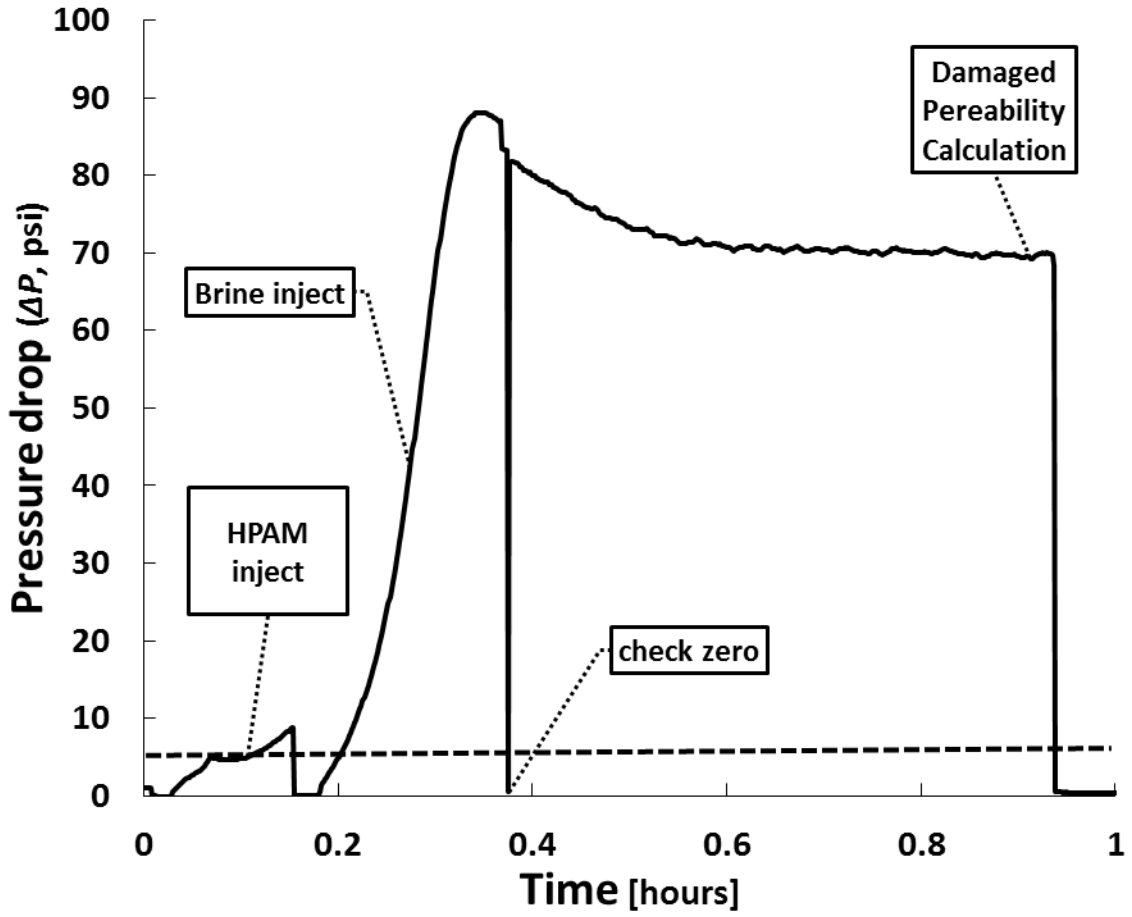

Figure 2.20 Example of core ILS-3 pressure profile during damage with polymer and brine flush for permeability measurement at a flowrate of 0.2 ml/min. Dotted line represents pressure at same flowrate for undamaged core.

5. While venting, 24 ml enzyme treatment was applied to the top of the core by filling the void space at a combined pump flowrate of 2 ml/min (1.0 ml/min for each pump). The excess reaction solution was circulated to ensure target treatment concentration. The top venting valve was left open to atmosphere and treatment solution was incubated on the core at 30 °C for 24 hours.

6. After 24 hours, brine circulated through the top of the void space (using the flow loop) evacuated the air and oxygen created above the core during the reaction. Then, brine was pumped through the core at a flow rate of 0.2 ml/min for 15 hours and recovered permeability was calculated based on the corresponding pressure (Figure 2.21).

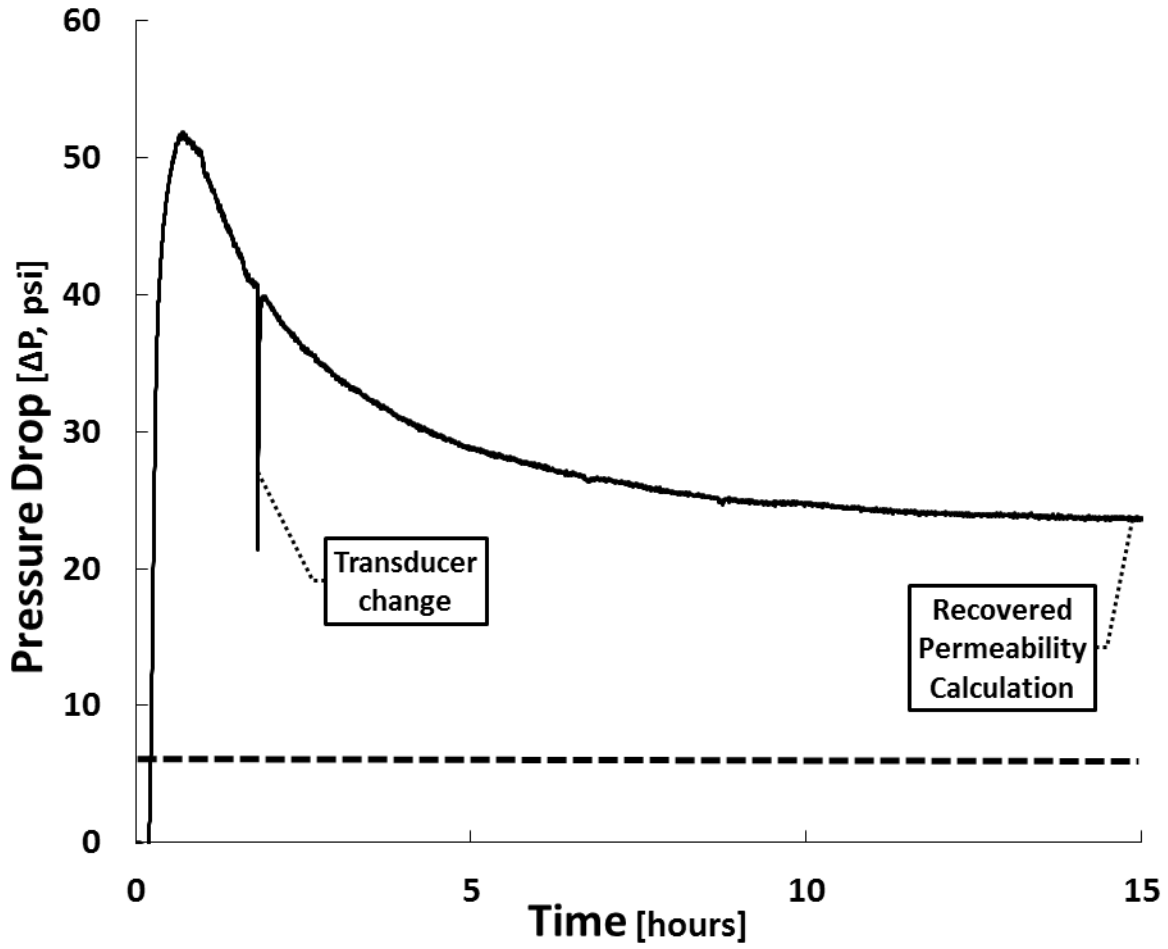

Figure 2.21 Example of core ILS-3 pressure profile after HRP/NADH/Peroxide treatment at a flowrate of 0.2 ml/min. Dotted line represents pressure at same flowrate for undamaged core.

As with the filtration experiments, various components were tested to quantify individual contribution to permeability recovery. The full experiment quantified the permeability recovery with treatment by the full HRP, NADH, and peroxide system. Additional tests were conducted to permeability recovery, after damage, attributed to the 15-hour flush, HRP and NADH without

peroxide, and peroxide alone. One additional study looked at the effects of the full enzyme treatment on the carbonate rock without HPAM damage.

2.6 Enzyme Immobilization on Silica Substrates

Enzyme immobilization was conducted to evaluate damage observed from flowing free enzyme through the core. Immobilization was conducted on glass beads and Ottawa fracturing sand and immobilized concentration and activity were quantified. The immobilized enzyme was tested for ability to degrade HPAM by measuring reduction in solution viscosity. Furthermore, immobilized samples were used to recover permeability in core flooding experiments and values were compared to results obtained using free enzyme.

2.6.1 Substrate Type and Preparation

The results of the core flooding study showed that forcing enzyme treatment solutions through the core creates additional permeability reduction. To eliminate the chances of the enzyme getting into the pore space, and reducing permeability, the enzyme was covalently bonded to a solid substrate. Enzyme immobilization on 75 µm, acid washed glass beads (Supleco, Bellefonte, PA) acted as a control to immobilization on crude Ottawa fracture sand. Both solid substrates were subjected to the same treatments and the immobilized activity and concentrations were determined. The following steps were taken to immobilize HRP with steps 1-3 illustrated in Figure 2.22. Base, acid, toluene, and peroxide were purchased from Fisher Scientific. Silanization was conducted using (3-aminopropyl) triethoxysilane (APTES, 99%, Sigma-Aldrich).

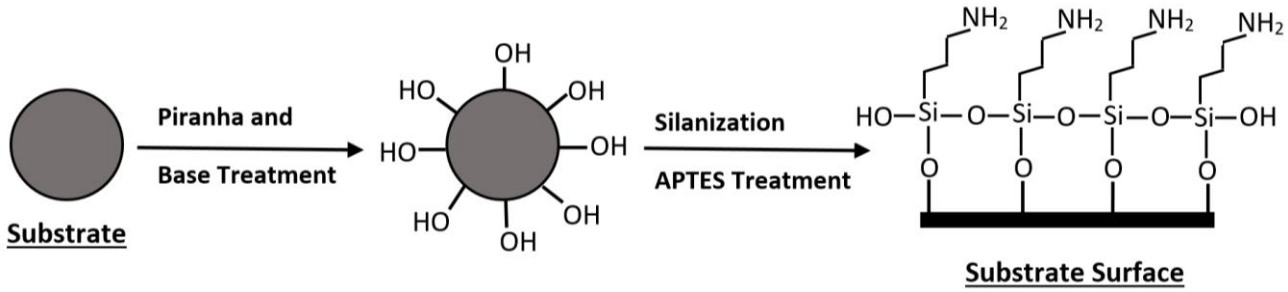

Figure 2.22: Steps for silanization of glass beads and Ottawa sand surfaces.

1. Cleaning the sand and glass surface was conducted by first subjecting substrates to a hydroxylating piranha etch, 3:1 H_2SO_4 (Fisher): 30% H_2O_2 in a beaker at 80°C for 1 hour according to Peltier.[230]
2. Following the same literature source, the substrate surface was then subjected to a base treatment. 5:1:1 H_20: NH_4OH: 30% H_2O_2 under sonication for a minimum of 1 hour.
3. The amine containing compound (3-aminopropyl) triethoxysilane (APTES), depicted in Figure 2.23, was then attached by submersing 20 grams substrate into 5% APTES solution made in anhydrous toluene for 4 hours at room temperature. APTES (shown below) undergoes dehydration to attach itself to the hydroxyl groups exposed on the sand/glass surface. After APTES treatment, the sand/glass was washed with toluene, acetone, and air-dried. Samples were stored and used as needed.

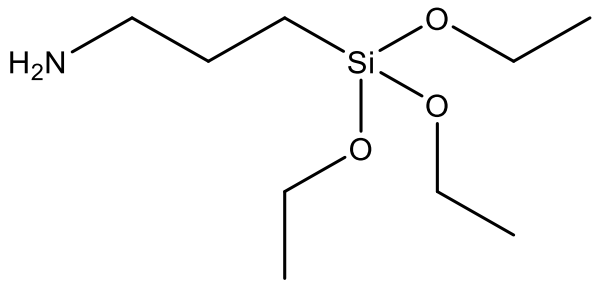

Figure 2.23 APTES compound used to pretreat glass and sand surface.

4. The next step used the cross linker glutaraldehyde (Figure 2.24) to bridge the NH_2 groups on the glass and amino acids in HRP. Sand and glass were treated with 2.5% glutaraldehyde (50% in water, Sigma) in 50 mM phosphate buffer saline (PBS, pH=7.4, Flucka) under agitation at room temperature for 1 hour.

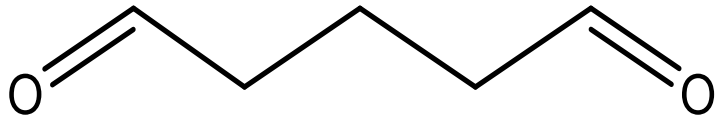

Figure 2.24: Glutaraldehyde cross linker.

5. After washing the sand and glass in 50 mM PBS, to remove excess glutaraldehyde, 5 ml of 113.3 µM (5 mg/ml) HRP was added per gram activated substrate. The HRP and substrates were agitated for 24 hours at 4°C. Analysis of the supernatant concentration change and sand activity was conducted. Enzyme activated sand was used to observe its ability to reduce the viscosity of HPAM in solution. In addition, the immobilized enzyme was used later in core flooding experiments to determine recovered permeability.

2.6.2 Concentration and Activity of Immobilized Enzyme

Concentration change was determined by analyzing the supernatant after enzyme 24-hour exposure to substrate. Concentrations were calculated by diluting all samples (5 mg/ml initial concertation) by 1:4 then measuring the absorbance at 405 nm. The standard curve in Figure 2.25 (n=3) was used to calculate the concentrations based on the absorbance values measured. The

immobilized concentration was quantified by the change in concentration measured in the supernatant.

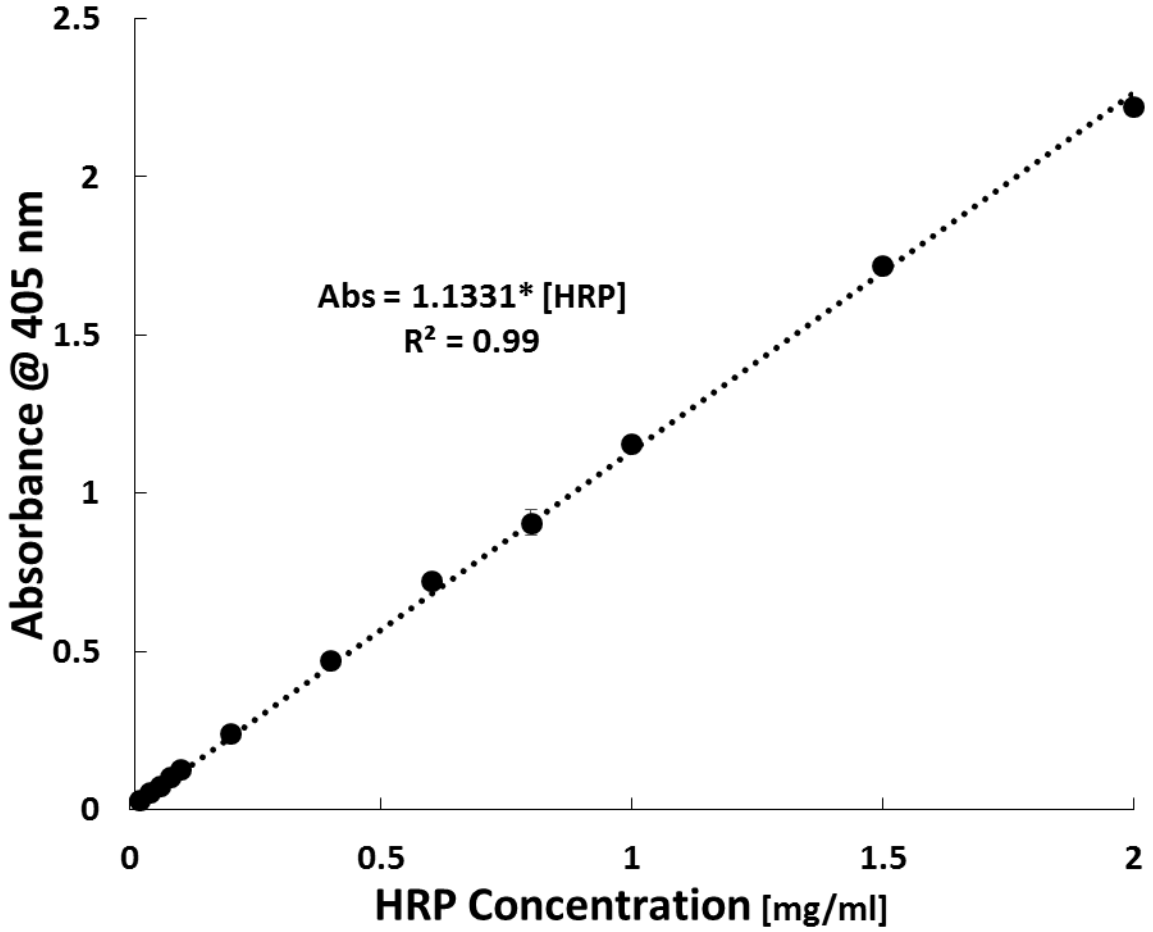

Figure 2.25 Standard curve used to calculate change of HRP concentration in supernatant after immobilization. Calibration created at 25°C, (n=3).

The activity of the immobilized enzyme and supernatant was measured using a colorimetric assay. In this assay Pyrogallol (99% ACS reagent, Sigma-Aldrich) is converted into Purpurgallan (Reaction 44) and the conversion can be measured spectrophotometrically at a wavelength of 420 nm. A Cary 300 Bio UV-Vis spectrophotometer (Varian) was used to measure the activity. The standard protocol (Sigma) for measuring free HRP in solution is as follows.

$$H_2O_2 + Pyrogallol \xrightarrow{HRP} H_2O + Purpurgallin \quad (44)$$

1. Reaction mixture was created in 3ml cuvette by addition of 2.10 ml RO water, 0.32 ml 100 mM PBS, 0.16 ml 0.027% (w/w) hydrogen peroxide, and 0.32 ml 0.5% (w/v) pyrogallol.
2. Solution was mixed using a stir bar and solution was allowed to equilibrate to a temperature of 20°C.
3. To activate the reaction, 0.10 ml of 0.04-0.07 unit HRP solution was added and the absorbance was monitored for 3 minutes. For solution blanks, 0.10 ml of 100 mM PBS was added in place of HRP.

The activity of free enzyme in the supernatant was calculated using Equation 45 where change in absorbance for blanks and test samples determined the difference in activity before and after immobilization. For the purpose of these tests the volume (*Vt*) was 3 ml, extinction coefficient (ε_c) was 12 (mM-cm)$^{-1}$ for Purpurgallan, the dilution factor (*DF*) was 625, and volume enzyme (V_e) was 0.10 ml.

$$\frac{Units}{ml\ HRP} = \frac{\left(\left(\frac{\Delta A_{420}}{20\ sec}\right) test - \left(\frac{\Delta A_{420}}{20\ sec}\right) blank\right) * Vt * DF}{\epsilon_c * Ve} \quad (45)$$

The standard protocol was modified slightly to measure the activity of immobilized enzyme. Solutions were made up to the concentrations used for the blank sample (mentioned above) and all components but peroxide were placed in the cuvette. Before addition of peroxide, about 10 mg of HRP treated sand or glass was placed in the cuvette. The cuvette was put in to the spectrophotometer and the solution was mixed with a stir bar. The peroxide was then added and

the data was collected for three minutes. Blank samples used the addition of 100mM PBS in place of peroxide. Equation 46 is the modified equation where the dilution factor and volume enzyme are zero and the unit activity was calculated per milligram substrate. An example of the absorbance vs time data collected is depicted in Figure 2.26 where dA/20 is the maximum velocity (V_{max}) from the absorbance vs time relationship.

$$\frac{Units}{mg\ Substrate} = \frac{\left(\left(\frac{\Delta A_{420}}{20\ sec}\right) test - \left(\frac{\Delta A_{420}}{20\ sec}\right) blank\right) * Vt}{\epsilon_c * Ms} \quad 46$$

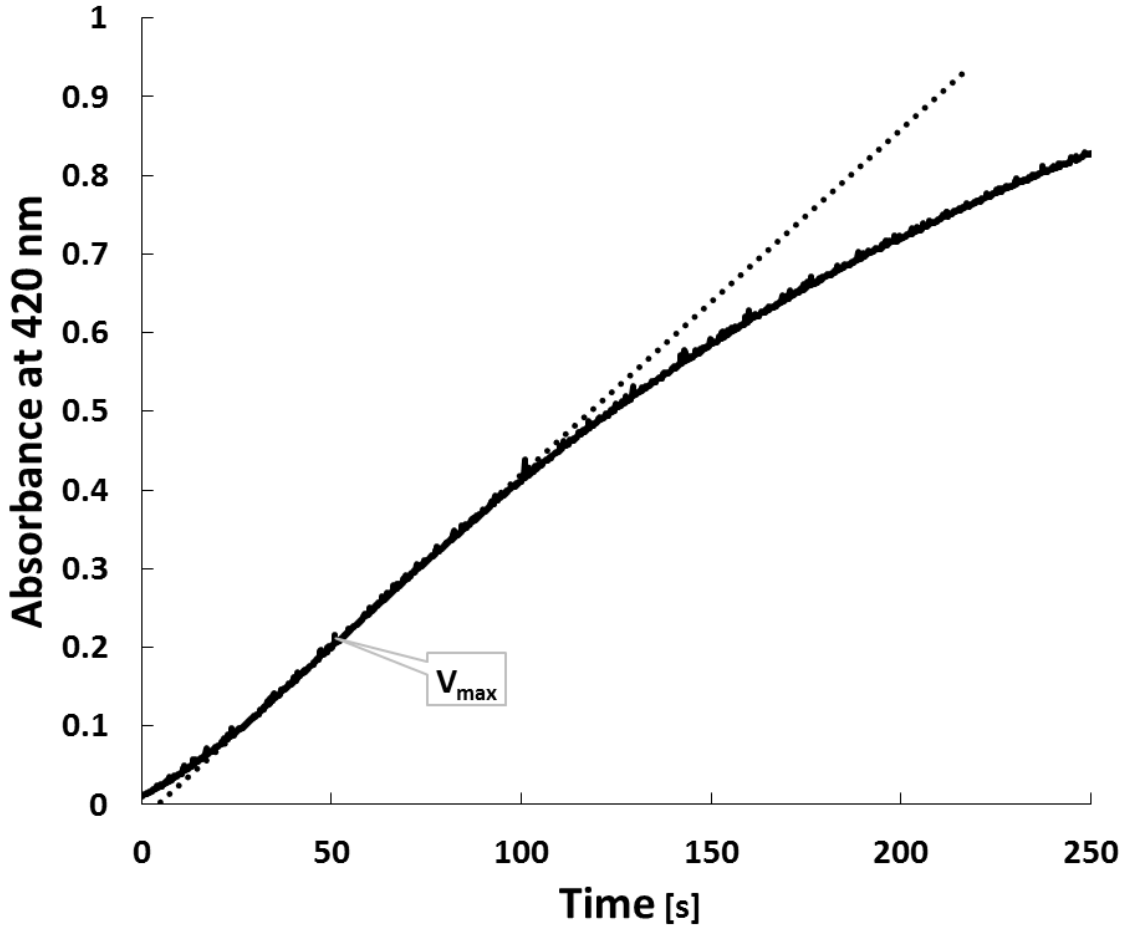

Figure 2.26 Example of absorbance vs time data collected for immobilized enzyme conversion of Pyrogallol to Purpurgallan.

2.6.3 Reduction in HPAM Viscosity with Immobilized HRP

Reduction in viscosity was measured vs time for immobilized free enzyme. The control for this experiment contained sand and peroxide but no HRP. The immobilized enzyme sample contained 0.5 g of *treated* sand. HRP, NADH and peroxide concentrations were used that mimicked the previous viscosity studies. First, 1.4 mM NADH was made up in 2000 ppm Alcoflood 935 and the polymer mixture was then added to the HRP immobilized sand in a 4:1 volume solution: weight sand ratio. The reaction was activated by addition of 10 µl/ml, 30% peroxide (96.9 mM final concentration) before the first viscosity measurement. The free enzyme sample contained 0.5 g of *untreated* Ottawa sand as a control. Solutions were prepared as deiscribed above but 0.516 mg of HRP was added to the sample. This amount of HRP was calculated from the previous concentration studies which determined an immobilized concentration of 1.032 mg HRP/gram sand. Samples with no HRP contained 0.5 g of *untreated* Ottawa sand. Measured volumes were placed back into reaction vials so not to change the enzyme concentration.

2.6.4 Immobilized HRP Application in Core Flooding

The same procedures were followed as for previous core flooding experiments (Section 2.5.2) but the sand was added to the top of the core after the damage permeability was measured. For example, after damage the headspace above the core was filled with air, the top of the core holder was removed, and 1g of HRP immobilized sand was added to the top of the core. The core holder was reassembled and the NADH/peroxide treatment was added the same procedure and concentration as previous core flooding experiments. The reaction was allowed to incubate at 30°C

for 24 hours at which time brine was flushed through the core for 15 hours. After the 15-hour brine flush, the recovered permeability was calculated. At the end of the experiment, the sand was removed from the top of the core and the recovered permeability was tested to observe permeability change due to sand addition.

2.7 References

224. Cross, M. M., J. Colloid Sci. 20, 417 1965.
225. Byron Bird, R.; Carreau, P. J., Chem. Eng. Sci. 23, 427 1968.
226. Sisko, A., Ind. Eng. Chem. 50, 1789 1958.
227. Mooney, M.; Black, S. A., J. Colloid Sci. 7, 204 1952.
228. Lewandowska, K., J. Appl. Polym. Sci. 103, 2235 2007.
229. Labet, M.; Thielemans, W., Chemical Society Reviews 38, 3484 2009.
230. Shafer-Peltier, K. E.; Haynes, C. L.; Glucksberg, M. R.; Van Duyne, R. P., J. Am. Chem. Soc. 125, 588 2003.

3 Viscosity and Molecular Weight Reduction

This chapter presents the viscosity and molecular weight data obtained using horseradish peroxidase (HRP) and soybean peroxidase (SBP) to degrade partially hydrolyzed polyacrylamide (HPAM). Preliminary viscosity studies and trends observed during method development can be found in Chapter 5. In the current chapter, Section 3.1 shows end-point viscosity measurements collected after protocol was established. These studies observe reduction in HPAM viscosity in the absence of various enzyme components (controls), with varying HRP (in the presence and absence of NADH), in 2% KCl brine, and in the presence of SBP in place of HRP. Section 3.2 presents the results obtained from periodically sampling the viscosity of HPAM in the presence of varying enzyme activities and peroxide concentrations. In Section 3.3 the molecular weight reduction was measured using size exclusion chromatography. Molecular weight reduction was quantified after 24-hour incubation in fresh water and brine. Additional periodic sampling was conducted using two HPAM concentrations. Although a thorough investigation is needed to properly quantify the kinetics, Section 3.4 describes general kinetic fits using the presented viscosity and molecular weight data. Further discussion is given in Section 3.4.1 and a summary of the findings can be found in Section 3.6.

3.1 Viscosity Reduction after 24-hour Incubation

Experiments were conducted after 24-hour incubation at 37°C to observe changes in viscosity and to compare degree of HPAM degradation. Viscosity of solutions were measured using the Anton Paar rheometer at various shear rates and 25°C before and after incubation for data normalization. Normalization is necessary to compare overall viscosity reduction of samples with

different component additions. Control experiments observed the effect viscosity reduction due to the addition of different components. Further investigation was conducted for samples containing different amounts of HRP in the presence and absence of NADH. Furthermore, reactions were conducted in both fresh water and 2% KCl brine solutions. Additionally, Alcoflood 935 degradation catalyzed by soybean peroxidase was tested and compared to results obtained using HRP.

3.1.1 Controls after 24-hour Incubation

Control experiments were conducted to identify the effect of each of the components on nominal initial viscosity (η_o) of the polymer solution with different additives e.g. water, peroxide solution, HRP solution, and NADH solution (Figure 3.1). The addition of any of these components, in amounts similar to the degradation experiments, to the stock polymer solution decreased the viscosity at all shear rates. The addition of HRP seemed to have a larger effect on diminishing the viscosity than the addition of NADH. Furthermore, there was little to no change in initial viscosity observed for HPAM solutions containing HRP and NADH when compared to HRP alone. The power law model (Equation 24) is used to describe data viscosity trends where viscosity is a product of the flow consistency index (K), the shear rate, and the power law index (n) where $n = 1$ is a Newtonian fluid, $n > 1$ is a shear thickening fluid, and $n < 1$ is a shear thinning fluid. Power law constants shown in Figure 3.1 are representative of the loss in viscosity and shear thinning associated with addition of components. These initial viscosities are used to normalize the reacted sample viscosity for comparison between samples with varying component additions and concentrations.

$$\eta = K\gamma^{n-1} \ or \ \sigma = K\gamma^{n} \quad (47)$$

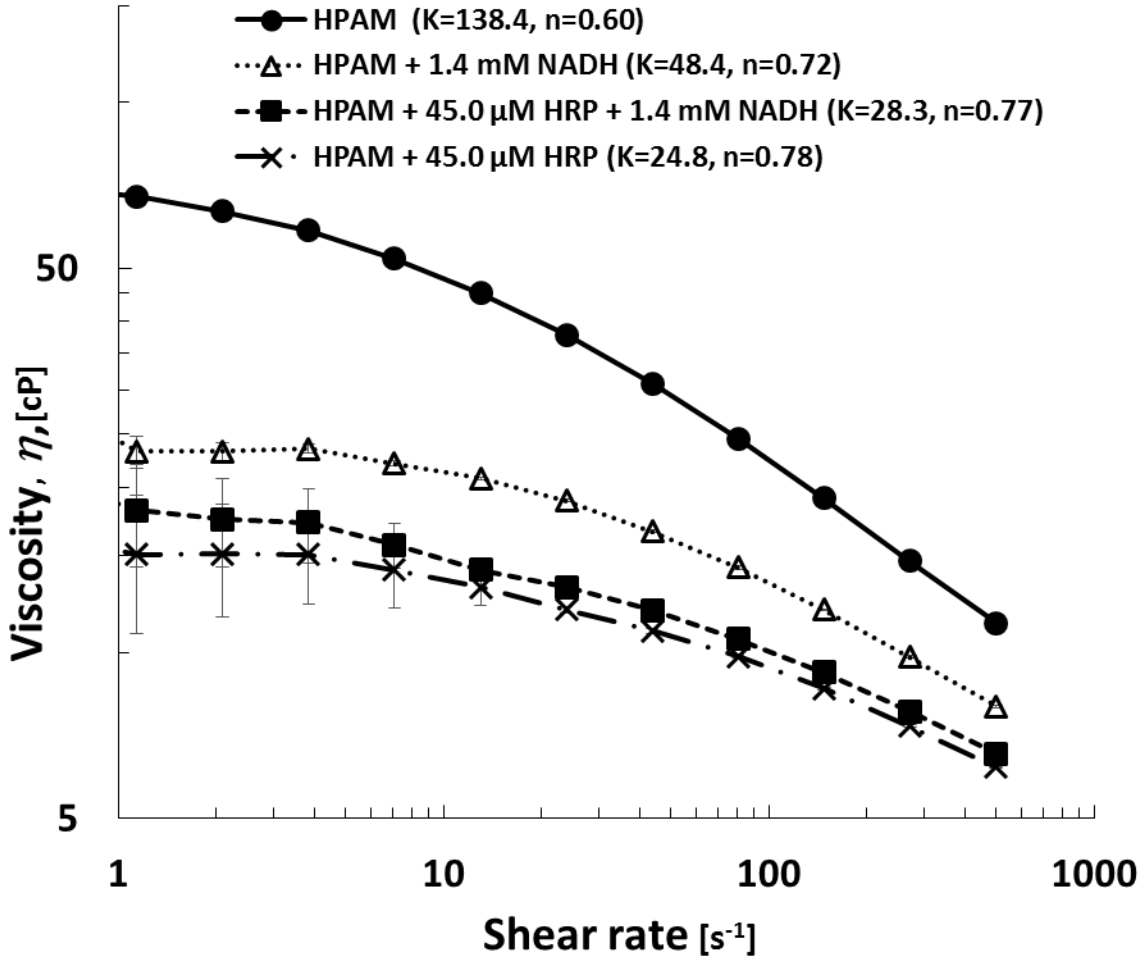

Figure 3.1 Viscosity of 1980 ppm HPAM and viscosity reduction observed from component addition. Initial viscosity was measured at 25°C before incubation; lines are smoothed data (n=3).

The use of hydrogen peroxide (H_2O_2) alone, after 24 hour incubation at 37 °C, has very little effect on HPAM solution viscosity. Figure 3.2 illustrates the change in viscosity relative to the initial solution viscosity at time zero (η_o) at each shear rate. As shown in Figure 3.2, after HPAM solutions undergo 24 hours incubation in the presence of peroxide the fractional change in viscosity decreases only slightly (~2-4%). When NADH is added, in addition to H_2O_2, virtually no reduction was noted within 24 hours. Therefore, without the enzyme, HRP, little to no

degradation of HPAM (as evidenced through solution viscosity) was observed. As solutions with NADH and H_2O_2 experience virtually no background degradation, NADH was added to most of the model studies performed here so that the effect of the HRP without the small background degradation could be determined. Studies comparing the degradation with and without NADH are included below, and in the following sections, demonstrate that NADH would be unnecessary in a practical application. For solutions containing HRP, the magnitude of the viscosity reduction is proportional to the amount of peroxide added to the solution. For mixtures with similar composition of HPAM, NADH, and HRP, increasing the concentration of peroxide results in increased degradation of HPAM as evidenced by lower viscosity after a 24-hour incubation. For instance at peroxide concentrations of 48.4mM and 96.9mM with NADH, the viscosity at a shear rate of 75 s^{-1} was reduced by about 65% and 70% respectively. As shown, the fractional decrease does change somewhat with shear rate. The fractional change indicates larger differences in fractional decrease at relatively large and small rates. The power law index (n) for the same solutions show increased shear thinning characteristics with increased peroxide concentration. The effect of NADH as a moderator of polymer degradation, in the presence peroxide, is seen in Figure 3.2 by the difference in samples not containing HRP. In addition, the greatest reduction in viscosity (about 81%) was observed using a peroxide concentration of 96.9mM without NADH. HPAM degradation under this condition showed similar rheological behavior to the unreacted sample (as noted by the relatively flat slope for normalized data).

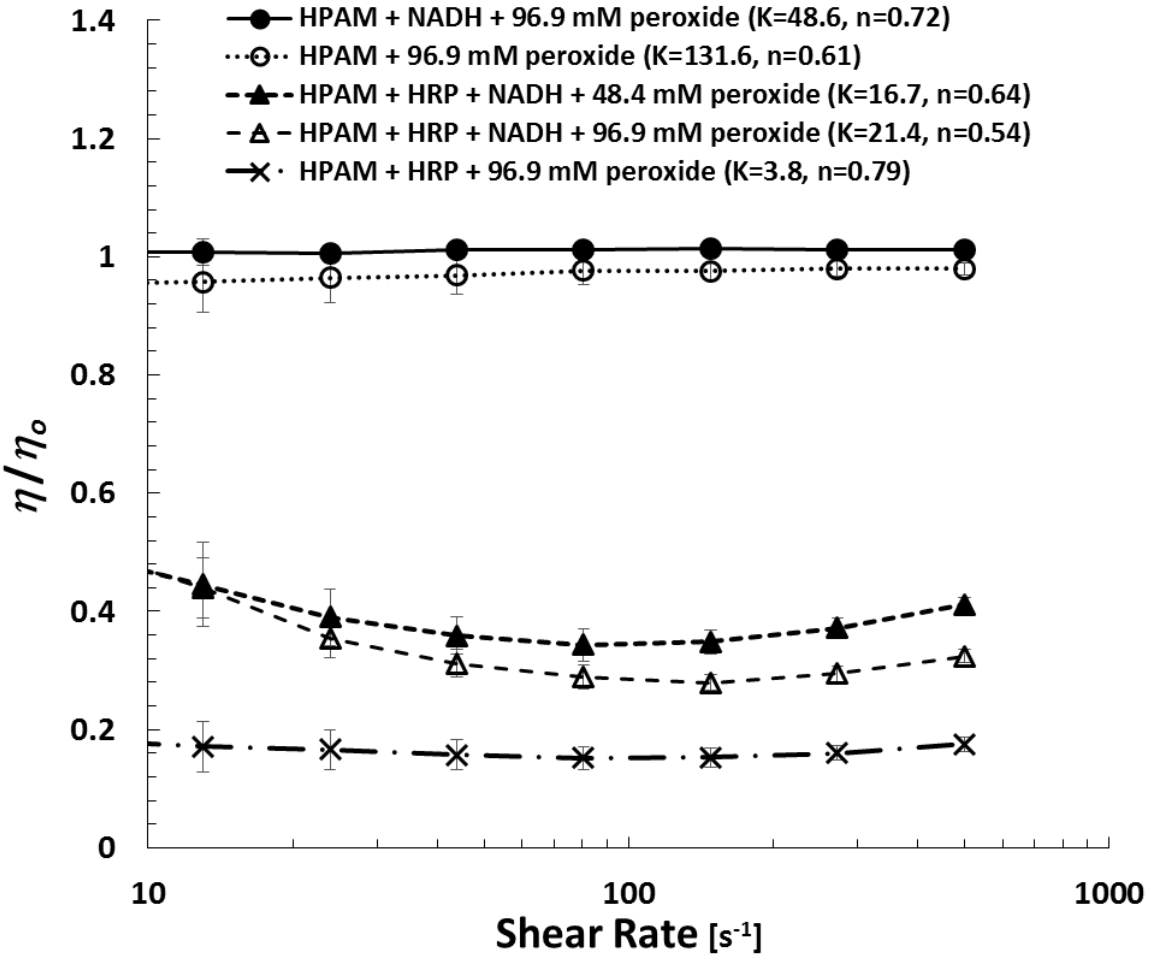

Figure 3.2 Variation of viscosity at 25°C with shear rate for 1980 ppm Alcoflood 935 samples containing varying peroxide concentration and the presence or absence of 45.0 μM HRP and/or 1.4 mM NADH after 24 hour incubation at 37°C. Power law constants K and n are representative of degraded HPAM trends; lines are smoothed data (n=3).

3.1.2 HRP Concentration on HPAM Viscosity Reduction

The amount of horseradish peroxidase affects the rheology of the resulting solution after incubation. Figure 3.3 illustrates the reduction in viscosity at different shear rates for three different concentrations of HRP (i.e. 5.6μM, 22.7 μM, and 45.0μM). At an enzyme concentration of 5.6 μM, the viscosity reduction is approximately 75% at a shear rate of 10 s^{-1} while at 500 s^{-1} the reduction is only ~58%. Thus, a weaker shear thinning (n=0.93), almost Newtonian, solution

remains after incubation. However, at an HRP enzyme concentration of 45.0 μM, a greater shear thinning solution results at low shear rates (n=0.77). While the mean viscosity over the range of shear rates is similar for all HRP concentrations, the rheology can be quite different. The increase in shear thinning characteristic observed at low shear rates could indicate that that polymer chains are undergoing hydrolysis. A study comparing unhydrolyzed and hydrolyzed polyacrylamide have shown increased shear thinning characteristics, at low shear rate, with increasing degree of hydrolysis.[228] In addition to hydrolysis, recombination could occur resulting is some branching. A study conducted with branched and linear HPAM showed that the branched polyacrylamide has a higher degree of shear thinning compared to linear polymer.[231] Furthermore, a more elastic response, and earlier viscoelastic transition at lower frequencies, has been observed for PAM polymers with branched, comb and star configuration when compared to a linear configuration.[232] The lower viscosity, and earlier onset of increased shear thinning behavior, suggests that the overall molar mass is being reduced but the final polymer products (after 24-hour exposure) may undergo some conformational change but further investigation is needed to determine the proper mechanism. If the polymer backbone is systematically cleaved, and no branching occurs, then the solution would exhibit a lesser degree of shear thinning and a reduced viscosity as seen with the 5.6 μM HRP concentration in Figure 3.3.

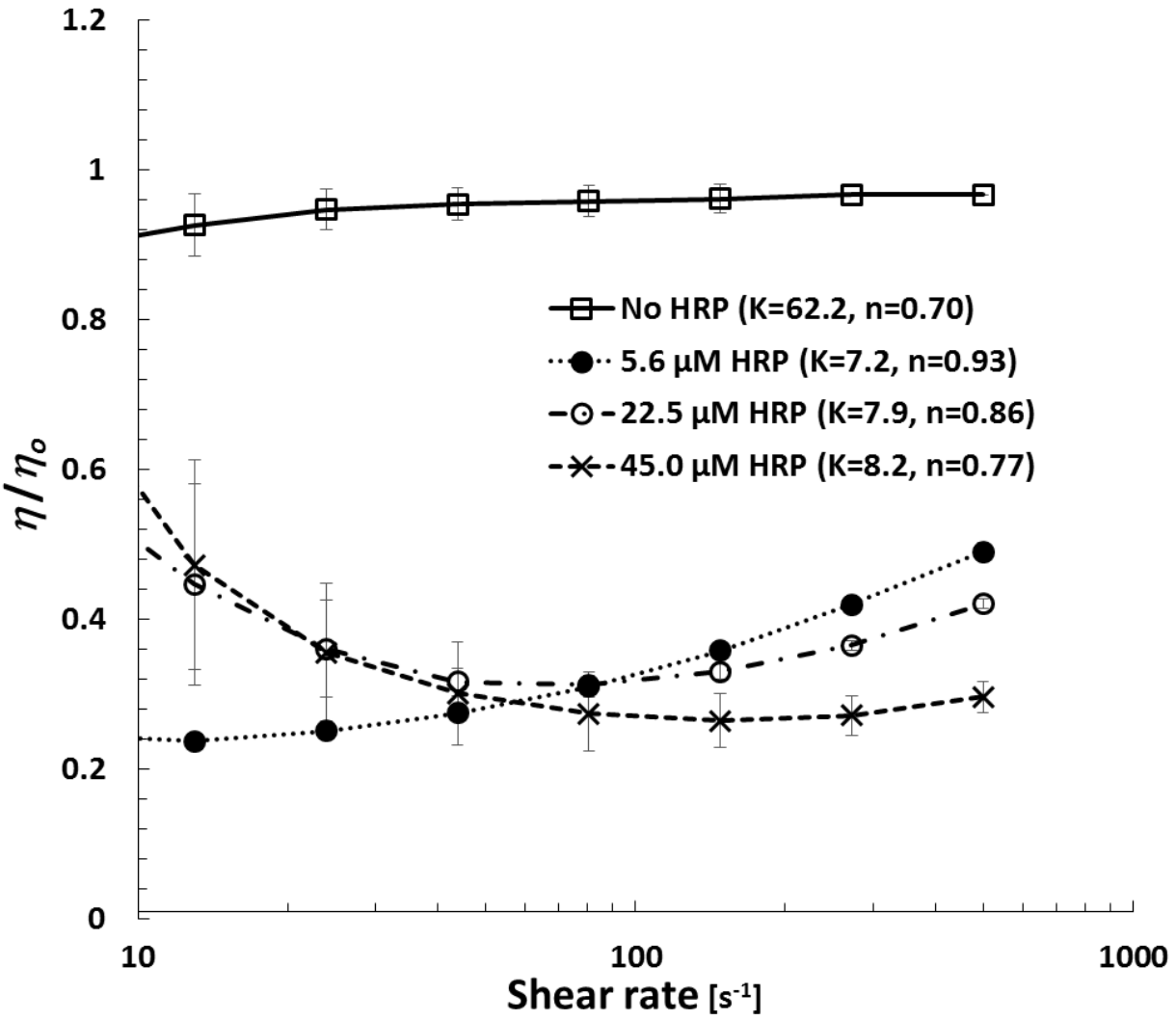

Figure 3.3 Viscosity of HPAM/NADH solutions with varying HRP concentration relative to original polymer solution over the same range of shear rates. Solutions concentrations for peroxide and NADH are 96.9 mM and 1.40 mM respectively. Samples were incubated for 24 hours at 37°C; lines represent smoothed data (n=3).

In the absence of NADH, degradation showed less variability with respect to HRP concentration but the magnitude of degradation was greater for all samples. Figure 3.4 illustrates the reduction in viscosity for three different concentrations of HRP without addition of NADH. In the absence of HRP, a slight change in viscosity occured only at low shear rates (as seen previously seen in Figure 3.2). Moderate and high concentrations of HRP resulted in similar profiles. As with the addition of NADH, theses concentrations resulted in greater shear thinning characteristics at

low shear rates (n=0.65 to n=0.4). An HRP concentration of 5.6 μM resulted in a power law index similar to the control sample (n=0.65). In addition, a greater reduction in viscosity was produced with the lowest HRP concentration. Unlike samples with the addition of NADH, the 5.6μM HRP concentration resulted in the lowest overall viscosity resulting in a mean viscosity reduction of about 90% at $75s^{-1}$.

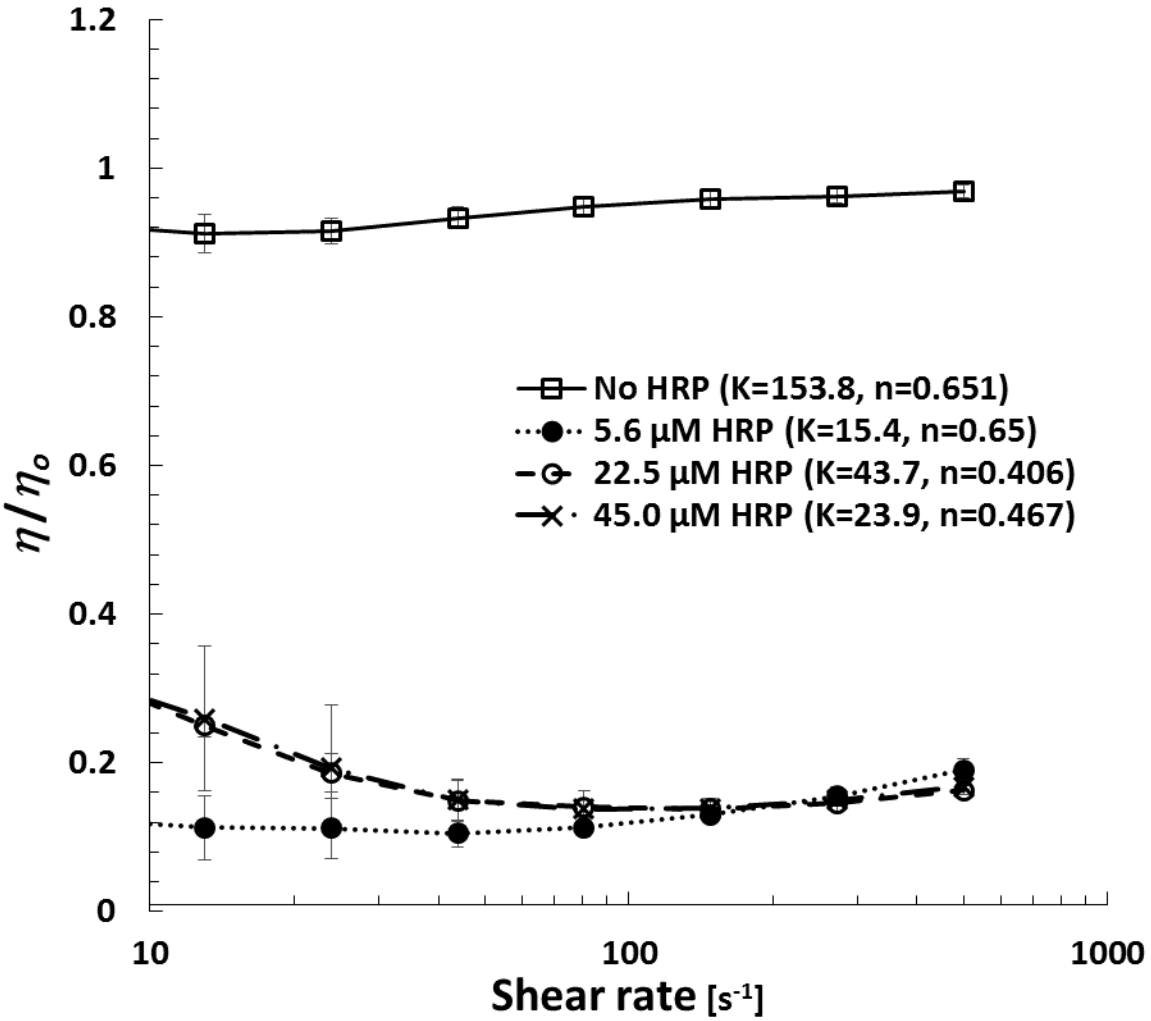

Figure 3.4 Viscosity of HPAM solutions (**in the absence of NADH**) with varying HRP concentration relative to original polymer solution over the same range of shear rates. Solutions concentrations for peroxide is 96.9 mM. Samples were incubated for 24 hours at 37°C; lines represent smoothed data (n=3).

3.1.3 Viscosity Reduction in 2% KCl

Viscosity reduction of HPAM solutions was tested in 2% KCl brine with the Bohlin rheometer at 25°C after 24-hour incubation. Figure 3.5 illustrates the viscosity difference in HPAM solutions containing HRP and NADH with and without the addition of salt. The degree of salt sensitivity has been shown to be a function of the polymer concentration, degree of hydrolysis, molecular weight, temperature, and side chain composition.[233] The observed reduction in viscosity is attributed to the ionic neutralization of repulsive electrostatic charge carried by the hydrolyzed carboxyl groups.[234] Neutralizing the repulsive charge allows the polymer to coil and decreases the resistance to flow. The reduction due to salt addition made quantifying the change in viscosity difficult. Figure 3.6 shows the viscosity change of reacted samples after 24-hour incubation. Unlike samples without salt, an increase in viscosity was observed for degraded HPAM samples at low shear rates. For 48.5 mM peroxide concentrations, an overall viscosity increase occurred when compared to unreacted samples. The higher peroxide concentration (96.9 mM) resulted in lower viscosity for most shear rates. As seen with experiments without salt, the reacted solutions resulted in greater shear thinning behavior. From this data, degradation of HPAM cannot be confirmed nor denied but a change in the solution is occurring. Further investigation is conducted in Section 3.3.1 using size exclusion chromatography to observe any change in molecular weight.

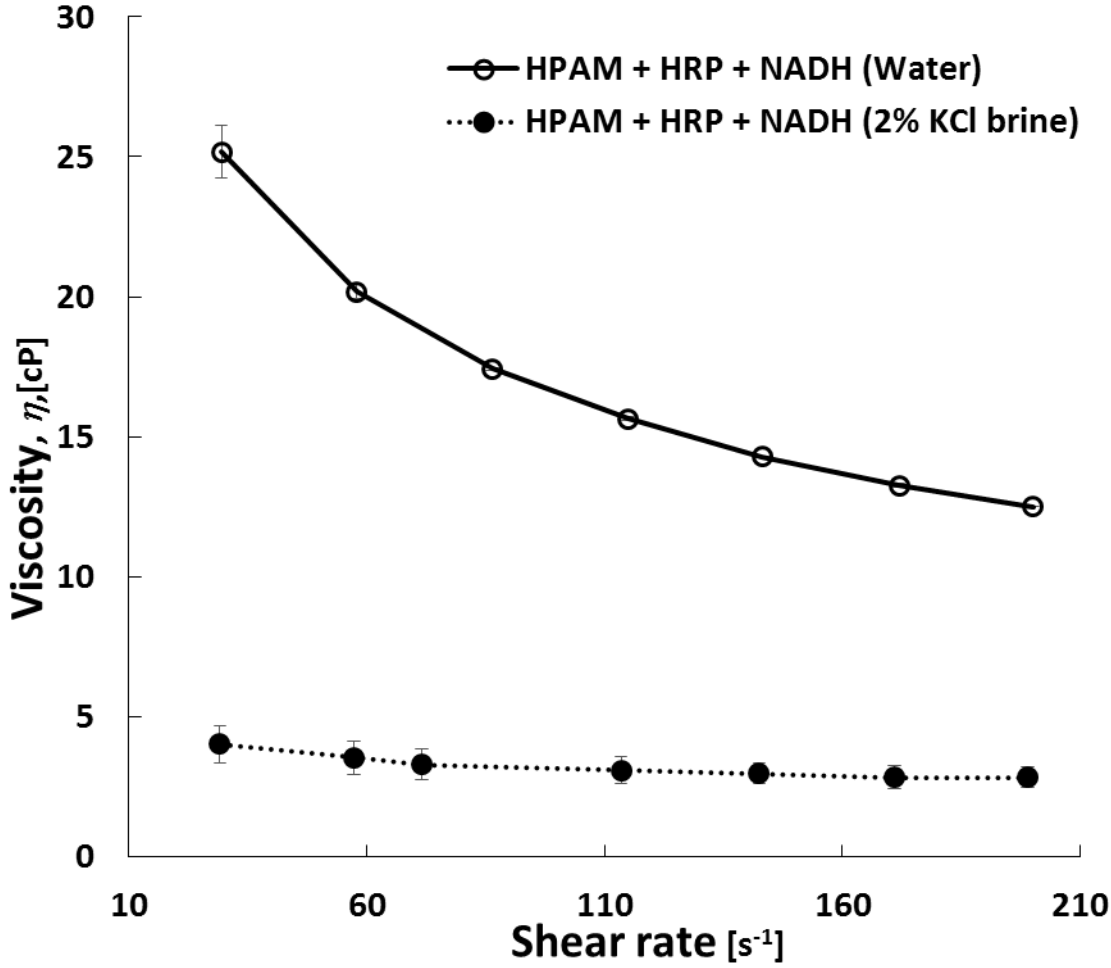

Figure 3.5 Viscosity profiles for 1980 ppm Alcoflood 935 solutions containing 45.0 μM HRP and 1.4 mM NADH in RO water and 2% KCl brine. Viscosity measured using the Bohlin rheometer at 25°C; lines are smoothed data (n=3)

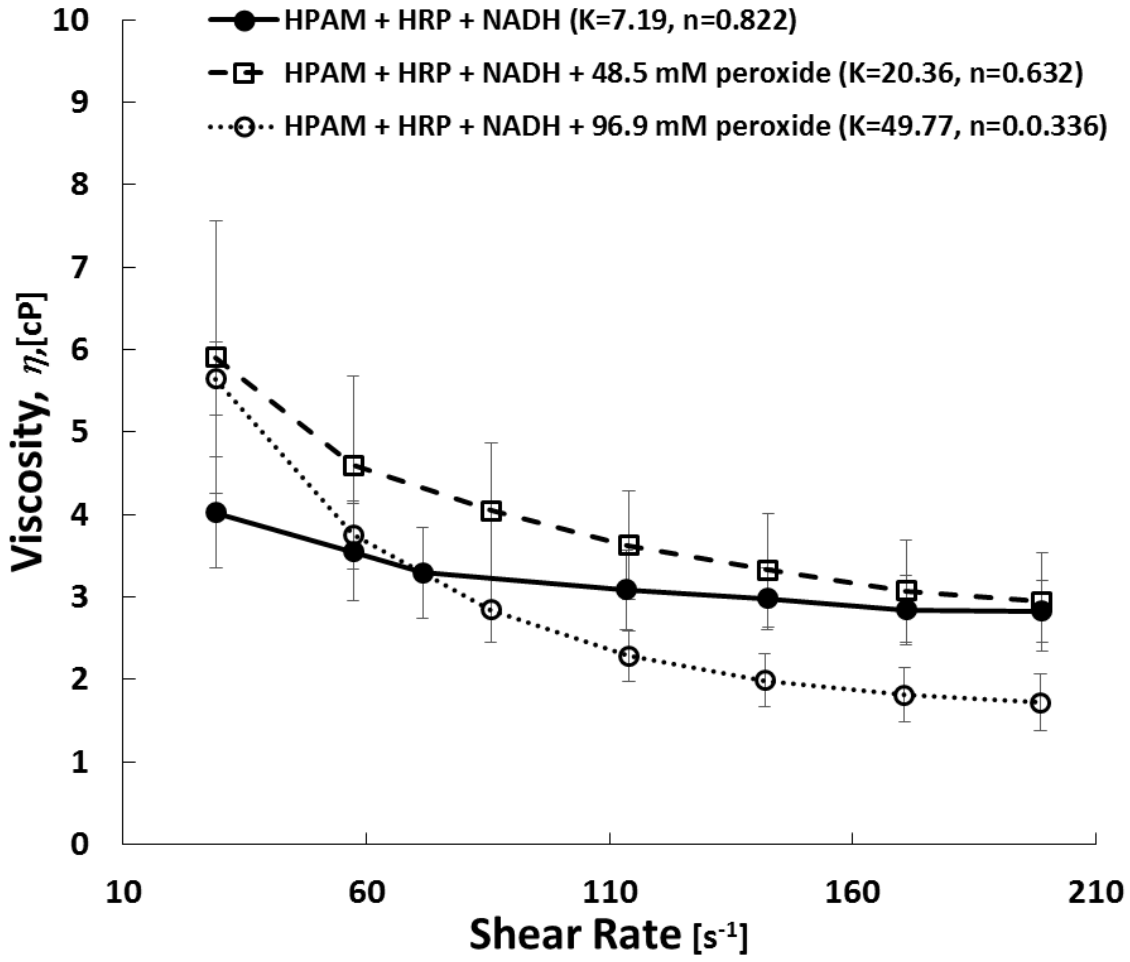

Figure 3.6 Viscosity reduction for 1980 ppm Alcoflood 935 solutions containing 45.0 μM HRP and 1.4 mM NADH in 2% KCl brine. Viscosity measured using the Bohlin rheometer at 25°C; lines are smoothed data (n=3)

3.1.4 HPAM Viscosity Reduction using Soybean Peroxidase

Experiments were conducted with soybean peroxidase (SBP) as an alternative for HRP. As stated in the introduction, SBP is a more economical alternative because the enzyme is easily extracted from soybean hulls, the hulls are a waste product of soybean processing, and the bean is abundant in the Midwest. The following experiment used Alcoflood 935 (HPAM) in conjunction with NADH at equivalent concentrations as used for HRP experiments. Data collected for SBP catalyzed degradation is shown in Figure 3.7 where control and 96.9 mM

peroxide concentrations represent three samples and 48.4 mM is represented by one sample. A single sample was used because SBP enzyme was limited. Figure 3.8 shows the comparison between SBP and HRP with equivalent concentrations. The data shown in this figure is a combination of data presented in Figure 3.1 and Figure 3.7.

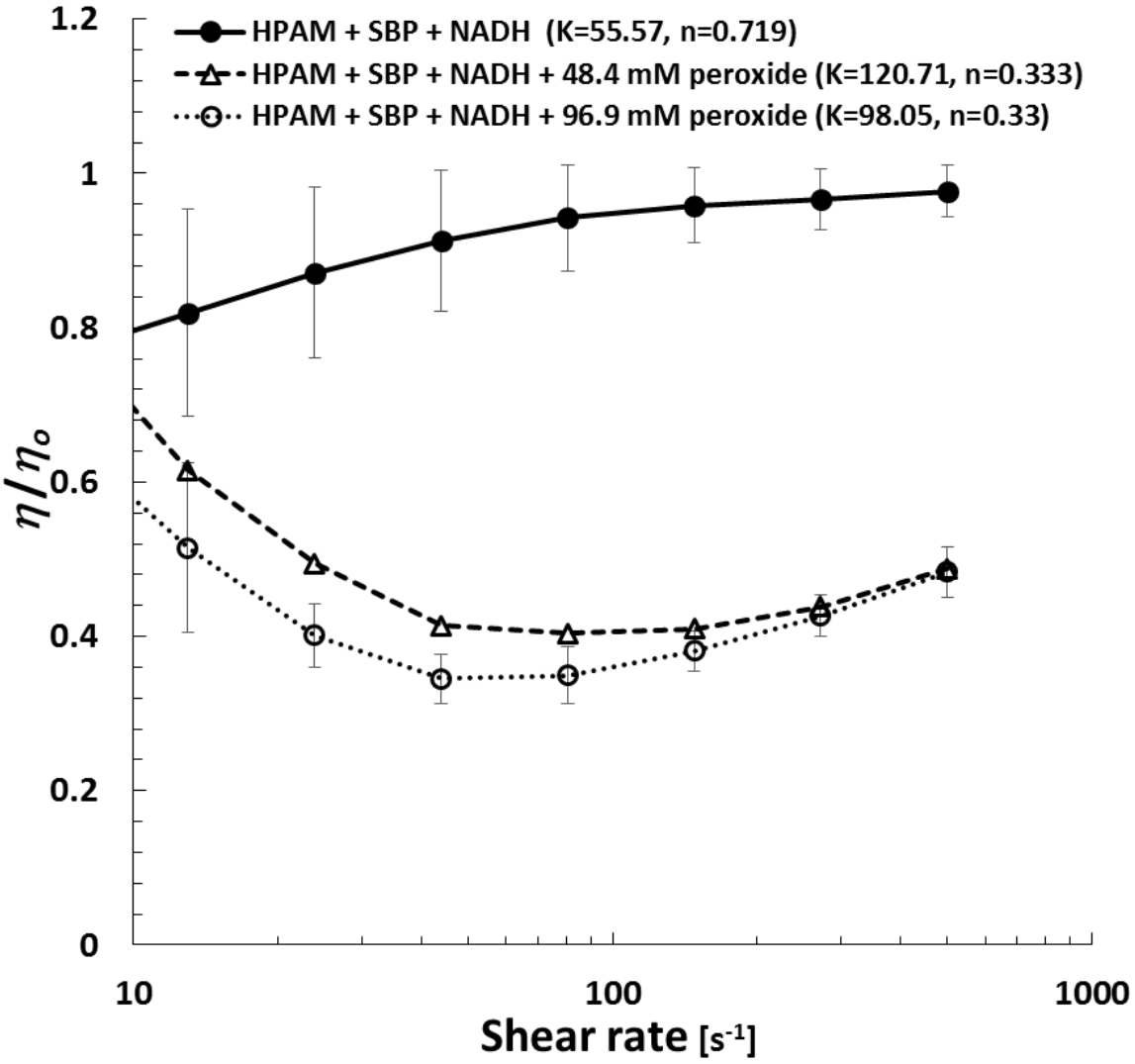

Figure 3.7 Reduction in 1980 ppm Alcoflood 925 viscosity observed using 45.0 μM soybean peroxidase, 1.4 mM NADH and varying peroxide concentration. Viscosity was measured using Anton Paar rheometer at 25°C after 24-hour incubation at 37°C; lines are smoothed data (n=3)

The use of soybean peroxidase, after 24-hour incubation at 37°C, produced a similar effect on HPAM solution viscosity as seen with reduction with HRP. Figure 3.7 illustrates the change in viscosity relative to the initial solution viscosity at time zero (η_o) at each shear rate. As shown, after HPAM solutions undergo 24 hours incubation, the fractional change in viscosity decreased only at low shear rate. Unlike solutions with HRP, SBP viscosity reduction was proportional to the amount of peroxide added to the solution only at low shear rates. At high shear rates the viscosity reduction was independent of peroxide added. Although similar at high shear, increasing the concentration of peroxide resulted in increased degradation of HPAM as evidenced by lower viscosity after a 24-hour incubation. The reduction observed was slightly less for SBP, compared to HRP, for 48.4 and 96.9 mM peroxide solutions at $75s^{-1}$ resulting about 60% and 65% respectively. As with the HRP experiments, the fractional decrease changed with shear rate. The fractional change indicates larger differences at relatively large and small rates. The power law index (n) for the same solutions show increased shear thinning characteristics with increased peroxide concentration at low shear rates. Furthermore, shear-thinning characteristics were more evident with using SBP as opposed to HRP resulting in power law indices of 0.33 and 0.54 for 96.9 mM peroxide respectively.

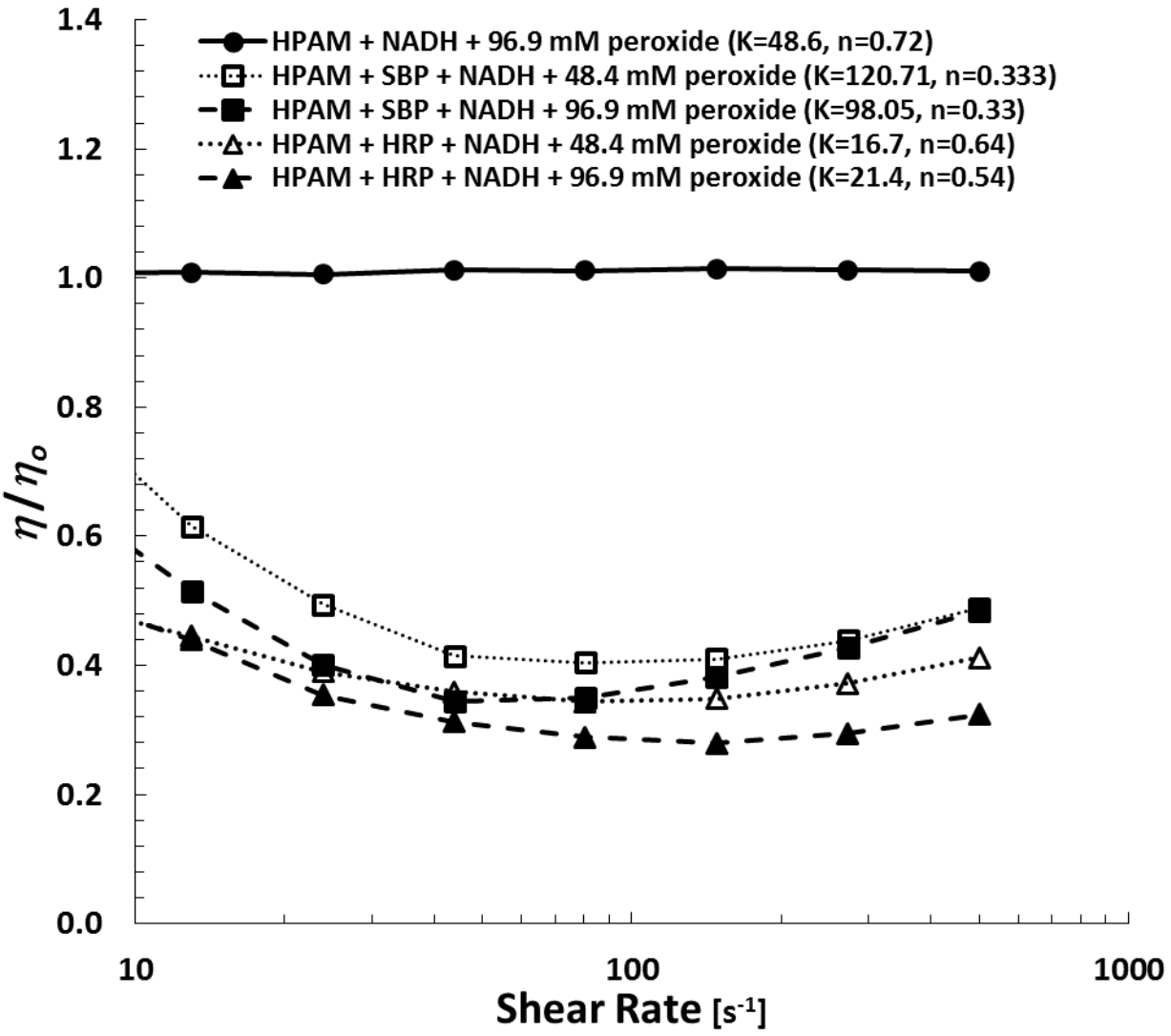

Figure 3.8 Viscosity profiles comparing HRP and SBP samples for two peroxide concentrations. Data is combination of studies illustrated in Figure 3.1 and Figure 3.7; Lines are smoothed data, n=3 for HRP and SBP with 96.9 mM peroxide.

3.2 Periodic Sampling of HPAM Viscosity Reduction

Periodic sampling was conducted in order to capture the rate of viscosity change. A previously mentioned, this method of sampling was conducted due to instrument limitations and because oxygen generated by the reaction skewed the results. Four sets of samples containing different activities were tested at 96.9 mM peroxide concentration to determine

differences (Section 3.2.1). Because peroxide concentration results in varying degradation after 24 hours, periodic sampling revealed differences in samples containing three peroxide concentrations (Section 3.2.2). Next, sampling was conducted on samples with and without NADH to observe the effects of extended incubation (Section 3.2.3).

3.2.1 Effects of HRP Activity

The effects of enzyme activity was tested for several reasons. First, the extent of this study used several samples containing different activities and samples ordered from Sigma and were within the 150-250 unit/mg solid range but differed from batch to batch. The data here compares the rate of viscosity reduction for samples used in several of the experiments. Next, the trend observed will help to estimate viscosity reductions observed when using HRP in the tested range. This information will be useful for deriving viscosity vs molecular weight relationship presented in later sections. All samples sets (n=3) contained 1980 ppm Alcoflood 935, 1.4 mM NADH, 96.9 mM peroxide, and 45.0 μM HRP. Data presented is normalized to the initial viscosity and samples were tested during 24-hour incubation at 35°C.

Horseradish peroxidase samples of different activities were tested as shown in Figure 3.9. The results of obtained for four HRP samples containing activities of 173-193 unis/mg HRP. The results of the study show that the initial activity of the enzyme has little influence on the degree of viscosity reduction. Samples of 173, 193, and 191 units/mg did vary in rate of reduction, with the lesser activity producing a slower rate, but all produced a final viscosity reduction of about 60%. The two samples with similar enzyme activities (191 and 193 units/mg) produced nearly identical results. The sample set containing 181 units/mg HRP seemed to produce a greater reduction in viscosity but based on the results of other samples is likely experimental error. The results of this

study show that the viscosity results obtained after 24-hour incubation are consistent despite the activity of HRP enzyme used but the degradation rate may vary.

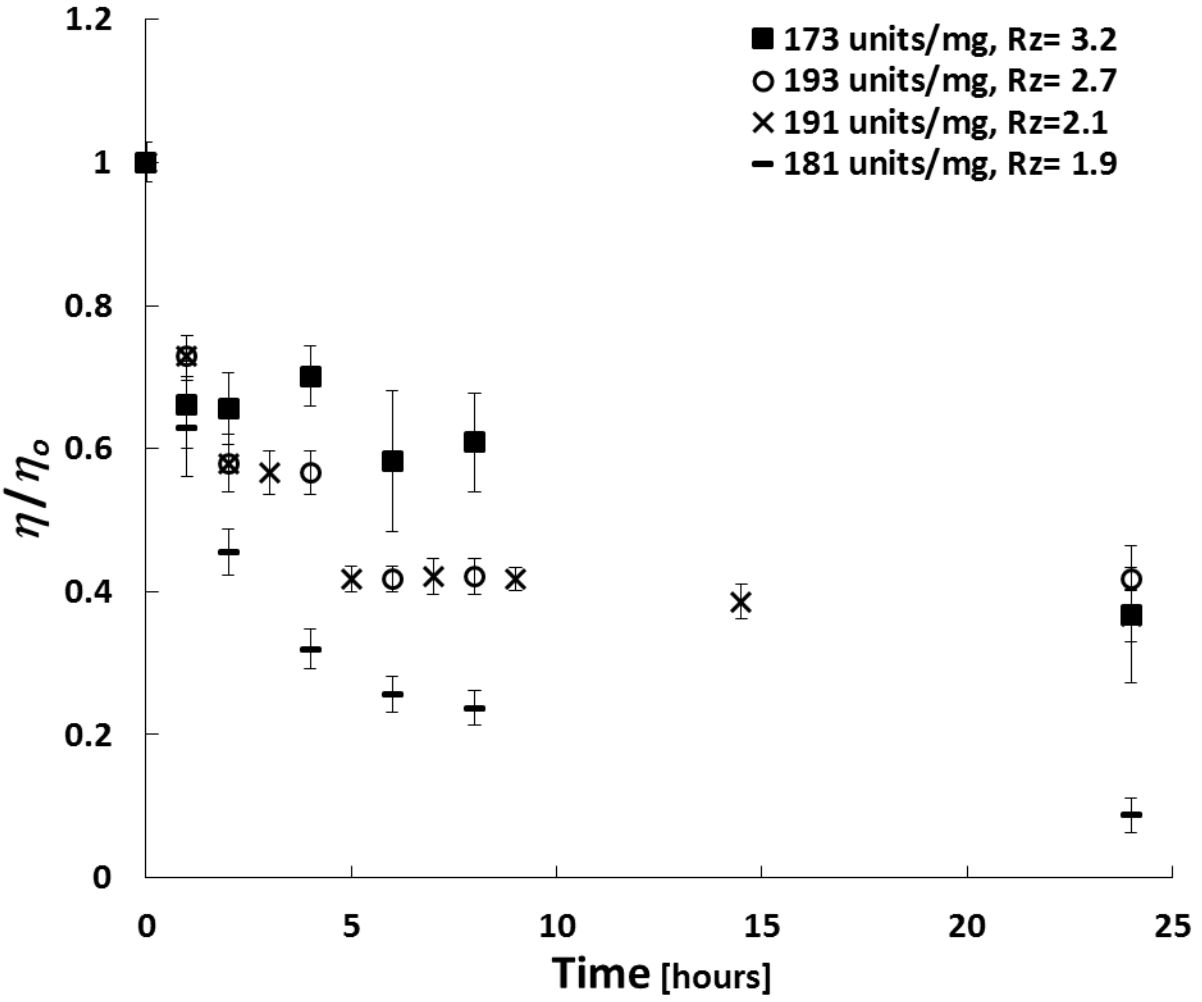

Figure 3.9 Normalized viscosity reduction observed for samples containing 1980 ppm Alcoflood 935, 1.4 mM NADH, 96.9 mM peroxide, and 45.0 μM HRP of different activity and Rz value. Viscosity was tested using the Bohlin rheometer at 75 s^{-1} and 25°C. (n=3)

3.2.2 Varying Peroxide Concentration

To observe the kinetics, viscosity at 75 s^{-1} was measured periodically over 24 hours for several peroxide concentrations. Figure 3.10 shows the change in normalized viscosity using 45.0 μM

HRP, 1.4 mM NADH, and varying peroxide concentrations. As seen in the control experiments, greater reduction in viscosity is associated with increased peroxide concentration. The reduction in viscosity calculated from Figure 6 is 17.6% ± 5.2, 37.7% ± 6.3, and 63.4% ± 3.9 for 9.69 mM, 48.4 mM, and 96.9 mM peroxide concentrations, respectively. The reduction in viscosity was seen to take place in two distinct regions with a faster reduction at earlier times. Results using varying peroxide concentration will be used to define the kinetic order of early polymer degradation.

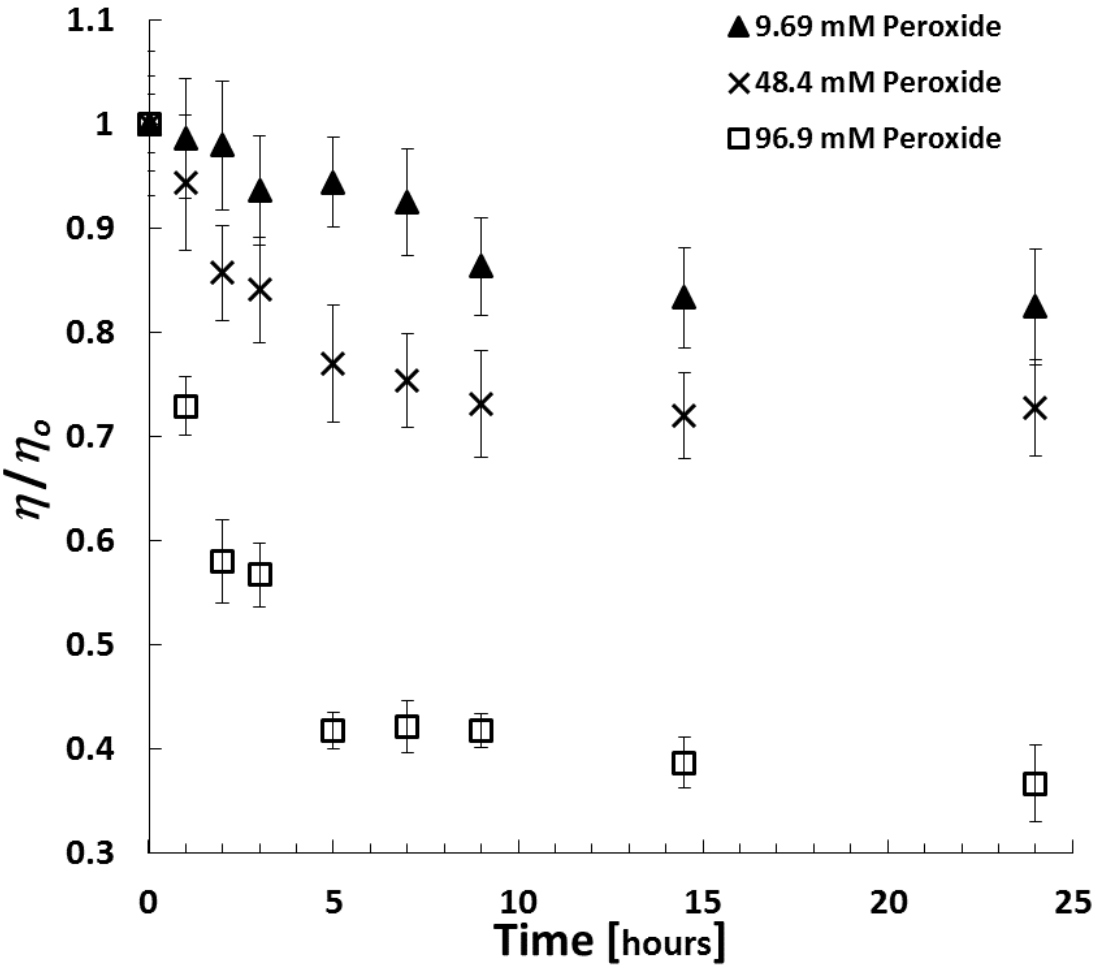

Figure 3.10 Normalized viscosity of 191 unit/mg HRP periodically sampled over 24 hours. Concentrations are 1980 ppm Alcoflood 935, 1.4 mM NADH, and 45.0 μM HRP with varying peroxide. Viscosity measurement taken at 75 s^{-1} at 25°C. (n=3)

3.2.3 Extended 75 hour Sampling

As seen in the earlier studies, a greater reduction in viscosity was observed for solutions containing 96.9 mM peroxide in the absence of NADH. In order to test whether NADH was delaying or inhibiting the viscosity reduction if HPAM, a separate study was conducted using equivalent concentrations to observe the reduction over an extended period. For this study samples containing 1980 ppm Alcoflood 935, 45.0 μM HRP, and 96.9 mM peroxide with and without the addition of 1.4 mM NADH. Sampling was conducted at 24, 48 and 75 hours and the viscosity of samples with and without NADH were compared. All samples were subjected to incubation at 37°C until sampling.

Figure 3.11 compares the viscosity profiles obtained after 24-hour incubation. The reduction in viscosity for samples not containing NADH show higher viscosity and shear thinning characteristics at low shear rates than seen in previous studies. On the other hand, the reduction in viscosity observed at high shear rates is comparable to the difference in curves observed previously. In the previous control experiments, normalized viscosity for solutions with and without NADH were about 0.3 and 0.2 respectively at a shear rate of 500 s^{-1}. At this time point, the viscosity profile reached the same viscosity at a shear rate of 43.9 s^{-1}.

As seen in Figure 3.12, after 48 hours of incubation the viscosity profiles for both solutions showed change. First, a reduction in viscosity was observed for both samples. In addition, the reduction was more pronounced at lower shear rates when compared to higher values. The magnitude of shear thinning did not change for solutions with NADH but less shear thing is seen in samples without NADH. Overall, solutions containing NADH showed the greatest reduction in viscosity between 24 and 48 hour. This difference can be observed by the shift in equivalent viscosities to a higher shear rate value of 148 s^{-1}.

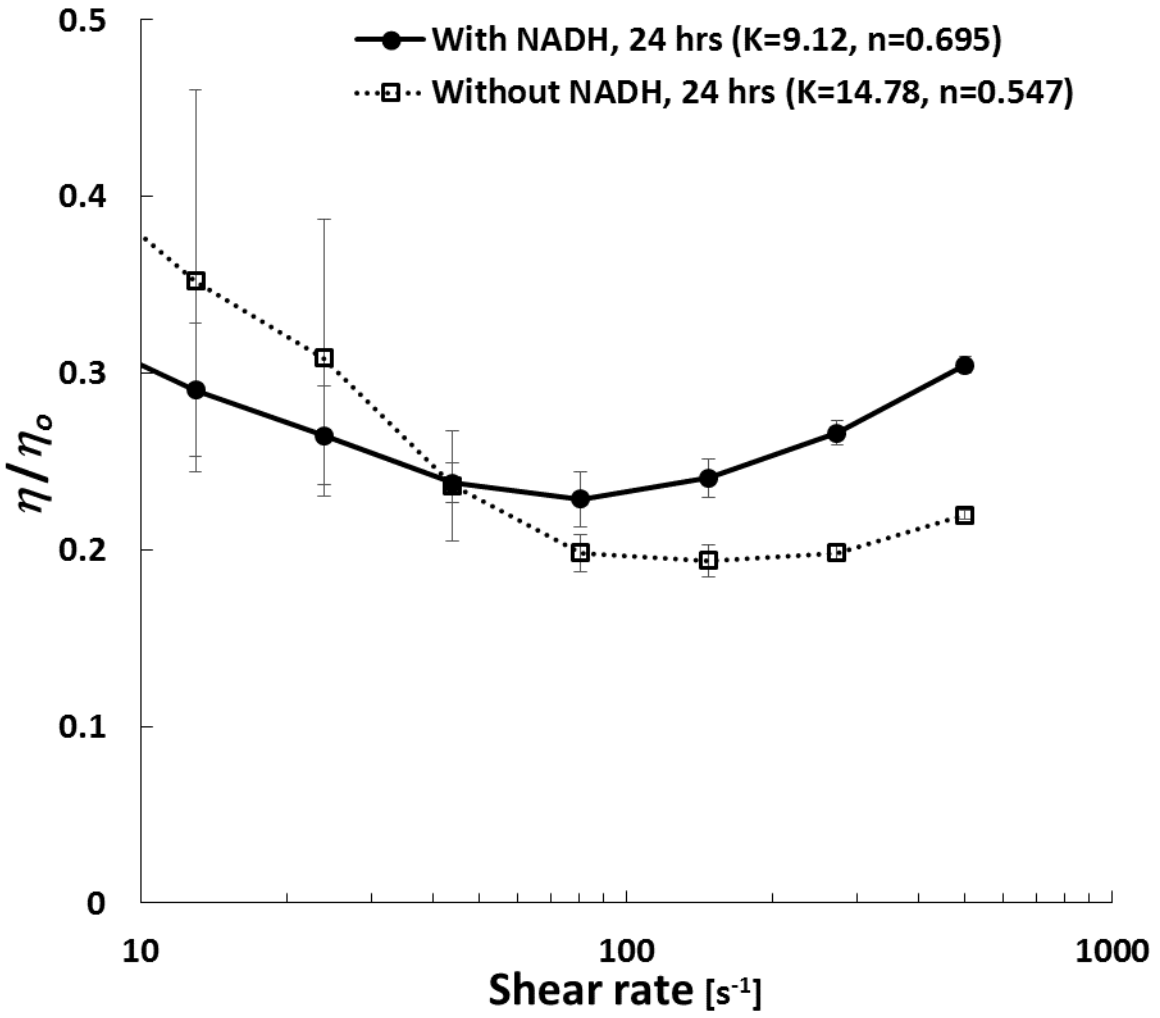

Figure 3.11 Normalized viscosity profile for solutions with and without NADH after **24-hour incubation** at 37°C. Samples containing 1980 ppm Alcoflood 935, 45.0 μM HRP, and 96.9 mM and tested at 25°C; lines are smoothed data (n=3).

Figure 3.13 shows the viscosity profiles obtained for those solutions incubated for 75 hours. The results show that similar viscosity reduction and profiles characteristic were achieved regardless of NADH addition. In addition, the power law fit was similar for both samples regardless of NADH addition. From these findings, we can conclude that NADH suppresses the rate at which HRP can oxidize the polymer but yields similar effects at longer times. Similar time lags, or inhibition, have been reported for other systems.[235,236]

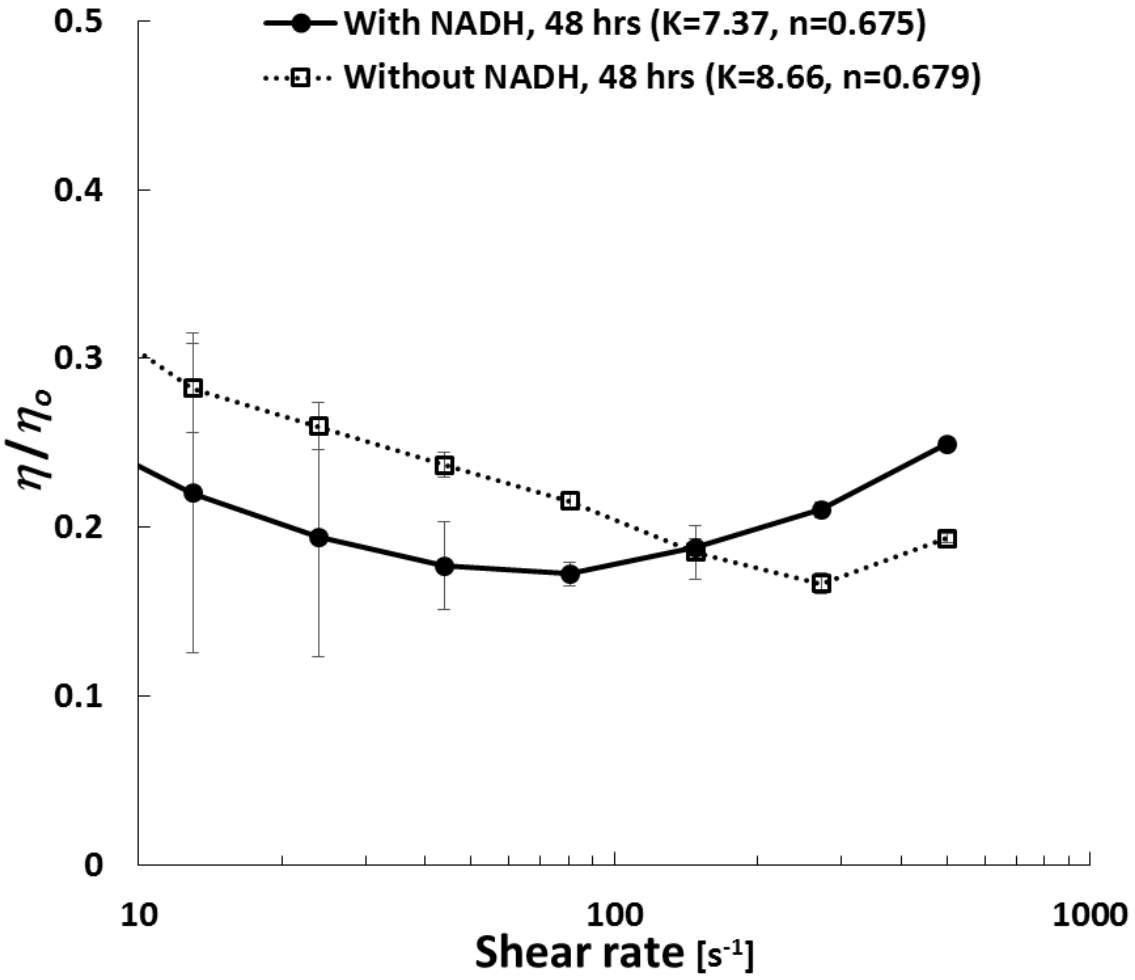

Figure 3.12 Normalized viscosity profile for solutions with and without NADH after **48-hour incubation** at 37°C. Samples containing 1980 ppm Alcoflood 935, 45.0 μM HRP, and 96.9 mM and tested at 25°C; lines are smoothed data (n=3)

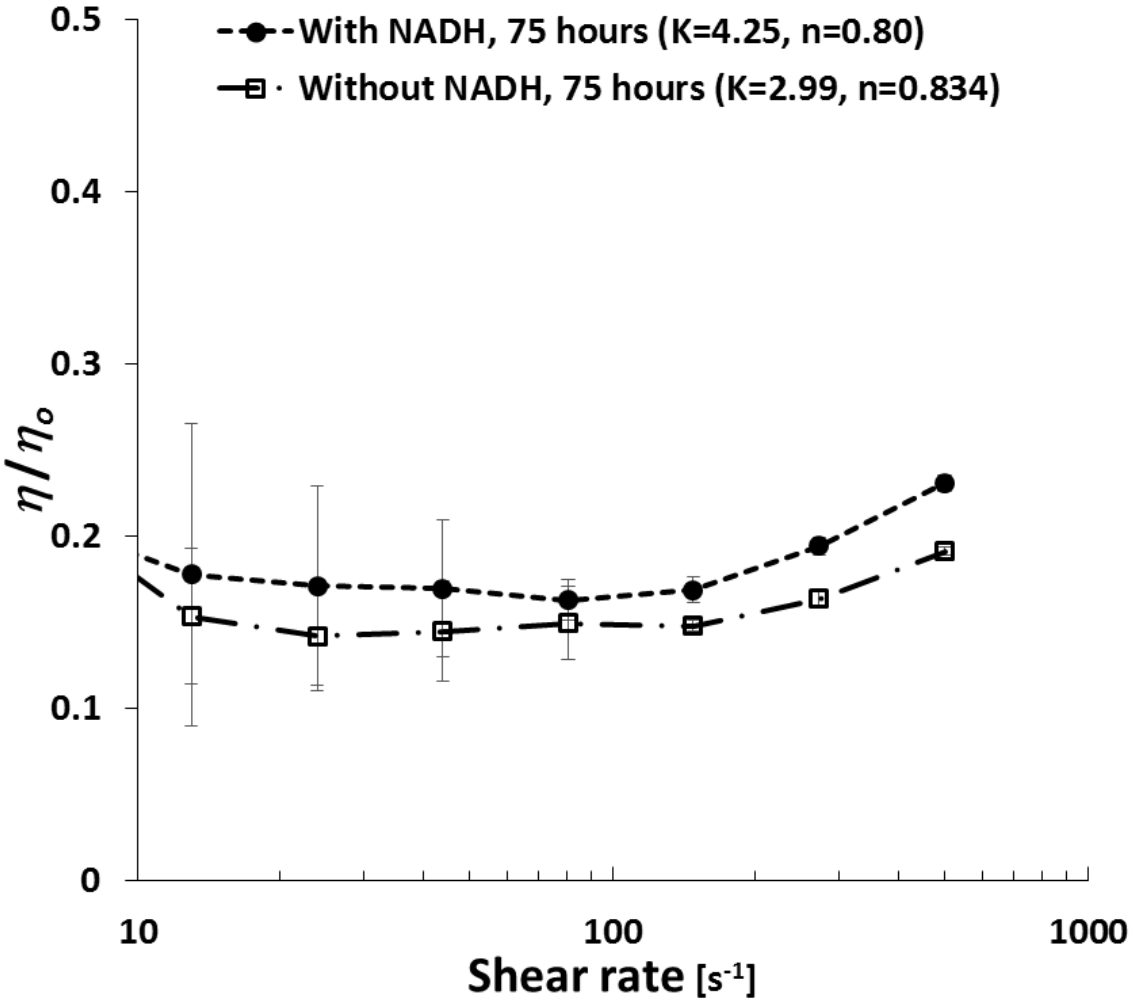

Figure 3.13 Normalized viscosity profile for solutions with and without NADH after **75-hour incubation** at 37°C. Samples containing 1980 ppm Alcoflood 935, 45.0 μM HRP, and 96.9 mM and tested at 25°C; lines are smoothed data (n=3)

3.3 Molecular Weight Reduction of HPAM Solutions

To verify that the changes in viscosity were due to reduction in molecular weight, studies were conducted using size exclusion chromatography (*SEC*). All data collected was analyzed for values of weight average molecular weight (M_w), number average molecular weight (M_n), and polydispersity (*PDI*). Samples contained 1980 ppm Alcoflood 935, 45.0 μM HRP, 1.4 mM NADH, and 96.9 mM peroxide concentrations for comparison to viscosity data. Several tests observed the

degradation of HPAM for 24-hour incubation at 37°C. First, endpoint measurements, taken after 24-hour incubation, were measured to establish molecular weight reduction in brine and RO water after 24 hours. Next, periodic sampling of the molecular weight established rate of reduction and a correlation to viscosity was established. Kinetic studies were conducted by measuring the rate of degradation with respect to time for samples containing different HPAM concentrations (i.e. 1000 and 10000 ppm). This study is incomplete due to column plugging but the data collected for 1000 ppm HPAM is presented.

3.3.1 Reduction after 24 Hour Incubation in Water and Brine

The weight average (M_w) and number average (M_n) molar masses were determined for the polymer after a 24-hour exposure to the HRP/NADH system at varying peroxide concentrations. Preliminary tests confirmed that there was a reduction in the molecular weight of HPAM after a 24-hour incubation period. Figure 3.14 illustrates the molecular weight reduction observed when the reaction was conducted in RO water. As inferred from the viscosity experiments, the reduction in molecular weight is peroxide dependent. The initial molecular weight was determined to be about 6000 kDa and corresponds with values reported in the literature.[237,238] The percent reductions in M_w were 14.0%, 40.2%, and 66.8% for 9.69 mM, 48.4 mM, and 96.9 mM peroxide concentrations respectively. The relative reductions in M_n mimic those observed for M_w and result in a more or less constant polydispersity (for example see Figure 3.16 inset). Identical 24-hour degradation tests were conducted in 2% KCl brine as shown in Figure 3.15. The reductions of M_w in brine were 13.3%, 31.6%, and 62.3% for 9.69 mM, 48.4 mM, and 96.9 mM peroxide concentrations. Again, the reduction in M_n followed M_w. Both RO water and brine experiments show a greater reduction in molecular weight as the peroxide concentration was increased. Furthermore, little change was observed when the reaction was conducted in a 2% KCl salt solution

as opposed to RO water. The reductions in molecular weight agree well with the observed reduction in viscosity at a shear rate of 75 s^{-1}.

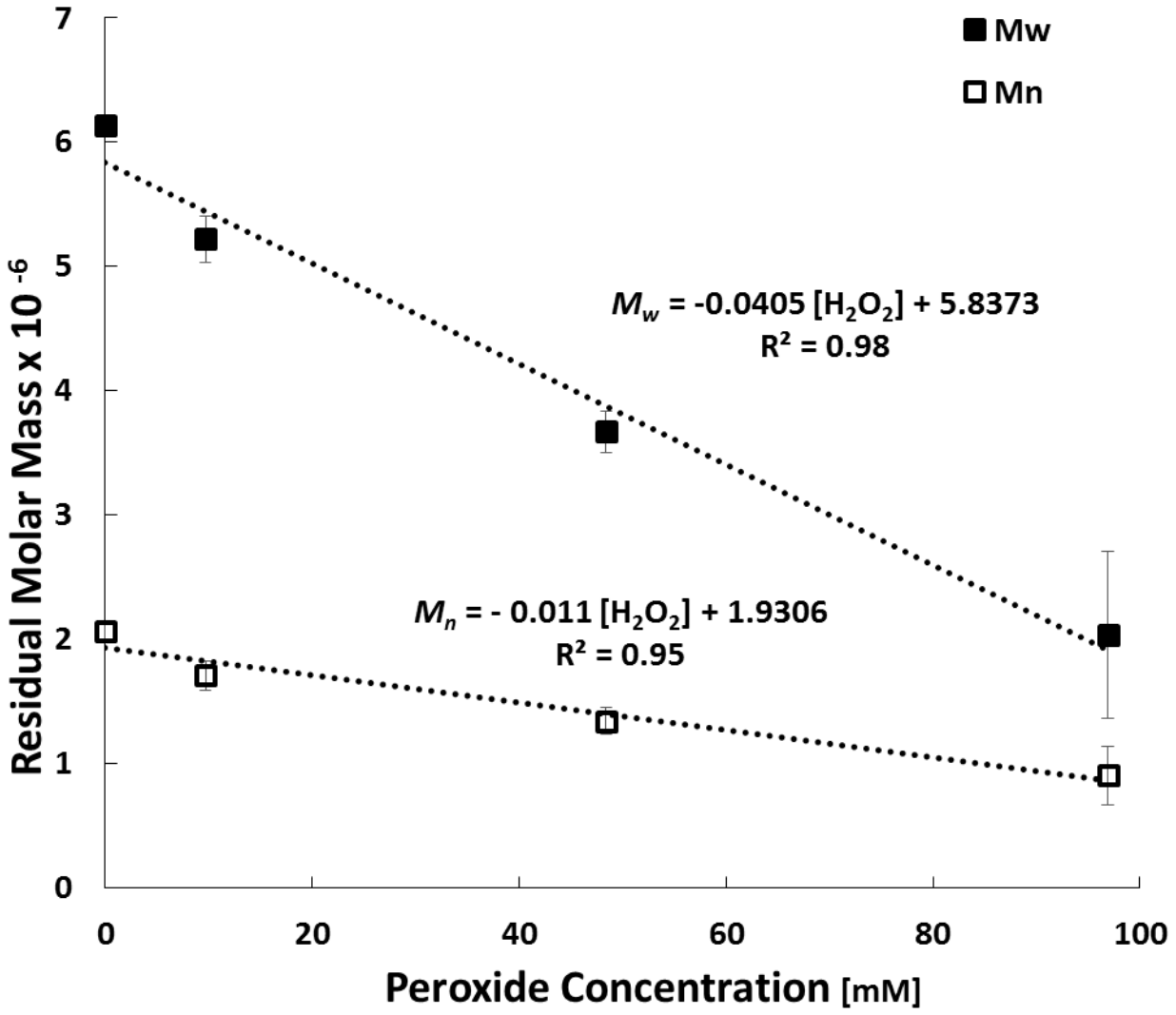

Figure 3.14: Number average (M_n) and weight average (M_w) molecular weight reduction of Alcoflood 935 solutions with 1.4 mM NADH and 45.0 μM HRP in **RO water** with varying peroxide concentrations after 24 incubation; lines are smoothed data (n=3)

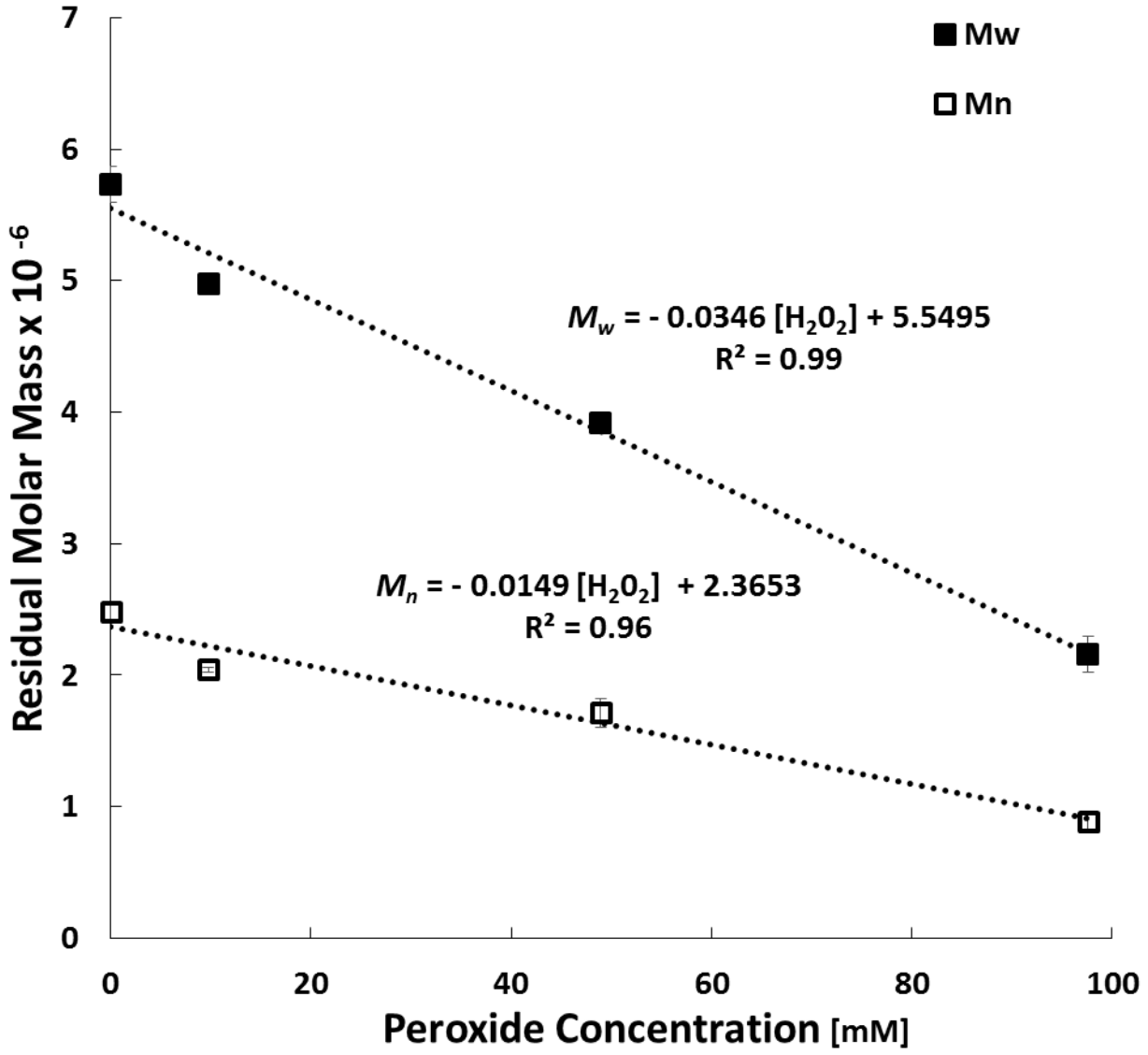

Figure 3.15: Number average (M_n) and weight average (M_w) molecular weight reduction of Alcoflood 935 solutions with 1.4 mM NADH and 45.0 μM HRP in **2% KCl** brine with varying peroxide concentrations after 24 incubation; lines are smoothed data (n=3)

3.3.2 Periodic Sampling of HPAM Molecular Weight Reduction

Periodic measurements of the molecular weight were made for HRP/NADH samples containing 96.9 mM peroxide concentration in RO water (Figure 3.16). During degradation, the polydispersity index decreased slightly from 2.64 to 2.34. The constant/slight decrease in polydispersity index suggests that the polymer backbone was cleaved randomly and under this

mechanism will result in a constant polydispersity of about 2.[239] A resulting polydispersity of 2 has been confirmed for random chain scission of linear polymers using a Monte Carlo method.[240] As with the viscosity experiments, a significant reduction was observed within the 2-3 first hours and displays two kinetically distinct regions.

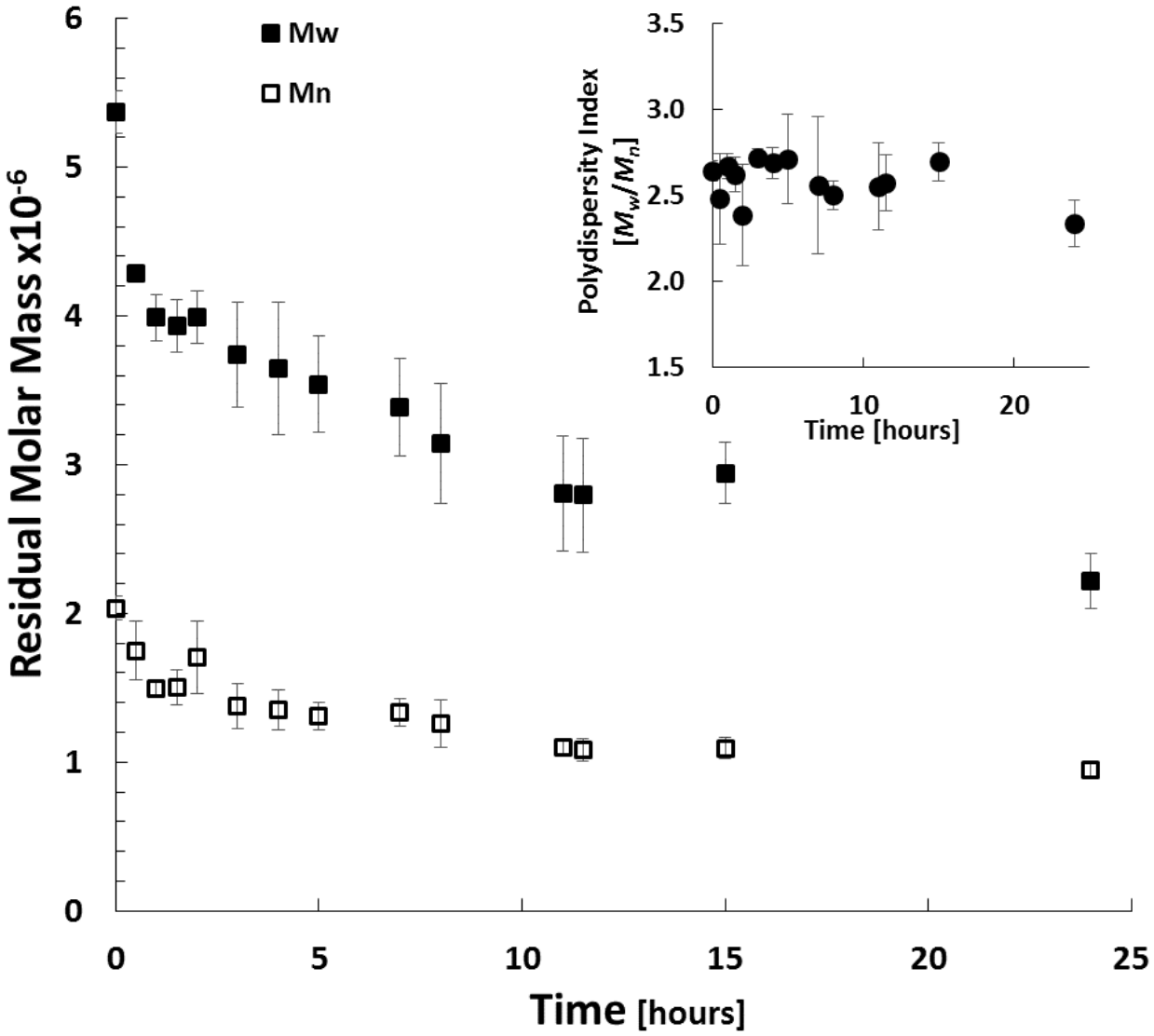

Figure 3.16 Number average (M_n) and weight average (M_w) molecular weight reduction of Alcoflood 935 with respect to time for solution containing 1.4 mM NADH, 45.0 μM HRP, and 96.9 mM peroxide concentration. Inset shows corresponding polydispersity index (*PDI*); (n=3).

Molecular weight reduction was calculated using 990 ppm Alcoflood 935. Significant time adjustments were made to the initial molecular weight calculation due to column plugging as earlier described in Section 2.2.2. The intended purpose of measuring the molecular weight for different HPAM concentration was to quantify the kinetic order and rate. Unfortunately, after completing the second HPAM concentration, column plugging prevented the analysis of a third HPAM concentration. Although the kinetics cannot be properly quantified, the data obtained for the second (990 ppm HPAM) experiment is shown here and compared to the 1980 ppm HPAM results. Figure 3.17 shows the residual Mw and corresponding percent reduction obtained for both HPAM concentrations. The results show that there is little to no difference in the molecular weight change or percent reduction observed when comparing concentrations.

The same plot comparing the two HPAM concentrations was created for the residual M_n and percent reduction. For unknown reasons, the values observed for 990 ppm HPAM were significantly higher ($\approx 3.2\times10^6$) than those observed using 1980 HPAM concentration ($\approx 2.0\times10^6$). In addition, an increase in M_n was observed at thirty minutes for 990 ppm. On the other hand, the percent reduction observed between concentrations was nearly identical and mimic the reductions observed for M_w.

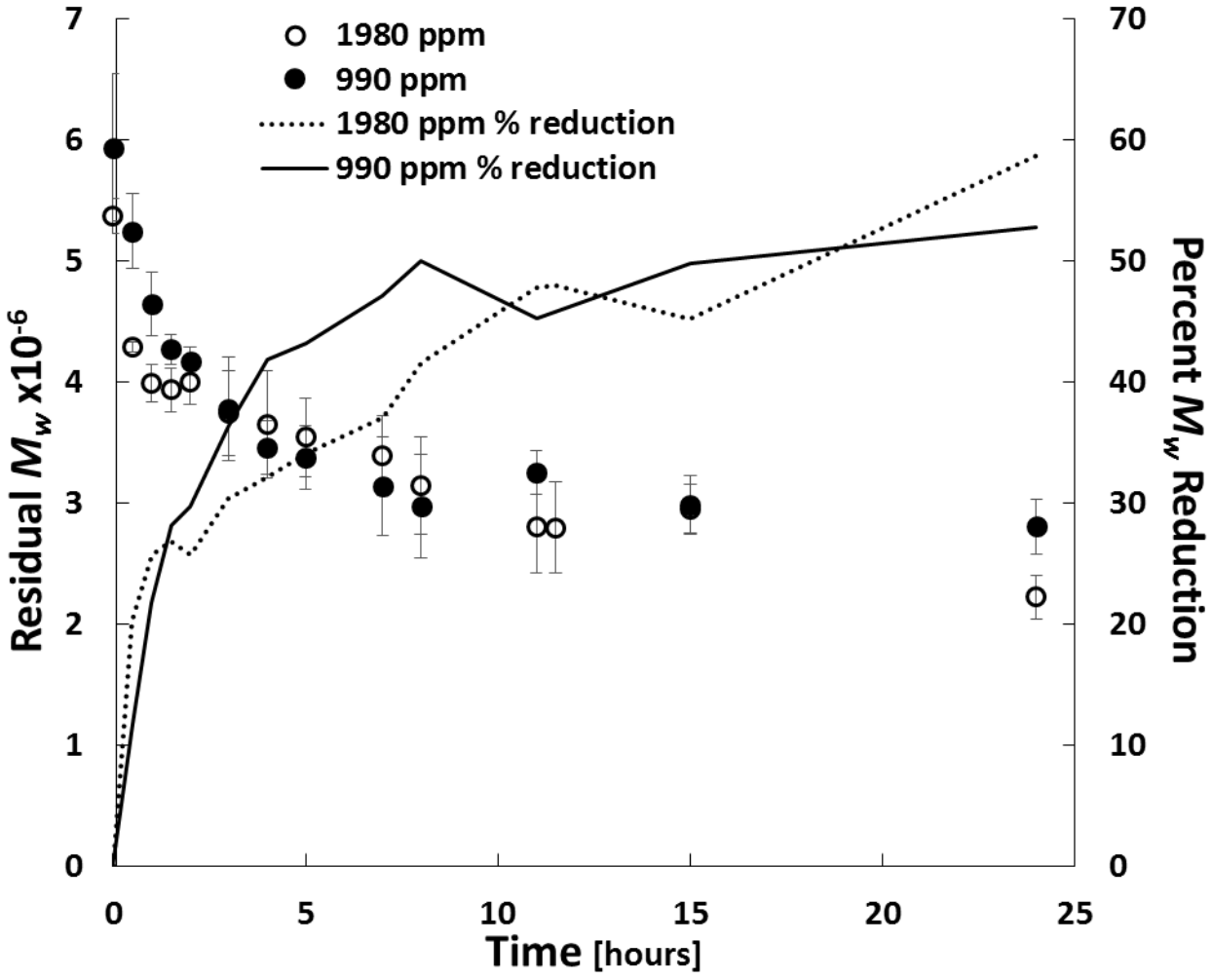

Figure 3.17 Weight average molecular weight (M_w) with time for samples containing 1980 and 990 ppm Alcoflood 935. Results presented as residual M_w and percent reduction for the HPAM concentrations; lines are smoothed data (n=3)

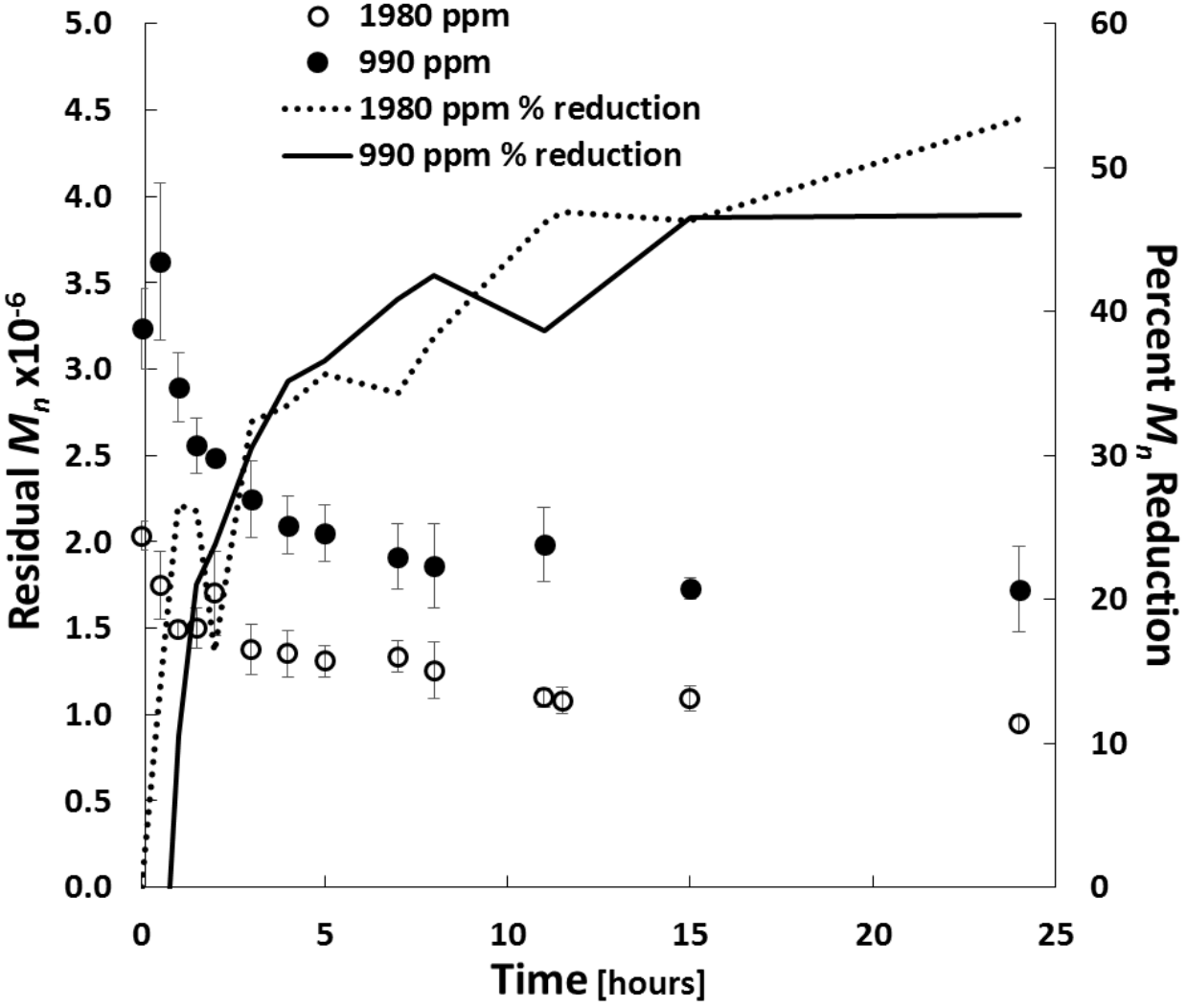

Figure 3.18 Number average molecular weight (M_n) with time for samples containing 1980 and 990 ppm Alcoflood 935. Results presented as residual M_n and percent reduction for the HPAM concentrations; lines are smoothed data (n=3)

3.4 Kinetic Evaluation of Viscosity and Molecular Weight Data

The kinetics of degradation can be evaluated using several of the previously presented data sets. First, the viscosity reduction was evaluated periodically using several peroxide concentrations (Figure 3.10). To determine the approximate kinetic order of the concentration of H_2O_2, the initial rates can be used to determine the relative magnitude of the exponent, α shown in Equation 48.

$$\frac{d\eta}{dt} \approx [H_2O_2]^{\alpha} \quad (48)$$

The initial slopes, evaluated from the first 3-5 hours, and concentrations were directly proportional indicating 1st order kinetics in peroxide concentration (Figure 3.19). The initial rates plotted with respect to peroxide concentration resulted in a linear correlation (R^2 = 0.99) and indicate first order kinetics.

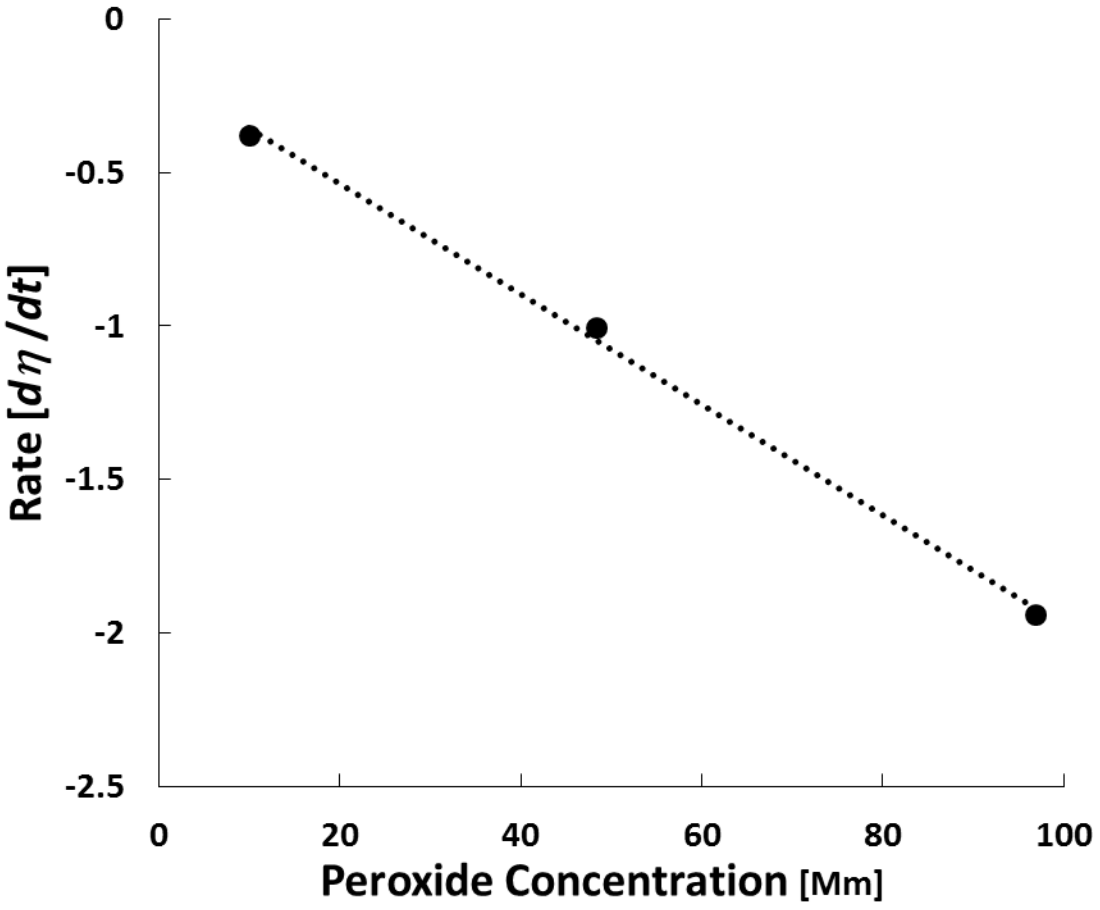

Figure 3.19 Trend fitting early time viscosity data presented in Figure 3.10.

In addition to evaluating the viscosity, the molecular weight change with respect to peroxide concentration can be kinetically described. Madras and Chattopadhyay[123] derived a kinetic model while studying the degradation of polyvinyl acetate in the presence of benzyl peroxide. In this

expression, the initial peroxide concentration (C_{po}) is plotted versus $1/M$ -$1/M_o$ as seen in Equation 49. For their results, the initial drop in molecular weight was very fast and after a period leveled out with very little change with time. This relationship uses the "endpoint" molecular weight to determine the kinetics, which is measured the current study as presented in Figure 3.14 and Figure 3.15 for degradation in RO and 2% KCl brine respectively.

$$\frac{1}{M_{nf}} - \frac{1}{M_{no}} = kC_{po} \qquad 49$$

Figure 3.20 shows the endpoint molecular weight data from Figure 3.14 plotted in accordance to Equation 49. For degradation in RO water, the trending fit showed $R^2 > 0.96$ and resulted in k_{Mw}= 3.16x10^{-9} mM/g and k_{Mn}= 6.25x10^{-9} mM/g. Using the same analysis for degradation in 2% KCl brine resulted in an $R^2 > 0.91$ and resulted in k_{Mwb}= 2.69x10^{-9} mM/g and k_{Mnb}= 6.72x10^{-9} mM/g.

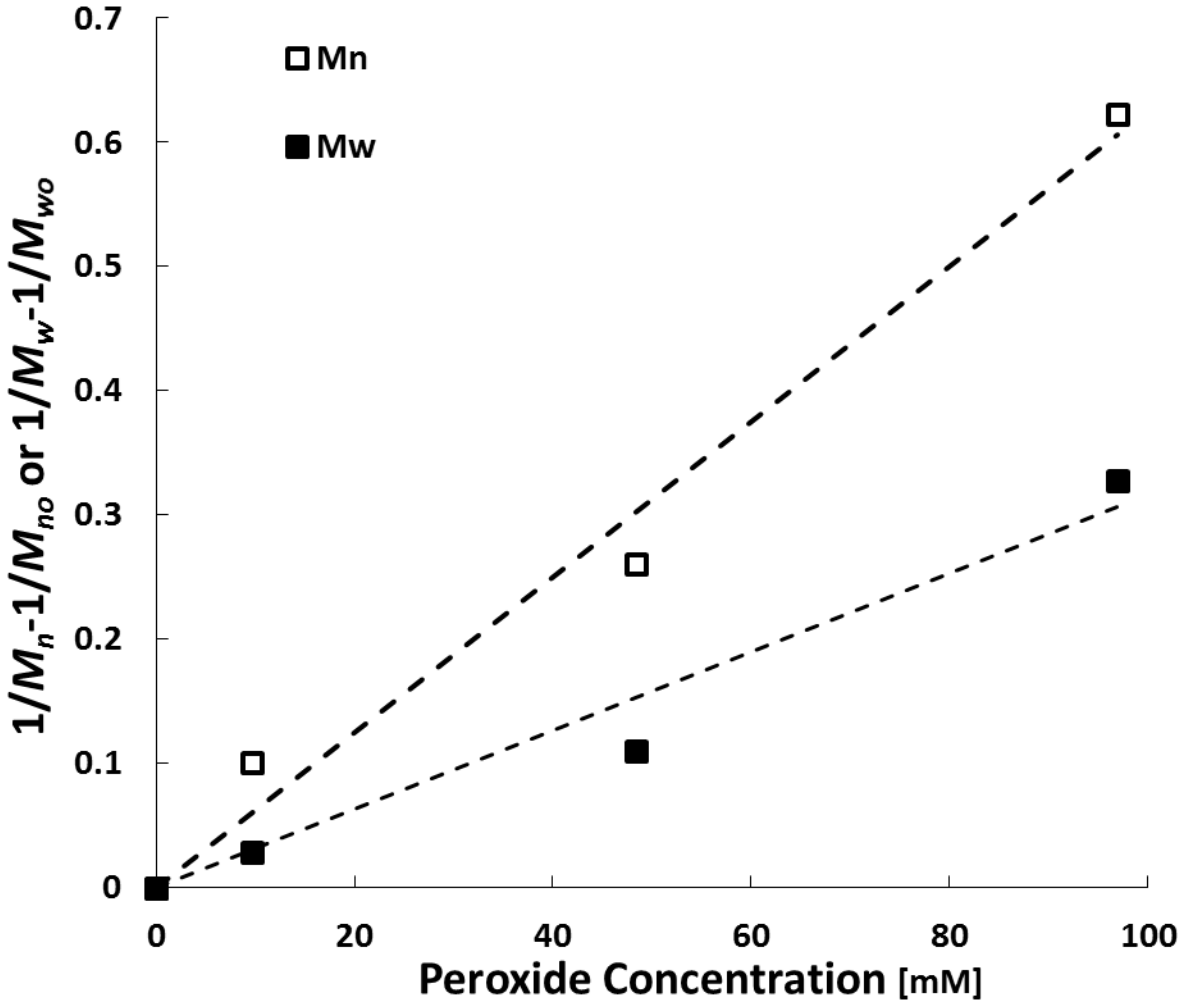

Figure 3.20 Inverse molecular weight data evaluated with varying peroxide concentrations in accordance to Equation 49. Data shown represents degradation in **RO water** and original values are presented in Figure 3.14.

Kinetic evaluation with respect to time is best done using two distinct regions. Traditional first order kinetic models, in addition to those presented by Basedow *et al.*[116] and Shukla *et al.*,[122] were not representative of the data. Conventionally in polymer degradation studies, the decrease in molecular weight (linkages of monomers) is often assumed to be a first order process.[241] Assuming a random molecular weight distribution and that the molecular weight of the polymer is much greater than the monomer, the kinetic expression becomes either: [118,119]

$$\frac{1}{M_{w\prime\, or\, n\prime}} - \frac{1}{M_{w\ or\ n,o}} = \left(\frac{k_{t'}}{mN_0}\right)(t') = \hat{k}_{t'}(t') \qquad 50$$

$$\frac{1}{M_{wt\ or\ nt}} - \frac{1}{M_{w'or\ n'}} = \left(\frac{k_t}{m}\right)(t - t') = \hat{k}_t(t - t') \qquad 51$$

where *m* is the monomer molecular weight, N_0 is the total number of molecules and initial zero order kinetics proceed to time *t'* followed by first order kinetics up to time *t*. As shown in Figure 3.21 when the inverse molecular weight is plotted versus time, two distinct slopes are observed. The steep initial slope implies zeroth order kinetics followed by 1st order for the remainder of the data. Equation 50 is used to obtain the zeroth order constant and Equation 51 is used to obtain the first order constant. The results are listed in Table 3.1 for 1980 ppm and 990 ppm HPAM concentrations respectively. Similar qualitative results have been reported in a large number of polymer degradation studies for random chain hydrolysis of polymers using chemical and enzymatic reagents and catalysts. For example, the hydrolysis of alginate,[120] cellulose linters,[121] carrageenan,[115] and glucomannan[118] with chemical reagents or enzymes results in two distinct kinetic regions. Most studies do not state a reason behind the distinct regions but a study conducted by Cheng and Prud'homme[242] showed a distinct correlation between kinetic rate and polymer substrate concentration for the enzymatic degradation rate of guar. For example, low polymer substrate concentration exhibited first order kinetics, intermediate concentrations showed zeroth order kinetics, and high concentrations were diffusion limited. However in the present study, the initial polymer concentration did not change but the concentration of the other reagent, H_2O_2, changed continually throughout the reaction. Thus, H_2O_2 was a rate-limiting reagent. In contrast, previous studies consisted of direct polymer/enzyme binding to facilitate degradation; technically

hydrolysis studies also have a second reagent that is always in great excess: water. The kinetic analysis here shows smaller apparent kinetic constants for all values of 990 ppm HPAM in comparison to the 1980 ppm. Also, values calculated using M_n indicated the best fit ($R^2 \geq 0.95$) and for both concentrations showed little change for early time data and greater change for later time data. These findings also indicate zeroth order kinetics followed by a higher order later. It should be reiterated that actual polymer degradation kinetics using peroxide and peroxidase enzymes is a culmination of a large number of elemental steps for H_2O_2, enzyme, radicals, polymers, etc. and therefore further investigation is needed to confirm reaction kinetics.

Table 3.1 Kinetic evaluation for data presented in Figure 3.21 and Figure 3.22 where $\hat{k}_{t'}$ is initial, apparent zero order rate constant and $\hat{k}_t$ is the apparent first order rate constant. Kinetics are evaluated for 1980 ppm and 990 ppm HPAM samples

	1980 ppm HPAM				**990 ppm HPAM**			
	$\hat{k}_{t'}$ **[1/hr/g/mol]**	R^2	$\hat{k}_t$ **[1/hr/g/mol]**	R^2	$\hat{k}_{t'}$ **[1/hr/g/mol]**	R^2	$\hat{k}_t$ **[1/hr/g/mol]**	R^2
M_w	7.037×10^{-7}	0.92	8.642×10^{-9}	0.91	3.550×10^{-8}	0.92	2.878×10^{-9}	0.70
M_n	1.743×10^{-8}	1.00	1.647×10^{-8}	0.95	4.644×10^{-8}	0.976	4.983×10^{-9}	0.95

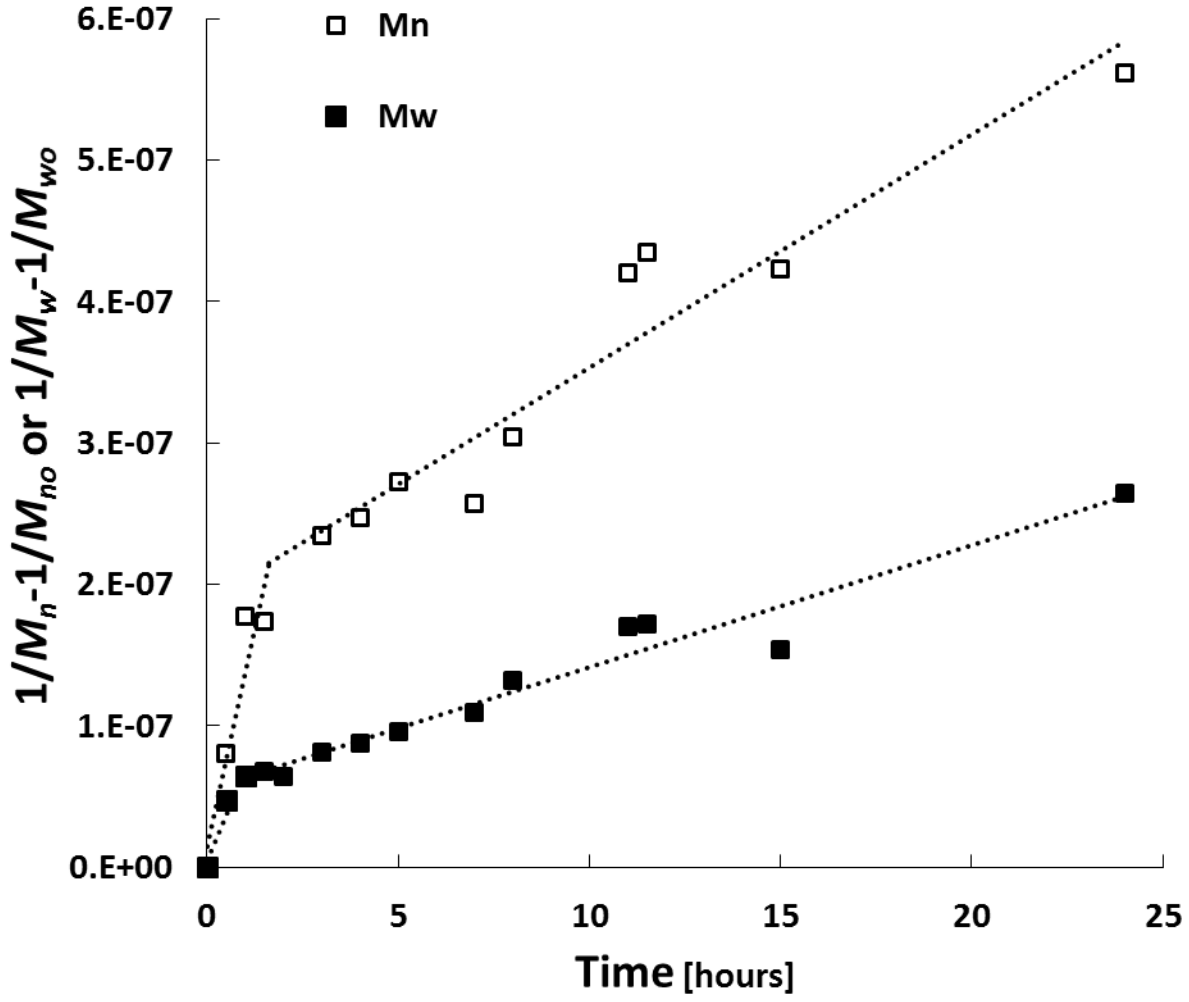

Figure 3.21: Inverse M_w and M_n for kinetic evaluation of **1980 ppm HPAM** previously illustrated in Figure 3.16. Corresponding rate constants are listed in Table 3.1.

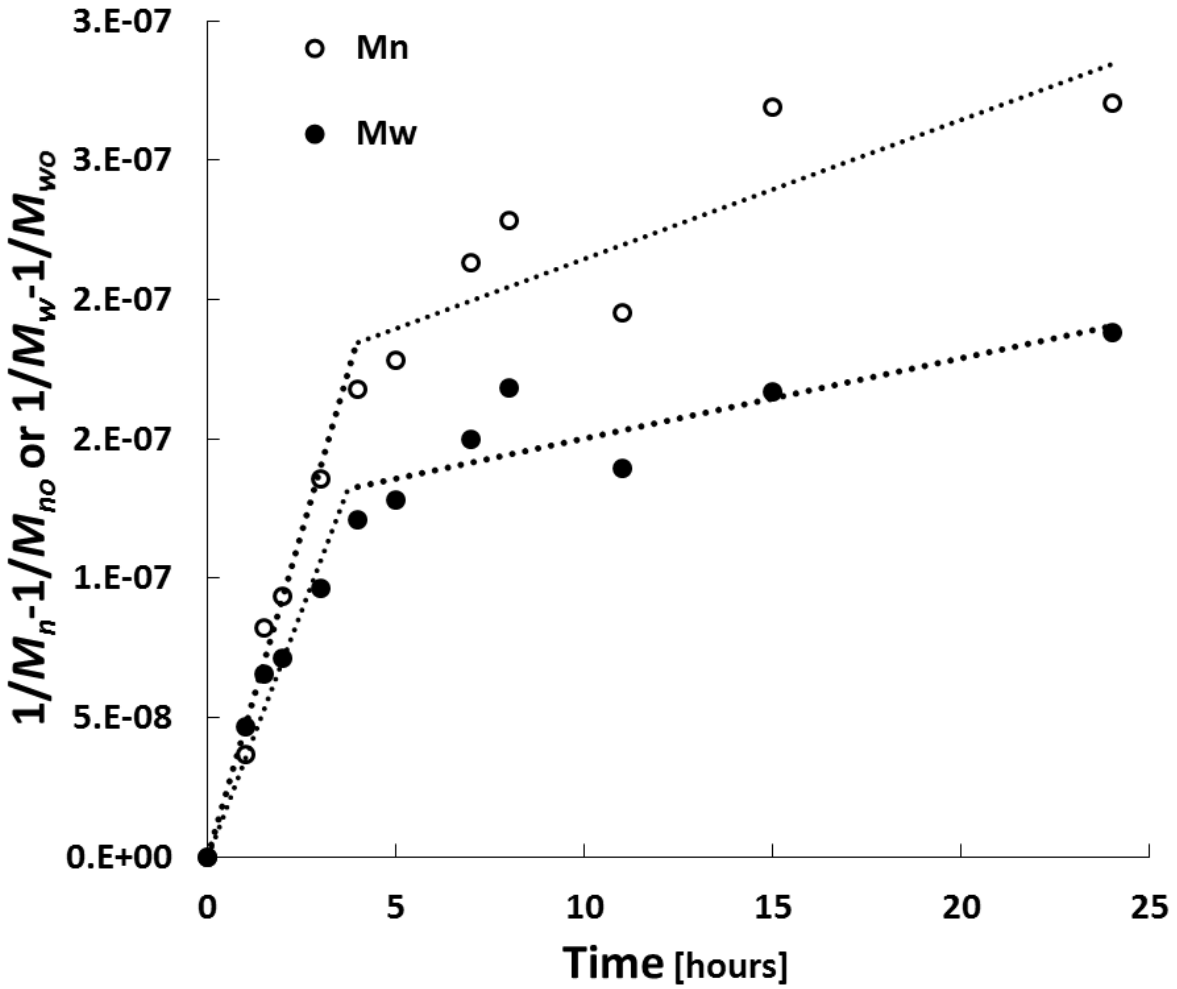

Figure 3.22 Inverse M_w and M_n for kinetic evaluation of **990 ppm HPAM** previously illustrated in Figure 3.17 and Figure 3.18. Corresponding rate constants are listed in Table 3.1.

3.4.1 Molecular Weight Viscosity Correlation

As shown in Figure 3.23, the fractional changes in viscosity and molecular weight with respect to their initial values are different at various times but proportional. A strong linear correlation ($R^2 \geq 0.9$) between the two properties exists, indicating that solution viscosity is a good indication of HPAM molecular weight reduction. The relationship between molecular weight and viscosity can be described by the following equation for times less than or equal to 24 hours: $M_w/M_{wo} = 0.795\ (\eta/\eta_o) + 0.236$. Viscosity measurements are much more facile than the lengthier analytical

techniques for molecular weight determination, i.e. SEC, etc. Thus, as viscosity is proportional to molecular weight, viscosity measurements alone should allow more rapid development and engineering of these systems in the future followed by molecular weight confirmation only of optimized systems.

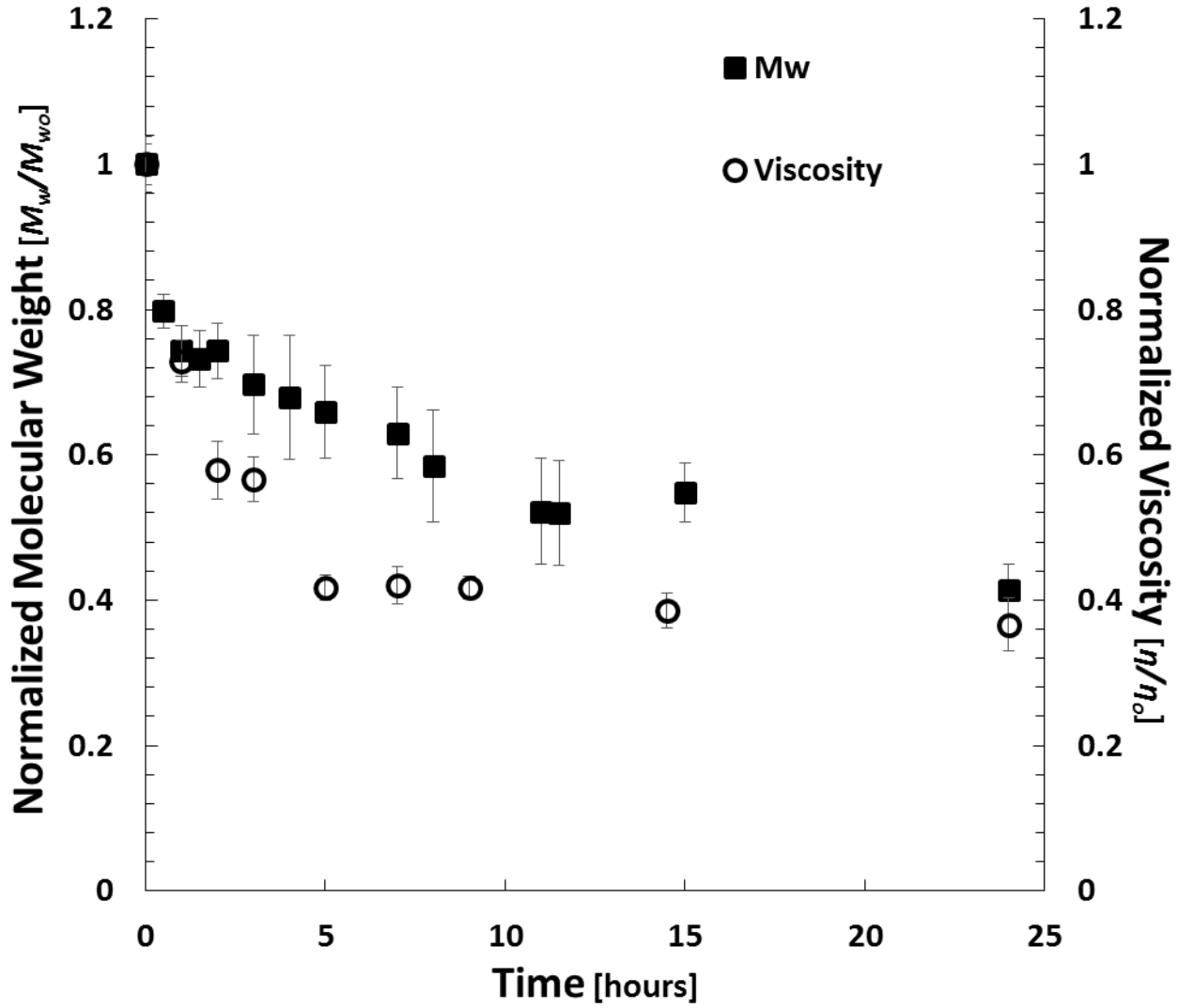

Figure 3.23 Kinetics of fractional molecular weight change and viscosity change. Error bars show standard deviation (n=3).

3.5 Data Comparison and Discussion

Persulfate oxidizers are the primary chemical breakers used during fracturing processes.[243] The results from these studies with HRP and H_2O_2 are comparable with other chemical breaker systems in the literature with similar polymer and conditions. A study by Gao *et al.*[100] demonstrated that amongst chemical breakers that potassium persulfate was more effective than ammonium persulfate, potassium persulfate-sodium-thiosulfate system, and hydrogen peroxide alone. In this study, little to no degradation was observed in the presence of hydrogen peroxide alone. At 0.4% PAM concentration, 40°C, and 30 mM potassium persulfate concentration the molecular weight of 12000 kDa PAM was reduced by about 35% after the first hour and a half. This fast initial reduction was followed by a slower degradation for PAM resulting in about 90% reduction after 10 hours of exposure. Similar percent reductions are achieved using HRP/H_20_2 in the absence of NADH after 24-hour reaction times. Although data shows 90% reductions after 24 hours, kinetic evaluation of this system was not conducted and therefore may happen faster than the tested time. The viscosity of degraded solutions reflected trends observed for the reduction in molecular weight. Reduction of PAM became more efficient with increased temperature, PAM concentration, and persulfate concentration. Although not shown, it can be expected that the efficiency of potassium persulfate would decrease for the 0.2% PAM concentration used in this study. While effective in the laboratory, the oil field application of persulfate breakers can create a number of issues. The non-specific nature of oxidative chemical breakers can react with well tubing, other reservoir fluid components, and show formation mineral incompatibility.[244,245] Field studies with the carbohydrate, guar gum, as the polymer have shown that guar specific enzyme breakers have been more successful than persulfates in actual oil filed application.[246] However,

these enzymes degrade polymers by direct binding and cannot degrade HPAMs like the current HRP/H_2O_2 system.

Fenton reagents are primarily used for remediation of petroleum contamination in soils and fracturing wastewater treatment.[247,248] The reduction in molecular weight observed using Fenton reagents is similar to that observed with persulfates but is notably slower at low temperatures. Mai et al.[249] observed the degradation of acrylamide, acrylic acid polymers, and copolymers in the presence of Fenton reagent at 30°C. Experimentally, the degradation was conducted in the presence of about 0.5% hydrogen peroxide, 0.247 mM Fenton reagent, and 5500 ppm (0.55% w/v) PAM with an initial molecular weight around 200 kDa. They showed that the molecular weight of PAM was reduced by 52% in 24 hours and about 85% after 120 hours. The results in this study show that polymer degradation using HRP is kinetically more rapid at lower temperatures than the use of Fenton reagents.

Radical generation by the HRP/reductant system has been extensively studied and the general reaction cycles were illustrated previously in Section 1.6.3. Figure 3.24[162] gives the overall reaction as it is hypothesized to work in the current study. This figure shows that enzyme conversion from the HRP resting state to compound I is initiated with hydrogen peroxide. From the viscosity studies, this holds true because no reduction in viscosity is observed for solutions containing HRP in the absence of peroxide. Next, in the presence of a reductant, compound I is converted to compound II though the addition of a hydrogen atom. In this case, the reductant can be a stable electron carrier, such as NADH, or can be hydrogen peroxide. Without the addition of NADH, the hydrogen peroxide is responsible for HRP conversion from compound I to compound II and compound II back to native HRP. During this mechanism, compound I can react with peroxide to release oxygen and the conversion results in compounds II and III. During the

conversion of compound I, hydroxyl and superoxide radicals are formed that degrade the polymer. Regardless of reductant addition, HRP has shown to undergo deactivation which can hinder the efficiency of the reaction.[148-150] The deactivation of proteins takes place through oxidation of amino acids and amino acid residues.[151] The addition of NADH to this system could decrease the overall rate by introducing an additional cycle (i.e the oxidative cycle) that promote the formation of compound III. Furthermore, the addition of NADH could act as a completive inhibitor in turn slowing the reaction. Overall, the proposed scheme in Figure 3.24 seems to be most feasible but further investigation is required to confirm exact mechanism.

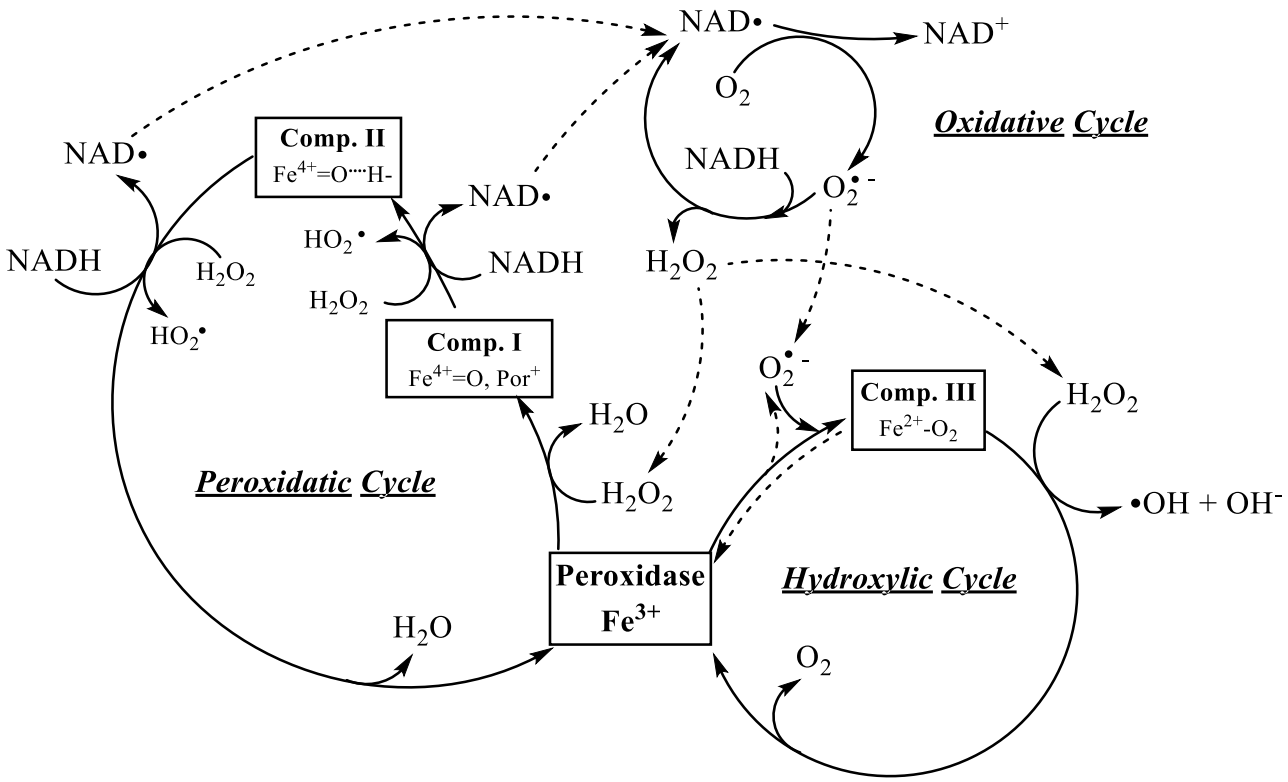

Figure 3.24 Peroxidase cyclic reaction scheme for catalyzed degradation of PAM/HPAM in the presence of NADH. Figure based off of Chen and Schopfer.[162]

3.6 Summary

With high molecular weight HPAM, both horseradish and soybean peroxidase significantly reduced the viscosity. The degree of viscosity reduction of HPAM solutions is dependent on many factors. Addition of HRP and NADH to HPAM solutions reduce the initial viscosity of solutions by varying degrees. A greater reduction in degraded HPAM solutions was observed in the absence of NADH. In the presence of NADH, the magnitude of degradation was dependent on peroxide concentration. In addition, NADH showed a "protective" effect against degradation of HAPM by peroxide in the absence of HRP. Furthermore, HPAM showed different rheological behavior (shear thinning characteristics) with varying HRP and peroxide concentrations in the presence and absence of NADH. Extended incubation (75-hours) revealed similar profiles to those obtained in the absence of NADH. In the presence of 2% KCl viscosity was significantly reduced but the molecular weight reduction showed similar results in brine and fresh water. Viscosity and molecular weight studies showed little difference in the degree of HPAM degradation with respect to enzyme activity and HPAM concentration. Kinetic analysis with molecular weight showed faster rate during initial times and with increasing HPAM concentration.

3.7 References

100. Gao, J., J. Appl. Polym. Sci. 69, 791 1998.
115. Masson, C., Can. J. Chem. 33, 597 1955.
116. Basedow, A. M.; Ebert, K. H.; Ederer, H. J., Macromol. 11, 774 1978.
118. Li, G.; Qi, L.; Li, A.; Ding, R.; Zong, M. in Macro. Symp.; Wiley Online Library: 2004, p 165.
119. Tayal, A.; Kelly, R. M.; Khan, S. A., Macromol. 32, 294 1999.
120. Bouhadir, K. H.; Lee, K. Y.; Alsberg, E.; Damm, K. L.; Anderson, K. W.; Mooney, D. J., Biotech. Prog. 17, 945 2001.
121. Marx-Figini, M., J. Appl. Polym. Sci. 33, 2097 1987.
122. Shukla, N. B.; Daraboina, N.; Madras, G., Polym. Degrad. Stabil. 94, 1238 2009.
123. Madras, G.; Chattopadhyay, S., Chem. Eng. Sci. 56, 5085 2001.

148. Hiner, A. N.; Ruiz, J. H.; López, J. N. R. g.; Cánovas, F. G. a.; Brisset, N. C.; Smith, A. T.; Arnao, M. B.; Acosta, M., J. Biol. Chem. 277, 26879 2002.
149. Hernandez-Ruiz, J.; Arnao, M. B.; Hiner, A. N.; Garcia-Canovas, F.; Acosta, M., Biochem. J 354, 107 2001.
150. Valderrama, B.; Ayala, M.; Vazquez-Duhalt, R., Chem. Biol. 9, 555 2002.
151. Stadtman, E., Annu. Rev. Biochem. 62, 797 1993.
162. Chen, S. x.; Schopfer, P., Eur. J. Biochem. 260, 726 1999.
228. Lewandowska, K., J. Appl. Polym. Sci. 103, 2235 2007.
231. Shi, L.-T., J. Chem. 17, 1 2013.
232. Wever, D. A. Z.; Picchioni, F.; Broekhuis, A. A., Eur. Polym. J. 49, 3289 2013.
233. Rashidi, M.; Blokhus, A. M.; Skauge, A., J. Appl. Polym. Sci. 117, 1551 2010.
234. Ait-Kadi, A.; Carreau, P.; Chauveteau, G., J. Rheol. (1978-present) 31, 537 1987.
235. Sakihama, Y.; Mano, J. i.; Sano, S.; Asada, K.; Yamasaki, H., Biochem. Biophys. Res. Commun. 279, 949 2000.
236. Marquez, L. A.; Dunford, H. B., Eur. J. Biochem. 233, 364 1995.
237. Johnson, S.; Trejo, J.; Veisi, M.; Willhite, G. P.; Liang, J. T.; Berkland, C., J. Appl. Polym. Sci. 115, 1008 2010.
238. Sydansk, R.; Al-Dhafeeri, A.; Xiong, Y.; Seright, R. S. SPE/DOE Symposium on Improved Oil Recovery, 2004. Document ID: SPE-89402-MS
239. Guaita, M.; Chiantore, O.; Luda, M. P., Macromol. 23, 2087 1990.
240. Tobita, H., Macromol. 29, 3000 1996.
241. af Ekenstam, A., Ber. Dtsch. Chem. Ges. 69, 549 1936.
242. Cheng, Y.; Prud'homme, R. K., Biomacromolecules 1, 782 2000.
243. Gulbis, J.; King, M.; Hawkins, G.; Brannon, H., SPE Prod. Eng. 7, 9 1992.
244. Malone, M. R.; Nelson, S. G.; Jackson, R. SPE Permian Basin Oil and Gas Recovery Conference, 2000. Document ID: SPE-59709-MS
245. Tjon-Joe-Pin, R. M.; Brannon, H. D.; Handren, P. J. SPE Production Operations Symposium, 1995. Document ID: SPE-29446-MS
246. Brannon, H. D.; Tjon-Joe-Pin, R. M.; Carman, P. S.; Wood, W. D. SPE Annual Technical Conference and Exhibition, 2003. Document ID: SPE-84213-MS
247. Yang, J.; Hong, L.; Liu, Y.-H.; Guo, J.-W.; Lin, L.-F., Environ. Technol. 35, 2878 2014.
248. Mota, A.; Albuquerque, L.; Beltrame, L. C.; Chiavone-Filho, O.; Machulek Jr, A.; Nascimento, C., Braz. J. Petrol. Gas 2, , 122 2009.
249. Mai, C.; Majcherczyk, A.; Schormann, W.; Hüttermann, A., Polym. Degrad. Stabil. 75, 107 2002.

4 Polymer Filtration, Core Flooding, and Enzyme Immobilization

The objective of this study was to evaluate the ability of hydrogen peroxide and a peroxidase catalyst to recover damage created by HPAM flooding when applied to porous media. Flow recovery was measured using synthetic filters and geologic core flooding tests where flow characteristics were measured in only the forward flow direction. It should be noted that measurements of unidirectional flow with different treatments is a conservative evaluation method since increased permeability of oil and/or gas in the reverse direction is the desired goal. However, the unidirectional flow of water/brine will serve as a stringent proxy in evaluating the current method and allow more fundamental calculations of the sizes of pore and polymer layer, etc. HPAM plugging of synthetic filters was initially evaluated to test the treatment system. Core flooding studies were conducted to measure the recovered permeability of HPAM damaged Indiana limestone using both free and immobilized HRP. HRP immobilization was conducted on Ottawa sand and the immobilized concentration and activity were characterized. In addition, HPAM viscosity reduction was measured using free and immobilized HRP. The enzyme-coated sand was then used in core flooding studies to observe permeability recovery in HPAM damaged cores. The final section constitutes a theoretical analysis derived from enhanced oil recovery to determine and explain the macro phenomena in terms of the average pore radius and polymer layer thickness before and after treatments given the experimental data.

In this chapter, Section 4.1 presents results obtained for filtration tests and filtration control experiments. Section 4.2 presents data collected for core flooding tests conducted using free enzyme in solution in consolidated cores. This section introduces core flooding by using Berea Sandstone modified with filter paper on the inlet side of the core. The modified core acted as an

intermediate between filtration tests and core flooding using lower permeability Indiana Limestone. Lastly, Indiana Limestone was used to measure permeability recovery after HRP treatments. The flow of treatment through the core resulted in additional permeability reduction and prompted the need for a new technique for applying treatment. Section 4.3 presents the data collected after HRP was covalently immobilized on glass beads and Ottawa sand. In this section, data is presented to describe the immobilized concentration, activity, ability to reduce the viscosity of HPAM, and recover permeability during core flooding.

4.1 Filtration Results and Controls

Filtration experiments compared the flowrate recovery when filter cake was created using HPAM alone or HPAM and treatment components (e.g. HRP and NADH). This set of experiments used a new brand of filter that resulted in greater HPAM retention compared to filters used in preliminary experiments (Section 5.2). The greater retention was observed following noticeable reduction in flowrates during filter cake formation. In response to the greater polymer retention, the volume of 2000 ppm HPAM used was reduced from 15 ml to 10 ml. First, undamaged flowrate (Q_i) to filter is measured with water.

Damage to the filter is created using 10 ml of components from Table 4.1 in the column labeled "cake formation", then the flowrate of damaged filter (Q_d) was measured with water. The excess water was vacuumed suctioned off and 10 ml of the corresponding treatment was applied. Two milliliters of the treatment was flushed through the filter to ensure contact with filter cake and the treatment is allowed to set at room temperature for 24 hours. After 24 hours, the excess treatment solution was carefully vacuum suctioned off and the recovered flowrate (Q_r) to water was measured. The percent flowrate damage after cake formation and recovery after treatment is calculated as shown in Equations 52 and 53.

$$\% \, Damage = (Q_i - Q_d)/Q_i * 100 \quad (52)$$

$$\% \, Recovery = (Q_r - Q_d)/Q_i * 100 \quad (53)$$

Initial experiments were performed using nylon filters as a proxy for low permeability rock to demonstrate the potential for use of peroxide and HRP for remediation of polymer damage to the filter; here "damage" will be used in the sense commonly understood in petroleum engineering to refer to permeability losses due to the buildup of polymer on the filter and not mechanical damage. Filtration tests were conducted using 0.1 µm nylon filters to evaluate the effect of HRP component addition order and quantify the flowrate recovery when filter paper was highly damaged with HPAM polymer. The permeability of the filter papers used was very uniform with the mean undamaged flowrate for all of the filters used at 64.1 ± 2.1 ml/min under constant pressure (20 psi). Approximately 10 ml of 2000 ppm polymer solution was flowed to build up a model "filter cake" and create flowrate decreases of 99.86 ± 0.02 % for all filters tested. Figure 4.1 shows pictures of undamaged and damaged filters. In this image, the texture of the woven filter can be seen on the wet undamaged filter (a), while the damaged filter shows a smooth, glossy gel-like layer that has developed (b). To recover the permeability of the damaged filter, various combinations of both the method of damage formation and the recovery technique were examined. As shown in Table 4.1, simply treating the polymer plugged (damaged) filter by adding hydrogen peroxide did little to remediate the filter permeability. However, when just one treatment was performed with H_2O_2 and the HRP enzyme (with or without NADH) in the solution above the plugged filter, the permeability improved to a modest but relevant, 2.0% to 6.4%. Here, NADH

was also investigated as in the previous viscosity study (Section 3.1) as it is known to reduce the very small amount of polymer degradation due to the peroxide alone; *i.e.* reduce any background side reactions. Interestingly, when the HRP was added to the polymer during the flow (not after as above) and resulting plugging from the polymer solution, the recovery with treatment of just peroxide (with or without NADH) improved to 13-14%. Here, the HRP becomes imbedded in the polymer film and filter as opposed to the previous scenarios where the HRP is in the solution above the filter. Thus, as the peroxide diffused into the HPAM polymer film, the reaction was initiated in the enzyme with concentrated polymer surrounding it to immediately react and degrade. This contributed to development of the HRP immobilization studies below. It should be noted that these treatments are un-optimized (concentrations, duration, number of treatments, etc.) and better results may be expected with further study. Although moderate recoveries were produced for these unidirectional tests, this indicates the potential of the peroxide and enzyme treatment for actual core samples (rock) (see next section).

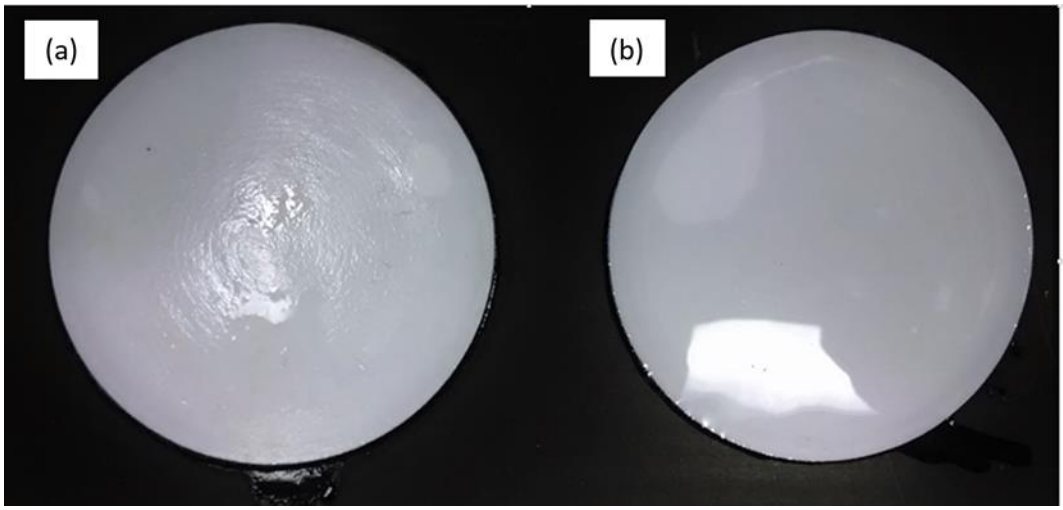

Figure 4.1 Example of wet filter as control (a) and filter damaged with 10 ml, 2000 ppm Alcoflood 935 (b).

Table 4.1 Mean percent recovery achieved when cake and treatment contain different components. Filtration conducted using 0.1 μm, nylon filter paper.

Cake formation	24-hour treatment	Mean Recovery (%)	Std dev	n
HPAM	water	0.1	0.0	3
HPAM	peroxide	0.1	0.0	3
HPAM	HRP, peroxide	2.0	0.8	3
HPAM	HRP, NADH, peroxide	6.4	3.9	4
HPAM & HRP	peroxide	13.1	10.3	4
HPAM & HRP	NADH, peroxide	14.0	7.4	4

10 ml of components to form "cake"; 24-hour treatments. Concentrations for HPAM, HRP, NADH, and peroxide are 2000 ppm, 45.0 μM, 1.4 mM, and 96.9 mM hydrogen peroxide respectively. Positive-pressure was 20 psig and treatment was applied for 24 hours at room temperature.

Control experiments were conducted to observe flowrate change attributed to polymer re-dissolution, i.e. polymer from the filter cake diffusing back into solution during the treatment time. After the filters were plugged, the polymer solution was removed and replaced with water and allowed to sit for 24 hours. Permeability change due to cake dissolution was tested by measuring flowrate of water through the undamaged filter, creating the cake with 10 ml HPAM, then adding 10 ml water in place of the treatment. After 24 hours, only a negligible recovery (0.08 ± 0.03 %) in flowrate was observed. Thus, re-dissolution of the polymer film does not appear to be factor within the time period of the study. Controls were repeated with a 24-hour treatment with peroxide (no HRP), and results were nearly identical to the water treatment (0.08 ± 0.02 %); again indicating that the enzyme catalyst, HRP, is necessary. In the absence of HPAM damage, filter exposure to the enzyme reaction resulted in a 9.061 ± 1.75% decrease in flowrate. The rate reduction can be attributed to the 2 ml flow through the filter after addition of treatment and from the residual enzyme in the filter holder after removal of the supernatant. This reduction would not exist for a fracturing treatment due to the reversal of flow during well production, and is an artifact of the

experimental procedure. In addition, the results solidify the fact that enzyme is incorporated into the filter cake when formed with HPAM and HRP.

4.2 Core Flooding with Resin Encapsulated Cores

Resin encapsulation of cores came with several advantages. First, unlike the Hassler-type core holder, the orientation of the core was vertical and a "head space" above the core provided excess room for applying treatment (see figures in Methods and Materials). With the Hassler core holder, solutions were directly injected through the core so pumping treatment solution into the core was unavoidable. With the resin-encapsulated cores, the ≈10 ml headspace allowed brine to be pushed through the core with air. This process creates a void above the core, without disturbing the polymer cake, so that treatment could be applied to the surface. Treating only the surface, and the vertical orientation of the core holder, allowed the experiments to be conducted at atmospheric pressure because generated oxygen would accumulate away from the core. Oxygen generated during the reaction did not enter the core, which can effect permeability measurement by changing the brine saturation in the core. Secondly, slow circulation of brine at the top of the core holder, after treatment, diluted the enzyme treatment before measuring recovered permeability. This can prevent some additional damage created by flowing enzyme through the core. Lastly, resin and PVC did not show signs of degradation in the presence of free radicals and therefore would not create addition damage (as seen in Hassler core holder, Chapter 5).

First, Berea sandstone cores, with the inlet surface modified with 0.1 micron nylon filters, were used to test flow recovery. The filters were placed on the inlet side of the core to filter out polymer, as done in filtration tests, and measure permeability recovery when damage contribution was limited to the surface and not internal pore plugging. This experiment gave a true cake recovery

since polymer had no measureable effect on permeability of Berea sandstone without filter. Lastly, low permeability Indiana Limestone was used to evaluate recovery after damage was created using HPAM.

4.2.1 Core Flooding using Filter Modified Berea Sandstone

Berea sandstone (BSS) cores were modified by placing a 0.1 micron filter on the inlet surface of the rock (Figure 4.2). The purpose of this test is to evaluate HRP ability to recover permeability when damage is created solely on the surface. The brine permeability of BSS before addition of filter paper was between 50-100 md and contained porosity around 0.15. Experiments wereconducted using PVC encapsulated method and damage was created using 1.5-1 ml, 2000 ppm HPAM. Due to the higher permeability, a flowrate of 1.0 ml/min was used during all stages of fluid flow. In low permeability cores, such as Indiana Limestone (1-4 md), damage to permeability is a combination of internal (pore plugging and adsorption) and external damage (filter cake). The filter on Berea Sandstone allowed damage to be created at the surface and the high permeability of the Berea sandstone allows polymer to flow through the core without creating measureable damage.

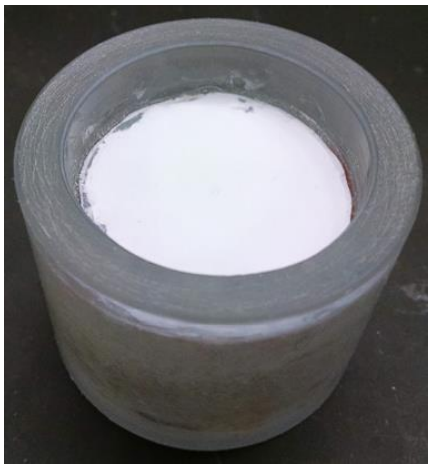

Figure 4.2 Berea sandstone core encapsulated in PVC and modified with filter paper.

The results of this study show favorable recoveries for all cores (Table 4.2). Core BSS #1 injected two polymer slugs of 0.5 and 1 ml because only 32% damage resulted from the first 0.5 ml injection. Although a total of 1.5 ml HPAM was used, only 55.8% reduction in permeability occurred. In addition to the minimal damage, a very high recovery of 83% resulted from treatment. Cores BSS #2 and #3 show very similar results with around 95% damage created using 1 ml HPAM and a recovery of about 50%. The permeability recovery observed for these cores after treatment was almost immediate. Unlike low permeability cores (discussed in the next section), the pressure stabilized after 15 minutes (15 ml) as opposed to 15 hours (180 ml) during experiments with Indiana Limestone. The quick pressure stabilization indicates that no internal pore plugging occurred. The results show that surface treatment is effective and that much of the damage observed in low permeability cores, as shown in the next section, was due to internal pore plugging and adsorption.

Table 4.2 Core flooding results obtained for Berea sandstone cores in PVC, modified with 0.1 micron, nylon filter paper.

Core #	Undamaged Ki (md)	HPAM volume (ml)	Damaged Kd (md)	Reduction (%)	Recovered Kr (md)	Residual Damage (%)	Damage Recovery (%)
BSS #1	59.33	1.5 ml	26.22	55.8	53.69	9.5	83.0
BSS #2	69.03	1 ml	2.93	95.8	38.12	44.8	53.2
BSS #3	73.01	1 ml	3.97	94.6	35.07	52.0	45.0

4.2.2 Free Enzyme: Core Flooding with Indiana Limestone

Indiana limestone (ILS, 1-4 md) was used to evaluate permeability recovery using HRP treatment. Indiana limestone was chosen due to low, but experimentally manageable, permeability

and is intended to simulate other types of low permeability geologic formations. Limestone fracturing is well established.[250,251] In all, about 20 cores originating from the same source were evaluated including method development studies. Little heterogeneity in dimensions or porosity was observed for the cores as a function of height of the total core (approximately 30+ cm total length). For instance, the cores (1.68 ± 0.07 cm long and 2.54 ± 0.01 cm diameter) had average pore volumes and porosity of 1.27 ± 0.09 cm^3, and 0.149 ± 0.008 respectively. However, initial brine permeability varied from about 1.5 to 3.7 md. Porosity and permeability relationships were previously mentioned in Section 2.5 but are shown again in Equations 54 and 55. Experimental sets are made of at least three core samples to evaluate the permeability change after treatments with standard deviations to represent the random error. Damage was created using 1.0 ml, 2000 ppm HPAM solution and flowrate for all steps was held at 0.2 ml/min. After damage, the temperature was increased from room temperature to 30°C then the treatment method was introduced for 24 hours. Brine was pumped through the core for 15 hours at 0.2 ml/min at which time the recovered permeability was measured. Percent permeability damage and recovery are a function of the initial undamaged permeability (K_i), damaged permeability (K_d), and recovered permeability (K_r). The mean percent damage created for all cores was 88.9 ± 2.9 % and resulted in significant pore plugging. All treatments and permeability measurements were obtained in the same direction (unidirectional) through the core as a means of testing the recovery. This method allowed for the analysis of residual resistance factor (*RRF*) and polymer layer thickness (β) to help quantify recovery (see below). It should be noted that measuring recovered permeability in the inward direction is a severe test of any potential remediation method as the degraded polymer would be forced through the pores of the core sample. In an actual reservoir, the most important permeability would be of oil or gas production (formation to wellbore) and not in the direction of

the hydraulic fracturing flow (wellbore to formation). However, this is beyond the scope of these studies which are aimed at demonstrating the proof of concept. It is therefore expected that any recovery from treatments and measurements from unidirectional flow of brine would lead to significant improvement for oil and gas production for any actual field treatment.

$$Porosity\ (\phi) = \frac{\frac{saturated\ weight - dry\ weight}{brine\ density}}{bulk\ volume} = \frac{pore\ volume}{bulk\ volume} \qquad 54$$

$$K_b = \frac{Q\eta L}{\Delta PA} \qquad 55$$

Table 4.3 illustrates the results of a variety of different treatment scenarios and control experiments. A set of control experiments was conducted whereby the damaged core was treated with brine instead of the HRP/H_2O_2 treatment. The results illustrate that no recovery occurred throughout the duration of treatment and 15-hour brine flush as indicated from the permeability (recovery of 0.04% ± 2.12%). Also, the absence of peroxide resulted in a negligible recovery of 3.8 ± 3.1%. However, when HRP and peroxide were added as a treatment, an average recovery of 9.6 ± 2.9 percent was obtained as shown in Table 4.3. This illustrates that the enzyme catalyzed treatment reduced the molecular weight and viscosity of the polymer filter cake and reduced the amount of pore plugging observed. The reduction in pore plugging is discussed in Section 4.3.4 by comparing polymer layer thickness (β) before and after treatment. Again, this permeability improvement is from a conservative test of unidirectional flow for damage, treatment, and permeability measurements.

However, a control study was conducted on the effect of peroxide alone on permeability recovery. For these experiments, a significant recovery was observed (17.7% ± 4.4% percent

permeability recovery). This is despite the fact that little to no reaction was observed with peroxide alone for degradation of the polymer in solution or in the previous nylon filter studies (Section 4.1). Hydrogen peroxide may slowly react with some types of carbonate rock.[252] However, the Indiana Limestone Institute of America actually recommends cleaning without damaging limestone surfaces with hydrogen peroxide to remove microorganisms such as algae.[253] In addition, Indiana Limestone contains a small amount (<1%) of iron oxide which may catalyze peroxide.[254,255] In the current study, Indiana Limestone was exposed to 96.9 mM peroxide for 24 hours and we believe the permeability recovery is more than likely a result of a slight reaction with the rock widening the pores. On the other hand, studies containing HRP consume most of the peroxide within the first couple of hours. For this reason, it is believed that reaction of the peroxide with the rock has a minor role in the results discussed for the HRP/H_2O_2 treatment discussed above.

The effect of the HRP/H_2O_2 treatment on an undamaged, native core was investigated. As shown in Table 4.3 forcing some of the remaining treatment solution through the core actually leads to a reduction in permeability of 24% ± 13 percent. While the solution is dilute in HRP, the enzyme is a biopolymer with a molecular weight of approximately 44,000 g/mol and a diameter of approximately 5 nm.[256,257] In addition, the HRP enzyme can form dimers and trimers, especially upon degradation.[216] Thus, it would potentially be trapped by some pore sizes in the core, depending on pore connectivity and throat diameters; in addition to being trapped in HPAM filled pores before a certain amount of degradation of the HPAM can take place.

Overall, core flooding results using free enzyme show that a significant recovery is possible using the full enzyme treatment but the rigorous method for testing the recovery creates residual permeability reduction by HRP. To elevate the actual permeability recovery, and eliminate negative contribution by the enzyme, HRP was covalently bound to Ottawa sand. Not only should

this eliminate the enzyme damage, it should also ensure that HRP is concentrated near the polymer damage, resulting in greater permeability recovery for filtration experiments.

Table 4.3 Recovery data for core flooding experiments using free enzyme. ($n \geq 3$)

Data Set #	Description	Initial Permeability (md)	Damaged Permeability (md)	Percent Damage (%)	Recovered Permeability (md)	Damage Recovery (%)
1	*No damage*: HRP/peroxide treatment	2.79 ± 0.71	-------	-------	2.07 ± 0.35	** -24.1 ± 12.5
2	Brine treatment	3.62 ± 0.48	0.51 ± 0.09	86.0 ± 1.9	0.50 ± 0.01	0.0 ± 2.1
3	HRP/NADH treatment	1.80 ± 0.50	0.20 ± 0.10	89.8 ± 0.5	0.26 ± 0.09	3.8 ± 3.1
4	HRP/NADH/ peroxide treatment	3.72 ± 0.94	0.43 ± 0.32	89.2 ± 5.8	0.79 ± 0.44	9.6 ± 2.9
5	Peroxide treatment only	1.48 ± 0.13	0.16 ± 0.02	89.2 ± 2.6	0.42 ± 0.06	17.7 ± 4.4

Indiana Limestone cores were damaged using 1 ml, 2000 ppm Alcoflood 935. Treatment solutions were applied for 24 hours at 30°C. Recovered permeability was measured after 15-hour brine flush to ensure steady state flow. ** Represents residual damage after HRP, NADH, and peroxide in the absence of HPAM.

4.3 Enzyme Immobilization and Application

Enzyme was immobilized on glass beads and Ottawa fracturing sand as a means of enzyme application in core flooding experiments. Ottawa sand provides a cheap alternative to glass substrate and immobilized enzyme could be used for bioremediation processes both in and out of fracture for a variety of compounds and applications. This study focused on the ability of immobilized HRP to catalyze the degradation of HPAM. Section 4.3.1 describes the immobilized concentration and activity measured for immobilization on glass and sand substrates. Section 4.3.2 tested the ability of enzyme immobilized on sand to reduce the viscosity of HPAM in solution. After viscosity reduction was confirmed, immobilized HRP was applied in core flooding studies

(Section 4.3.3). Overall, immobilization showed a greater permeability recovery in HPAM damaged core when compared to free enzyme.

4.3.1 Immobilized Enzyme Concentration and Activity

Immobilize HRP concentration was determined by measuring the change in HRP concentration of sample supernatant for 75-micron glass bead and Ottawa sand samples. The concentration of immobilized enzyme is equivalent to the change in concentration observed in the sample supernatant. After incubation at 4°C, the effluent of samples were collected diluted 4:1 in water. This dilution reduced the enzyme concentration from about 5 ml/ml to about 1 mg/ml. Two methods for finding concentration were tested. First, Bradford reagent was made and evaluated spectrophotometrically according to the literature.[258] The results of the standard curve were not repeatable so HRP concentration was evaluated directly using UV-Vis spectrometer.

The HRP immobilized on sand was initially characterized to determine the amount of bonded enzyme. Standard HRP activity assays were employed using UV-vis absorption spectroscopy. To generate a standard curve, 2 mg/ml HRP in 50 mM PBS was diluted with water to create solutions ranging from 2-0.01 mg/ml. The absorption spectra, shown in Figure 4.3, revealed three peaks that were characteristic of HRP. A plot of the absorbance values for peaks found at 205, 280, and 405 nm are is shown in Figure 4.4 for the various concentrations. The plotted results revealed that a wavelength of 405 nm is best suited for evaluating the concentration change in HRP solutions. At a wavelength of 205 nm, the correlation is nonlinear and generates significant error. On the other hand, at a wavelength of 280 nm, a good linear correlation was developed but a lower intensity is observed making it less sensitive to small changes in concentration. The concentration for following experiments were evaluated using the correlation shown in Figure 4.4 at 405 nm.

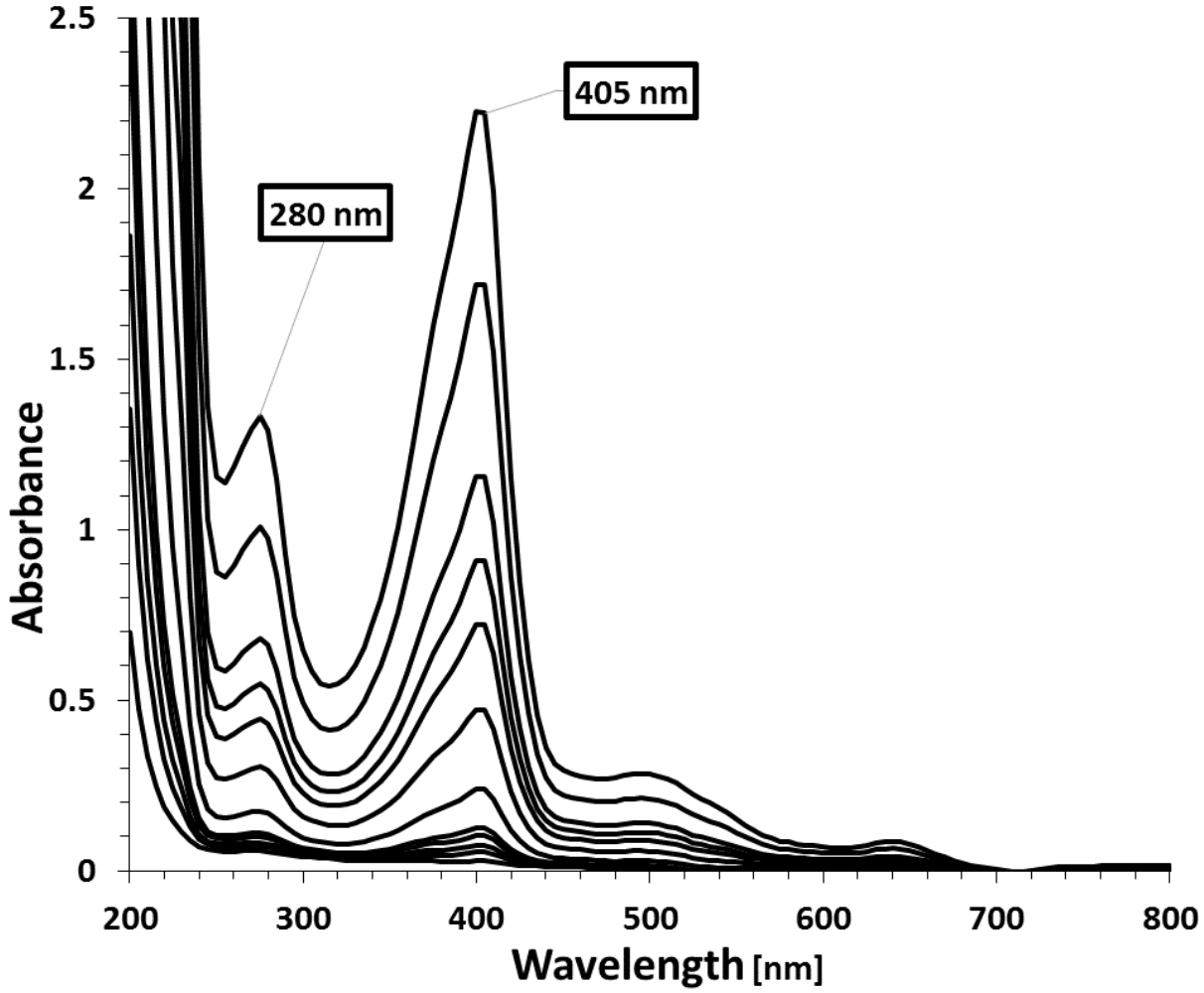

Figure 4.3 Wavelength scan of HRP at various concentrations.

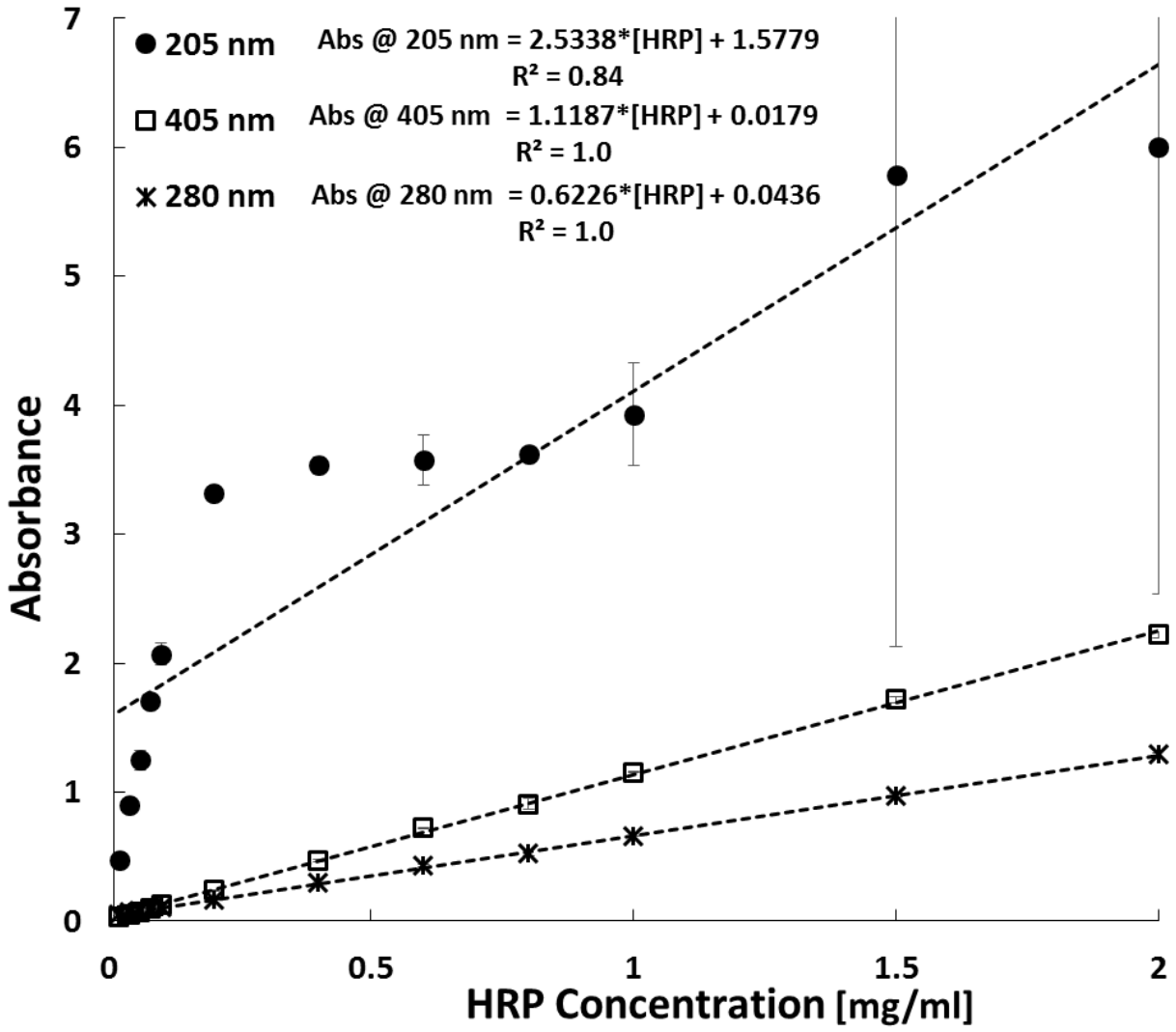

Figure 4.4 Absorbance for varying concentration of HRP at three wavelengths.

Experiments evaluated the concentration of immobilized enzyme on 0.2 grams of 75-micron glass beads and Ottawa sand. Solutions were incubated at 4°C for 24 hours before evaluating the concentration and activity. The final immobilized concentration was calculated as 1.03 ± 0.18 mg HRP per gram sand and 0.26 ± 0.11 mg HRP per gram glass beads. Preliminary studies indicated that a longer sand/enzyme exposure time of 96 hours did not significantly change the amount of immobilized HRP concentration on sand resulting in about 1.07 mg HRP per gram sand. In

addition, longer enzyme exposure times to glass resulted a much higher immobilized of 1.779 mg HRP per gram glass after 96 hour enzyme exposure.

The activity of the immobilized enzyme was determined and compared to a control of free enzyme in solution. The values represented here were measured for the same samples represented by the reported concentrations. For the control (subjected the same conditions as immobilized samples in the absence of sand), and immobilized HRP on sand, experimental results showed that this unoptimized immobilization technique decreased the activity versus the control of free enzyme, under the same dilution (4:1, water to enzyme solution). The activity results for Ottawa sand and glass are listed in Table 4.4. The results indicate that a lower enzyme concentration was achieved for glass but the retained activity was much greater.

Table 4.4 Unit Activity (U) of control versus HRP immobilized on Ottawa sand 75-micron glass beads.

	Ottawa Sand		**75-micron glass beads**	
	[U/ml solution]	[U/mg HRP]	[U/ml solution]	[U/mg HRP]
Control	214.2 ± 15.8	214.2 ± 15.8	197.1 ± 16.6	197.1 ± 16.6
HRP-Solid substrate	1.1 ± 0.6 [U/g sand]	1.1 ± 0.6 [U/mg HRP on Sand]	7.2 ± 3.8 [U/g glass]	27.7 ± 18.0 [U/mg HRP on glass]
Silanized substrates were subjected to 5 mg/ml HRP for 24 hours at 4°C.				

4.3.2 Immobilized Enzyme for HPAM Viscosity Reduction

To confirm that the immobilized enzyme was able to catalyze the breakdown of HPAM, the viscosity of 1980 ppm Alcoflood 935 was observed in the presence of free and immobilized enzyme. For samples containing no HRP, untreated Ottawa sand and peroxide was added to HPAM solutions. The amount of free enzyme used was based on previous concentration studies using HRP immobilized on Ottawa sand (1.032 mg HRP/mg sand). The reduction in viscosity was

measured periodically over a 24-hour period and the results are depicted in Figure 4.5. The initial viscosity was 13.34 ± 0.56 centipoise (n=6) using samples with and without free HRP. The results of this study show that there was a significant reduction in viscosity for both the free and immobilized enzyme in comparison to sample containing no HRP. Furthermore, a greater reduction in viscosity and rate was observed for the free enzyme when compared to the immobilized sample as expected for the higher unit activity. The results of this study confirm that there is a decreased activity observed with the immobilized enzyme sample but it is still sufficient to catalyze significant breakdown of HPAM.

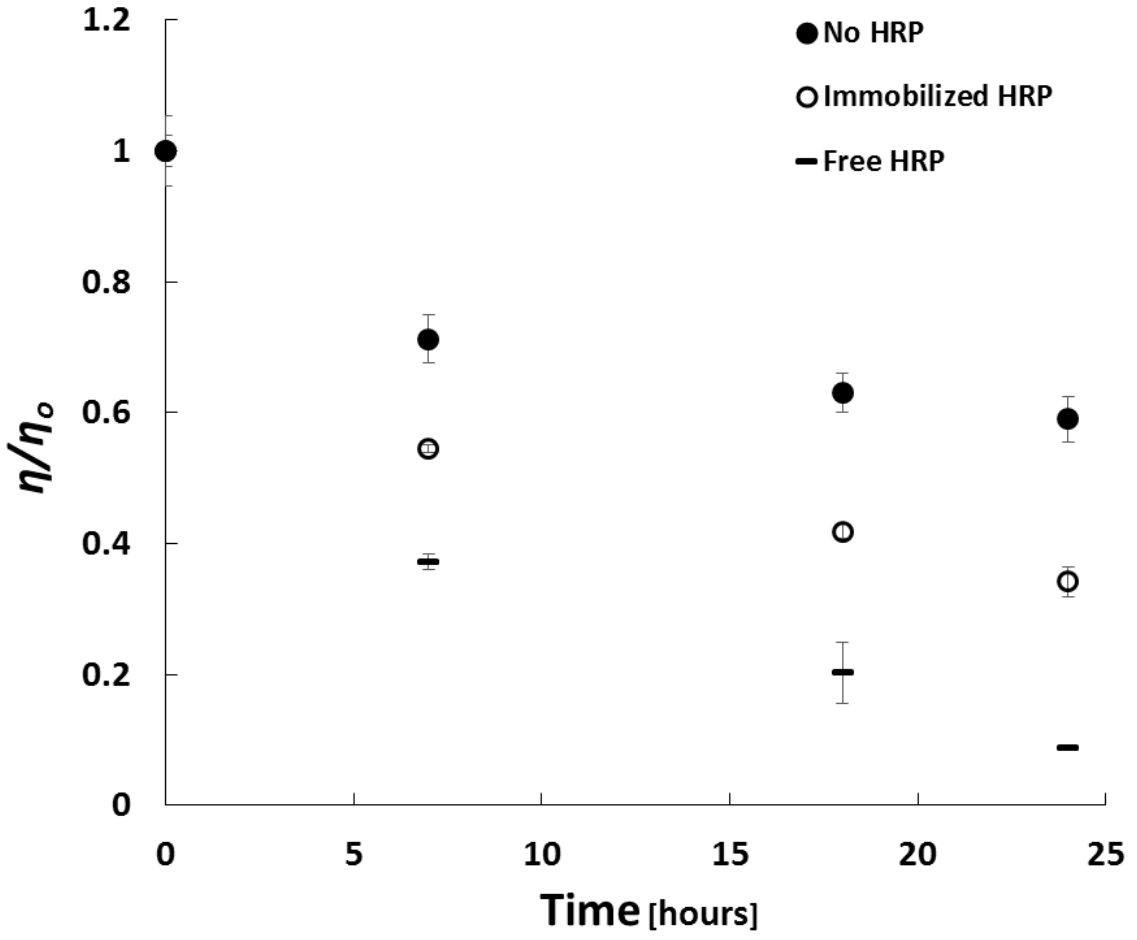

Figure 4.5 The reduction in HPAM viscosity observed in the presence of HRP treated and untreated Ottawa sand. Viscosity measured at $75s^{-1}$ and 25°C. (n=3)

As a control, sand without immobilized HRP was investigated. As shown in Figure 4.5, a reduction in viscosity was observed for HPAM samples containing no HRP and just H_2O_2. This is in contrast to previous studies where little to no degradation of HPAM occurred in solution containing only H_2O_2. Ravlkumar and Gurol[259] studied the decomposition of hydrogen peroxide in the presence of sand. They showed percent decomposition values 5-10 times higher in the presence of sand when compared to glass beads. Higher peroxide percent decomposition was observed in sands containing higher iron content up to 22% depending on the sample. Ottawa sand used in the current study contains about 99.8 SiO2, 0.02% Fe_2O_3, 0.06% Al_2O_3, with the remaining content consisting of trace minerals. Therefore, 0.5 g untreated sand would be equivalent to 0.1 mg iron oxide. Although the iron content in the Ottawa sand sample is low, this may be catalyzing the observed viscosity reduction for samples not containing HRP.

4.3.3 Core Flooding with HRP Immobilized on Ottawa Sand

The immobilized enzyme was used in the core flooding studies to reevaluate the HPAM damage recovery and eliminate the chance for any plugging from the treatment procedure itself. Experimental procedure mimicked that used for core flooding studies but one gram of enzyme treated Ottawa sand was placed on top of the core after damage was created. The results using the immobilized samples show a recovery of 32.0 ± 0.4 percent (see Table 4.5). These results are a 75% improvement compared to free enzyme treatment. As expected, the sand itself, with much higher porosity than the limestone, showed no measurable change in permeability. Data for free and immobilized HRP correlate well with the damage observed from the free enzyme reaction alone. For example, addition of the permeability reduction caused by the HRP/peroxide reaction (24.1%) added to the recovery from the same reaction (9.6%) should yield about 33.7% recovery. During an actual field treatment, the immobilized sand would be imbedded within the polymer

filter cake upon fracture closure, and possibly provide even better degradation of the film. Therefore, this technology could be further developed as more cost effective fluid remediation technique.

Table 4.5 Recovery data for core flooding experiments using free and immobilized enzyme. ($n \geq 3$)

Data Set #	Description	Initial Permeability (md)	Damaged Permeability (md)	Percent Damage (%)	Recovered Permeability (md)	Damage Recovery (%)
1	*No damage*: HRP/peroxide treatment	2.79 ± 0.71	-------	-------	2.07 ± 0.35	** -24.1 ± 12.5
2	Brine treatment	3.62 ± 0.48	0.51 ± 0.09	86.0 ± 1.9	0.50 ± 0.01	0.0 ± 2.1
3	HRP/NADH treatment	1.80 ± 0.50	0.20 ± 0.10	89.8 ± 0.5	0.26 ± 0.09	3.8 ± 3.1
4	HRP/ peroxide treatment	3.72 ± 0.94	0.43 ± 0.32	89.2 ± 5.8	0.79 ± 0.44	9.6 ± 2.9
5	Peroxide treatment only	1.48 ± 0.13	0.16 ± 0.02	89.2 ± 2.6	0.42 ± 0.06	17.7 ± 4.4
6	Immobilized HRP treatment	2.49 ± 0.87	0.31 ± 0.18	87.7 ± 2.7	0.99 ± 0.40	28.0 ± 0.7

Indiana Limestone cores were damaged using 1 ml, 2000 ppm Alcoflood 935. Treatment solutions were applied for 24 hours at 30°C. Recovered permeability was measured after 15-hour brine flush to ensure steady state flow. ** Represents residual damage after HRP, NADH, and peroxide in the absence of HPAM.

4.3.4 Further Core Flooding Analysis

Much of the literature for analysis of permeability with HPAM solutions relate to intentionally reducing permeability for enhanced oil recovery (EOR). In this process, concentrated HPAM solutions are injected into the rock matrix to reduce the permeability of highly water flooded areas in order to divert the flow to lesser flooded areas. Thus, similar analysis techniques for EOR permeability (but with opposite goals) may also be useful for these studies. In these studies, the permeability reduction quantified by means of the resistance factor (*RF*) and residual resistance factor (*RRF*) as described by Equations 56 and 57 and are measured at steady state.[260-262] In

addition, the average pore radius (r_p, μm) and the average thickness of the polymer layer (β, μm) can be calculated using Equations 58 and 59.[260] The resistance factor is a measure of the polymer's effective viscosity as it flows through porous media and was not calculated in this study because steady state polymer flow was not achieved. The residual resistance factor, *RRF*, is a measure of the polymer induced reduction of brine permeability. Due to the constant flowrate (0.2 ml/min) used throughout the experiment, the residual resistance factor can be calculated using undamaged (K_i) and damaged permeability (K_d) values from previously presented tables.

$$RF = \frac{\Delta P_{Polymer}}{\Delta P_{Brine}} \quad (56)$$

$$RRF = \frac{\Delta P_{\text{Brine after HPAM injection}}}{\Delta P_{\text{Brine before HPAM injection}}} \; or \; \frac{K_{\text{Brine before HPAM injection}}}{K_{\text{Brine after HPAM injection}}} \quad (57)$$

$$r_p = \left(\frac{8 * K_i}{\phi}\right)^{\frac{1}{2}} \quad (58)$$

$$\beta = r_p * (1 - RRF^{-\frac{1}{4}}) \quad (59)$$

where ΔP is the pressure drop, Φ is the porosity, and r_p is the average pore radius. First, using the above equations, the values for *RRF*, r_p, and polymer layer thickness were calculated based from the average porosity, undamaged, and damaged permeability (Table 4.6). The mean of all cores was used for this calculation in order to find the overall average pore radius and polymer layer thickness. The mean pore radius is used in subsequent calculations to find the change in polymer layer thickness before and after applying treatment. As shown, the mean polymer film thickness (0.16 ± 0.03 μm) for the damaged cores (88.9 ± 2.9 % damage) is close to half of the mean pore radius (0.36 ± 0.07 μm) and indicates significant flow damage.

Table 4.6 Shows mean undamaged permeability (K_i), porosity (ϕ), residual recovery factor (*RRF*), pore radius, and polymer layer thickness (β) from all core flooding experiments. Values are based off all core flooding studies using Indiana Limestone damaged with 1ml, 2000 ppm Alcoflood 935.

K_i (md)	ϕ	*RRF*	r_p (μm)	β (μm)
2.43 ± 0.95	0.149 ± 0.008	9.43 ± 2.45	0.36 ± 0.07	0.16 ± 0.03

To quantify the magnitude of recovery, the residual resistance factor is recalculated using recovered permeability values (K_r) measured after treatment from individual data sets. When compared to the initial values, calculated using (K_d), the reduction in effective polymer layer thickness can be compared before and after treatment. The new residual resistance factors and corresponding polymer layer thicknesses, calculated after treatment, are designated as RRF_α and β_α respectively and used the mean pore radius (r_p) calculated in Table 4.7. Since there is significant variation in recoveries, the calculations were conducted using mean recovered permeability values obtained from individual data sets. Table 4.7 lists the calculated residual resistance factors and polymer layer thicknesses for each data set. The data show some variation in RRF between sets but no significant difference is apparent. In addition, little difference was seen in the polymer layer thickness (before treatment) with three of the data sets resulting in a thickness of 0.16 μm. After treatment with the full enzyme system (i.e. HRP, NADH, peroxide), the polymer layer thickness was reduced by 0.04 μm and the residual resistance factor was reduced by half. Little to no change was observed when the cake was subjected to a 15-hour brine flush, in the absence of treatment, and with the enzyme without peroxide. Core exposure to treatment alone (no HPAM) did appear to create a residual resistance factor, which resulted in an absorbed thickness of 0.03 ± 0.02 μm.

Table 4.7 Residual resistance factors and polymer layer thickness calculated for each data set. Abbreviations (*RRF*) an (β) correspond to resistance factors calculated using damaged permeability (K_d). Abbreviations (RRF_α) an (β_α) correspond to resistance factors calculated using recovered permeability (K_r)

Data Set #	Description	Undamaged K_i (md)	Damaged K_d (md)	Recovered K_r (md)	*RRF*	β (µm)	RRF_α	β_α (µm)
1	No damage: HRP/peroxide treatment	2.79 ± 0.71	------	2.07 ± 0.35	-------	-------	1.35 ± 0.25	0.03 ± 0.02
2	Damaged: Brine treatment	3.62 ± 0.48	0.51 ± 0.09	0.50 ± 0.01	7.23 ± 1.08	0.14 ± 0.01	7.20 ± 0.91	0.14 ± 0.01
3	Damaged HRP/NADH treatment	1.80 ± 0.50	0.20 ± 0.10	0.26 ± 0.09	9.54 ± 2.74	0.16 ± 0.01	7.12 ± 1.75	0.14 ± 0.01
3	Damaged HRP/peroxide treatment	3.72 ± 0.94	0.43 ± 0.32	0.79 ± 0.44	11.1 ± 5.20	0.16 ± 0.03	5.22 ± 1.52	0.12 ± 0.02
4	Damaged: Peroxide treatment	1.48 ± 0.13	0.16 ± 0.02	0.42 ± 0.06	9.53 ± 2.00	0.16 ± 0.01	3.51 ± 0.26	0.10 ± 0.01
5	Immobilized HRP	2.42 ± 0.87	0.31 ± 0.12	1.0 ± 0.40	8.41 ± 1.84	0.15 ± 0.01	2.49 ± 0.13	0.07 ± 0.01

4.3.5 Immobilization Discussion and Literature Comparison

The immobilized HRP concentration and activity was very low when compared to the literature. Literature studies indicate that modified immobilization techniques can often lead to much higher retained activities upon immobilization even up to 77-78% of free enzyme.[212,215] Many immobilizations are conducted with porous aminopropyl glass beads that have controlled mesh size and pore diameter. Immobilizations conducted in this study used 75-micron glass beads from Supelco and no information on pore size could be found suggesting that they have a smooth surface. The following literature used the different bead types but similar enzyme attachment by attachment of amine containing compound to the glass surface and using the glutaraldehyde crosslinking for HRP attachment. The literature is discussed to show the wide range of results achieved and to compare these results and methods to those used in this study.

Bodalo *et al.*[213] and Gomez *et al.*[212] both studied the immobilization of horseradish and soybean on 200-400 mesh controlled pore glass. These studies conducted all aspects of attachment and testing in a jacketed reactor to study the ability of HRP to remove phenol compounds. The pretreatment of the glass consisted of exposure to 5% nitric acid at 80°C for 1 hour. Activation with APTES was done in water at pH 3-4 and 75°C for two hours. Glutaraldehyde cross linker was applied at 2.5% (v/v) in 50 mM phosphate buffered saline (PBS) (pH=7) for one hour and immobilization applied 2 mg/ml HRP or SBP at 4°C overnight. The study conducted by Bodalo *et al.*[213] showed slightly higher immobilization concentrations of 42.3 mg/g dry support (45.2%) for SBP and 23.1 mg/g dry support (40.6%) for HRP. The immobilized enzyme showed retained activities 82.4% for SBP and 52.5% for HRP. The study conducted by Gomez *et al.*[212] resulted in concentrations of 35 mg/g dry support (45.2%) and 18 mg/g dry support (40.6%) for soybean and horseradish peroxidase respectively. Furthermore, the immobilized enzyme showed retained activities of 74% for SBP and 78% for HRP. This study suggested that SBP was more suitable for immobilization, compared to HRP, because it contained more free amino groups. In addition, SBP showed greater phenol conversion with increased peroxide concentration. As shown in the viscosity studies SBP can reduce the viscosity of HPAM in solution and, from the results presented in these two papers, may be a better candidate for recovering permeability. In addition, immobilizing the enzyme was shown to protect against inactivation resulting in higher degradation in some cases.

A study conducted by Lai and Lin[214] used 200-400 mesh porous, pre-salinized, aminopropyl glass beads containing a pore diameter of 170 nm. This study did not pretreat the beads and used 2.5% (v/v) glutaraldehyde in 50mM PBS (pH=7) for 8 hours. The beads were then exposed to 2.5 mg/ml HRP in 50 mM PBS (pH=7) at for 12-15 hours. The resulting immobilized enzyme

concentration was 9.6 mg/g support and displayed a specific activity of 5.3 U/g glass. In addition, increasing the HRP load decreased the specific activity. For example, 5.63 mg HRP/g glass lead the specific activity of 43.2 U/g and increasing the enzyme load to 9.6 mg HRP/g glass dropped the specific activity by 30% to 5.3 U/g. The study suggested that the decrease in activity might be a consequence of steric hindrance and glutaraldehyde cross linker may cause extensive protein denaturation. The results of this study show much higher immobilized enzyme concentration than achieved for glass or sand samples in the current study but comparable specific activity for glass samples.

A similar study conducted by Azevedo *et al.*[216] used pretreated, alkylamine controlled pore glass (80–120 mesh, 700nm pore size). Again, no pretreatment was conducted and they used 5% (v/v) glutaraldehyde cross linker in 0.1 M PBS (pH=7) for 2 hours. An HRP concentration of 20 mg/ml in 0.1 M PBS (pH=7) at 4°C for 18 hours. The higher glutaraldehyde and HRP concentrations resulted in a higher enzyme immobilization of 21 mg/g glass with an activity of 17.4 U/cm^3 in a mini-packed bed reactor. In addition, this study showed that upon peroxidation, conjugation between HRP creates enzyme dimers and trimers, which could explain permeability damage created from enzyme treatment during core flooding experiments.

An additional paper by Arica *et al.*[263] studied the immobilization of laccase on non-porous beads. The concentration of immobilized enzyme was much lower compared to porous beads resulting in 4.9-5.6 mg laccase/g substrate. The resulting immobilization showed 53-88% activity compared to free enzyme but values as low as 1-20% have been observed for similar systems.[264] These studies show values closer to the results obtained using the 75 micron glass beads in the current study.

In all of these studies, higher concentration and activity was achieved. When comparing the literature protocols to the current study, only slight deviations from the main procedure exist. First, the glass beads used in the literature were porous and therefore contained greater surface area. This gives the potential for higher protein loading and therefore activity. The second major difference was observed for substrate cleaning. Some studies used pre-coated, arylamine or alklamine, glass and did not describe the substrate cleaning or amine attachment procedure. Gomez *et al.*[217] and Bodalo *et al.*[218] used a less harsh 5% nitric acid treatment before APTES attachment. In the current study, nitric acid proved to be unsuccessful during preliminary studies and this led to the use of piranha solution. The need for a harsher pre-cleaning suggested impurities existed on the glass surface. A longer duration of surface cleaning may be necessary to improve enzyme load. In most cases, glutaraldehyde concentration remains consistent at 2.5% (v/v) but exposure times vary from 1-8 hours. HRP solution concentration seems to play a role in the enzyme load. In most cases, higher HRP concentration applied to the activated substrate results in higher immobilization concentrations.

Very little research has been conducted on enzyme immobilization using sand. The literature has shown that ligand concentrations for controlled pore glass (CPG) vary depending on the type but two publications reported values of 33.8 and 47.6 μmol/g for CPG-2000 and CPG 500 respectively.[217,218] Salinization of Celite, a naturally occurring siliceous sedimentary rock, resulted in slightly lower values of ligand concentration (20.1 μmol/g).[219] A study conducted by Brotherton *et.al* [220] showed that sand contained the lowest ligand concentration resulting in 3.0 μmol/g. The lower concentration of available binding sites on sand will result in lower immobilized enzyme concentrations. In addition to Celite and sand, enzyme immobilization has been studied using other naturally occurring substances such as vermiculite[221], kaolinite, hornblende, biotite, muscovite,

and feldspar[222]. The study conducted by Johnson and Thornton[222] compared immobilization of lactoperoxidase on porous glass, hornblende, biotite, muscovite, feldspar, and sand using APTES and glutaraldehyde binding method in addition to a metal linking method. The results of this study showed that APTES/glutaraldehyde method resulted in the highest specific activity for porous glass (2.5 U/g) and no detectable activity for sand. Using the metal linking method, the highest specific activity was observed for hornblende (5.74 U/g) with the lowest activity of 0.23 U/mg observed for sand. In the current study, 1.1 U/g specific activity was achieved for enzyme immobilization on sand using the APTES/glutaraldehyde binding method. Additional studies have shown that trypsin can be covalently bound to sand. One study using 3-aminopropyltriethoxysilane (APTS) and glutaraldehyde cross linker studied the amount of trypsin binding achieved from iron and non-iron containing sand.[223] The results of the study showed that between 1.88 and 2.31 mg/g bound protein was achieved for all samples. In addition, the study showed that protein binding is covalent and more prevalent with quartz sand. The concentration of trypsin immobilized on sand corresponds well with the finding in the current study.

The reduction in viscosity observed for samples containing treated and untreated Ottawa sand showed degradation for samples containing peroxide and untreated sand. Ravikumar and Gurol[259] studied the decomposition of hydrogen peroxide in the presence of sand. The study showed percent decomposition values 5-10 times higher using sand when compared to glass beads. Higher peroxide percent decomposition was observed in sands containing higher iron content. For example, 1.9% and 4.3% peroxide decomposition was observed in glass samples without iron and with addition of 1 mg ferrous sulfate respectively. The iron content in sand played a direct role in the decomposition of peroxide. Sand samples of varying diameter (0.5-1.4 mm) resulted in similar percent decompositions regardless of the size. Sand samples containing 4.0, 6.0, and 8.0 mg iron

resulted in about 11, 16, and 22 percent peroxide decomposition respectively. Ottawa sand used in the current study contains about 99.8 SiO_2, 0.02% Fe_2O_3, 0.06% Al_2O_3, with the remaining content consisting of trace minerals. For the current viscosity study, 0.5 g untreated sand was present, in the sample not containing HRP, which is equivalent to 0.1 mg iron oxide. Although the iron content in the Ottawa sand sample is low, this still may be the contributing factor for the observed viscosity reduction.

Overall, glass samples showed mixed results for immobilized concentration but the specific activity was higher than that observed for Ottawa sand. The immobilized enzyme concentration on Ottawa sand correlates well with data obtained from the literature. Viscosity reduction using treated and untreated sand samples resulted in viscosity reduction in all samples regardless of HRP addition. A slight decrease in viscosity was observed for samples containing untreated Ottawa sand in the presence of peroxide, which is thought to be caused by trace mineral content in the sand. Furthermore, free HRP resulted in greater viscosity reduction than immobilized samples. Immobilization has shown to reduce the activity and therefore expected to see less viscosity reduction. In core flooding studies, the immobilization alleviated the damage observed from reacted HRP/NADH/peroxide solutions. The reaction of these components have been show to create protein dimers and trimers that can have a greater contribution to pore plugging and further permeability damage.

4.4 Summary

This chapter showed the proof-of-concept for a sustainable enzyme-catalyzed degradation of polymer damaged rock from polyacrylamide solutions with the “green” oxidant hydrogen peroxide. The HRP/H_2O_2 treatment was initially tested on synthetic flat filters plugged with

HPAM. The un-optimized treatment method was able to increase the permeability. Indiana limestone core samples with low permeability (< 4 md) were damaged and then the HRP/H_2O_2 treatment was used to improve the flow. It was noticed that the enzyme treatment method actually both increases and decreases the damage in unidirectional flow system; which would not occur in an actual field treatment. However, immobilizing the enzyme on sand alleviated any further damage due to the enzyme plugging pores and increased the recovery of the damaged cores. This immobilized system may be a useful platform for remediation of polymer damage in hydraulic fracturing operations. Through immobilization, the biocatalyst-activated proppant can act as a excellent means of breaker transport and utilization. Moreover, the renewable and biodegradable reactant and catalyst may be able to help remediate other target chemicals in the fracturing fluid reducing the need for large-scale flowback water treatment.[27] In a broader scope, using silica sand provides an in inexpensive substrate alternative when compared to glass beads and could act as a viable alternative to many HRP bioremediation processes in addition to degradation of HPAM.

4.5 References

27. Gregory, K. B.; Vidic, R. D.; Dzombak, D. A., Elements 7, 181 2011.
212. Gomez, J.; Bodalo, A.; Gomez, E.; Bastida, J.; Hidalgo, A.; Gómez, M., Enzyme Microb. Technol. 39, 1016 2006.
213. Bódalo, A.; Bastida, J.; Máximo, M. F.; Montiel, M. C.; Gómez, M.; Murcia, M. D., Bioprocess Biosyst. Eng. 31, 587 2008.
214. Lai, Y.-C.; Lin, S.-C., Process Biochem. 40, 1167 2005.
215. Pundir, C.; Malik, V.; Bhargava, A.; Thakur, M.; Kalia, V.; Singh, S.; Kuchhal, N., J Plant Biochem Biotechnol. 8, 123 1999.
216. Azevedo, A.; Vojinović, V.; Cabral, J.; Gibson, T.; Fonseca, L., J. Molec. Cat. B 28, 121 2004.
217. Janolino, V. G.; Swaisgood, H. E., Biotech. Bioeng. 24, 1069 1982.
218. Swaisgood, H., Food Enzymology 2, 309 1991.
219. Huang, X. L.; Catignani, G. L.; Swaisgood, H. E., J. Biotech. 53, 21 1997.
220. Brotherton, J. E.; Emery, A.; Rodwell, V. W., Biotech. Bioeng. 18, 527 1976.
221. Chellapandian, M., Process Biochem. 33, 169 1998.
222. Johnson, D. B.; Thornton, D.; Ryan, P. D., Biochem. Soc. Trans. 2, 494 1974.
223. Puvanakrishnan, R.; Bose, S.; Reddi, B., J. Biosci 4, 51 1982.

250. Zillur, R.; Bartko, K.; Al-Qahtani, M. Y. SPE Annual Technical Conference and Exhibition, 2002. Document ID: SPE-77677-MS
251. Abass, H.; Ortiz, I.; Khan, M.; Beresky, J.; Sierra, L. SPE Saudi Arabia Section Technical Symposium, 2007. Document ID: SPE-110973-MS
252. Štelcl, J.; Kubešová, S., Environ. Pollut. 122, 417 2003.
253. Cleaning Indiana Limestone, Website: http://www.iliai.com/pages/Cleaning_Indiana_Limestone
254. McGregor, D. J., High-Calcium Limestone and Dolomite in Indiana, 1963.
255. Lin, S.-S.; Gurol, M. D., Environ. Sci. Tech. 32, 1417 1998.
256. Dvorak, A.; Kohn, S.; Morgan, E. S.; Fox, P.; Nagy, J. A.; Dvorak, H. F., J. Leukoc. Biol. 59, 100 1996.
257. Feder, N., J. Cell Biol. 51, 339 1971.
258. Bradford, M. M., Anal. Biochem. 72, 248 1976.
259. Ravikumar, J. X.; Gurol, M. D., Environ. Sci. Tech. 28, 394 1994.
260. Zaitoun, A.; Kohler, N. SPE Annual Technical Conference and Exhibition, 1988. Document ID: SPE-18085-MS
261. Wever, D. A. Z.; Picchioni, F.; Broekhuis, A. A., Ind. Eng. Chem. Res. 52, 16352 2013.
262. Wei, B., J. Appl. Polym. Sci. 1322015.
263. Arıca, M. Y.; Altıntas, B.; Bayramoğlu, G., Bioresour. Technol. 100, 665 2009.
264. Rekuć, A.; Kruczkiewicz, P.; Jastrzembska, B.; Liesiene, J.; Peczyńska-Czoch, W.; Bryjak, J., Int. J. Biol. Macromolec. 42, 208 2008.

5 Preliminary Studies and Additional Data

This section outlines the experiments and steps taken to develop experimental protocol used in previously presented experiments (Chapters 3 and 4). Preliminary viscosity studies (Section 5.1) were conducted to evaluate the feasibility of HRP as a catalyst to degrade PAM/HPAM in solution. Initially, studies were conducted using 10000 MW PAM and in later experiments, tests are conducted on high molecular weight, commercially available partially hydrolyzed polyacrylamide (HPAM) Alcoflood 935. Using Alcoflood 935 polymer, preliminary studies consisted of end-point (24-hour incubation) measurements as well as continuous sampling.

For filtration tests (Section 5.2), a complete data set was completed in addition to the final experimental set presented in Chapter 4. The preliminary studies used filters found in the lab and showed different flow characteristics to those purchased for the final data set. Preliminary experiments were conducted with and without a back pressure regulator in an attempt to reduce variation in baseline flow (to water) created by trapped oxygen in the filter holder. Although deviation in the data prevented this set from being used, trends in flowrate recovery are similar to those observed for the final data set.

Before core flooding with the Hassler core holder (later explained), oxygen generation via HRP catalyzed decomposition of peroxide was studied (Section 5.3). The study was used to determine the amount of backpressure necessary to keep generated oxygen in solution. Liberated oxygen in the brine saturated cores can change the brine saturation and therefore, the brine permeability. First, a theoretical calculation was conducted based on theoretical peroxide and brine concentrations. Next, UV-Vis spectroscopy was used to measure the initial peroxide concentration and the amount of peroxide consumed during HRP reaction. The theoretical calculation is used, in

conjunction with the corrected peroxide concentrations, to recalculate pressure. Lastly, a high-pressure view cell was used to visualize the oxygen liberation by incrementally reducing the pressure after HRP/peroxide reaction was complete.

Core flooding studies were conducted using the Hassler-type core holder (Section 5.4). This section explains the experimental progression that led to the final, resin encapsulated core holder presented in Chapter 4. This data was included for informational purposes because no relevant data was extracted due to experimental setup.

Lastly, Section 5.5 outlines development of enzyme immobilization protocol. This section explains the methodology used to immobilize HRP on Ottawa sand and glass beads. In addition to the methodology, data is presented that shows preliminary immobilized concentration studies for both Ottawa sand and glass beads after 24 and 96 hour incubation in HRP solution.

5.1 Preliminary Viscosity Studies

This section outlines the experiments and steps taken to develop the concentrations and experimental protocol used in previously presented experiments (Chapters 3). Furthermore, these studies were conducted to evaluate the feasibility of HRP as a catalyst to degrade PAM/HPAM in solution. To start, the viscosity of 10000 MW PAM, at a concentration of 18 wt% in water, was used to observe changes in viscosity. HRP concentration was held constant at 45.3 μM and NADH and peroxide concentrations were varied. In later experiments, tests were conducted on high molecular weight, commercially available partially hydrolyzed polyacrylamide (HPAM) Alcoflood 935. Using this polymer, preliminary studies consisted of end-point (24-hour incubation) measurements as well as continuous sampling.

5.1.1 Preliminary 10,000 Molecular Weight Polyacrylamide

Multiple concentrations of NADH and peroxide concentrations were investigated. Initially the viscosity was observed for 1 hour but this was extended to three hours to observe trends. The starting viscosity of 18 wt% PAM with addition of components was 11-13 centipoise (cP). Viscosity was observed using NADH concentrations of 2.82, 9.09, and 18.33 mM in conjunction with 4.5, 9.69, 22.5, and 96.9 mM hydrogen peroxide. An increase in the viscosity with respect to time was seen in all peroxide activated experiments. Figure 5.1 depicts the normalized viscosity with time where (η_o) is the viscosity at time zero. The data shown uses 2.82 mM NADH and varying peroxide concentrations but also represents trends observed with other NADH concentrations. In this example, no change in viscosity was observed in the absence of peroxide. A greater rate and magnitude in viscosity increase was observed for samples containing higher concentrations of peroxide. In all experiments, samples that did not contain peroxide and/or HRP showed consistant viscosity with time.

The increase in viscosity is indicative of hydrolysis. The hydrolysis of PAM increases the viscosity because the created anionic charges increase the hydrodynamic radius of the polymer.[265,266] Because of the observed increase in viscosity, further experimentation was conducted on a high molecular weight partially hydrolyzed polyacrylamide (HPAM). Alcoflood 935 was estimated to have 6000 kDa molecular weight and is more representative of the polymer used in fracturing applications.

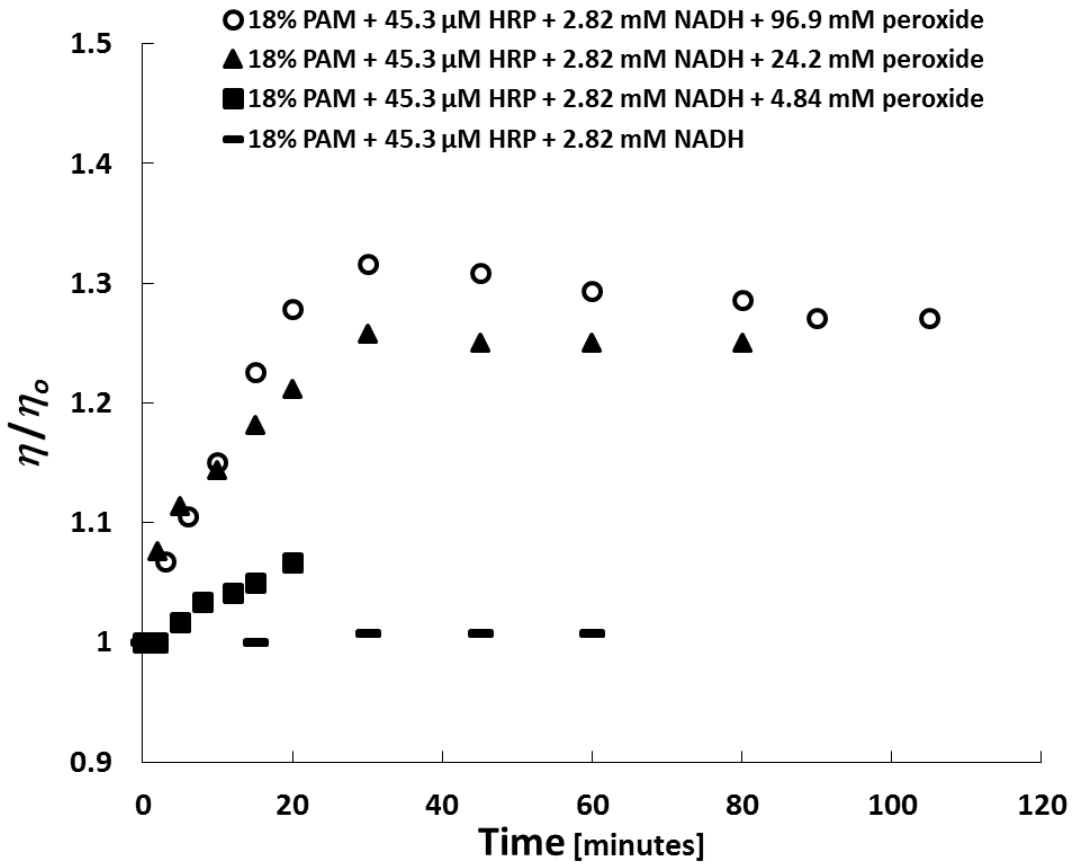

Figure 5.1 Viscosity of 10000 molecular weight PAM solutions over time with varying additions of peroxide. Viscosity measured at a shear rate of 75 s^{-1} and 25°C.

5.1.2 Preliminary Alcoflood 935 Data

The partially hydrolyzed polyacrylamide (HPAM) polymer Alcoflood 935 was used because it is analogous to the high molecular weight HPAM used in fracturing applications. Estimated polymer molecular weight, as suggested from the literature and manufacturer, is 6,000 kDa. Again, the Brookfield DV-II+ viscometer was used to measure the viscosity of solutions. In contrast to previous experiments, the viscosity was measured after 24-hour incubation 35°C and over a range of shear rates. Solutions initially contained 18.33 mM NADH and viscosity was measured for a variety of peroxide additions. Figure 5.2 illustrates a pilot study in Cartesian coordinates conducted to observe the viscosity of these solutions after incubation. The results indicated that no reduction

in viscosity was observed with the 9.69 mM peroxide concentration. On the other hand, a distinct reduction in the viscosity was observed for the highest peroxide (96.9 mM) addition. During this set of experiments, the concentration of the polymer was not the same between samples due to peroxide addition. Later experiments compensated for peroxide dilution by adding an equivalent volume of peroxide or water for all samples.

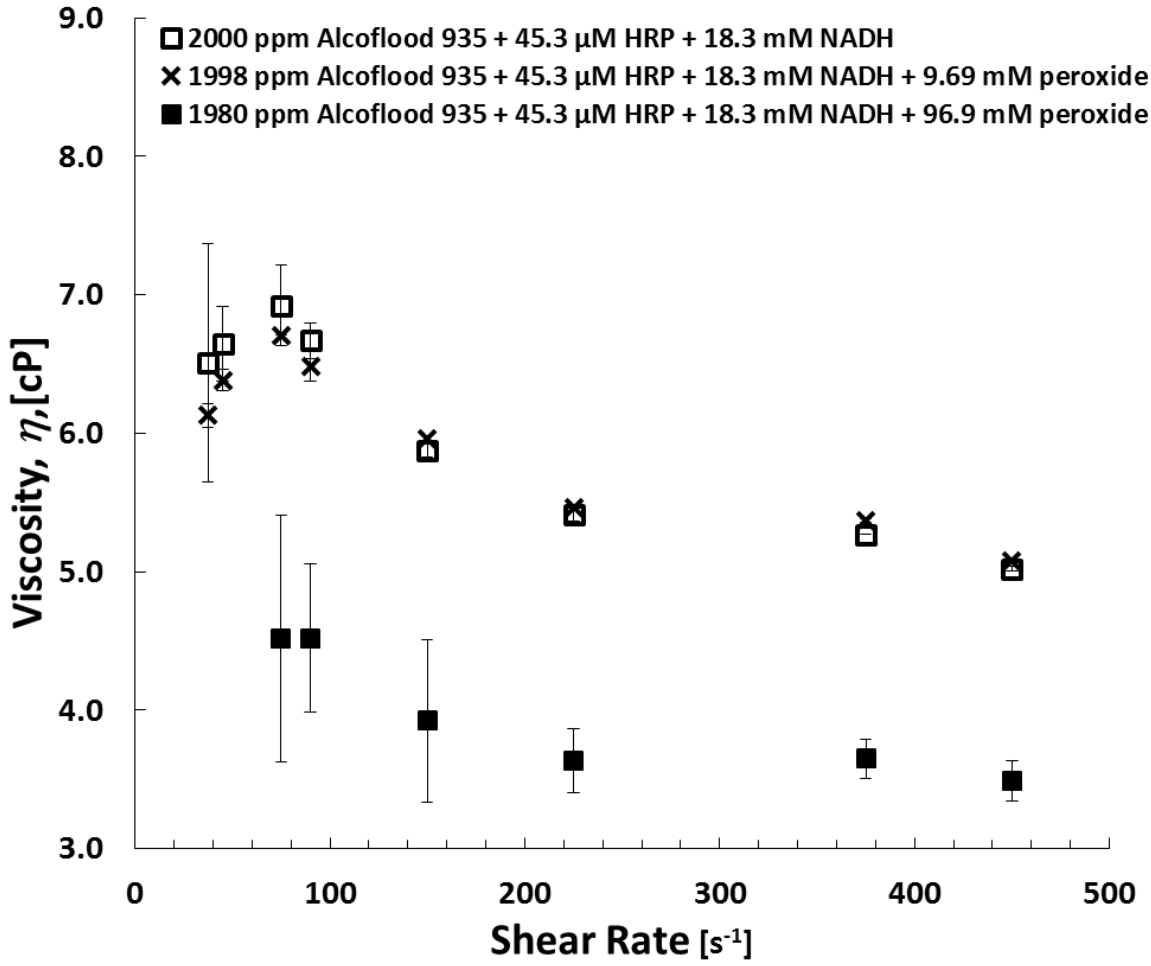

Figure 5.2 Viscosity reduction observed for Alcoflood 935 solutions containing 18.33 mM NADH and varying peroxide concentrations. Viscosity measured at various shear rates and 25°C.

Further experimentation revealed that the addition of NADH without the other reagents created a significant initial reduction in viscosity. Figure 5.3 shows the results obtained for Alcoflood with

and without the addition of NADH. The results show that there was a slight drop in viscosity attributed to the addition of hydrogen peroxide, but a very significant reduction was observed for the addition of NADH. Data is shown at different shear rate range due the Brookfield viscometer torque limitations where a minimum 10% is required. The results of this study prompted the need to further study the viscosity effects observed from NADH addition. Results depicting the effects of NADH concentration are shown in Figure 5.4 and an increase in viscosity was observed when less NADH was used. Reduction in NADH concentration to 1.4 mM doubled the viscosity observed compared to 18.3 mM and further testing was conducted using this concentration.

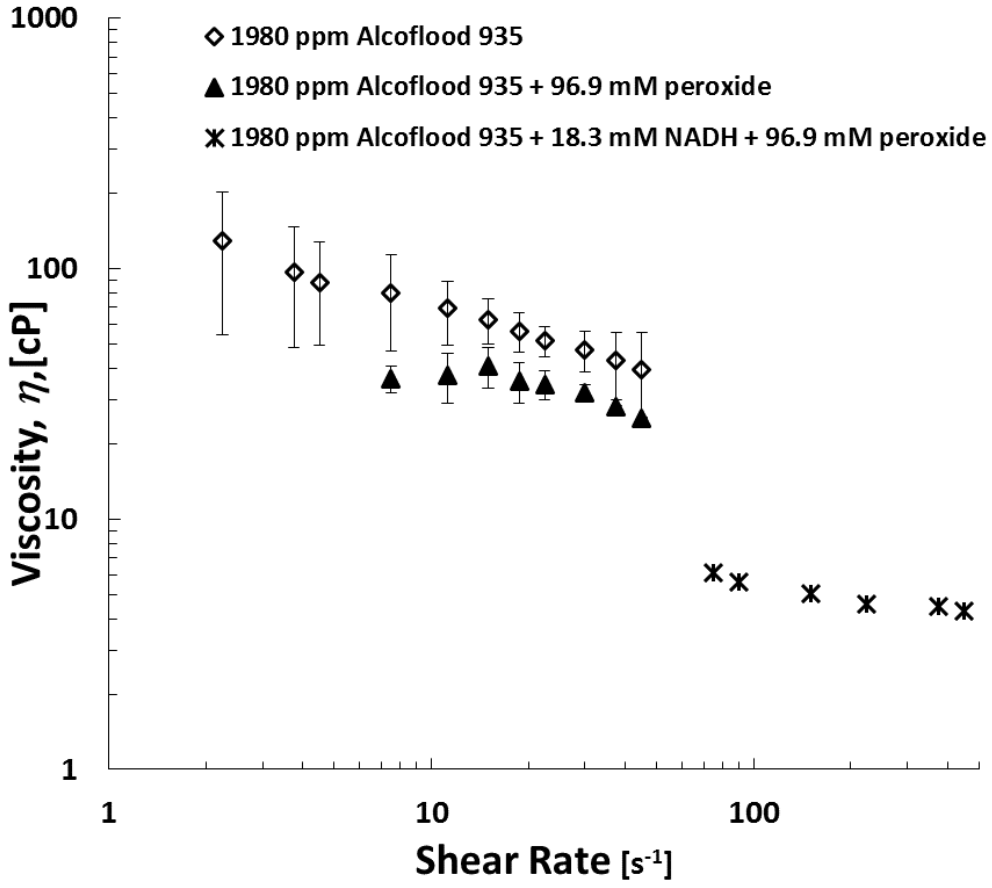

Figure 5.3 Viscosity reduction observed for Alcoflood solutions with and without the addition of 18.33 mM NADH. Viscosity measured at various shear rates and 25°C.

Figure 5.5 depicts the reduction in viscosity for samples using 1.4 mM NADH concentration after 24-hour incubation. Comparable concentrations in all samples are created by dilution with 10 μL/ml peroxide, or water, at the various concentrations. The results of this study showed that there was still a significant reduction from the addition of components but separation between trends was achieved. In this experiment, there is a notable reduction in viscosity at lower peroxide additions. The component concentrations used in this study are further investigated in later experiments (Chapter 3). After concentrations were established, continuous sampling of the polymer degradation was attempted as outlined in the next section.

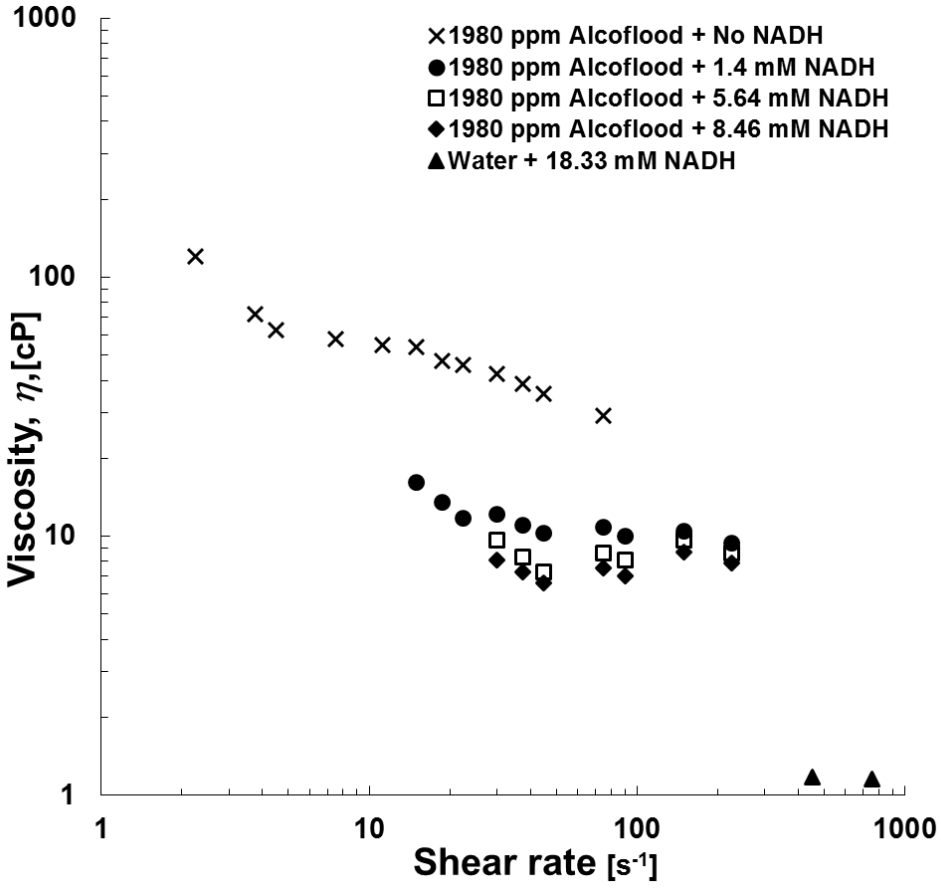

Figure 5.4 Effect of NADH concentration on HPAM viscosity. Viscosity measured at various shear rates and 25°C.

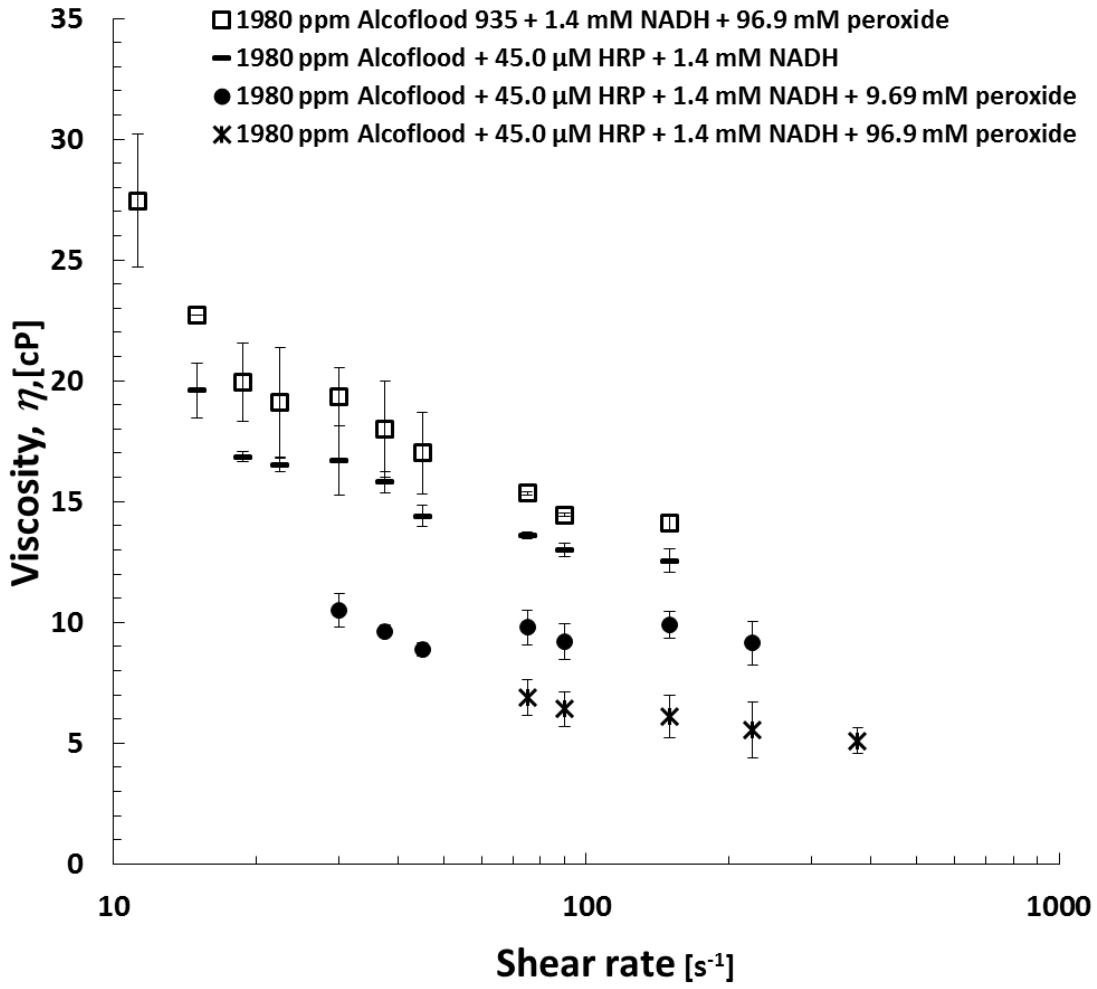

Figure 5.5 Viscosity profiles obtained for Alcoflood Solutions containing 1.4 mM NADH concentration and varying peroxide concentration. Viscosity measured at various shear rates and 25°C.

5.1.3 Continuous Sampling of Alcoflood 935

Continuous sampling was attempted to describe the kinetics of HPAM degradation by monitoring the change in viscosity of reacting solutions for 15 hours at a shear rate of 75 s^{-1} and a temperature of 35°C. The final concentration of components in solution are 1980 ppm Alcoflood 935, 1.4 mM NADH, 45.0 µM HRP and 96.9 mM peroxide. First, these studies were conducted using the Brookfield DVII Pro viscometer. Figure 5.6 shows the results obtained from three runs. Although the data obtained shows a significant decrease in viscosity, a systematic fluctuation in

the data was observed. The after the first run, fluctuation in the data was thought to be caused by torque limitations associated with the decreasing viscosity of the polymer. Because of this, subsequent experiments consisted of two experiments with shear rates changing from 75 s^{-1} to 150 s^{-1} after 4.5 hours. Although the shear rate was increased, no improvement in the data was observed.

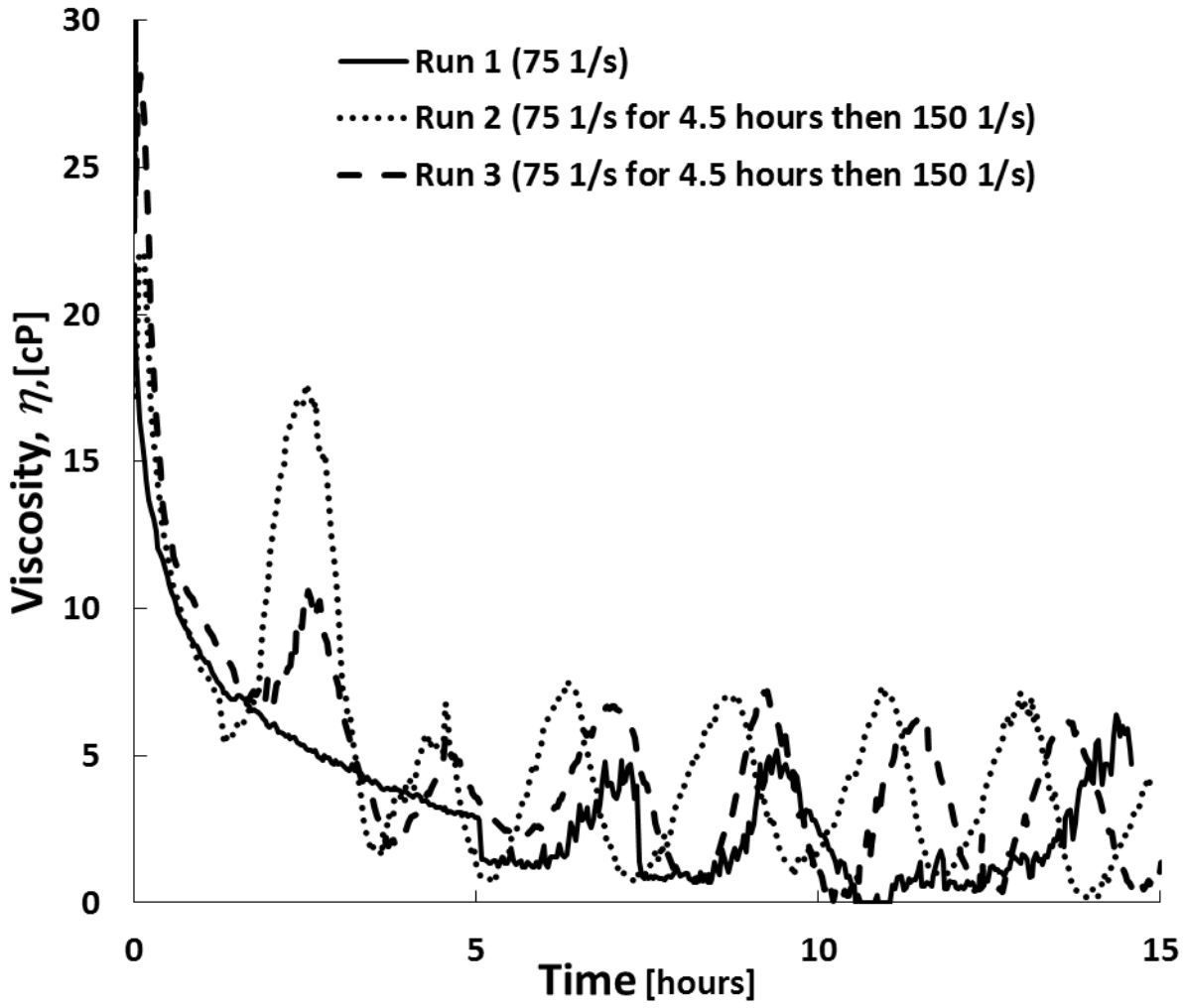

Figure 5.6 Viscosity of 1980 ppm Alcoflood 935 solutions in the presence of 1.4 mM NADH, 45.0 μM HRP, and 96.9 mM peroxide. Viscosity monitored at shear rates indicated in legend for 15 hours at 35°C. (Lines represent smoothed data)

To eliminate the possibility that the fluctuations were due to the solution, a standard oil was monitored overnight (Figure 5.7). A viscosity standard with 6-7 cP at 35°C was chosen because of the similarity in viscosity to experimental values where fluctuation was first observed. As seen from the results, similar fluctuations were observed for the standard oil suggesting that artifacts in that data were due to the equipment. Furthermore, the onset of fluctuations occurred near the same time observed in HPAM degradation experiments. Because of this, all subsequent experiments were conducted using air driven rheometers. Next, the Bohlin CS10 Rheometer was used to repeat these experiments.

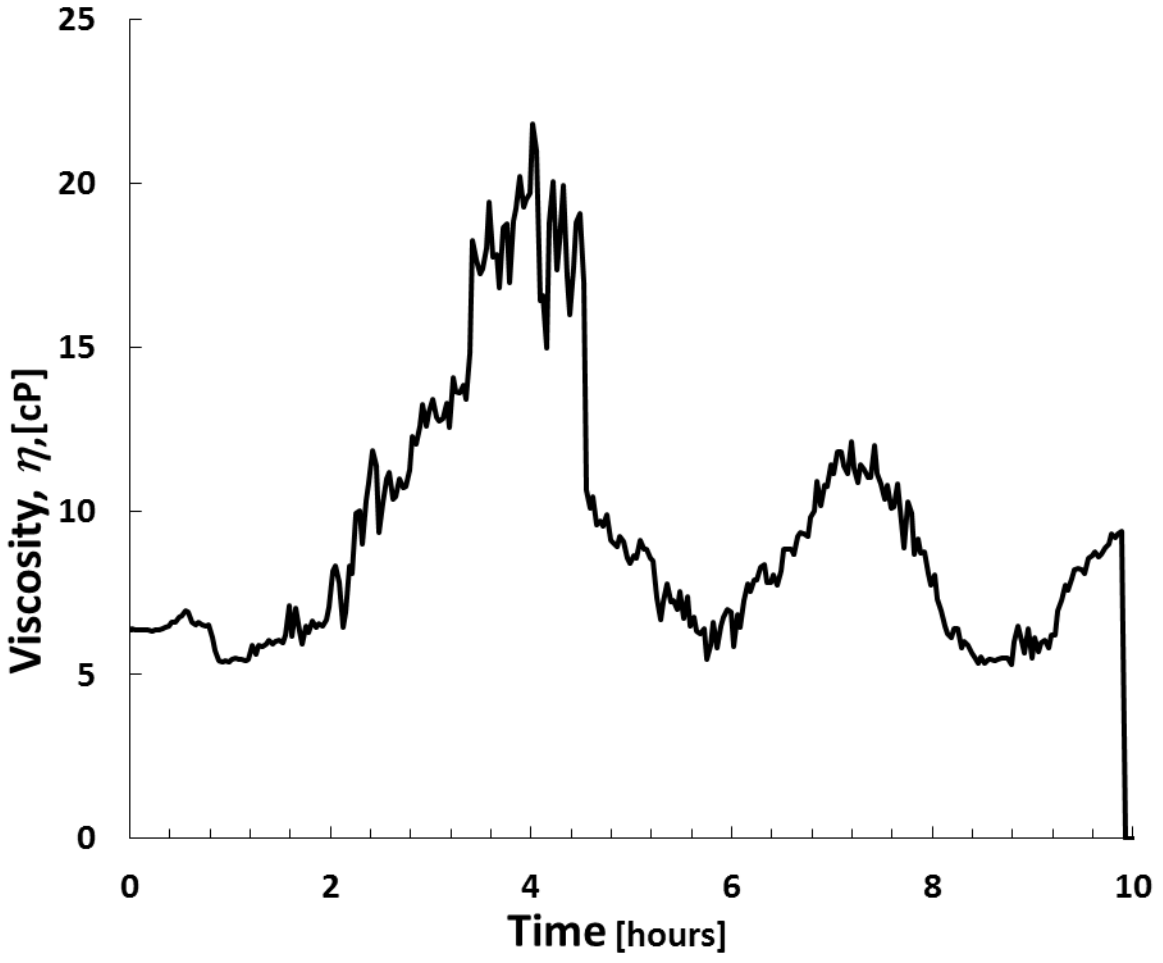

Figure 5.7 Oil viscosity standard monitored for 10 hours using the Brookfield DVII Pro viscometer at a shear rate of 75 s^{-1} and 35°C; Line represent smoothed data

Figure 5.8 depicts the same experiments repeated using the Bohlin CS10 Rheometer. Again, a significant decrease in viscosity is observed for all six runs but initial viscosities showed inconsistent data. Furthermore, the viscosity of the solutions showed an initial increase in viscosity followed by a gradual decrease. Through visual observation, it was concluded that the increase in viscosity was due to the creation of oxygen during the reaction. The soapy nature of the HPAM/HRP solution, in conjunction with oxygen generation, caused bubbles to form on the edge of the cone during the viscosity measurement. Most of the bubbles were created within the first few hours, because a majority of the peroxide is consumed within the same period (Section 5.3.2), which is the reason for the increase in viscosity. As the bubbles dissipate, the viscosity is reduced and becomes more consistent across all trials. As with the Brookfield viscometer, a standard oil was observed over time for fluctuations in viscosity. Results from the standard oil sample showed a constant viscosity for the full 15-hour period. Due to the formation of oxygen by the reaction, periodic sampling was conducted using the Bohlin rheometer to observe the kinetics.

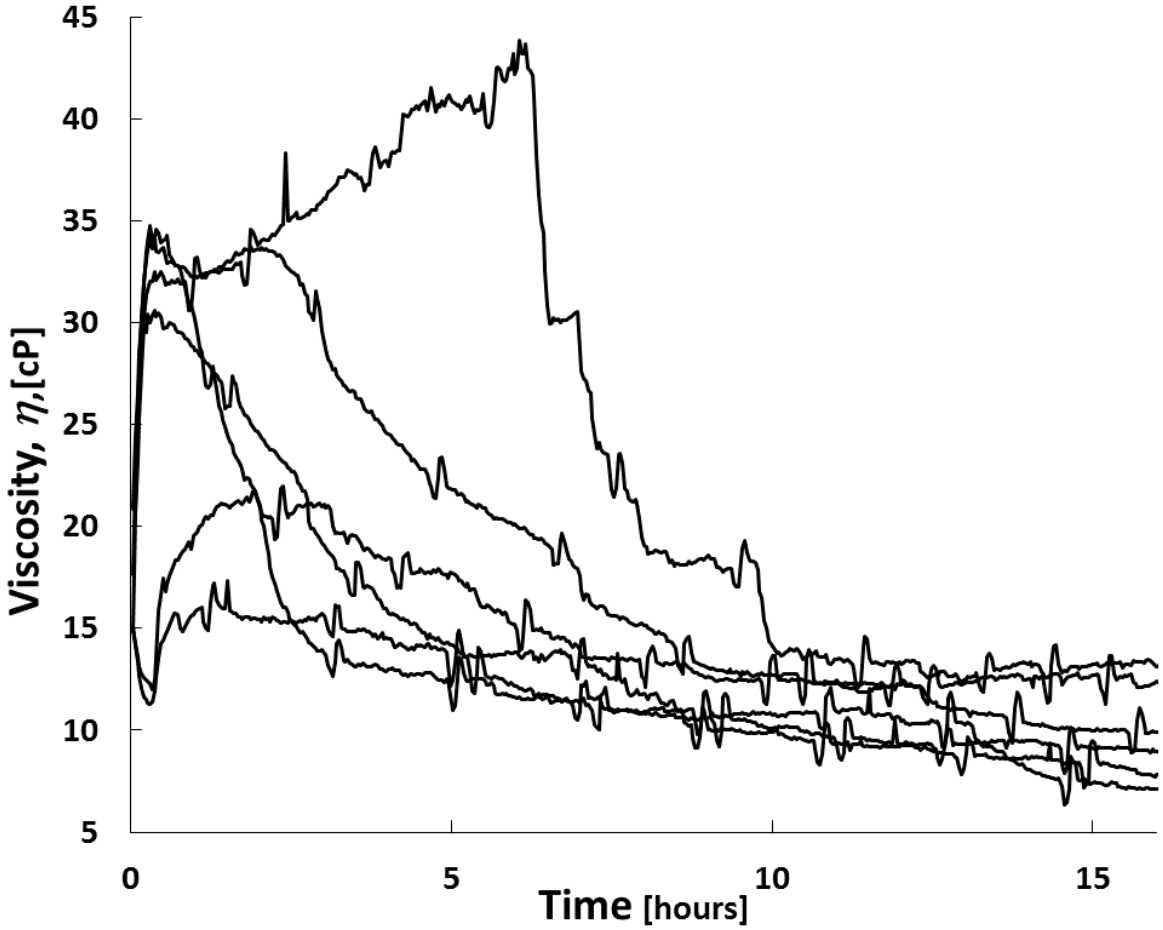

Figure 5.8 Viscosity of 1980 ppm Alcoflood 935 solutions in the presence of 1.4 mM NADH, 45.0 μM HRP, and 96.9 mM peroxide. Viscosity monitored with the Bohlin rheometer for 15 hours at a shear rate of $75s^{-1}$ and 35°C; Lines represent smoothed data.

5.2 Preliminary Filtration Experiments

Preliminary experiments were conducted to find the best technique for filter cake cleanup. These experiments measured the flowrate across 0.1μm nylon filter paper to observe flowrate recovery. The filters used in these experiments were found in the lab and had significantly different flow characteristics to newly purchased filters used for the final tests. Although the same filters were not used, the recovery trends remained the same. Flowrate was measured by weighing the effluent with time when a constant pressure of 20 psi was applied. Furthermore, some experiments

were conducted using a 40 psi back pressure regulator to minimize filter surface area blocked by trapped oxygen and air bubbles. First, control experiments were conducted to measure the change in flowrate observed from polymer resuspension (from filter cake back into solution) when allowed to set for 24 hours. In addition, control experiments were conducted to observe effects of peroxide exposure and enzyme reaction exposure to the filter paper and holder. The control experiments were followed by a set of tests that measured the flowrate recovery after treatment was applied to the filter cake. The applied treatments varied in order of addition where filter cake was created using HPAM alone and with the addition of other components. Additionally, a few dynamic experiments measured the increase in flowrate with time by flushing the HRP enzyme system through the filter cake at constant pressure.

5.2.1 Experimental Development

The first step in establishing a protocol was to find a suitable pressure and volume for creating a filter cake. The goal of this test was to establish the lowest applied pressure to create a filter cake within a suitable time. Preliminary tests using 2000 ppm Alcoflood 935 revealed that 20 psi positive pressure application created greater than 99% reduction in flow rate by applying 10 ml polymer. The filter cake was formed in about 60 mins and, although flow was fast, the undamaged flowrate to filter could be accurately measured under the same pressure. For consistency, all flowrate measurements were conducted using the same pressure applied for creating damage with HPAM polymer. Figure 5.9 shows an example of the final measurements using a 20-psi positive pressure. The test was conducted by establishing flow with the undamaged filter, creating the filter cake, measuring the flowrate to water for damaged filter, and measuring the recovered flowrate to water after 24-hour treatment. As seen from the plot, there is a distinct difference established between undamaged, damaged, and recovered flowrates.

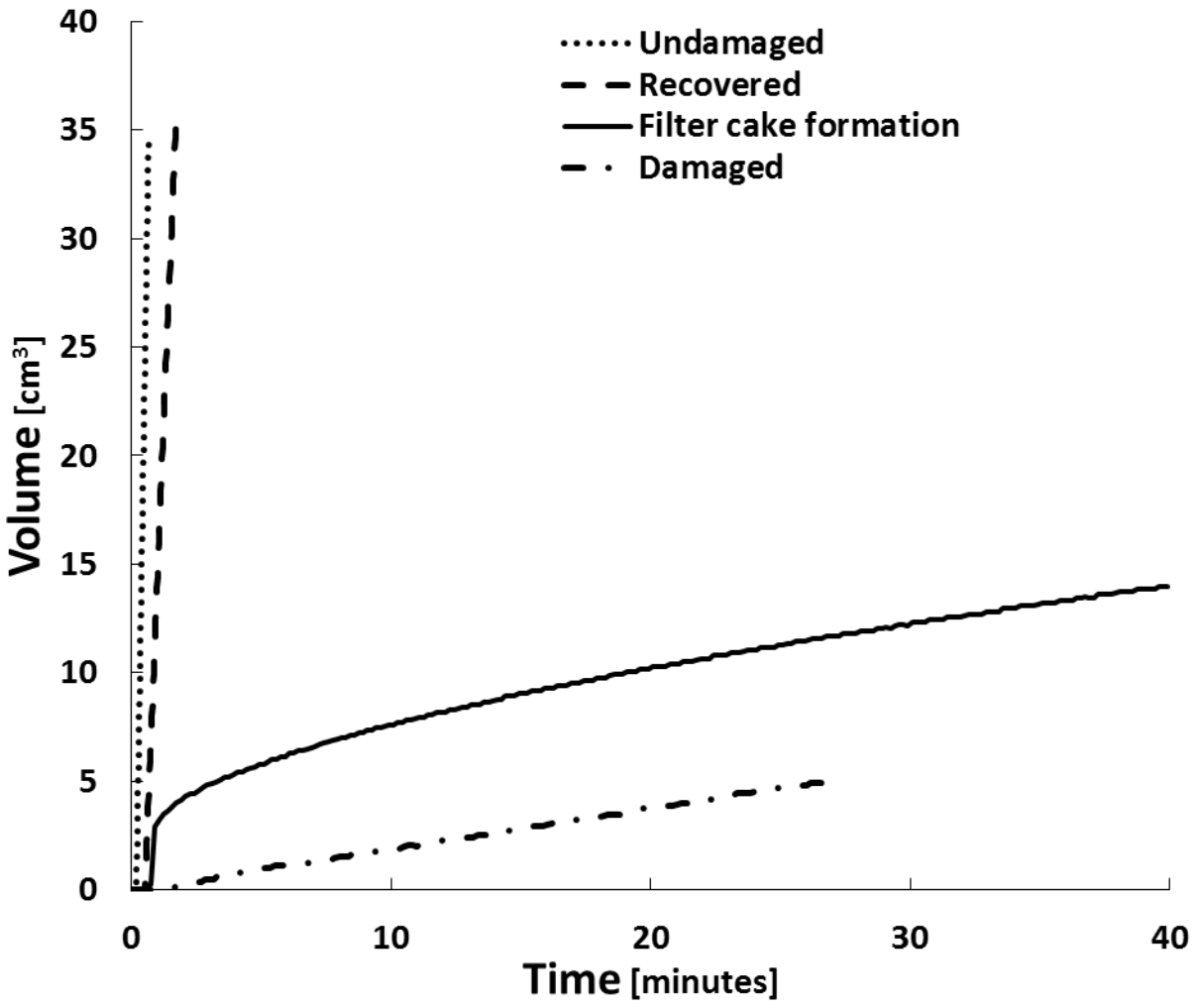

Figure 5.9 Example of flow measurements used to calculate flowrate recovery. Example used HPAM filter cake and HRP, NADH, and peroxide treatment. All runs conducted at 20 psi differential pressure; Line represent smoothed data.

Baseline flow tests observed the mean water flowrate through the undamaged filter paper. Preliminary tests showed variation in baseline flow results and the difference was thought to be caused by air trapped in the filter holder. During filter cake treatment, a significant amount of oxygen is generated from the enzymatic breakdown of peroxide and some of this oxygen is trapped in the filter holder. The trapped oxygen adheres to the filter paper, which reduces the filter paper surface area available for water flow. The reduction in flow directly impacts the results obtained

and can drastically change the calculated recoveries. In all, eleven filters tested resulted in a mean flow rate of 62.8 ± 5.4 ml/min. To test the effect of air entering the system one filter was placed in the filter holder and all of the air was evacuated. Then, three flowrate tests were completed without air entering the system resulting in a mean flow rate of 64.7 ± 1.2 ml/min. After the last run, air was allowed to flow through the filter paper and the flow rate to water was tested again. This was repeated with resulting in a mean flow rate of 65.7 ± 0.5 ml/min. The results of this test show that there is not a significant change in flow rate observed if air entered the system before damage occurs.

5.2.2 Filter Permeability

In addition to the previously mentioned experimentation, an attempt was made to measure the permeability of the filters. A thickness of 0.0508 cm was determined using Vernier calipers (with negligible error) for four stacked filters. The filters were saturated and placed into the filter holder where the flowrate to water was determined as various pressures. Figure 5.11 shows the volume versus time, and corresponding flowrates and pressures, for data obtained for four filters. The calculated flowrates were plotted against pressure drop ($R^2 > 0.99$) and the permeability was determined from the slope using Darcy's equation (Equation 42). Data was collected for two sets of four stacked filters and two sets of single filters. The thickness used in single filter experiments was the thickness determined using four filters divided by four. Calculated permeability was 0.470 ± 0.024 md and 0.642 ± 0.003 md for one filter and four filters respectively.

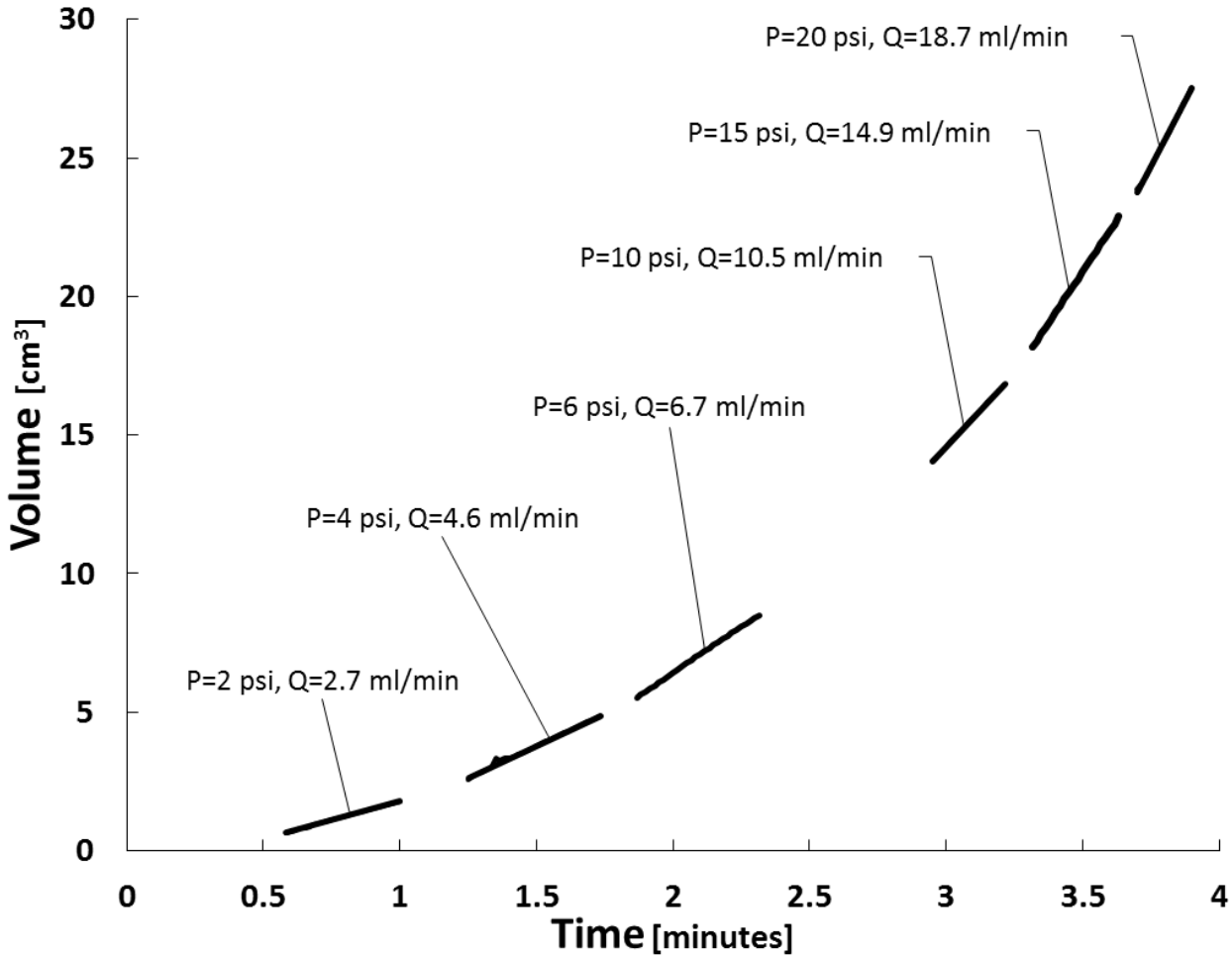

Figure 5.10 Volume with time measured for the flow of water through four filters. From this data, the flowrate was calculated and plotted with respect to pressure to determine permeability; lines represent smoothed data.

5.2.3 Continuous Flow for Treatment of Filter Cake

One of the first experiments attempted observed the change in flowrate with respect to time. Although only two experiments were attempted, valuable information for future procedure was obtained. The experiment measured the undamaged flowrate to water, applied polymer damage, and then applied treatment. Flowrate measurements used 10 psi driving pressure and filter cake formation used 20 psi pressure application. Damage was created using 15 ml, 2000 ppm Alcoflood

935 and treatments consisted of 45.0 μM HRP, 1.4 mM NADH and/or 96.9 mM hydrogen peroxide. Effluent mass with respect to time was obtained and data was fit with a fourth degree polynomial (R^2= 1). The derivative of the polynomials represent flowrate and is depicted in Figure 5.11. Data shown in Figure 5.11 represents the same volume of treatment (30 ml) in both cases. The undamaged flowrate (at 10-psi pressure) was 44.8 and 43.1 ml/min for the peroxide and HRP, NADH, peroxide treatments respectively. Damage was created using 15 ml HPAM and treatment was immediately applied after cake formation. The results show that a fast initial increase in flowrate occurred but that flow decreases with respect to time for the treatment containing HRP. Although the recovery was more rapid with solutions containing HRP, the damage created with the enzyme counteracted the recovery. Furthermore, damage created by HRP resulted in an overall lower flowrate recovery obtained compared to peroxide alone. The results of this study showed the need for batch experiments where only the surface of the cake is treated and large volumes HRP solution do not pass through the filter. In addition, flowing treatment through the cake is not indicative of field applications as flow is reversed during the production stage and therefore using the same direction in flow represents a harsh test condition.

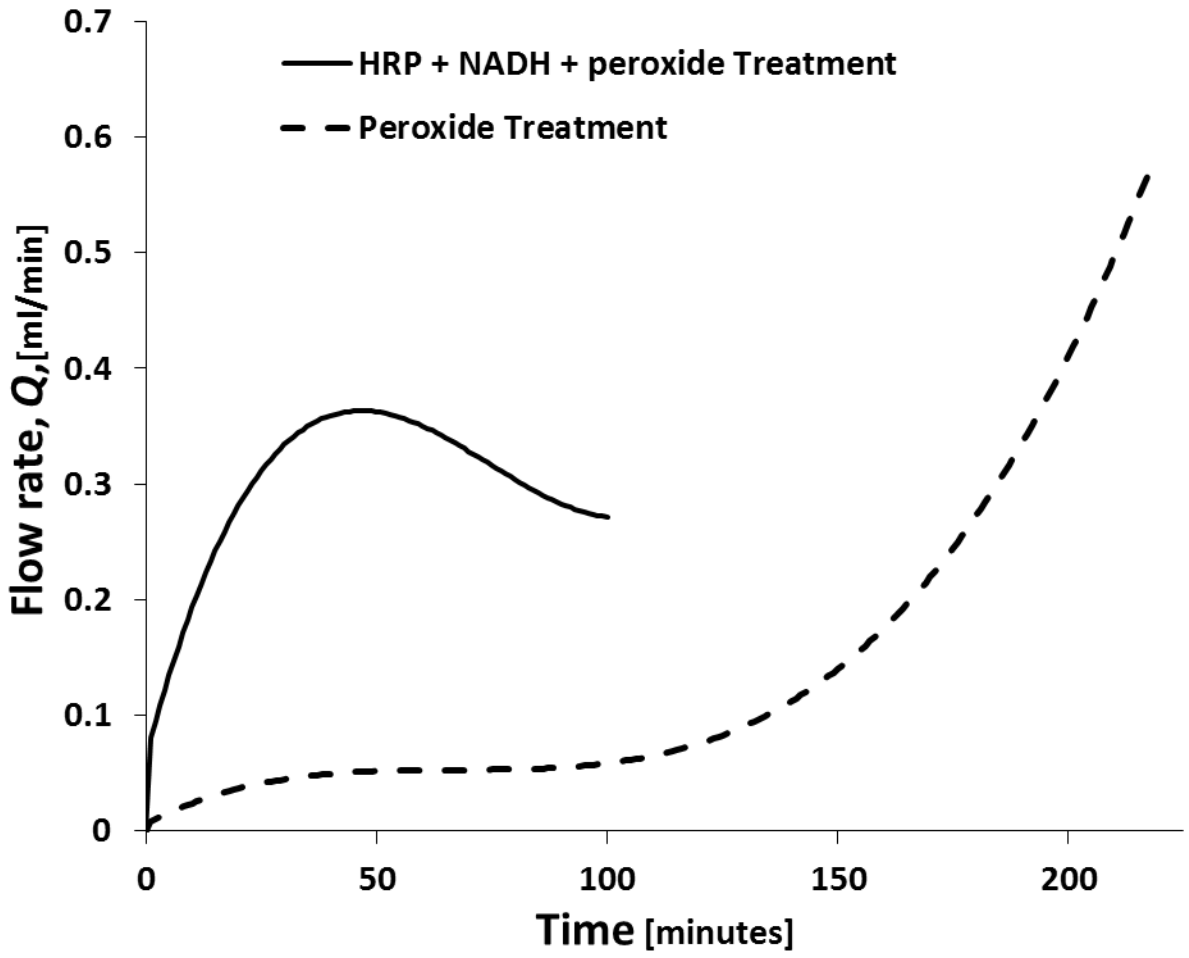

Figure 5.11 Plot represents flowrate change for the treatment flow through damaged filter and HPAM cake. Two treatments were tested (i.e. peroxide and HRP, NADH, and peroxide) at a pressure of 10 psi.

5.2.4 Preliminary Filtration Results

The following studies were conducted as batch experiments. First, undamaged flowrate (Q_i) to filter was measured with water. Damage to filter was created using 15 ml of components from Table 5.1 in the column labeled "cake formation", then the flowrate of damaged filter (Q_d) was measured with water. The excess water was vacuumed suctioned off and 10 ml of the corresponding treatment was applied. Two milliliters of the treatment was flushed through the filter to ensure contact with HPAM and the treatment was allowed to set at room temperature for 24 hours. After 24 hours, the excess treatment solution was carefully removed and the recovered

flowrate (Q_r) to water was measured. The percent damage and flowrate recovery are calculated as stated in the methods but is shown again in Equation 60 and 61 respectively.

$$\% \, Damage = (Q_i - Q_d)/Q_i * 100 \quad (60)$$

$$\% \, Recovery = (Q_r - Q_d)/Q_i * 100 \quad (61)$$

Initial baseline flow tests had indicated that air in the filter holder did not affect the flowrate observed for undamaged filter paper. Although this may be true, for the first two trials inconsistencies were observed for flowrate of water after treatment and was thought to be caused by oxygen created during the reaction. A 40-psi backpressure regulator was placed downstream of the filter to help with the issue. Table 5.1 outlines the results obtained using the backpressure regulator and indicated the best recoveries when HPAM formed the filter cake and the entire HRP treatment was applied. The results are only composed of one or two experiments because the backpressure regulator was inconsistent. It was then decided that that a set of experiments would be conducted at atmospheric pressure.

A set of experiments conducted without the use of a backpressure regulator are shown in Table 5.1. For this set of experiments, a minimum of three sample per formulation was tested. The mean damage created by the filter cake for all formulation was 99.7 ± 0.4%. The results of this study again showed that the best recovery is achieved when damage was created using HPAM and treated with HRP, NADH, and peroxide. Further evaluation of the results revealed that the greatest recoveries were achieved in the presence of NADH. These results are counter to trends observed for viscosity reduction because in the viscosity studies, much greater recoveries are observed in the absence of NADH. Although 3-5 experimental sets represented each formulation, a high

deviation from the mean is observed. Combining the results obtained with and without the backpressure regulator did complement the results. Further testing was planned in order to bring the error down, and conduct control experiments, but the filter supply was diminished and more could not be obtained from the same manufacturer. Similar filters, purchased from another company, retained more HPAM when creating damage. Because of this, the polymer volume was reduced to 10 ml for the final set of tests.

Table 5.1 Lists the mean percent recoveries achieved when cake and treatment contain different components. Results shown represent experiments conducted with and without 40-psi backpressure regulator and a combination of the results.

Cake formation	Treatment	% Recovery With Backpressure			% Recovery Without Backpressure			Combined Results		
		Mean (%)	Std dev	n	Mean (%)	Std dev	n	Mean (%)	Std dev	n
HPAM	**peroxide**	0.2	0.1	2	3.3	7.2	5	2.4	6.1	7
HPAM	**HRP, peroxide**	28.1		1	10.8	2.8	4	14.3	8.1	5
HPAM	**HRP,NADH, peroxide**	28.5	17.7	2	23.2	12.1	4	24.9	12.6	6
HPAM, HRP	**peroxide**	6.3		1	12.8	11.3	3	11.2	9.8	4
HPAM, HRP	**NADH, peroxide**	21.8		1	21.3	13.9	3	21.4	11.4	4
HPAM, HRP, NADH	**peroxide**				20.1	13.1	3	20.1	13.1	3

5.3 Oxygen Generation and Peroxide Consumption

From previous filtration studies, it was anticipated that oxygen generation would be an issue when testing core samples. If the treatment solution is injected into a fully brine saturated core, and oxygen is internally generated through the degradation of peroxide, then the permeability can change due to the change in brine saturation. This would not be an issue under field conditions, due to the high pressure, but is important for lab conditions. In order to alleviate the change in

permeability, a backpressure would have to be applied to keep oxygen in solution during the duration of testing. In this section, several studies were conducted to find the necessary pressure application needed for the treatment system. First, hand calculations were conducted to find the pressure necessary to keep oxygen in solution. These calculations were based off of the 96.9 mM peroxide concentration used in experiments. Next, a spectrophotometric study monitored the peroxide concentration of a reacting solution with respect to time. The last study observed the presence of oxygen in the reaction solution via a high pressure view cell. The results of this study determined the backpressure necessary for flooding cores using the Hassler core holder.

5.3.1 Theoretical Calculation

The first step to finding a suitable pressure was to conduct hand calculations. For these calculations, it is assumed that all of the peroxide is consumed and the peroxide to oxygen ratio is 1:1. The calculations were based off of the study presented by Tromans[267] where a model for calculating oxygen solubility in brine is presented. Equations 62 and 63 represent the equations used in the calculation. In this model the concentration of oxygen in brine (C_{aq}, mol/kg water) is a function of the partial pressure of oxygen (P_o, atm), the concentration of salt (C_I, mol/kg water), and the constants Y, κ, H. The constants used in this equation are directly related to the electrolyte and are 1.116, 0.407, and 0.842 for KCl respectively. For a 2% KCl brine, and a molecular weight of 74.5513 g/mol, the concentration of salt (C_I) is 0.268 mol/kg water. The peroxide concentration in the core flooding experiment is 0.0969 mol/kg water and a temperature (T) of 303.15 Kelvin is used to incubate the reaction. Rearranging Equation 62 and solving for (P_o) gives a theoretical pressure of 88.6 atm or 1302 psi. This calculation assumes that the peroxide stock solution is a minimum of 30% and that all of the peroxide is consumed. Ideal conditions do not exist and for this reason, experimental testing was done to obtain a better idea of actual reaction conditions.

$$C_{aq} = P_o K(1 + \kappa C_I^Y)^{-H} \quad (62)$$

$$K = \exp\left(\frac{0.046T^2 + 203.35Tln\left(\frac{T}{298}\right) - (299.379 + 0.092T)(T - 298) - 20591}{8.3144T}\right) \quad (63)$$

5.3.2 Peroxide Consumption measured with UV-Vis

Spectrophotometric tests were conducted to monitor the consumption of peroxide in the reaction with respect to time at a temperature of 37°C. As stated in the materials and methods, baseline spectra confirmed that the characteristic absorbance wavelength of hydrogen peroxide was 240 nm. The absorbance wavelengths of HRP and NADH did not overlap the peroxide spectra. As seen in Figure 5.12, a peroxide concentration of 96.9 mM (theoretical) showed an actual concentration of 75 mM calculated using an extinction coefficient of 43.6. This value is smaller than the 96.9 mM theoretical concentration, which can be attributed to stock solution degradation with time. The concentration was monitored for one hour in the absence of HRP. There was no change in peroxide concentration observed over the one-hour period so it was assumed that no concentration change would be seen for the duration of reacted sample. After a baseline was established, 3 ml solution containing 45.0 μM HRP and 1.4 mM NADH was placed into a quartz cuvette. The temperature was allowed to equilibrate, the baseline was zeroed, and then the reaction was activated with addition of peroxide to a final concentration of 96.9 mM. The results in Figure 5.12 show that upon initiation of the reaction the absorbance did not reach baseline values. This could be due to the speed of the reaction or from poor initial mixing. In

either case, the data shows similar trends as seen with previous studies (i.e viscosity and molecular weight reduction with time) where a fast initial rate is followed by a slower rate.

In light of the new initial concentration, and the fact that only 77% of peroxide is consumed, Equations 62 and 63 are again used to calculate pressure requirements. The results of the spectrophotometric study show that a pressure of 1013.6 psi is required at 30°C and 2% KCl salt concentration. If 77% total peroxide concentration is consumed, as shown here, then the required pressure would be reduced to 781 psi under the same conditions. Although this gives a better understanding of the efficiency of the reaction, visual confirmation was conducted using a high-pressure view cell.

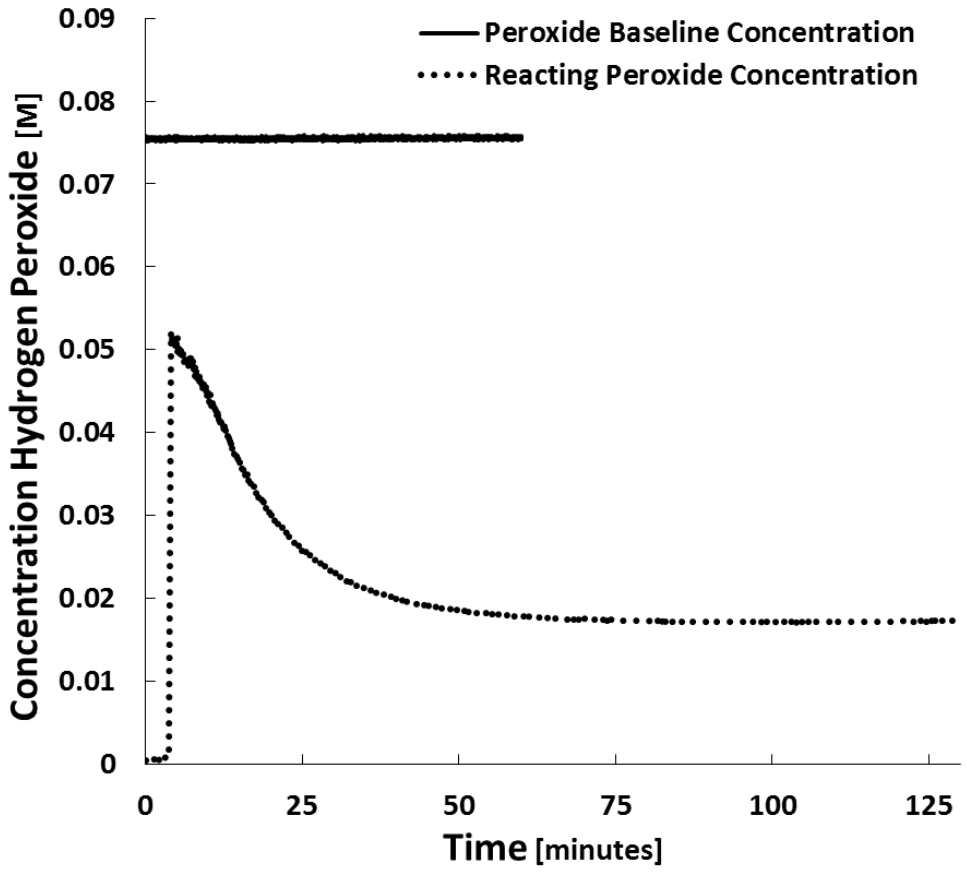

Figure 5.12 Absorbance and molar concentration observed for peroxide control and reacting sample.

5.3.3 Pressure and O_2 Generation in High Pressure View Cell

The pressure at which oxygen formed in solution was observed using a high-pressure view cell. In the figures below, the solution in the view cell is shown at various pressure milestones. First, the cell was filled with 96.9 mM peroxide to evacuate the air. Then the cell was filled with 45.0 μM HRP, 1.4 mM NADH, and 96.9 mM peroxide by pumping the solutions in to the cell. During this, and core flooding studies, HRP/NADH solutions were delivered using the ISCO syringe pump and peroxide solutions were delivered using an Eldex pump at a backpressure of 2000 psi. Solutions were originally at two times the target concentration but diluted by half when injecting solutions into the cell at the same rates. A volume of about five times the view cell volume was flushed through to ensure correct concentration. The reaction set at a pressure of 2000 psi and 30°C for 24 hours. After the reaction pressure in the view cell was incrementally released, from a starting pressure of 1944 psi, while internally stirring with a small stir bar, and observed for oxygen formation in solution. As the succession of figures show, no oxygen was present for the theoretical pressure value (1302 psi) calculated from Tromans model[267] with 96.9 mM peroxide in 2% KCl at 30°C. From the spectrophotometry study, the initial peroxide concentration was calculated to be 75.5 mM with a reaction efficiency of 77% (58.1 mM consumed peroxide). The calculated pressure values for these peroxide concentrations were 1014 and 781 psi respectively and no oxygen was present in solution for these pressures. Although no gas was observed at a pressure of 740 psi, small chunks of enzyme aggregates became visible. Gas was visually observed coming out of solution when pressure was reduced from 475 psi to 435 psi. A stable pressure of 435 psi was maintained for about 30 seconds before bubbles became visible. Further reducing the pressure created large amounts of oxygen and large protein aggregates appeared.

Pressure = 2000 psi: Image of view cell after HRP, HADH, and peroxide after loading (before incubation).

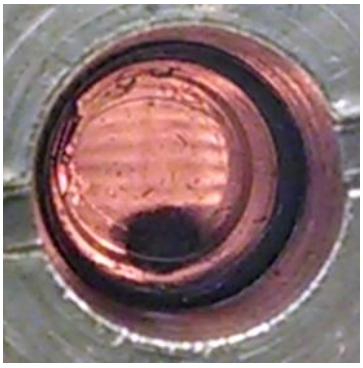

Pressure = 1944 psi: Image of view cell after 24-hour incubation at 30°C. Pressure was reduced to observe oxygen.

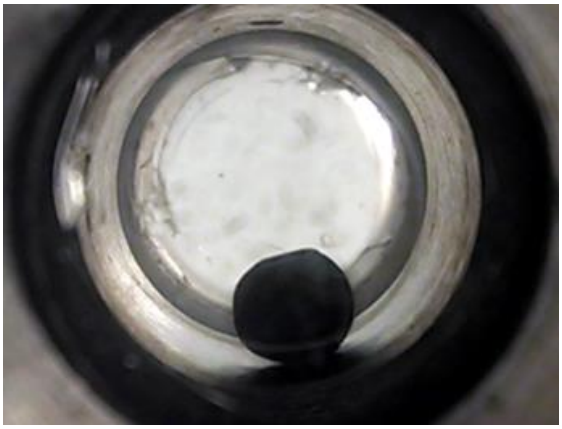

Pressure = 1311 psi: Pressure of 1302 psi was estimated using Tromans model for 96.9 mM H_2O_2 (Section 5.3.1)

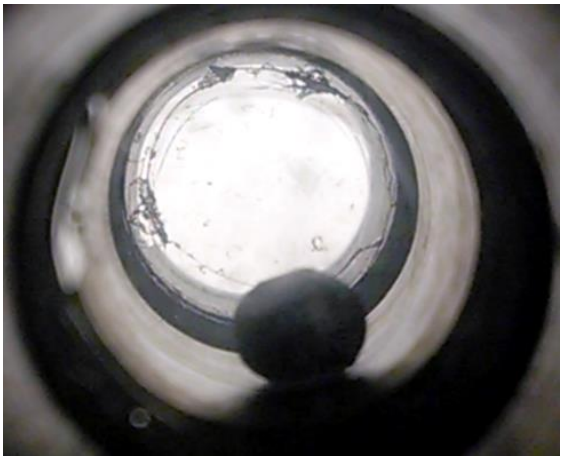

Pressure = 978 psi: Pressure of 1014 psi was estimated using the baseline peroxide measurement of 75.5 mM H_2O_2 (5.3.2)

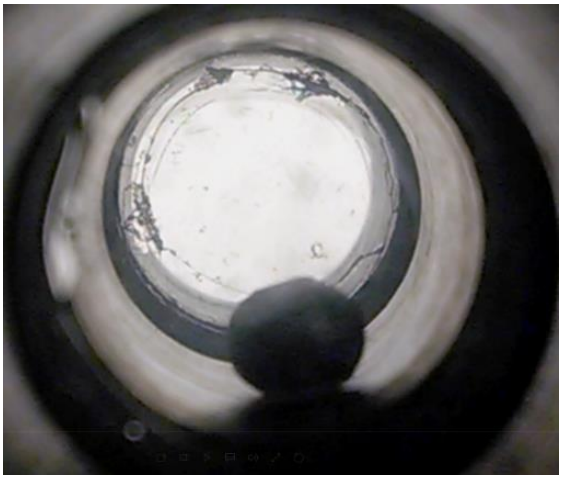

<u>Pressure = 740 psi</u>: Pressure of 781 psi was estimated using the 77% reaction efficiency of starting 75.5 mM H_2O_2 concentration. (Section 5.3.2) First sign of HRP aggregation is circled in red.

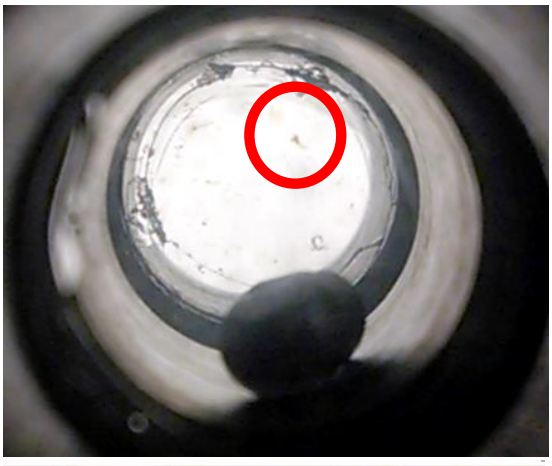

<u>Pressure = 435 psi</u>: First sign of oxygen present in solution. Pressure was reduced from 475 psi to 435 psi. Protein aggregation is more apparent.

<u>Pressure = 260 psi</u>: Larger oxygen bubbles and more protein aggregation is apparent.

<u>Pressure = 10 psi</u>: View cell was filled with oxygen near atmospheric pressure.

From this study, a few things are apparent. First, the pressure where oxygen was observed is lower than theoretical and measured values. Secondly, increasing the pressure created protein aggregation. One reason for this may be due to the effects of pressure on the enzyme activity. Change in pressure (under 1000 bar) has shown to affect enzyme activity and thought to be a function of protein folding.[268] The lower activity could cause less peroxide conversion to oxygen. In this system, pressure alone could not be responsible for denaturation or aggregation. Studies have shown that disassociation of compounds containing multiple proteins and oligomeric proteins take place between 1-2 kbar.[269] Moreover, disassociation of small monomeric proteins take place at much higher pressures of 4-8 kbar.[270] More than likely both, reduced peroxide conversion and aggregation are due to increased oxygen in solution. As previously explained, the breakdown of hydrogen peroxide creates radical oxygen species. By keeping the oxygen in solution radicals could be more abundant causing protein denaturation and aggregation. After this study, backpressures of no less than 600 psi were applied to core flooding studies that were not conducted at atmospheric pressure.

5.4 Preliminary Core Flooding Studies

The results and discussion in this section outline unsuccessful methods in evaluating the permeability recovery. The knowledge gained from these methods and trials resulted in the creation of a modified core flooding apparatus that encapsulated the cores in PVC and resin (presented later). The goal of this section is to outline the methodology that led to the final, successful apparatus and procedure. Initially, traditional fluid loss tests were attempted and presented a couple of issues. Then, a Hassler-type core holder was used and a variety of alterations and modifications to the core flood in system were attempted. Several core types tested showed no damage due to high permeability but Indiana Limestone ($k \approx 1\text{-}4$ md) showed significant damage

for low volumes of 2000 ppm Alcoflood 935 injected. Indiana Limestone was used for all preliminary core flooding experiments. Solutions were made in 2% KCl and permeability was measured using the same brine solution. Although the data showed unsuccessful recoveries, valuable knowledge is gained about issues that would be prevenient during real world application.

5.4.1 Fluid Loss Cell

The fluid loss cell presented some issues. First, large volumes are required due to the cell size. In the manner that the cell is constructed, a 12 ml dead volume existed around the core and additional solution is needed for flow recovery or static treatment. At the treatment concentrations used, significant cost would have went to purchasing materials used in the treatment solutions. Secondly, the low permeability of Indiana Limestone cores could not be accurately measured using this apparatus. While conducting the first experiment an attempt to measure the permeability, as done with filter permeability (Section 5.2.2), resulted in erroneous data. It was concluded that the variation in the data was attributed to the pressure regulation of gas used to push the fluid through the core. To test the theory, an Isco syringe pump was used in place of the nitrogen gas cylinder to apply positive pressure. The results using this modification is shown in Figure 5.13 where an improved linear correlation between pressure drop and flowrate was obtained in comparison to data previously obtained. Although improved, the data shown is not linear and the correlation intercept is not zero. These small variations resulted in significantly lower permeability calculated for the fluid loss cell when compared to the Hassler core holder. The permeability measured using the fluid loss cell and Hassler core holder was 0.6 md and 1.4 md respectively. The system was tested for leaks but none could be found. Due to these issues, subsequent experiments used the Hassler core holder.

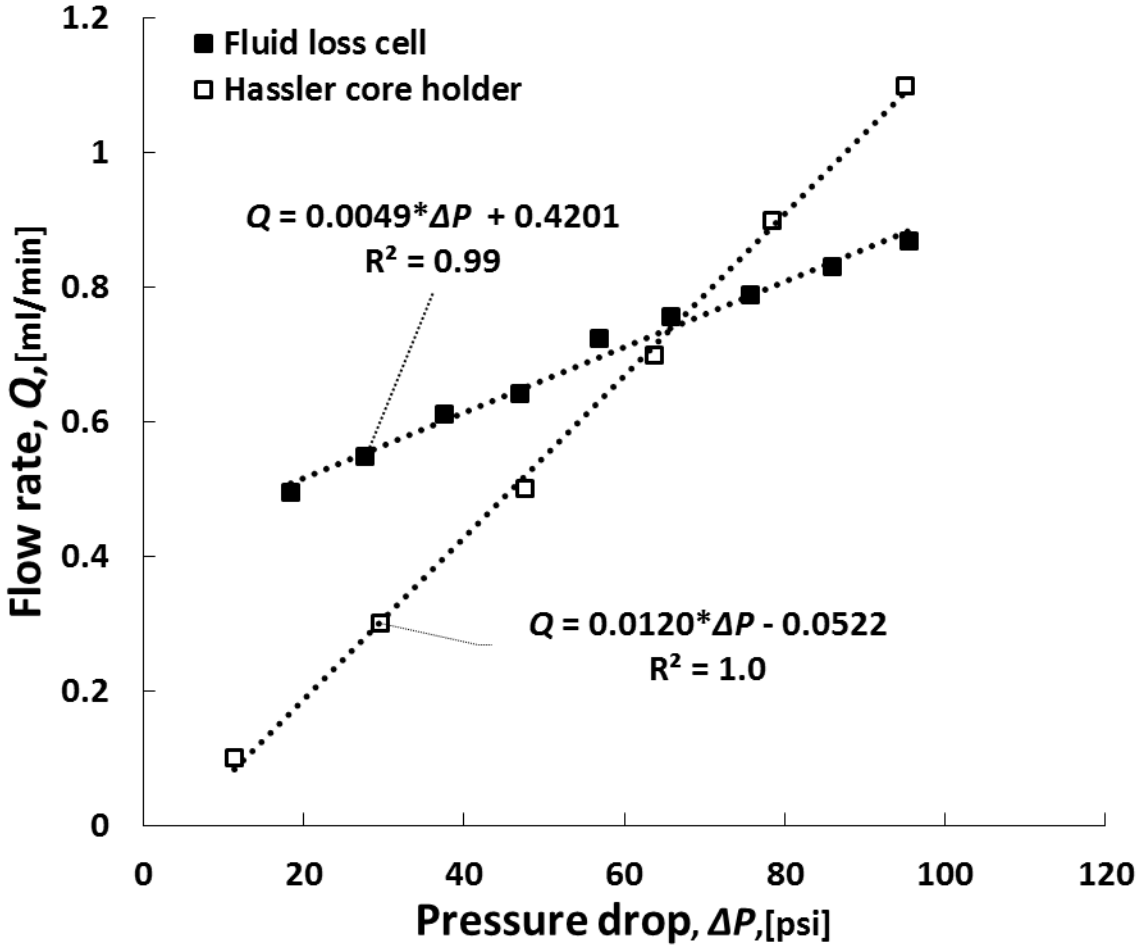

Figure 5.13 Pressure drop versus flowrate obtained using fluid loss cell and Hassler core holder using the same Indiana Limestone core. Linear correlation was used to obtain rock permeability.

5.4.2 Hassler Core Holder

In these studies, Indiana Limestone (1-4 md) was used and all permeability measurements were made using 2% KCL brine. Procedurally, the undamaged permeability (K_i) was measured, damage was created using 2000 ppm Alcoflood 935 and the damaged permeability (K_d) was measured, treatment was applied for 24 hours at 30°C, then the recovered permeability (K_r) was measured after 15 hour flow time. Data collected using the Hassler core holder is separated into three sections. The first set of studies (cores 1-4) show that data collected before reversing flow to

measure the permeability. The second set (cores 6-8) show data collected using reversed flow. Reverse flow was used in order to minimize additional damage by enzyme observed in the previous set. The third set (10-14) show forward flow with additional modifications to the core flooding procedure and apparatus in order to minimize variation in results. Reverse flow was discontinued because results still showed additional damage and high variability of results. Cores missing in the succession were used for collection additional data related to observations and are explained throughout the section. All core-flooding tests used Indiana Limestone with an mean brine permeability of 2.02 ± 0.83 md.

The first set of cores contributed in developing the use of backpressure and revealed the additional damaging effects of HRP (results listed in Table 5.2). As previously mentioned flowing all components through the core is a rigorous and harsh method for proving HRP recovery ability and is not indicative of field conditions. Core #1 was damaged using an unmeasured amount of polymer and pressure after damage was not allowed to stabilize. In addition, porosity (Φ) and pore volume (PV) was not measured. Results from this core are unreliable and unusable but also revealed that oxygen generation by enzyme system caused problems. The oxygen observed in the core resulted in the study conducted in Section 5.3 to establish a suitable backpressure. Core #2 (Φ= 0.12, PV= 1.50 ml) was flooded using a backpressure of 1000 psi and core was damaged using 10 PV of polymer. Leaks in the system resulted in a backpressure of 270 psi after 24-hour incubation of treatment and oxygen was observed in the core due to the loss of pressure. The initial damage created from the HPAM was 39.6% and the 16 pore volume (PV) treatment enhanced the damage by 28.1%. Core #3 (Φ= 0.11, PV= 1.36 ml) repeated the previous test but damage was created using 15 pore volumes and the treatment consisted 17 pore volumes. The backpressure was maintained at 1000 psi but the treatment again resulted in an additional 44.2% reduction in

permeability. Observation of the inlet side of the core revealed enzyme damage and aggregates were observed in the effluent. Core #4 (Φ= 0.151, PV= 1.86 ml) repeated the previous experiment, and used 15 pore volume damage, but treatment volume and backpressure were both reduced to minimized damage from enzyme. The backpressure was reduced to 600 psi and treatment was reduced to two pore volumes but additional damage of 26.5% was observed after treatment. The results of these studies led to the next set of experiments where reverse flow was used to measure the permeability. This was done in an attempt to minimize the damage created by flowing enzyme through the core after treatment is applied and is more realistic to field conditions.

Table 5.2 Data collected for Indiana Limestone cores 1-4 flooded in Hassler core holder.

Core #	Back pressure (psi)	Undamaged K_i (md)	Damaged K_d (md)	Reduction (%)	Treatment Vol (PV)	Recovered K_r (md)	Residual Damage (%)	Recovery (%)
1	------	1.69	0.35	79.3	20 ml	0.586	65.3	17.6
2	270	1.03	0.62	39.6	16.0	0.331	67.7	-71.2
3	1000	1.42	0.68	51.8	17.0	0.0571	96.0	-85.3
4	600	1.60	0.67	58.4	2.0	0.241	84.9	-45.3

Core #5 was used to test damage created using enzyme treatment alone, was the first test using forward, and reverse flow to measure permeability using a backpressure of 600 psi. First, undamaged permeability was measured in forward and reverse flow directions resulting in permeability of 1.91 md and 2.02 md respectively. The core was then treated with two pore volumes (3.23 ml) treatment and incubated at 30°C for 24 hours. After incubation, the permeability was first measured in the forward direction (K_{rf}) resulting in 25.2% permeability damage from treatment. The flow was then reversed and the permeability measured resulting in complete flow recovery (K_{rr} =2.05 md). This test proved that residual enzyme damage could be recovered using reverse flow. In light of these results, three core samples were damaged using HPAM and treatment tested for recovery using reverse permeability measurements.

For the reverse flow experiments listed in Table 5.3, permeability was measured in the forward (K_{if}) and reverse (K_{ir}) directions for undamaged (K_{if}) and recovered permeability. The damaged permeability was only measured in the reverse direction and percent reduction is considered the reduction observed after reverse flow. Core samples were tested using a minimum backpressure of 600 psi and treatment consisted of two pore volumes enzyme solution. Core #6 (Φ= 0.123, PV= 1.67 ml) showed only 24% damage after 15 pore volume HPAM and after reverse flow. The treatment added additional damage for both forward and reverse flow directions of 34.0% and 35.7% respectively. After conducting this experiment, a black residue was observed on the inlet face of the core and upon further investigation; groves were observed in the core holder's rubber sleeve. Further research indicated that the Viton rubber sleeve was not compatible with free radicals. For subsequent experiments, heat shrink wrap was placed around core and spacers to alleviate enzyme treatment contact with rubber sleeve. Core #7 (Φ= 0.114, PV= 1.42 ml) repeated the previous experiment but damage was created using only 8.4 pore volumes because pressure drop reached 500 psi transducer limit. Reverse flow resulted in 47.9% damage and after treatment, recovered permeability resulted in additional loss in permeability of 44.8% and 16.3% for forward and reverse flow respectively. Results of this study show less damage using reverse flow indicating that heat shrink was effective in reducing additional damage created by rubber residue. Core #8 (Φ= 0.118, PV= 1.49 ml) was an attempt to repeat previous experiment but issues were encountered when creating damage. Damage was created using 15 ml HPAM but reverse flow resulted in 11.0% greater permeability than initial measurement. It is thought that the gain in permeability can be attributed to poor sealing by the heat shrink-wrap. Later experiments were conducted using only forward flow so contribution from heat shrink could be compared to previously obtained data.

Table 5.3 Results obtained using forward and reverse flow for cores 6-8.

Core #	Undamaged K_{if} (md) (forward)	Undamaged K_{ir} (md) (reverse)	Damaged K_{dr} (md) (reverse)	Reduction (%)	Recovered K_{rf} (md) (forward)	Recovered K_{rr} (md) (reverse)	Recovery forward (%)	Recovery reverse (%)
6	2.14	2.03	1.55	27.4	0.825	0.749	-124.1	-167.6
7	1.53	1.41	0.73	47.9	0.112	0.505	-77.8	-39.9
8	2.18	2.19	2.44	-11.8	-----	-----	-----	-----

Core #9 (Φ= 0.117, PV= 1.42 ml) tested the difference in undamaged permeability for forward and reverse flow with and without heat shrink wrap. The results of the study indicated that slightly higher permeability was observed with addition of heat shrink for both flow directions. This core also indicated a greater difference in permeability with respect to flow direction regardless of heat shrink application. For forward flow, the resulting permeability with and without heat shrink was 1.21 md and 1.16 md respectively. Reverse flow resulted in 1.57 md and 1.44 md with and without heat shrink wrap respectively.

Core flooding experiments were repeated using only forward flow (rigorous method) with heat shrink (Table 5.4). To ensure that heat shrink was sealed properly, the undamaged permeability was measured before and after heat shrink application. For this set, cores 10-14 were flooded with a backpressure of 600 psi and were damaged using 15 pore volumes HPAM. Core #10 (Φ= 0.121, PV= 1.58 ml) indicated significant improvement to previous observations resulting in only 8.2% residual damage after a two pore volumes treatment. In a final attempt to improve results, an inline mixer was used to ensure HRP and peroxide solutions were well mixed before reaching the core. In addition to the inline mixer, treatment volume was reduced to 0.5 pore volume. Core #11 (Φ= 0.121, PV= 1.58 ml) shows the results obtained from using inline mixer and reduced treatment volume. Using this core, a 24% stimulation was observed after treatment.

Core #12 (Φ= 0.126, PV= 1.61 ml) showed the highest undamaged permeability up to this point (K_i= 4.33 md) and injection of 15 pore volumes indicated no significant damage. Two more experiments were conducted with core 13 (Φ= 0.121, PV= 1.56 ml) and core 14 (Φ= 0.123, PV= 1.59 ml) in order to repeat results observed for core # 11. The results of these two core flooding experiments did show permeability recovery but not stimulation as seen with core #11. The resulting permeability recovery was 1.3% and 0.7% for cores 13 and 14 respectively. Results from this set of experiments showed that HPAM damage recovery was possible. Rubber residue (from rubber sleeve) as well as large treatment volumes counteracted the recovery from enzyme treatment.

Table 5.4 Results obtained using forward flow, heat shrink, and inline mixer for cores 10-14.

Core #	Undamaged K_i (md)	Damaged K_d (md)	Reduction (%)	Recovered K_r (md)	Residual Damage (%)	Recovery (%)
10	2.57	0.356	86.1	0.145	94.3	-9.5
11	1.47	0.688	53.1	1.789	-21.9	141.3
13	1.82	0.707	61.2	0.87	52.3	1.3
14	2.58	1.118	56.7	1.137	55.9	0.7

Results of this study show that flowing all components is a rigorous method because additional damage can be created from flowing enzyme through the core. Although flowing treatment and degraded polymer through the core is not a practical application in fracturing, it does demonstrate a viable treatment method if recovery can be accomplished. On the other hand, fracturing does cause filtration of fluids at the fracture face (fluid leak off). One particular study showed that significant leak off can occur in cores with 1-5 md permeability when using crosslinked fluid-loss additives.[271] Furthermore, the fluid loss observed for linear polymers is greater than that of crosslinked additives. In order evaluate the permeability recovery exhibited by the enzyme system,

enzyme flow through the core must be minimized. In a real world scenario, flow is reversed after damage is created. In the case of this study flow is not reversed so that recovery can be more easily quantified and is a greater indication of the magnitude damage recovered. To achieve this goal, a new core flooding apparatus was created to simulate a fluid loss cell. The final core flooding apparatus encapsulated cores in clear PVC and resin and is covered Chapter 4.

5.5 Enzyme Immobilization: Method Development and Preliminary Data

Enzyme was immobilized on glass beads and Ottawa fracturing sand as a means of enzyme application in core flooding experiments. Ottawa sand provides a cheap alternative to glass substrate and sand immobilized enzyme could be used for bioremediation processes both in and out of fracture for a variety of compounds and applications. This study focused in immobilized HRP ability to catalyze the degradation of HPAM. Because little literature could be found for HRP immobilization on sand, Section 5.5.1 covers the immobilization method development and observations. Section 5.5.2 describes the preliminary immobilized concentration and activity measured for immobilization on glass and sand substrates.

5.5.1 Method Development

Initially, two methods were considered for improving the core flooding results. The first method was attachment of HRP to the HPAM polymer using glutaraldehyde cross linker. Glutaraldehyde is a nonspecific cross linker that will form bonds between amine groups. Covalently attaching HRP to HPAM would ensure that radical generation takes place near HPAM and that the HPAM is incorporated into the filter cake. This method may improve the recovery, as seen with the filtration experiments, but still has the ability to increase the permeability damage. The second method consists of covalently attaching the enzyme to the fracturing sand. Immobilizing HRP to the

fracture sand would not only alleviate the possibility of HRP causing further damage to the rock matrix, but would also provide a means of breaker transport throughout the fracture. In addition, sand could be a cheap alternative to glass substrates for other bioremediation processes. One such process could be remediation of contaminants and additives in flow back water. With this in mind, HRP attachment to fracturing sand was pursued and the method development for this technique is discussed.

Literature search on the subject revealed that HRP attachment to glass surfaces was well established and for this reason the 75-micron, acid washed glass beads were used as a control. Initially, four different substrates were tested and included 75-micron, acid washed glass beads (control), potters glass beads, 30-50 mesh Ottawa sand, and unseparated Ottawa sand. From the literature, the main method for covalently bonding the enzyme to the substrate remained the same where the substrate would be cleaned, treated with (3-aminopropyl) triethoxysilane (APTES), and the enzyme would be attached to the substrate using glutaraldehyde cross linker. Although many studies used these steps, several variations existed for cleaning the substrate and attaching the enzyme.

The first attempt at HRP attachment washed the substrates in 5% nitric acid for one hour at 80°C in an attempt to activate the surface. The substrates were washed with RO water and dried in the oven at 110°C for 24 hours. The surface was activated using 10% (v/v) APTES in RO water with the pH adjusted to 4-4 using 6N HCl. The substrates were exposed to APTES for 2 hours at 75°C the washed with distilled water and again dried overnight at 110°C. Activated substrates subjected to 2.5% (v/v) glutaraldehyde in 50mM phosphate buffer solution (PBS, pH=7.0) under agitation for 8 hours at room temperature. Substrate was washed using 50mM PBS by decantation until pH=7. Substrate was then exposed to 56.5 μM HRP at a 1:1 ratio (ml HRP: mg substrate)

for 15 hours at 4°C. The supernatant was then collected and substrates were washed with 50 mM PBS to remove free enzyme. A bench top test observed the activity of enzyme treated sand by exposing the substrates to 96.9 mM peroxide. Peroxide was added to 200 mg treated and untreated sand samples, placed into 15 ml centrifuge tubes, and observed over time for oxygen generation. Results of this study showed no activity in treated samples but oxygen formation did take place in untreated samples (Figure 5.14).

Further literature search showed that glass required a more aggressive treatment, when compare to other substrate types, in order to activate the substrate surface.[272] After learning this, 20 grams of each substrate was first cleaned with piranha solution (3:1, H_2SO_2: H_2O_2) for 3 hours at 80°C followed by a base treatment (5:1:1, H_2O: NH_4OH: H_2O_2) for 1 hour under sonication. The samples were then dried at 70°C overnight. Substrates were salinized using 5% (v/v) APTES in anhydrous toluene for 4 hours. Substrates were washed with toluene, acetone then dried and stored for later use. After dried the substrates were cemented together and had to be broken apart. This indicated that the APTES treatment was successful and the surface of the substrates had been modified. Another enzyme attachment using previous procedure was attempted. Again, no detectable activity was visually observed upon exposure to peroxide.

Adjustments were made to the procedure and attachment was attempted again. The first adjustment was with the duration of glutaraldehyde treatment. The same 2.5% (v/v) was used exposure time was reduced from 8 hours to 1 hour. In addition, the enzyme concentration was increased from 56.5 μM to 135.9 μM HRP. Again, enzyme exposure was for 24 hours at 4°C under agitation. Upon observation, it was clear that attachment took place by the darker color and another test was conducted with exposure to peroxide. Figure 5.15 shows an image of sand with immobilized enzyme (left) and an untreated sample (right) after washing excess enzyme away by

decantation. During exposure to peroxide the enzyme treated samples showed activity by continuous generation of oxygen. This method for immobilization applied in all future studies.

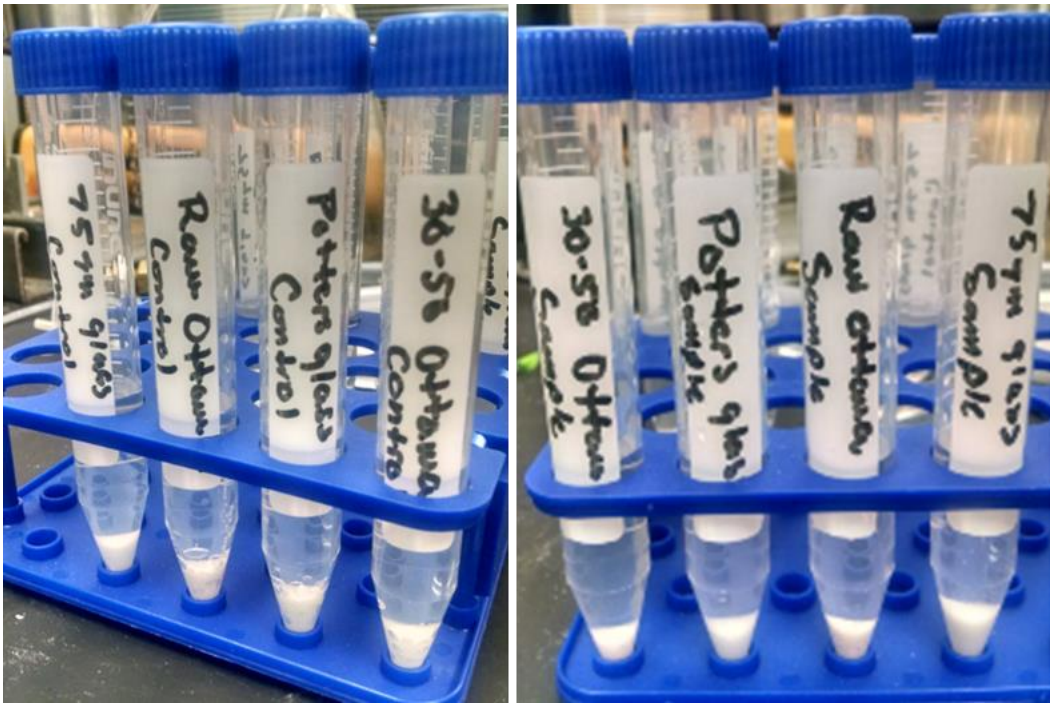

Figure 5.14 Observations of peroxide exposure to untreated (control. left) and treated substrate (right) samples.

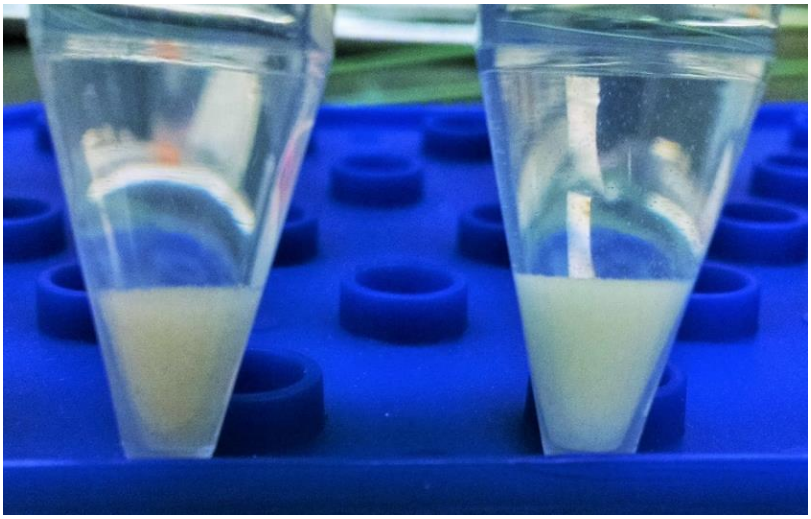

Figure 5.15 Image showing enzyme attachment on sand using glutaraldehyde cross linker, (left is immobilized and right is untreated.

A study conducted by Kadima and Tenshuka[273] showed two methods of attaching HRP to porous glass beads. The first method was using traditional procedure of exposing substrate to glutaraldehyde and then applying enzyme as previously explained. The novel technique used the enzyme isoelectric point (IP) to ionically attach the enzyme to the substrate surface before crosslinking everything together using glutaraldehyde. The study concluded that using the enzyme isoelectric point resulted in greater attachment and therefore this was attempted in the current study. Enzyme solutions were exposed to the salinized glass beads at a concentration 56.5 μM HRP in 50 mM PBS adjusted to various pH from 5-9. Solutions were incubated at 4°C for 24 hours at which time the supernatant was removed and samples were washed with 50 mM PBS. Observations showed a slight color difference for sample at pH=8 indication enzyme binding (Figure 5.16). Although enzyme showed ionic bonding, the enzyme easily washed away and could not be crosslinked to the substrate. Kadima and Tenhuka[273] noted the same issue but were able to reduce the loss of enzyme by change in buffer salt content. Further testing was conducted on the effect of salt (PBS) concentration but better results were not achieved. Future testing is conducted using the traditional method of glutaraldehyde pretreatment then enzyme binding.

All experiments presented in Chapter 4 used the successful method of attachment with exposure to glutaraldehyde then attaching enzyme. Ottawa sand and 75-micron glass samples were evaluated for concentration and activity. Further investigation was conducted to evaluate enzyme activated Ottawa sand for ability to reduce HPAM viscosity and recover permeability in core flooding experiments.

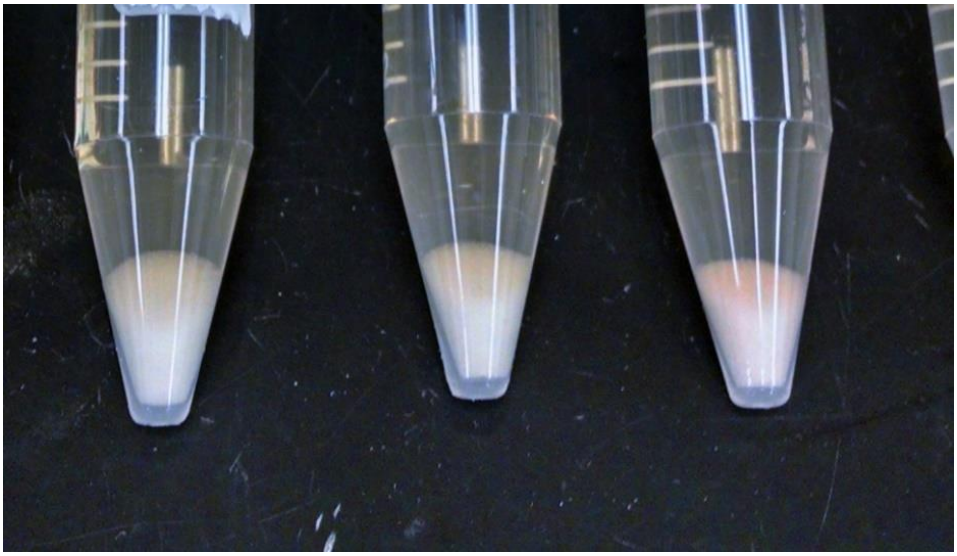

Figure 5.16 HRP ionically bound to salinized glass sample at pH=8. Samples in picture are pH=6 (left), pH=7 (middle), and pH=8 (right).

5.5.2 Preliminary Immobilized Enzyme Concentration Data

Immobilized HRP concentration was determined using UV-Vis spectroscopy (absorbance at 405 nm) by measuring the change in HRP concentration of sample supernatant for 75-micron glass bead and Ottawa sand samples. Experiments evaluated the concentration of immobilized enzyme on 0.2 grams of 75-micron glass beads. Solutions incubated at 4°C for 24 and 96 hours before evaluation. Enzyme solutions were made to a concentration of 5.0 mg/ml (113 μM HRP) and 3 ml of the solution was set aside for the control. All samples were subjected to the same conditions but solid substrates were not added to the control.

For glass beads, Table 5.5 shows the results obtained for HRP immobilization after 24 and 96 hours exposure to enzyme solution. The measured absorbance values closely predicted the diluted concentration of HRP resulting in 0.989 mg/ml HRP for control sample. After 24 hours, the diluted sample showed a 0.031 mg change in HRP concentration. Multiplying that value by the dilution factor (DF) of 5 resulted in a 0.155 mg change in the original solution. In addition, the change in

concentration resulted in an enzyme concentration of 0.773 mg HRP per gram glass. Allowing a longer exposure time of 96 hours resulted in significantly higher immobilization of HRP. The 96-hour exposure resulted in an immobilization of 1.779 mg HRP per gram glass. Based on the activity listed in the bottle (163 U/mg), and assuming the enzyme shows the same activity while immobilized, the immobilized enzyme would show an activity of 126 U/g glass and 289 U/g glass for 24 and 96 hour exposures respectively.

Table 5.5 Enzyme concentration on 75-micron glass beads evaluated after 24 and 96 hours incubation at 4°C.

	Abs @ 405 nm	**[HRP] (mg/ml)**	**Δ[HRP] (mg/ml)**	**Δ[HRP]*DF (mg/ml)**		**[HRP]/substrate (mg/g)**
Control	1.125	0.989	-------	-------		-------
Supernatant (24 hrs)	1.090	0.958	0.031	0.155	===>	0.773
Supernatant (96 hrs)	1.045	0.918	0.071	0.356	===>	1.779

For Ottawa sand, Table 5.6 shows the results obtained for HRP immobilization after 24 and 96 hours exposure to enzyme solution. The measured absorbance values closely predicted the diluted concentration of HRP resulting in 0.961 mg/ml HRP for control sample. After 24 hours, the diluted sample showed a 0.037 mg change in HRP concentration. Multiplying that value by the dilution factor (DF) of 5 resulted in a 0.183 mg change in the original solution. In addition, the change in concentration resulted in an enzyme concentration of 0.916 mg HRP per gram beads. Allowing a longer exposure time of 96 hours did not significantly change HRP concentration. The 96-hour exposure resulted in an immobilization of 1.068 mg HRP per gram sand. Based off the activity listed in the bottle (163 U/mg), and assuming the enzyme shows the same activity while immobilized, the immobilized enzyme should show an activity of 149 U/g sand and 174 U/g sand for 24 and 96 hour exposures respectively. Compared to the 75-micron glass beads, immobilization

in the first 24 hours is more significant. In addition, longer exposure time did not show further immobilization as seen with the glass beads.

Table 5.6 Enzyme concentration on Ottawa sand evaluated after 24 and 96 hours incubation at 4°C.

	Abs @ 405 nm	[HRP] (mg/ml)	Δ[HRP] (mg/ml)	Δ[HRP]*DF (mg/ml)		[HRP]/substrate mg/g
Control	1.093	0.961	-------	-------		-------
Supernatant (24 hrs)	1.052	0.924	0.037	0.183	===>	0.916
Supernatant (96 hrs)	1.045	0.918	0.043	0.214	===>	1.068

5.6 References

265. Levitt, D.; Pope, G. A. SPE Symposium on Improved Oil Recovery, 2008. Document ID: SPE-113845-MS
266. Seright, R. S.; Campbell, A.; Mozley, P.; Han, P., SPE Journal 15, 341 2010.
267. Tromans, D., Ind. Eng. Chem. Res. 39, 805 2000.
268. Boonyaratanakornkit, B. B.; Park, C. B.; Clark, D. S., Biochim. Biophys. Acta 1595, 235 2002.
269. Silva, J. L.; Weber, G., Annual Review of Physical Chemistry 44, 89 1993.
270. Mozhaev, V. V.; Heremans, K.; Frank, J.; Masson, P.; Balny, C., Trends Biotech. 12, 493 1994.
271. Vinod, P.; Flindt, M.; Card, R.; Mitchell, J. SPE Production Operations Symposium, 1997. Document ID: SPE-37486-MS
272. Shafer-Peltier, K. E.; Haynes, C. L.; Glucksberg, M. R.; Van Duyne, R. P., J. Am. Chem. Soc. 125, 588 2003.
273. Kadima, T. A.; Pickard, M. A., Applied and Environmental Microbiology 56, 3473 1990.

6 Conclusions

This study has presented a novel biocatalytic system for the degradation of partially hydrolyzed polyacrylamide (HPAM) typically used in hydraulic fracturing fluids. Horseradish peroxidase catalyzes the radical degradation of the HPAM with hydrogen peroxide as shown in viscosity and molecular weight studies. For viscosity studies, a wide range of solutions showed that the HRP could efficiently degrade HPAM solutions in the presence of peroxide. First, viscosity measurements were conducted to observe change attributed to the addition of components (i.e HRP, NADH). The results showed that the addition of any of these components, in amounts similar to the degradation experiments, to the stock polymer solution decreased the viscosity at all shear rates with HRP having the greatest effect. Although the viscosity was reduced, the shear thinning characteristics of solution remained similar.

In the absence of HRP, HPAM solutions showed slight reductions in viscosity after 24 hours when peroxide was added. Furthermore, the addition of NADH eliminated the small reduction attributed to peroxide. Degradation studies tested after 24 reaction time showed varying results. In the presence of HRP and peroxide alone, a viscosity reduction of about 81% was achieved. Further investigation using HRP and peroxide revealed that HPAM viscosity reduction of 90% could be achieved by reducing the HRP concentration (from 45μM to 5.6 μM). Furthermore, the magnitude of viscosity reduction did not change when HRP concentration was reduced by half (from 45μM to 22.5μM).

In the presence of HRP, NADH, and peroxide, results showed significant reduction in HPAM solution viscosity (60-75%) after 24-hour reaction time. Reduction of HRP concentration created HPAM solutions with different rheological behavior. For example, in the presence of NADH the

power law indices (*n*) were 0.77, 0.86, and 0.93 for HRP concentrations of 45μM, 22.5μM, 5.6μM HRP respectively. Although the solution showed a systematic change in the power law index, all solutions had the same fractional change (η/η_o) at a shear rate of about 70-75s^{-1}. Soybean peroxidase was investigated at comparable concentrations in the presence of NADH. Compared to HRP, soybean peroxidase achieved similar viscosity reductions.

Further investigation was conducted using the HRP/NADH/peroxide system. First, periodic sampling was conducted (over 24 hours) to observe the effects of varying peroxide concentration. The results showed that viscosity reduction was directly related to the amount of peroxide added with greater viscosity reduction achieved for higher peroxide concentrations. Furthermore, small changes in enzyme activity and RZ value resulted in similar viscosity reductions after 24-hour reaction time. Periodic sampling over a 24-hour period revealed that a majority of the viscosity reduction takes place within the first 5 hours and follows a first order kinetic relationship with respect to peroxide concentration. Periodic sampling was extended to 75 hours to compare the viscosity reduction of HPAM solutions with and without the addition of NADH. Results showed that similar viscosity was archived (in both profile and magnitude) after 75 hours.

Size exclusion chromatography was used to quantify the molecular weight change when HPAM solutions were subjected to the HRP/peroxide system. After 24-hour reaction time, results show a linear relationship between molecular weight reduction and peroxide concentration in both fresh water and 2% KCl brine solutions. Little to no change in the magnitude of reduction was observed with the addition of resulting in about 65% molecular weight reduction using the highest peroxide concentration. Periodic sampling confirmed viscosity observations by showing a majority of degradation within the first few hours. Analysis of the data revealed two kinetically distinct regions at early and late degradation times.

The HRP/peroxide system was tested for the ability to degrade filter cake and recover damaged permeability in consolidated core samples. In both filtration and core flooding tests, recoveries were measured in only the forward flow direction. The unidirectional flow of water/brine served as a stringent proxy in evaluating the flow recoveries in both filtration and core flooding studies. First, experiments investigated the flowrate recovery, to 0.1 µm nylon filters, when greater than 99% flowrate reduction was created using HPAM solutions. When the filter cake consisted of HPAM alone, no recovery was archived for water and peroxide treatments. Using HRP and peroxide (without NADH) resulted in a minimal recovery of about 2%. A higher flowrate recovery of 6% was observed for treatments consisting of HRP, NADH, and peroxide. The higher recovery observed in the presence of NADH is counter to findings reported in viscosity experiments. Further testing revealed that greater flowrate recoveries were achieved (13-14%) when HRP was incorporated into the filter cake.

Core flooding was conducted to measure HPAM damage recovery in low permeability (1-4 md) Indiana Limestone cores. Treatment solutions included NADH due to the greater flowrate recoveries observed during filtration tests. The mean permeability damage was 89% and the full treatment (i.e HRP, NADH, and peroxide) resulted in 10% recovery. Core exposure HRP reaction (without HPAM damage) revealed an additional 24% reduction in permeability. This additional reduction was observed from flowing treatment solutions through the core samples and is an artifact of the testing protocol. To ameliorate the additional permeability loss, HRP was covalently immobilized on Ottawa fracturing sand. The immobilization on sand was a unique approach to delivering a catalyst and yielded positive results.

Immobilization of HRP was achieved on 75-micron glass bead (control) and Ottawa sand samples. The immobilization consisted of substrate surface silanization using APTES followed by

covalently binding the enzyme with glutaraldehyde crosslinker. The protocol was un-optimized and achieved 1.03 mg HRP per gram sand and 0.26 mg HRP per gram glass. The corresponding immobilized activities were 1.1 U/g sand and 27.7 U/g glass. Overall, the results show a higher enzyme load using Ottawa sand but a much lower specific activity compared to glass. Further investigation was conducted using HRP on Ottawa sand to evaluate the system's ability to reduce the viscosity of HPAM solutions. The immobilized enzyme showed considerable viscosity reduction compared to peroxide alone but was less effective than free enzyme at an equivalent HRP concentration. Lastly, the enzyme activated sand was used to recover permeability in HPAM damaged cores. Using similar procedures to previous core floods (with free HRP), the immobilized enzyme showed a greatly improved recovery of 28% when compared to the 10% archived using free HRP. Overall, immobilizing the enzyme on sand alleviated any further damage due to pore plugging by the enzyme and increased the permeability recovery in damaged cores. This immobilized system may be a useful platform for remediation of polymer damage in hydraulic fracturing operations. Moreover, the renewable and biodegradable reactant and catalyst may be able to help remediate other target chemicals in the fracturing fluid and reduce the need for large-scale flowback water treatment.

Appendix A: Nomenclature

Categories	Characters	Description
Viscosity	η	General expression for viscosity (cP)
	η_o	Initial viscosity (cP) at time= 0
	η_i	Initial viscosity (cP) low shear rate (zero shear viscosity)
	η_{oo}	Viscosity (cP) high shear rate
	η_a	Apparent viscosity
	τ_{yx}	Momentum Flux
	σ	Shear stress (N/m^2)
	γ	Shear rate (s^{-1})
	α_c	Constant related to polymer relaxation time
	λ_c	Constant related to polymer relaxation time
	z	graphically determined constant (dimensionless)
	N	graphically determined constant (dimensionless)
	K, K_s	Flow consistency index
	n, n_s	Power law index
Polymer Degradation Kinetics	C_{2i}	Initiator concentration at time=0
	C_{po}	Initial peroxide concentration
	a	scaling constant
	α	Kinetic exponent used to determine order
	k_{Mw}	Rate constant: weight average molecular weight (reaction in water)
	k_{Mn}	Rate constant: number average molecular weight (reaction in water)
	k_{Mwb}	Rate constant: weight average molecular weight (reaction in brine)
	k_{Mnb}	Rate constant: number average molecular weight (reaction in brine)
	$k\hat{}_{t'}$, $k\hat{}_t$	Apparent rate constant of zero and first order reactions respectively
	k	General reaction rate constant
	N_o	Total number of molecules
	m	monomer molecular weight
Molecular Weight	M_n, M_{nt}	Number average molecular weight at any time (t)
	M_{no}	Number average molecular weight at time= 0
	M_{nf}	Final reduced number average molecular weight
	M_w, M_{wt}	Weight average molecular weight at any time (t)

	M_{wo}	Weight average molecular weight at time= 0
	M_{wf}	Final reduced weight average molecular weight
	M_i	Incremental Molecular weight
	M_t	Molecular weight at any time (t), generic
	m	Monomer molecular weight
	n_i	Moles polymer
	c_i	Incremental polymer concentration
	k_p	proportionality constant
	Q_o	Detector readout
	PDI	Polydispersity Index
	a	Scaling constant
Filtration and Core flooding	RRF	Residual resistance factor
	RRF_α	Residual resistance factor after treatment
	RF	Resistance Factor
	r_p	Average pore radius
	β	Polymer layer thickness (μm)
	β_α	Polymer layer thickness after treatment (μm)
	$\Delta P_{(polymer)}$	Pressure drop observed during polymer flow
	$\Delta P_{(brine)}$	Pressure drop observed for brine flow before damage
	$\Delta P_{(after\ polymer)}$	Pressure drop after polymer damage (psi)
	$\Delta P_{(before\ polymer)}$	Pressure drop before polymer damage (psi)
	ΔP	General expression for pressure drop (psi)
	Φ	Porosity
	K_b	General expression for rock permeability (Darcy)
	K_i	Initial rock permeability (Darcy)
	K_d	Damaged rock permeability (Darcy)
	K_r	Recovered rock permeability (Darcy)
	K_{if}, K_{ir}	Initial rock permeability in forward and reverse flow directions (Darcy)
	K_{df}, K_{dr}	Damaged rock permeability: forward and reverse flow directions(Darcy)
	K_{rf}, K_{rr}	Recovered rock permeability:forward and reverse flow directions (Darcy)
	Q_i	Initial Flowrate (ml/min)
	Q_d	Damaged flowrate (ml/min)
	Q_r	Recovered flowrate (ml/min)
	Q	Flowrate (ml/min)
	m_b	Slope from ΔP vs Q relationship
	PV	Pore volume

Enzyme Activity	ΔA_{420}/20 sec	Change in absorbance measurement with respect to time
	V_t	Total volume in cuvette (ml)
	DF	Dilution factor
	ε_c	Extinction coefficient (m-cm^{-1})
	V_e	Volume of enzyme addition
	M_s	Mass substrate
Oxygen generation	C_{aq}	Oxygen concentration in brine (mol/kg)
	C_I	Salt concentration in brine (mol/kg)
	Po	Partial pressure of oxygen (atm)
	Y, κ, H	Constants related to salt type
General Characters	T	Temperature
	t	Time
	A	area
	v,V_x, V_{max}	velocity, velocity in x direction, maximum velocity
	F	tangential force
	r	Radius
	θ	angle (degrees)
	Ω	Angular frequency (revolutions per minute)
	τ	Torque
	V, ΔV	Volume, volume increment
	C	Concentration (mol/L)
	ε	absorptivity
	l	Light path length (cm)
	L	Length

Appendix C: Plotted Data Tables

Figure 3.1 Viscosity of 1980 ppm HPAM and viscosity reduction observed from component addition. Initial viscosity was measured at 25°C before incubation; lines are smoothed data (n=3).

	HPAM		HPAM + 1.4 mM NADH		HPAM + 45.0 µM HRP + 1.4 mM NADH		HPAM + 45.0 µM HRP	
Shear rate (s^{-1})	**viscosity (η_0) (cP)**	**σ**	**viscosity (η_0) (cP)**	**σ**	**viscosity (η_0) (cP)**	**σ**	**viscosity (η_0) (cP)**	**σ**
1.1	67.4	2.7	23.2	1.6	18.1	3.9	15.1	4.2
2.1	63.4	1.3	23.2	0.9	17.5	3.2	15.1	3.5
3.9	58.6	1.1	23.5	0.4	17.2	2.7	15.1	2.8
7.1	52.0	1.0	22.1	0.2	15.7	1.5	14.1	2.1
13.0	45.1	0.7	20.7	0.2	14.1	0.3	13.2	1.0
23.9	37.9	0.6	18.9	0.1	13.2	0.2	12.0	0.2
43.9	30.8	0.4	16.6	0.1	11.9	0.1	11.0	0.1
80.6	24.5	0.3	14.3	0.1	10.6	0.1	9.9	0.1
148.0	19.1	0.2	12.0	0.1	9.2	0.1	8.6	0.0
272.0	14.7	0.1	9.8	0.1	7.8	0.0	7.4	0.0
500.0	11.3	0.1	8.0	0.0	6.6	0.0	6.2	0.0

Figure 3.2 Variation of viscosity relative to the initial viscosity (Figure 3.1 data) at 25°C with shear rate for 1980 ppm Alcoflood 935 samples containing varying peroxide concentration and the presence or absence of 45.0 μM HRP and/or 1.4 mM NADH after 24 hour incubation at 37°C. Power law constants K and n are representative of degraded HPAM trends; lines are smoothed data (n=3).

	HPAM + 96.9 mM peroxide			**HPAM + NADH + 96.9 mM peroxide**			**HPAM + HRP + NADH + 96.9 mM peroxide**			**HPAM + HRP + NADH + 48.4 mM peroxide**			**HPAM + HRP + 96.9 mM peroxide**		
Shear rate	**viscosity (η)**	**η/ηo**	**σ**	**viscosity (η)**	**η/ηo**	**σ**	**viscosity (η)**	**η/ηo**	**σ**	**viscosity (η)**	**η/ηo**	**σ**	**viscosity (η)**	**η/ηo**	**σ**
(s^{-1})	**(cP)**			**(cP)**			**(cP)**			**(cP)**			**(cP)**		
7.1	49.7	0.95	0.07	22.27	1.01	0.03	7.99	0.51	0.09	7.82	0.50	0.11	2.57	0.18	0.06
13.0	43.1	0.96	0.05	20.90	1.01	0.02	6.20	0.44	0.05	6.29	0.45	0.07	2.25	0.17	0.04
23.9	36.5	0.96	0.04	19.00	1.01	0.01	4.66	0.35	0.03	5.13	0.39	0.05	1.99	0.17	0.03
43.9	29.9	0.97	0.03	16.83	1.01	0.01	3.73	0.31	0.02	4.28	0.36	0.03	1.72	0.16	0.03
80.6	23.9	0.98	0.02	14.47	1.01	0.01	3.06	0.29	0.02	3.64	0.34	0.03	1.50	0.15	0.02
148.0	18.6	0.98	0.01	12.13	1.01	0.01	2.57	0.28	0.01	3.20	0.35	0.02	1.31	0.15	0.02
272.0	14.4	0.98	0.01	9.95	1.01	0.01	2.30	0.29	0.01	2.91	0.37	0.02	1.18	0.16	0.01
500.0	11.1	0.98	0.01	8.07	1.01	0.01	2.12	0.32	0.01	2.70	0.41	0.01	1.09	0.18	0.01

Figure 3.3 Viscosity of HPAM/NADH solutions with varying HRP concentration relative to original polymer solution over the same range of shear rates. Solutions concentrations for peroxide and NADH are 96.9 mM and 1.40 mM respectively. Samples were incubated for 24 hours at 37°C; lines represent smoothed data (n=3).

	45.3 µM HRP				22.7 µM HRP				5.6 µM HRP				No HRP			
Shear Rate	**ηo**	**η**	**η/ηo**	**σ**	**ηo**	**η**	**η/ηo**	**σ**	**ηo**	**η**	**η/ηo**	**σ**	**ηo**	**η**	**η/ηo**	**σ**
(s^{-1})	**(cP)**	**(cP)**			**(cP)**	**(cP)**			**(cP)**	**(cP)**			**(cP)**	**(cP)**		
7.1	15.1	10.7	0.71	0.24	23.1	13.4	0.58	0.22	28.3	7.0	0.25	0.03	31.1	27.3	0.89	0.04
13.0	13.8	6.5	0.47	0.14	20.1	9.0	0.45	0.13	25.5	6.1	0.24	0.01	27.5	24.5	0.93	0.04
23.9	13.0	4.6	0.36	0.09	17.4	6.3	0.36	0.06	23.0	5.8	0.25	0.00	23.4	22.0	0.95	0.03
43.9	12.1	3.6	0.30	0.07	15.2	4.8	0.32	0.02	20.1	5.5	0.27	0.01	20.4	19.4	0.95	0.02
80.6	10.9	3.0	0.27	0.05	13.4	4.2	0.31	0.02	17.1	5.3	0.31	0.01	17.4	16.7	0.96	0.02
148.0	9.6	2.5	0.26	0.04	11.5	3.8	0.33	0.01	14.3	5.1	0.36	0.01	14.6	14.0	0.96	0.02
272.0	8.3	2.3	0.27	0.03	9.7	3.5	0.37	0.01	11.7	4.9	0.42	0.01	11.9	11.5	0.97	0.00
500.0	7.1	2.1	0.30	0.02	8.1	3.4	0.42	0.01	9.5	4.7	0.49	0.01	9.7	9.3	0.97	0.00

Figure 3.4 Viscosity of HPAM solutions (in the absence of NADH) with varying HRP concentration relative to original polymer solution over the same range of shear rates. Solutions concentrations for peroxide is 96.9 mM. Samples were incubated for 24 hours at 37°C; lines represent smoothed data (n=3).

	45.3 µM HRP				22.7 µM HRP				5.6 µM HRP				No HRP			
Shear Rate	**ηo**	**η**	**η/ηo**	**σ**	**ηo**	**η**	**η/ηo**	**σ**	**ηo**	**η**	**η/ηo**	**σ**	**ηo**	**η**	**η/ηo**	**σ**
(s^{-1})	**(cP)**	**(cP)**			**(cP)**	**(cP)**			**(cP)**	**(cP)**			**(cP)**	**(cP)**		
7.1	19.6	6.2	0.32	0.09	30.9	9.9	0.32	0.04	52.2	6.5	0.12	0.05	65.7	60.6	0.92	0.08
13	17.4	4.5	0.26	0.10	26.7	6.7	0.25	0.01	43.4	4.9	0.11	0.04	55.4	50.6	0.91	0.03
23.9	15.9	3.1	0.19	0.08	23.5	4.4	0.19	0.03	36.5	4.1	0.11	0.04	45.8	41.9	0.92	0.02
43.9	14.4	2.2	0.15	0.03	20.2	3.0	0.15	0.03	30.3	3.2	0.10	0.02	37.0	34.5	0.93	0.01
80.6	12.8	1.8	0.14	0.01	17.2	2.4	0.14	0.02	24.6	2.8	0.11	0.01	29.2	27.7	0.95	0.01
148	11.0	1.5	0.14	0.01	14.4	2.0	0.14	0.01	19.5	2.6	0.13	0.01	22.7	21.8	0.96	0.01
272	9.3	1.4	0.15	0.01	11.7	1.7	0.15	0.01	15.3	2.4	0.15	0.01	17.5	16.9	0.96	0.01
500	7.8	1.3	0.17	0.00	9.5	1.6	0.16	0.01	12.1	2.3	0.19	0.01	13.5	13.1	0.97	0.01

Figure 3.5 and Figure 3.6 Viscosity profiles for 1980 ppm Alcoflood 935 solutions containing 45.0 μM HRP and 1.4 mM NADH in RO water and 2% KCl brine. Viscosity measured using the Bohlin rheometer at 25°C; lines are smoothed data (n=3)

	HPAM + 45.0 μM HRP + 1.4 mM NADH (water)		**HPAM + 45.0 μM HRP + 1.4 mM NADH (2% KCl)**		**HPAM + 45.0 μM HRP + 1.4 mM NADH +48.5 mM H2O2 (2% KCl)**		**HPAM + 45.0 μM HRP + 1.4 mM NADH +48.5 mM H2O2 (2% KCl)**	
Shear rate	**viscosity (η_0)**	**σ**	**viscosity (η_0)**	**σ**	**viscosity (η_0)**	**σ**	**viscosity (η_0)**	**σ**
(s^{-1})	**(cP)**		**(cP)**		**(cP)**		**(cP)**	
29	25.2	0.95	4.0	0.67	5.9	1.65	5.6	0.44
58	20.2	0.27	3.5	0.59	4.6	1.09	3.8	0.41
86	17.4	0.03	3.3	0.55	4.0	0.81	2.8	0.39
115	15.6	0.08	3.1	0.48	3.6	0.66	2.3	0.30
143	14.3	0.01	3.0	0.38	3.3	0.68	2.0	0.32
172	13.3	0.05	2.8	0.42	3.1	0.62	1.8	0.33
200	12.5	0.00	2.8	0.37	2.9	0.59	1.7	0.35

Figure 3.7 Reduction in 1980 ppm Alcoflood 925 viscosity observed using 45.0 μM soybean peroxidase, 1.4 mM NADH and varying peroxide concentration. Viscosity was measured using Anton Paar rheometer at 25°C after 24-hour incubation at 37°C; lines are smoothed data (n=3)

	HPAM SBP NADH				HPAM SBP NADH + 48.4 mM peroxide				HPAM SBP NADH + 96.9 mM peroxide			
Shear Rate	**ηo**	**η**	**η/ηo**	**σ**	**ηo**	**η**	**η/ηo**	**σ**	**ηo**	**η**	**η/ηo**	**σ**
(s^{-1})	**(cP)**	**(cP)**			**(cP)**	**(cP)**			**(cP)**	**(cP)**		
7	37.8	28.9	0.77	0.16	37.8	30.3	0.80	N/A	37.8	25.0	0.66	0.17
13	31.2	25.6	0.82	0.13	31.2	19.2	0.62	N/A	31.2	16.1	0.51	0.11
24	26.1	22.7	0.87	0.11	26.1	12.9	0.49	N/A	26.1	10.5	0.40	0.04
44	21.9	20.0	0.91	0.09	21.9	9.1	0.41	N/A	21.9	7.6	0.34	0.03
81	17.9	16.9	0.94	0.07	17.9	7.2	0.40	N/A	17.9	6.3	0.35	0.04
148	14.6	14.0	0.96	0.05	14.6	6.0	0.41	N/A	14.6	5.6	0.38	0.03
272	11.8	11.4	0.97	0.04	11.8	5.2	0.44	N/A	11.8	5.0	0.43	0.03
500	9.5	9.3	0.98	0.03	9.5	4.6	0.49	N/A	9.5	4.6	0.48	0.03

Figure 3.9 Normalized viscosity reduction observed for samples containing 1980 ppm Alcoflood 935, 1.4 mM NADH, 96.9 mM peroxide, and 45.0 μM HRP of different activity and Rz value. Viscosity was tested using the Bohlin rheometer at 75 s-1 and 25°C. (n=3)

	173 units/mg, Rz= 3.2		193 units/mg, Rz= 2.7		191 units/mg, Rz= 2.1		181 units/mg, Rz= 1.9	
Time	Viscosity (η)	σ	Viscosity (η)	σ	Viscosity (η)	σ	Viscosity (η)	σ
(hours)								
0	18.3	0.2	18.3	0.4	18.3	0.4	19.1	0.2
1	12.1	1.1	13.3	0.5	13.3	0.5	12.0	1.3
2	12.0	0.9	10.6	0.7	10.6	0.7	8.7	0.6
3					10.4	0.5		
4	12.8	0.8	10.4	0.5			6.1	0.5
5					7.6	0.3		
6	10.7	1.8	7.6	0.3			4.9	0.5
7					7.7	0.4		
8	11.1	1.2	7.7	0.4			4.5	0.5
9					7.6	0.3		
14.5					7.1	0.4		
24	6.7	1.8	7.6	0.3	6.7	0.7	1.7	0.5

Figure 3.10 Normalized viscosity of 191 unit/mg HRP periodically sampled over 24 hours. Concentrations are 1980 ppm Alcoflood 935, 1.4 mM NADH, and 45.0 μM HRP with varying peroxide. Viscosity measurement taken at 75 s-1 at 25°C. (n=3)

	96.9 mM peroxide		48.4 mM peroxide		9.69 mM peroxide	
Time (hours)	Viscosity (η)	σ	Viscosity (η)	σ	Viscosity (η)	σ
0.0	18.3	0.4	18.8	0.9	18.9	0.6
1.0	13.3	0.5	17.7	0.9	18.7	0.9
2.0	10.6	0.7	16.1	0.4	18.5	1.0
3.0	10.4	0.5	15.8	0.6	17.7	0.8
5.0	7.6	0.3	14.5	0.8	17.9	0.6
7.0	7.7	0.4	14.2	0.5	17.5	0.8
9.0	7.6	0.3	13.7	0.7	16.3	0.7
14.5	7.1	0.4	13.5	0.4	15.8	0.8
24.0	6.7	0.7	13.7	0.6	15.6	0.9

Figure 3.11 - Figure 3.13 Normalized viscosity profile for solutions with and without NADH after 24, 48, and 75-hour incubation at 37°C. Samples containing 1980 ppm Alcoflood 935, 45.0 μM HRP, and 96.9 mM and tested at 25°C; lines are smoothed data (n=3)

		Without NADH, 24 hours			Without NADH, 48 hours			Without NADH, 75 hours		
Shear Rate	ηo	η	η/ηo	σ	η	η/ηo	σ	η	η/ηo	σ
[1/s]	(cP)	(cP)			(cP)			(cP)		
7	14.1	5.9	0.41	0.16	4.7	0.33	0.05	2.9	0.21	0.06
13	13.2	4.6	0.35	0.11	3.7	0.28	0.03	2.0	0.15	0.04
24	12.0	3.7	0.31	0.08	3.1	0.26	0.01	1.7	0.14	0.03
44	11.0	2.6	0.24	0.03	2.6	0.24	0.01	1.6	0.14	0.03
81	9.9	2.0	0.20	0.01	2.1	0.22	0.01	1.5	0.15	0.02
148	8.6	1.7	0.19	0.01	1.6	0.19	0.02	1.3	0.15	0.00
272	7.4	1.5	0.20	0.00	1.2	0.17	0.01	1.2	0.16	0.00
500	6.2	1.4	0.22	0.00	1.2	0.19	0.00	1.2	0.19	0.00

		With NADH, 24 hours			With NADH, 48 hours			With NADH, 75 hours		
Shear Rate	ηo	η	η/ηo	σ	η	η/ηo	σ	η	η/ηo	σ
[1/s]	(cP)	(cP)			(cP)			(cP)		
7	15.7	5.1	0.32	0.06	4.1	0.26	0.10	3.2	0.20	0.12
13	14.1	4.1	0.29	0.04	3.1	0.22	0.09	2.5	0.18	0.09
24	13.2	3.5	0.26	0.03	2.6	0.19	0.07	2.3	0.17	0.06
44	11.9	2.8	0.24	0.01	2.1	0.18	0.03	2.0	0.17	0.04
81	10.6	2.4	0.23	0.02	1.8	0.17	0.01	1.7	0.16	0.01
148	9.2	2.2	0.24	0.01	1.7	0.19	0.01	1.6	0.17	0.01
272	7.8	2.1	0.27	0.01	1.6	0.21	0.00	1.5	0.19	0.01
500	6.6	2.0	0.30	0.00	1.6	0.25	0.00	1.5	0.23	0.00

Figure 3.14 Number average (Mn) and weight average (Mw) molecular weight reduction of Alcoflood 935 solutions with 1.4 mM NADH and 45.0 μM HRP in RO water with varying peroxide concentrations after 24 incubation; lines are smoothed data (n=3)

	M_n x 10^{-6}	σ	M_w x 10^{-6}	σ	PDI= M_w/M_n	σ
Control	2.06	0.06	6.14	0.07	2.98	0.07
0.979 M Peroxide Addition	1.71	0.11	5.22	0.19	3.06	0.09
4.89 M Peroxide Addition	1.34	0.11	3.67	0.17	2.75	0.12
9.79 M Peroxide Addition	0.90	0.23	2.04	0.67	2.20	0.23

Figure 3.15 Number average (Mn) and weight average (Mw) molecular weight reduction of Alcoflood 935 solutions with 1.4 mM NADH and 45.0 μM HRP in 2% KCl brine with varying peroxide concentrations after 24 incubation; lines are smoothed data (n=3).

	M_n x 10^{-6}	σ	M_w x 10^{-6}	σ	PDI= M_w/M_n	σ
Control	2.49	0.06	5.73	0.1361	2.31	0.00
0.979 M Peroxide Addition	2.04	0.02	4.97	0.0406	2.44	0.01
4.89 M Peroxide Addition	1.71	0.11	3.92	0.0372	2.30	0.15
9.79 M Peroxide Addition	0.89	0.05	2.16	0.1374	2.44	0.08

Figure 3.16 Number average (Mn) and weight average (Mw) molecular weight reduction of Alcoflood 935 with respect to time for solution containing 1.4 mM NADH, 45.0 μM HRP, and 96.9 mM peroxide concentration. Inset shows corresponding polydispersity index (PDI); (n=3).

Time (hours)	$M_n \times 10^{-6}$	σ	$M_w \times 10^{-6}$	σ	PDI=M_w/M_n	σ
0.0	2.04	0.08	5.37	0.15	2.64	0.06
0.5	1.75	0.20	4.29	0.04	2.48	0.26
1.0	1.50	0.05	3.99	0.16	2.67	0.07
1.5	1.50	0.12	3.93	0.18	2.62	0.10
2.0	1.70	0.24	3.99	0.18	2.38	0.30
3.0	1.38	0.15	3.74	0.35	2.72	0.05
4.0	1.35	0.14	3.65	0.45	2.69	0.09
5.0	1.31	0.09	3.54	0.33	2.71	0.26
7.0	1.34	0.09	3.38	0.33	2.56	0.40
8.0	1.26	0.16	3.14	0.40	2.50	0.08
11.0	1.10	0.06	2.81	0.39	2.55	0.25
11.5	1.08	0.08	2.79	0.38	2.57	0.16
15.0	1.09	0.07	2.94	0.20	2.70	0.11
24.0	0.95	0.05	2.22	0.18	2.34	0.14

Figure 3.17 and Figure 3.18 Number average molecular weight (Mn) and weight average molecular weight (Mw) with time for samples containing 990 ppm Alcoflood 935. Results presented as residual Mn and percent reduction for the HPAM concentrations; lines are smoothed data (n=3)

Time	M_n x 10^{-6}	σ	M_w x 10^{-6}	σ	PDI=M_w/M_n	σ
(hours)						
0.0	3.24	0.23	5.94	0.61	1.83	0.06
0.5	3.45	0.25	5.55	0.74	1.60	0.16
1.0	2.88	0.21	4.71	0.27	1.64	0.09
1.5	2.50	0.19	4.32	0.13	1.74	0.12
2.0	2.47	0.03	4.19	0.15	1.70	0.08
3.0	2.25	0.23	3.78	0.43	1.68	0.04
4.0	2.10	0.17	3.45	0.22	1.65	0.03
5.0	2.05	0.17	3.37	0.26	1.64	0.02
7.0	1.91	0.19	3.14	0.41	1.64	0.06
8.0	1.86	0.24	2.97	0.43	1.59	0.03
11.0	1.98	0.21	3.25	0.18	1.65	0.09
15.0	1.73	0.06	2.98	0.24	1.72	0.07
24.0	1.72	0.25	2.81	0.23	1.64	0.10

Chapter 4

Indiana Limestone Core Flooding Data Sets (Free and Immobilized HRP)

Data Set 1: Results for core exposure to full reaction treatment in the absence of HPAM damage.

Core #	Undamaged K_i (md)	Recovered K_r (md)	Residual Damage (%)
ILS 1-7	2.81	2.37	15.5
ILS 1-10	2.07	1.69	18.4
ILS 1-11	3.49	2.14	38.5
Mean	2.79	2.07	**24.1**
Std Dev	0.71	0.35	**12.5**

Data Set 2: Contribution to permeability recovery from 15-hour brine flow alone.

Core #	Undamaged K_i (md)	Damaged K_d (md)	Reduction (%)	Recovered K_r (md)	Residual Damage (%)	Damage Recovery (%)
ILS 1-1	3.65	0.431	88.2	0.490	86.6	1.6
ILS 1-5	3.13	0.480	84.7	0.506	83.8	0.8
ILS 1-9	4.09	0.610	85.1	0.513	87.4	-2.4
Mean	3.623	0.507	85.984	0.503	85.9	**0.04**
Std Dev	0.478	0.093	1.934	0.012	1.9	**2.12**

Data Set 3: Contribution to permeability recovery from HRP and NADH exposure.

Core #	Undamaged K_i (md)	Damaged K_d (md)	Reduction (%)	Recovered K_r (md)	Residual Damage (%)	Damage Recovery (%)
ILS 1-12	2.12	0.210	90.1	0.269	87.3	2.8
ILS 1-13	1.90	0.200	89.5	0.276	85.5	4.0
ILS 1-14	2.28	0.303	86.7	0.373	83.6	3.1
ILS 1-15	1.98	0.214	89.2	0.216	89.1	0.1
ILS 1-18	1.30	0.101	92.2	0.214	83.6	8.7
ILS 1-24	1.57	0.181	88.5	0.292	81.4	7.1
ILS 2-2	1.87	0.187	90.0	0.210	88.8	1.2
Mean	1.80	0.197	89.3	0.261	85.3	**3.8**
Std Dev	0.50	0.101	2.8	0.091	3.2	**3.1**

Data Set 4: Permeability recovery observed using full treatment consisting of HRP, NADH, and peroxide.

Core #	Undamaged K_i (md)	Damaged K_d (md)	Reduction (%)	Recovered K_r (md)	Residual Damage (%)	Damage Recovery (%)
ILS 1-2	2.72	0.240	91.2	0.414	84.8	6.4
ILS 1-3	3.85	0.238	93.8	0.699	81.8	12.0
ILS 1-4	4.59	0.796	82.7	1.281	72.1	10.6
Mean	3.72	0.425	89.2	0.798	79.6	**9.6**
Std Dev	0.94	0.322	5.8	0.442	6.6	**2.9**

Data Set 5: The effect of peroxide alone on permeability recovery.

Core #	Undamaged K_i (md)	Damaged K_d (md)	Reduction (%)	Recovered K_r (md)	Residual Damage (%)	Damage Recovery (%)
ILS 1-25	1.53	0.145	90.5	0.471	69.2	21.3
ILS 2-3	1.34	0.185	86.2	0.356	73.4	12.8
ILS 2-4	1.58	0.145	90.8	0.447	71.7	19.1
Mean	1.48	0.158	89.1	0.424	71.4	**17.7**
Std Dev	0.13	0.023	2.6	0.061	2.1	**4.4**

Data Set 6: Permeability recovery using immobilized HRP on Ottawa sand.

Core #	Undamaged Ki (md)	Damaged Kd (md)	Reduction (%)	Recovered Kr (md)	Residual Damage (%)	Damage Recovery (%)
ILS 2-1	3.38	0.506	85.0	1.425	57.8	27.2
ILS 2-3	2.23	0.272	87.8	0.905	59.4	28.4
ILS 2-4	1.66	0.161	90.3	0.634	61.9	28.5
Mean	2.42	0.313	87.7	0.988	59.7	**28.0**
Std Dev	0.87	0.176	2.7	0.402	2.1	**0.7**

Figure 4.4 Absorbance for varying concentration of HRP at three wavelengths.

Concentration [HRP]	Wavelength 205 nm		Wavelength 280 nm		Wavelength 405 nm	
mg/ml	Abs	σ	Abs	σ	Abs	σ
2.00	6.003	3.462	1.292	0.011	2.221	0.022
1.50	5.782	3.655	0.976	0.011	1.719	0.025
1.00	3.929	0.400	0.661	0.001	1.156	0.001
0.80	3.627	0.012	0.531	0.027	0.907	0.041
0.60	3.574	0.193	0.430	0.009	0.722	0.006
0.40	3.536	0.067	0.294	0.005	0.472	0.009
0.20	3.315	0.045	0.168	0.006	0.239	0.007
0.10	2.069	0.084	0.106	0.004	0.126	0.006
0.08	1.709	0.034	0.095	0.002	0.103	0.000
0.06	1.247	0.078	0.079	0.004	0.075	0.005
0.04	0.898	0.007	0.069	0.003	0.054	0.002
0.02	0.475	0.022	0.055	0.003	0.029	0.003

Glass Beads

Immobilized enzyme concentration after 24 hours on 75-micron glass beads (n=3).

	Abs	[HRP] (mg/ml)	Δ[HRP] (mg/ml)	Δ[HRP]*DF (mg/ml)		[HRP]/substrate mg/g
Control	1.149 ± 0.006	1.011 ± 0.005	-------	-------		-------
Supernatant	1.138 ± 0.011	1.001 ± 0.009	0.010 ± 0.004	0.051 ± 0.022	===>	0.255 ± 0.109

Activity of control, supernatant, and HRP immobilized on 75-micron glass beads. Values correspond to data presented in concentration table (above). (n=3)

Control	182.9 ± 2.9	HRP activity (U/ml)
Supernatant	197.1 ± 16.6	HRP activity (U/ml)
Glass beads	7.2 ± 3.8	HRP specific activity (U/g)

Ottawa Sand

Immobilized enzyme concentration after 24 hours on Ottawa sand (n=3).

	Abs	[HRP] (mg/ml)	Δ[HRP] (mg/ml)	Δ[HRP]*DF (mg/ml)		[HRP]/substrate mg/g
Control	1.208 ± 0.002	1.063 ± 0.002	-------	-------	===>	-------
Supernatant	1.161 ± 0.006	1.022 ± 0.005	0.041 ± 0.007	0.206 ± 0.036	===>	1.032 ± 0.180

Activity of control, supernatant, and HRP immobilized on Ottawa sand. Values correspond to data presented in concentration table (above). (n=3)

Control	214.2 ± 15.8	HRP activity (U/ml)
Supernatant	198.8 ± 16.5	HRP activity (U/ml)
Sand	1.1 ± 0.6	Specific activity (U/g)

Figure 4.5 The reduction in HPAM viscosity observed in the presence of HRP treated and untreated Ottawa sand. Viscosity measured at 75s-1 and 25°C. (n=3)

	Free HRP		Immobilized HRP		No HRP	
Time (hours)	Viscosity (η)	σ	Viscosity (η)	σ	Viscosity (η)	σ
0	13.29	0.23	13.34	0.56	13.40	0.51
7	4.95	0.13	7.24	0.08	9.54	0.33
18	2.69	0.61	5.56	0.15	8.44	0.23
24	1.17	0.03	4.54	0.30	7.90	0.36

Figure 5.1 Viscosity of 10000 molecular weight PAM solutions over time with varying additions of peroxide. Viscosity measured at a shear rate of 75 s-1 and 25°C.

	18% PAM + 45.3 µM HRP + 2.82 mM NADH		18% PAM + 45.3 µM HRP + 2.82 mM NADH + 4.84 mM peroxide		18% PAM + 45.3 µM HRP + 2.82 mM NADH + 24.2 mM peroxide		18% PAM + 45.3 µM HRP + 2.82 mM NADH + 96.9 mM peroxide	
Time	η	η/ηo	η	η/ηo	η	η/ηo	η	η/ηo
[minutes]	(cP)		(cP)		(cP)		(cP)	
0	13.5	1.00	12	0.26	13.2	1.00	13.3	1.00
2			12	0.22	14.2	1.08	14.2	1.07
5			12.2	0.19	14.7	1.11	14.7	1.11
8			12.4	0.18				
10					15.1	1.14	15.3	1.15
12			12.5	0.17				
15	13.5	1.00	12.6	0.19	15.6	1.18	16.3	1.23
20			12.8	0.21	16	1.21	17	1.28
30	13.6	1.01			16.6	1.26	17.5	1.32
45	13.6	1.01			16.5	1.25	17.4	1.31
60	13.6	1.01			16.5	1.25	17.2	1.29
80					16.5	1.25	17.1	1.29
90							16.9	1.27
105							16.9	1.27

Figure 5.2 Viscosity reduction observed for Alcoflood 935 solutions containing 18.33 mM NADH and varying peroxide concentrations. Viscosity measured at various shear rates and 25°C.

	2000 ppm Alcoflood 935 + 45.3 µM HRP + 18.3 mM NADH		**1998 ppm Alcoflood 935 + 45.3 µM HRP + 18.3 mM NADH + 9.69 mM peroxide**		**1980 ppm Alcoflood 935 + 45.3 µM HRP + 18.3 mM NADH + 96.9 mM peroxide**	
Shear rate (s^{-1})	**viscosity (η_0) (cP)**	**σ**	**viscosity (η_0) (cP)**	**σ**	**viscosity (η_0) (cP)**	**σ**
37.5	6.5	0.86	6.1	0.08		
45	6.6	0.27	6.4	0.08		
75	6.9	0.29	6.7	0.00	4.5	0.89
90	6.7	0.13	6.5	0.11	4.5	0.54
150	5.9	0.05	6.0	0.02	3.9	0.59
225	5.4	0.05	5.5	0.01	3.6	0.23
375	5.3	0.00	5.4	0.01	3.7	0.14
450	5.0	0.02	5.1	0.01	3.5	0.14

Figure 5.3 Viscosity reduction observed for Alcoflood solutions with and without the addition of 18.33 mM NADH. Viscosity measured at various shear rates and 25°C.

	1980 ppm Alcoflood 935		1980 ppm Alcoflood 935 + 96.9 mM peroxide		1980 ppm Alcoflood 935 + 18.3 mM NADH + 96.9 mM peroxide	
Shear rate	**viscosity (η_0)**	**σ**	**viscosity (η_0)**	**σ**	**viscosity (η_0)**	**σ**
(s^{-1})	**(cP)**		**(cP)**		**(cP)**	
2.3	128.8	74.4	out of range		out of range	
3.8	97.2	48.8	out of range		out of range	
4.5	88.4	38.9	out of range		out of range	
7.5	80.3	33.4	36.3	4.5	out of range	
11.3	69.2	20.0	37.4	8.3	out of range	
15.0	62.6	12.9	40.9	7.4	out of range	
18.8	56.4	10.1	35.5	6.5	out of range	
22.5	51.5	6.9	34.6	4.6	out of range	
30.0	47.5	9.0	32.1	2.5	out of range	
37.5	42.9	12.9	28.1	0.2	out of range	
45.0	39.7	16.0	25.4	0.1	out of range	
75.0					6.1	**NA**
90.0					5.6	**NA**
150.0					5.1	**NA**
225.0					4.6	**NA**
375.0					4.5	**NA**
450.0					4.3	**NA**

Figure 5.4 Effect of NADH concentration on HPAM viscosity. Viscosity measured at various shear rates and 25°C.

	1980 ppm Alcoflood + No NADH	1980 ppm Alcoflood + 1.4 mM NADH	1980 ppm Alcoflood + 5.64 mM NADH	1980 ppm Alcoflood + 8.46 mM NADH	Water + 18.33 mM NADH
Shear rate	**viscosity (η_0)**	**viscosity (η_0)**	**viscosity (η_0)**	**viscosity (η_0)**	**viscosity (η_0)**
(s^{-1})	**(cP)**	**(cP)**	**(cP)**	**(cP)**	**(cP)**
2	120.6	out of range	out of range	out of range	out of range
4	72.3	out of range	out of range	out of range	out of range
5	62.8	out of range	out of range	out of range	out of range
8	57.6	out of range	out of range	out of range	out of range
11	54.6	out of range	out of range	out of range	out of range
15	53.8	16.2	out of range	out of range	out of range
19	47.6	13.5	out of range	out of range	out of range
23	46	11.7	out of range	out of range	out of range
30	42.5	12.2	9.7	8.1	out of range
38	38.7	11.0	8.3	7.3	out of range
45	35.4	10.3	7.3	6.6	out of range
75	29.1	10.8	8.6	7.5	out of range
90		10.0	8.1	7.1	out of range
150		10.5	9.6	8.7	out of range
375					0.9
450					1.2
750					1.2

Figure 5.5 Viscosity profiles obtained for Alcoflood Solutions containing 1.4 mM NADH concentration and varying peroxide concentration. Viscosity measured at various shear rates and 25°C.

	1980 ppm Alcoflood 935 + 1.4 mM NADH + 96.9 mM peroxide		**1980 ppm Alcoflood + 45.0 µM HRP + 1.4 mM NADH**		**1980 ppm Alcoflood + 45.0 µM HRP + 1.4 mM NADH + 9.69 mM peroxide**		**1980 ppm Alcoflood + 45.0 µM HRP + 1.4 mM NADH + 96.9 mM peroxide**	
Shear rate	**viscosity (η_0)**	**σ**	**viscosity (η_0)**	**σ**	**viscosity (η_0)**	**σ**	**viscosity (η_0)**	**σ**
(s^{-1})	**(cP)**		**(cP)**		**(cP)**		**(cP)**	
11.25	27.5	2.8	out of range		out of range		out of range	
15	22.7	0.0	19.6	1.1	out of range		out of range	
18.75	20.0	1.6	16.9	0.2	out of range		out of range	
22.5	19.1	2.3	16.5	0.3	out of range		out of range	
30	19.4	1.2	16.7	1.4	10.5	0.7	out of range	
37.5	18.0	2.0	15.8	0.4	9.6	0.3	out of range	
45	17.0	1.7	14.4	0.4	8.9	0.3	out of range	
75	15.4	0.1	13.6	0.1	9.8	0.7	6.9	0.7
90	14.5	0.1	13.0	0.3	9.2	0.8	6.4	0.7
150	14.1	0.3	12.6	0.5	9.9	0.6	6.1	0.9
225					9.1	0.9	5.6	1.1
375							5.1	0.5